

**Exploring the links between the *ZDHHC9* gene
and intellectual disability**

A thesis presented by

Marianna Kouskou

BSc, MSc

In fulfilment of the requirement for the degree of

Doctor of Philosophy

2018

University of Strathclyde

Strathclyde Institute of Pharmacy and Biomedical Sciences

Declaration of Authenticity and Author's Rights:

This thesis is the result of the author's original research. It has been composed by the author and has not been previously submitted for examination which has led to the award of a degree.

The copyright of this thesis belongs to the author under the terms of the United Kingdom Copyright Acts as qualified by University of Strathclyde Regulation 3.50. Due acknowledgement must always be made of the use of any material contained in, or derived from this thesis.

Signed:

Date: 10/07/18

A handwritten signature in black ink, appearing to read "M. K. K. K. K.", with a long, sweeping underline.

Acknowledgments

A thesis is a collaborative work, consisting of supervisors, colleagues, friends and family. First of all, I would like to thank with all my heart my supervisor Professor Luke Chamberlain for supporting me throughout the whole Phd. He was always very helpful and happy to give me advice on my experimental work and to give me many ideas on future work. His positivity even when things were not working out gave me the motivation to continue until the end. A big thanks for all the support, the understanding and the patience!

I would also like to thank my second supervisor Professor Judith Pratt for her valuable input on my publication and for her understanding and patience during the period I was trying to finish the writing of my Phd and working at the same time in her group.

Then I would like to thank Dr David Mark Thomson for teaching me Behavioural Neuroscience. His love for the subject made my Phd an enjoyable experience, he was always happy to give me feedback and advice on my experimental work and support me when experiments were not going as expected. He was also a friend for me apart from colleague.

I would also like to thank all the Chamberlain lab members consisting of Dr Christine Salaun, Dr Kimon Lemonidis, Dr Jennifer Greaves and Dr Cinta Diez-Ardanuy. They were always happy to help me and to discuss about my experimental problems, they were also friends for me apart from colleagues. I will miss the friendly work environment of the Chamberlain lab as it is not easy to find a team where you always feel welcome.

Friends are an important part of the supporting system during the Phd process so I would like to thank Olga Łapieś for being there for me when I needed her. Thanks for being patient and listening to me! I would also like to thank James

for his every day support and interest on my progress, even though he is not from the same field he always enjoyed learning about my work and discussing about my progress, a big thanks!

Last but not least, an enormous thanks to my family, my mother Mina, my father Giorgos and my sister Mersy for the whole support. They always believed I can do it!

Publications

Kouskou, M., Thomson, D.M., Brett, R.R., Wheeler, L., Tate, R.J., Pratt, J.A., Chamberlain, L.H. (2018) 'Disruption of the *Zdhhc9* intellectual disability gene leads to behavioural abnormalities in a mouse model', *Experimental Neurology*, pii: S0014-4886(18)30204-8. doi: 10.1016/j.expneurol.2018.06.014. [Epub ahead of print]

Lemonidis, K., Salaun, C., Kouskou, M., Diez-Ardanuy, C., Chamberlain, L.H., Greaves, J. (2017) 'Substrate selectivity in the zDHHC family of S-acyltransferases', *Biochemical Society Transactions*, 45(3), pp. 751-758. doi: 10.1042/BST20160309.

Conference communications

Kouskou, M., Thomson, D.M., Wheeler, L., Collins, M., Brett, R.R., Pratt, J.A., Chamberlain, L.H. (2017) Knockout of *ZDHHC9*, a gene associated with X-linked intellectual disability, causes reduced anxiety and a spatial learning deficit in adult male mice. Unpublished poster presentation at Society for Neuroscience annual conference in Washington, DC, USA, November 2017. Appendix I.

Kouskou, M., Thomson, D.M., Wheeler, L., Collins, M., Brett, R.R., Pratt, J.A., Chamberlain, L.H. (2016) Exploring the links between the *ZDHHC9* gene and intellectual disability. Oral communication and unpublished poster presentation at the Biochemical Society conference 'Protein S-Palmitoylation: from mechanism to application', Oxford, UK, September 2016. Appendix II.

Kouskou, M., Thomson, D.M., Wheeler, L., Collins, M., Brett, R.R., Pratt, J.A., Chamberlain, L.H. (2016) Exploring the links between the *ZDHHC9* gene and intellectual disability. Oral communication and unpublished poster presentation at the Scottish Neuroscience group meeting, Glasgow, UK, August 2016. Appendix II.

Kouskou, M., Thomson, D.M., Collins, M., Chamberlain, L.H. (2016) Exploring the links between the *ZDHHC9* gene and intellectual disability. Unpublished poster presentation in Glasgow Neuroscience Day, Glasgow, UK, January 2016. Appendix III.

Table of contents

Declaration of Authenticity and Author's Rights	I
Acknowledgments	II
Publications.....	IV
Conference communications.....	V
Table of contents.....	VI
List of Figures	XIII
List of Tables.....	XIX
List of Abbreviations.....	XX
Abstract.....	XXIV
CHAPTER 1.....	1
1 General introduction	1
1.1 PROTEIN PALMITOYLATION	1
1.2 ENZYMES REGULATING PALMITOYLATION.....	4
1.3 ZDHHC9 (ZINC FINGER DHHC DOMAIN-CONTAINING PROTEIN 9).....	5
1.3.1 The <i>ZDHHC9</i> gene and its transcripts	5
1.3.2 <i>ZDHHC9</i> transcript expression in brain	5
1.3.3 Transcriptional regulation of <i>ZDHHC9</i>	6
1.3.4 zDHHC9 structure and function	7
1.3.5 Protein alignment between human and mouse zDHHC9	8
1.4 GCP16 (GOLGI COMPLEX-ASSOCIATED PROTEIN OF 16KDA).....	9
1.5 ZDHHC9-GCP16 COMPLEX	9

1.6	A PALMITOYLATION- DEPALMITOYLATION CYCLE REGULATES THE SUBCELLULAR TRAFFICKING OF RAS FAMILY GTPASES, SUBSTRATES OF ZDHHC9	11
1.7	PALMITOYLATION AND NERVOUS SYSTEM FUNCTION	14
1.8	OTHER POST-TRANSLATIONAL MODIFICATIONS IMPORTANT IN NERVOUS SYSTEM FUNCTION.....	18
1.9	ZDHHC MUTATIONS AND DISEASE	20
1.9.1	Intellectual disability	23
1.9.2	Effects of ZDHHC9 mutations on the nervous system	24
1.9.2.1	ZDHHC9 mutations and epilepsy	25
1.9.2.2	ZDHHC9 mutations are associated with hypoplasia of corpus callosum.....	26
1.9.3	ZDHHC9 dysfunction as a cause of other disorders.....	28
1.10	GENETIC ANIMAL MODELS OF ID	29
1.10.1	Down Syndrome	29
1.10.2	Fragile X syndrome.....	31
1.10.3	Rett syndrome.....	32
1.10.4	Non-syndromic XLID.....	34
1.11	MOLECULAR AND CELLULAR MECHANISMS IMPLICATED IN ID	35
1.12	METABOLIC BIOMARKERS OF INTELLECTUAL DISABILITY	36
1.13	AIMS OF THIS THESIS	37
CHAPTER 2.....		39
2	Materials and Methods	39
2.1	ZDHHC9 KNOCK-OUT MICE	39
2.2	MOUSE COLONY AND GENOTYPING	39
2.3	BEHAVIOURAL TESTS	40
2.3.1	SHIRPA.....	40
2.3.2	Hanging wire task.....	42
2.3.3	Rotarod task	42

2.3.4	Open field test.....	42
2.3.5	Elevated plus maze.....	43
2.3.6	Startle curve	43
2.3.7	Pre-pulse inhibition	43
2.3.8	Morris water maze	44
2.3.8.1	Reversal learning version of Morris water maze.....	46
2.3.8.2	Working memory version of Morris water maze	46
2.3.9	Three-chamber apparatus for sociability and social novelty.....	47
2.3.10	Sucrose preference task.....	48
2.3.11	Pairwise discrimination task	48
2.3.12	Same paired associated learning (sPAL)	49
2.3.13	Five Choice Serial Reaction Time Test.....	51
2.4	MOUSE TRANSCARDIAL PERFUSION FOR EX VIVO MRI	52
2.5	FAST LOW ANGLE SHOT MAGNETIC RESONANCE IMAGING (FLASH MRI) AND ANALYSIS	53
2.6	MOUSE BRAIN ISOLATION AND STORAGE FOR NON-MRI EXPERIMENTS.....	54
2.7	MOLECULAR BIOLOGY	54
2.7.1	DNA extraction from mouse brain tissue.....	54
2.7.2	RNA isolation from mouse brain tissue	55
2.7.3	Spectrophotometric quantification of DNA and RNA	57
2.7.4	End-point polymerase chain reaction (PCR)	57
2.7.5	Agarose gel electrophoresis.....	60
2.7.6	Reverse transcription PCR.....	60
2.7.7	Quantitative PCR (qPCR)	61
2.7.8	Plasmids	61
2.7.9	Sequencing	62
2.7.10	Cloning of Zdhhc9 KO cDNA into the pEF-BOS-HA plasmid.....	62
2.7.11	Plating HEK293T cells	64
2.7.12	Transfection of HEK293T cells.....	64
2.8	BIOCHEMISTRY.....	65

2.8.1	HEK293T cell lysates.....	65
2.8.2	Determination of protein concentration	65
2.8.3	Polyacrylamide gel electrophoresis and Western blot equipment	66
2.8.4	Sodium dodecyl sulphate (SDS) - polyacrylamide gel electrophoresis (PAGE).	66
2.8.5	Antibodies	67
2.8.6	Western blotting	69
2.8.7	Cell fractionation and Resin-Assisted Capture of S-acylated proteins (Acyl-RAC).....	70
2.9	IMMUNOFLUORESCENCE AND CONFOCAL MICROSCOPY	73
2.10	DATA ANALYSIS	74
2.11	OMICS APPROACHES	74
2.11.1	Proteomics	74
2.11.2	Metabolomics	75
2.11.3	Integrated metabolomic and transcriptomic analysis	76
CHAPTER 3.....		78
3	Initial characterisation of the <i>Zdhhc9</i> mouse line	78
3.1	INTRODUCTION	78
3.2	RESULTS	79
3.2.1	<i>Zdhhc9</i> KO mice are born at a lower frequency than WT mice.....	79
3.2.2	Qualitative analysis of <i>Zdhhc9</i> expression in brain samples from WT and <i>Zdhhc9</i> KO mice	80
3.2.3	Quantitative analysis of <i>Zdhhc9</i> expression in brain samples from WT and <i>Zdhhc9</i> KO mice	82
3.2.4	Analysis of the mRNA transcript detected in <i>Zdhhc9</i> KO mouse brain .	86
3.2.5	Analysis of expression of mutant <i>Zdhhc9</i> in HEK293T cells.....	89
3.2.6	Localisation of mutant <i>ZDHHC9</i> in HEK293T cells	90

3.2.7	A new antibody against zDHHC9 confirms KO of zDHHC9 expression and the absence of a truncated zDHHC9 protein in KO brain	92
3.3	DISCUSSION	93
CHAPTER 4.....		98
4	Behavioural and anatomical investigation of the effect of Zdhhc9 KO in mouse brain	98
4.1	INTRODUCTION	98
4.2	RESULTS	99
4.2.1	Physical gross examination of Zdhhc9 KO mice.....	99
4.2.2	Zdhhc9 KO mice exhibit hypotonia in the hanging wire	102
4.2.3	Zdhhc9 KO mice show normal motor coordination on the rotarod	104
4.2.4	Effect of age on hanging wire and rotarod task.....	105
4.2.5	Zdhhc9 KO mice exhibit normal locomotor activity in the open field test but different thigmotactic behaviour during the habituation period compared to WT mice	107
4.2.6	Zdhhc9 KO mice exhibit reduced anxiety levels in the elevated plus maze.....	112
4.2.7	Zdhhc9 KO mice exhibit reduced startle reactivity in the startle curve.....	114
4.2.8	Zdhhc9 KO mice exhibit normal pre-pulse inhibition	115
4.2.9	Zdhhc9 KO mice exhibit a different pattern of spatial learning in the Morris water maze	116
4.2.10	Zdhhc9 KO mice exhibit a different pattern of reversal learning in Morris water maze	120
4.2.11	Zdhhc9 KO mice show normal working memory in Morris water maze.....	125
4.2.12	Zdhhc9 KO mice show normal sociability and social novelty	130
4.2.13	Zdhhc9 KO mice show normal sucrose and water intake.....	132

4.2.14	Zdhhc9 KO mice show normal learning and cognitive flexibility in the pairwise discrimination task	134
4.2.15	Analysis of the performance of Zdhhc9 KO mice in same paired associated learning (sPAL).....	136
4.2.16	Zdhhc9 KO mice complete more trials than the WT mice but they have similar correct responses to the WT animals in the Five Choice Serial Reaction Time Task (5CSRTT)	138
4.2.17	Zdhhc9 KO mice react faster when responding correctly while they have similar percentage of correct responses and they complete similar number of trials to the WT mice in the final week of the 5CSRTT	140
4.2.18	Zdhhc9 KO mice register more beam breaks while they have similar number of premature responses to the WT mice in the final week of the 5CSRTT.....	142
4.2.19	Zdhhc9 KO mice have decreased volume of corpus callosum but not of hippocampus.....	143
4.3	DISCUSSION	151
CHAPTER 5.....		164
5	Biochemical and proteomic investigation of the effect of Zdhhc9 KO in mouse brain	164
5.1	INTRODUCTION	164
5.2	RESULTS	165
5.2.1	H-Ras and N-Ras protein levels are not affected in whole brain homogenates of Zdhhc9 KO mice.	165
5.2.2	H-Ras and N-Ras levels in membrane fractions are not affected in whole brain homogenates of Zdhhc9 KO mice.....	167
5.2.3	H-Ras palmitoylation is not affected in whole brain or hippocampus of Zdhhc9 KO mice	169
5.2.4	Analysis of palmitoylated pre-synaptic proteins in Zdhhc9 KO brain..	171

5.2.5	Analysis of palmitoylated post-synaptic proteins in Zdhhc9 KO brain.	185
5.2.6	Proteomic analysis of changes in palmitoylated proteins in Zdhhc9 KO mouse brain	194
5.2.7	Validation of proteomics with immunoblotting	206
5.3	DISCUSSION	211
CHAPTER 6.....		217
6	Metabolomic investigation of the effect of Zdhhc9 KO.....	217
6.1	INTRODUCTION	217
6.2	RESULTS	218
6.2.1	Metabolomics	218
6.2.2	Integrated pathway analysis	220
6.3	DISCUSSION	222
CHAPTER 7.....		231
7	General Discussion	231
CHAPTER 8.....		238
8	References	238
Appendix I.....		274
Appendix II.....		275
Appendix III.....		276

List of Figures

Figure 1.1 Protein alignment between human (top sequence) and mouse (bottom sequence) zDHHC9 using Emboss Water	8
Figure 1.2 Subcellular distribution of zDHHC9 and GCP16 in HEK-293 cells	10
Figure 1.3 The Ras palmitoylation cycle.....	13
Figure 1.4 Schematic representation of the various classes of proteins that are palmitoylated.	15
Figure 2.1 Map of the Morris water maze, the submerged platform (white circle) and the various release points.....	45
Figure 2.2 Illustration of the sPAL task.	50
Figure 3.1 Average ratios of numbers of Zdhhc9 KO versus WT male animals weaned and HET versus WT female animals weaned	80
Figure 3.2 Agarose gel electrophoresis of end-point PCR products from WT and KO brain cDNA samples	81
Figure 3.3 Comparison of the average ΔC_t values of WT and KO mouse brain samples (n=3 WT, 3 KO) for MA2 and z9v1 after normalisation against TBP and HPRT1	83
Figure 3.4 Expression fold change (EFC) for MA2 and z9v1 target genes after normalisation against reference genes TBP and HPRT1.....	84
Figure 3.5 Agarose gel electrophoresis of end-point PCR products from WT and KO mouse brain cDNA samples	87
Figure 3.6 Nucleotide alignment between the Zdhhc9 transcript 1 (top sequence) and the transcript isolated from the KO mouse brain (bottom sequence) using EMBOSS Water	89
Figure 3.7 Expression of full-length and truncated zDHHC9 in HEK293T cells.....	90
Figure 3.8 Localisation of full-length and mutant zDHHC9 in HEK293T cells.	91
Figure 3.9 Confirmation of the KO of zDHHC9 expression in protein level.....	93
Figure 4.1 Weight of male Zdhhc9 KO and WT animals before conducting the SHIRPA task (n=18 KO, 24 WT).....	102

Figure 4.2 Comparison of wild- type and Zdhhc9 KO mice in the Hanging Wire test	103
Figure 4.3 Comparison of wild- type and Zdhhc9 KO mice on a rotarod.....	104
Figure 4.4 Effect of age on the hanging wire task.	105
Figure 4.5 Effect of age on rotarod performance	106
Figure 4.6 Distance moved in open field test for Zdhhc9 KO and WT mice	108
Figure 4.7 Thygmotactic behaviour and velocity of Zdhhc9 KO and WT mice during the habituation period of open field test.	110
Figure 4.8 Thygmotactic behaviour and velocity of Zdhhc9 KO and WT mice during the test period of open field test	112
Figure 4.9 Performance of Zdhhc9 KO and WT mice in the elevated plus maze	113
Figure 4.10 Startle reactivity of Zdhhc9 KO and WT mice.	114
Figure 4.11 Analysis of pre-pulse inhibition of Zdhhc9 KO and WT mice.....	115
Figure 4.12 Performance of Zdhhc9 KO and WT mice in the Morris water maze...	117
Figure 4.13 Performance of Zdhhc9 KO and WT mice in the probe trial of Morris water maze.....	118
Figure 4.14 Comparison of Zdhhc9 KO and wild- type mice in the visual cue trial of the Morris Water Maze.....	119
Figure 4.15 Performance of Zdhhc9 KO and WT mice in Morris water maze and reversal learning test	121
Figure 4.16 Performance of Zdhhc9 KO and WT mice in the probe trial of Morris water maze.....	122
Figure 4.17 Comparison of Zdhhc9 KO and wild- type mice in the visual cue trial of the Morris Water Maze.....	123
Figure 4.18 Performance of Zdhhc9 KO and WT mice in the probe trial of Morris water maze after reversal learning.....	124
Figure 4.19 Comparison of Zdhhc9 KO and wild- type mice in the visual cue trial of Morris water maze after reversal learning	125
Figure 4.20 Performance of Zdhhc9 KO and WT mice in Morris water maze	126

Figure 4.21 Performance of Zdhhc9 KO and WT mice in the probe trial of Morris water maze.....	128
Figure 4.22 Performance of Zdhhc9 KO and wild- type mice in the visual cue trial of Morris Water Maze	129
Figure 4.23 Performance of Zdhhc9 KO and WT mice during the working memory experiment of Morris water maze	130
Figure 4.24 Residence time of Zdhhc9 KO and wild- type mice in zones of the sociability and social novelty tests.....	131
Figure 4.25 Distance moved and mean velocities for Zdhhc9 KO and WT mice in the 3 chamber apparatus for sociability and social novelty	132
Figure 4.26 Preference of Zdhhc9 KO and wild- type mice for sucrose and water..	133
Figure 4.27 Performance of WT and Zdhhc9 KO mice in pairwise discrimination task and reversal learning.....	135
Figure 4.28 Performance of WT and Zdhhc9 KO mice in sPAL task.....	138
Figure 4.29 Performance of WT and Zdhhc9 KO mice in the test period of the Five Choice Serial Reaction Time Task.....	139
Figure 4.30 Performance of WT and Zdhhc9 KO mice in the final segment of the Five Choice Serial Reaction Time Task.....	141
Figure 4.31 Number of premature responses (A) and beam breaks (B) of WT and Zdhhc9 KO mice in the final segment of the Five Choice Serial Reaction Time Task	143
Figure 4.32 Coronal images from WT (A) and KO (B) mouse brains after ex vivo MRI scan in a 9.4 Tesla magnet	145
Figure 4.33 Transverse plane images from WT (A) and KO (B) mouse brains after ex vivo MRI scan in a 9.4 Tesla magnet	146
Figure 4.34 Sagittal images from WT (A) and KO (B) mouse brains after ex vivo MRI scan in a 9.4 Tesla magnet	147
Figure 4.35 3D reconstruction of a WT (A) and KO (B) mouse brain using Amira 6.01 software after ex vivo MRI scan.....	149
Figure 4.36 Box and whiskers graphs showing the various data points for the volume of corpus callosum and hippocampus made using GraphPad Prism7.....	151

Figure 5.1 Quantification of H-Ras protein level in brain homogenates	166
Figure 5.2 Quantification of N-Ras protein level in brain homogenates	167
Figure 5.3 Quantification of H-Ras protein level in membrane fractions from brain homogenates	168
Figure 5.4 Quantification of N-Ras protein level in membrane fractions from brain homogenates	169
Figure 5.5 Quantification of H-Ras palmitoylation in whole brain and hippocampi of WT and Zdhhc9 KO mice	170
Figure 5.6 Western blots of β -actin as a negative control for Acyl-RAC in whole brain and hippocampi of WT and Zdhhc9 KO mice	171
Figure 5.7 Quantification of Csp protein level in brain homogenates.....	172
Figure 5.8 Quantification of Csp palmitoylation in whole brain and hippocampi of WT and Zdhhc9 KO mice	173
Figure 5.9 Quantification of Snap25 protein level in brain homogenates	174
Figure 5.10 Quantification of Snap25 palmitoylation in whole brain and hippocampi of WT and Zdhhc9 KO mice	175
Figure 5.11 Quantification of VAMP1/2 protein level in brain homogenates.....	176
Figure 5.12 Quantification of VAMP1/2 palmitoylation in whole brain and hippocampi of WT and Zdhhc9 KO mice.....	177
Figure 5.13 Quantification of VAMP2 protein level in brain homogenates	178
Figure 5.14 Quantification of VAMP2 palmitoylation in whole brain of WT and Zdhhc9 KO mice	179
Figure 5.15 Quantification of VAMP3 protein level in brain homogenates	180
Figure 5.16 Quantification of Synaptotagmin 1 protein level in brain homogenates	181
Figure 5.17 Quantification of Synaptotagmin 1 palmitoylation in whole brain and hippocampi of WT and Zdhhc9 KO mice.....	182
Figure 5.18 Quantification of VGLUT1 and VGLUT2 protein level in brain homogenates	183

Figure 5.19 Quantification of VGLUT1 palmitoylation in whole brain of WT and Zdhhc9 KO mice	184
Figure 5.20 Quantification of VGLUT2 palmitoylation in whole brain and hippocampi of WT and Zdhhc9 KO mice	185
Figure 5.21 Quantification of GluR1 protein level in brain homogenates.....	186
Figure 5.22 Quantification of phospho-GluR1 (Ser845) protein level in brain homogenates	187
Figure 5.23 Quantification of GluR1 palmitoylation in whole brain and hippocampi of WT and Zdhhc9 KO mice	188
Figure 5.24 Quantification of GluR2 protein level in brain homogenates.....	189
Figure 5.25 Quantification of GluR2 palmitoylation in whole brain of WT and Zdhhc9 KO mice	190
Figure 5.26 Quantification of PSD95 protein level in brain homogenates	191
Figure 5.27 Quantification of PSD95 palmitoylation in whole brain and hippocampi of WT and Zdhhc9 KO mice	192
Figure 5.28 Quantification of NR2b protein level in brain homogenates.....	193
Figure 5.29 Quantification of NR2b palmitoylation in whole brain of WT and Zdhhc9 KO mice	194
Figure 5.30 CCR5 expression in Acyl-RAC fractions and brain homogenates from WT and Zdhhc9 KO mice.	207
Figure 5.31 Pde10a expression in Acyl-RAC fractions and brain homogenates from WT and Zdhhc9 KO mice	208
Figure 5.32 Synaptophysin expression in Acyl-RAC fractions from WT and Zdhhc9 KO mice.....	209
Figure 5.33 Calnexin expression in Acyl-RAC fractions and brain homogenates from WT and Zdhhc9 KO mice	210
Figure 5.34 Flotillin 2 expression in Acyl-RAC fractions and brain homogenates from WT and Zdhhc9 KO mice	211
Figure 6.1 The pathway of tryptophan metabolism from KEGG pathway website.	223

Figure 6.2 The pathway of phenylalanine, tyrosine and tryptophan biosynthesis from KEGG pathway website 226

Figure 6.3 The pathway of taurine and hypotaurine metabolism from KEGG pathway website..... 229

List of Tables

Table 1.1 Links of zDHHC enzymes to disease	21
Table 1.2 Key features of zDHHC9	27
Table 2.1 List of behaviours that were scored for each animal.....	41
Table 2.2 DNA sequences for all the primers used in this study (shown in 5' to 3' orientation)	58
Table 2.3 Primary and secondary antibodies used in this study for Western blotting or immunofluorescence	67
Table 3.1 Difference in expression of <i>Zdhhc9</i> between KO and WT mouse brain normalised against two reference genes.....	86
Table 4.1 List of behaviours that were scored for each animal while the animal was in the arena for a 5 minute period or restrained.....	100
Table 5.1 Proteins with reduced palmitoylation in <i>Zdhhc9</i> KO mouse brain.	195
Table 6.1 Pathways that are potentially dysregulated in <i>Zdhhc9</i> KO mice based on metabolomic data analysis using MetaboAnalyst.	218
Table 6.2 Pathways that are dysregulated in <i>Zdhhc9</i> KO mice based on integrated metabolomic and transcriptomic data analysis using MetaboAnalyst.....	221

List of Abbreviations

5CSRTT	Five Choice Serial Reaction Time Test
5-HIAA	5-Hydroxyindoleacetic acid
aa	Amino acids
ABE	Acyl-biotinyl exchange
Acyl-RAC	Acyl resin-assisted capture
ADHD	Attention Deficit Hyperactivity Disorder
Akr1p	Ankyrin-repeat containing protein 1
AMPA	α -amino-3-hydroxyl- 5 methyl-4-isoxazole-propionate
ANOVA	Analysis of variance
AP	Alkaline phosphatase
APS	Ammonium persulfate
APT	Acyl protein thioesterase
ARID1B	AT-Rich Interaction Domain 1B
ASD	Autism Spectrum Disorders
BCA	Bicinchoninic acid
BDNF	Brain derived neurotrophic factor
BH	Bound HA treated fraction
BK	Big Potassium
BSA	Bovine serum albumin
BT	Bound Tris treated fraction
CCR5	C-C chemokine receptor type 5
CREB	Cyclic-AMP response element binding protein
C-RP	C-reactive protein
Csp	Cysteine string protein
Ct	Cycle threshold
DCR-1	Down syndrome Critical Region 1
dH2O	Distilled H2O
DMEM	Dulbecco's Modified Eagle Medium
DS	Down Syndrome
DTT	Dithiothreitol
E	East
EEF1A2	Eukaryotic elongation factor 1, alpha-2
EEG	Electroencephalogram
EFC	Expression fold change
EPM	Elevated plus maze
ER	Endoplasmic reticulum
Erf2	Effect on Ras Function 2
FBS	Foetal bovine serum
FKBP	FK506 Binding Protein
FLASH MRI	Fast low angle shot magnetic resonance imaging
FMRP	Fragile X Mental Retardation Protein
FXS	Fragile X syndrome
GABA	γ -aminobutyric acid

Gad1	Glutamate Decarboxylase 1
GCP170	Golgi Complex-Associated Protein of 170 KDa
GDI1	GDP Dissociation Inhibitor 1
GOLGA7	Golgi Autoantigen Golgin subfamily a7
GRIP1b	Glutamate receptor interacting protein 1
HD	Huntington's disease
HEK293T	Human Embryonic Kidney 293 cells that express a mutant of the SV40 large T antigen
HET	Heterozygous
HMGB1	High mobility group box-1
HPRT1	Hypoxanthine guanine phosphoribosyl transferase
HSA21	Human chromosome 21
HTT	Huntingtin protein
ID	Intellectual disability
IL1RA	Interleukin 1 receptor antagonist
IL1RAPL1	IL-1 receptor accessory protein-like 1
IL1 β	Interleukin 1 beta
IL6	Interleukin 6
KO	Knock- out
LB	Lysogeny broth
LC-MS/MS	Liquid Chromatography– Mass Spectrometry/Mass Spectrometry
LIMK1	LIM kinase 1
LJS	Lujan-Fryns syndrome
LTP	Long-Term Potentiation
MA1	mRNA Confirmation assay 1
MA2	mRNA Confirmation assay 2
MeCP2	Methyl-CpG binding protein 2
MED12	Mediator Complex Subunit 12
MEF	Mouse embryonic fibroblasts
MKP	Mitogen-activated protein kinase phosphatase
MMRRC	Mutant Mouse Regional Resource Centers
MMTS	S-methyl methanethiosulfonate
MMU16	Mouse chromosome 16
MRI	Magnetic resonance imaging
MS	Mass Spectrometry
MWM	Morris water maze
N	North
NCS-1	Neuronal calcium sensor-1
NE	Northeast
Neo	Neomycin
NMDA	N-methyl-D-aspartate
nNOS	Neuronal nitric oxide synthase
NW	Northwest
OFT	Open field test
OPHN1	Oligophrenin 1
ORA	Over-representation analysis

PAGE	Polyacrylamide gel electrophoresis
PAT	Protein acyl- transferases
PBS	Phosphate-buffered saline
PCR	Polymerase chain reaction
Pde10a	cAMP and cAMP-inhibited cGMP 3,5-cyclic phosphodiesterase 10A
PKU	Phenylketonuria
PM	Plasma membrane
PPF	Paired pulse facilitation
PPI	Pre-pulse inhibition
PPIA	Peptidylprolyl isomerase A
PPT1	Palmitoyl-protein thioesterase 1
PSD95	Post-synaptic density protein-95
PTP	Protein tyrosine phosphatase
qPCR	Quantitative polymerase chain reaction
RT	Room temperature
RTT	Rett syndrome
S	South
SAA	Serum amyloid A
SDS	Sodium dodecyl sulphate
SE	Southeast
SEM	Standard error of the mean
SH	Sulfhydryl
SHIRPA	SmithKline Beecham, Harwell, Imperial College, Royal London Hospital, Phenotype Assessment
SILAM	Stable Isotope Labeling in Mammals
Snap25	Synaptosomal-associated protein of 25kDa
SNARE	Soluble NSF Attachment Protein Receptor
SNR	Signal to noise ratio
sPAL	Same paired associate learning
SST+	Somatostatin positive
STP	Short-term synaptic plasticity
STREX	Stress-regulated exon
STXBP1	Syntaxin-binding protein 1
SW	Southwest
TBP	TATA box binding protein
TEMED	N,N,N',N'-tetramethyl-ethane-1,2-diamine
TI	Total input
TLR	Toll-like receptor
TMD	Transmembrane domain
Tph2	Tryptophan hydroxylase 2
TRN	Thalamic reticular nucleus
TUBB3	Tubulin Beta 3 Class III
UDG	Uracil-DNA Glycosylase
UH	Unbound HA treated fraction
UP	Ultra-pure
UT	Unbound Tris treated fraction

VAMP	Vesicle-associated membrane protein
VGLUTs	Vesicular glutamate transporters
W	West
WT	Wild type
XLID	X-linked intellectual disability
ZDHHC9	Zinc Finger DHHC domain-containing protein 9

Abstract

Protein palmitoylation (also known as S-acylation) is a widespread post-translational modification that regulates the trafficking and function of a diverse array of proteins. This modification is catalysed by a family of twenty-three zDHHC enzymes that exhibit both specific and overlapping substrate interactions. Mutations in the gene encoding zDHHC9 cause mild-to-moderate intellectual disability, seizures, speech and language impairment, hypoplasia of the corpus callosum and reduced volume of sub-cortical structures. In this thesis, behavioural phenotyping, magnetic resonance imaging (MRI), isolation of S-acylated proteins and metabolomics were conducted to investigate the effect of knock-out (KO) of the *Zdhhc9* gene in mice in a C57BL/6 genetic background. As a first step, end-point and quantitative Polymerase Chain reaction (PCR) were used to confirm KO of *Zdhhc9* expression. Interestingly, although the mutant mice had ablated expression of mRNA encoding full-length zDHHC9, the mice did express reduced levels of a shorter *Zdhhc9* transcript. However, immunoblotting analysis suggested that this shorter mRNA fragment did not lead to expression of a stable truncated form of zDHHC9 and further confirmed loss of zDHHC9 expression. Thus, the mouse line appears to be a true knock-out. The *Zdhhc9* KO male mice exhibit a range of abnormalities compared with their wild-type littermates: altered behaviour in the open-field test, elevated plus maze and acoustic startle test that is consistent with a reduced anxiety level; a reduced hang time in the hanging wire test that suggests underlying hypotonia but which may also be linked to reduced anxiety; deficits in the Morris water maze test of hippocampal-dependent spatial learning and memory; and a 36% reduction in corpus callosum volume revealed by MRI. Surprisingly, palmitoylation of several important pre- and post-synaptic proteins was not disrupted in either whole brain or hippocampus of *Zdhhc9* KO mice, including H-Ras which has previously been proposed to be a key substrate of zDHHC9. This suggests that other unidentified substrates of zDHHC9 are linked to the observed changes.

Metabolomic profiling identified the pathways of tryptophan metabolism and of phenylalanine, tyrosine and tryptophan biosynthesis as significantly dysregulated in *Zdhhc9* KO mice. Overall, this study highlights a key role for zDHHC9 in brain development and behaviour and supports the utility of the *Zdhhc9* KO mouse line to investigate molecular and cellular changes linked to intellectual disability and other deficits in the human population.

CHAPTER 1

1 General introduction

1.1 Protein palmitoylation

Cellular proteins can be covalently modified with lipids, such as fatty acids, isoprenoids and cholesterol. These lipid modifications are important in regulating protein localization and function and are broadly categorized in two groups based on the location that they take place (Nadolski and Linder, 2007). The first category includes modifications that take place in the cytoplasm or on the cytoplasmic surface of membranes while the second category includes modifications that take place in the lumen of the secretory pathway (Nadolski and Linder, 2007). Proteins that are lipidated in the secretory pathway include the secreted proteins Wnt, Hedgehog and Ghrelin (Resh, 2016). However, the vast majority of lipidation takes place in the cytoplasm of cells.

Among the most common lipid modifications that take place in the cytoplasm of cells are N-myristoylation, S-acylation and prenylation. N-myristoylation is the attachment of myristic acid onto an N-terminal glycine following cleavage of the initiating methionine residue, with the typical consensus sequence MGXXS/T (M, methionine; G, glycine; X, any amino acid; S, serine; T, threonine). Prenylation, on the other hand, typically involves modification of the C-terminal end of a protein, in which farnesyl or geranylgeranyl groups are added to the cysteine residue of a CAAX motif (C, cysteine; A, any aliphatic amino acid; X any amino acid) (Resh, 2006). S-acylation is the covalent addition of palmitate and other long-chain fatty acids by thioester linkages to proteins at cysteine residues present in a variety of sequence contexts (Chamberlain and Shipston, 2015). Apart from palmitate, the addition of stearate, oleate and arachidonate to S-acylated proteins has been described (El-Husseini and Brecht, 2002). Because the lipid palmitate is

most often found at these sites of S-acylation, this modification is also commonly referred to as palmitoylation.

Palmitoylation was first reported to occur on a glycoprotein from vesicular stomatitis virus and subsequently on mammalian proteins in cultured cells (Schmidt and Schlesinger, 1979; Schlesinger et al., 1980). In the following years, many other mammalian proteins were reported to undergo this modification including heterotrimeric and monomeric G proteins, G protein-coupled receptors and other signalling proteins (Milligan et al., 1995). In recent years, there have been several proteomic studies that have profiled the palmitoylated proteins in many eukaryotic cells from yeast to neurons. These analyses have highlighted the broad diversity of proteins that undergo palmitoylation, with reports that 10% of the proteome can be modified in this way (Blanc et al., 2015). In contrast to N-myristoylation and prenylation, palmitoylation was shown to be reversible on some proteins, such as the monomeric G proteins, H-Ras and N-Ras. Specifically, pulse-chase experiments using ^3H palmitic acid estimated the half-life of palmitoylation of H-Ras and N-Ras to be 90 and 20 minutes, respectively (Magee et al., 1987). In addition, many other signalling and structural proteins also display dynamic palmitoylation cycles and proteins can undergo several rounds of palmitoylation and depalmitoylation during their lifetime, either in a constitutive manner or in response to specific signals (El-Husseini et al., 2002).

Palmitoylation is known to occur on a wide variety of proteins and, in contrast to N-myristoylation and prenylation, does not need a specific sequence other than the presence of a cysteine residue. Proteins that undergo palmitoylation can be categorized in two main groups: proteins that are synthesized on free ribosomes and associate peripherally with membranes and integral membrane proteins that contain transmembrane domains (TMDs) (Nadolski and Linder, 2007). The key factor determining the palmitoylation of cysteine residues in transmembrane proteins appears to be the close positioning of cysteines to the membrane interface. Indeed, recent work suggested that palmitoylation of cysteine residues in

transmembrane proteins is stochastic and determined by the accessibility of cysteines to membrane-bound palmitoylation enzymes (Rodenburg et al., 2017). A similar principle appears to apply for soluble proteins, which are frequently palmitoylated at sites adjacent to N-myristoylated or prenylated residues (Chamberlain and Shipston, 2015).

The most commonly described function of palmitoylation is to increase the affinity of a soluble protein for membranes, which can thereby affect the protein's localization and function. For example, palmitoylation of H- and N- Ras is essential to mediate stable membrane binding to endoplasmic reticulum and Golgi membranes and allow transport to the plasma membrane, whereas palmitoylation of the post-synaptic scaffold PSD95 in neurons is essential for association with transport vesicles that target the protein to synapses (Hancock et al., 1989; Apolloni et al., 2000; El-Husseini et al., 2002). Although integral membrane proteins are stably associated with membranes, palmitoylation can also regulate membrane attachment of cytosolic domains of such proteins, affecting localization and function. For example, palmitoylation of G protein-coupled receptors has been shown to affect trafficking to the plasma membrane, internalization and/or interaction with effector proteins (Chamberlain and Shipston, 2015).

Palmitoylation can also regulate the membrane micro- localisation of modified proteins and is often proposed to target proteins to cholesterol-rich "raft" domains. For example, the extent of palmitoylation of SNAP25 is proposed to modulate association of this membrane fusion protein with rafts and in so- doing regulate exocytosis in neuroendocrine cells (Salaun et al., 2004). Another effect of palmitoylation is on protein stability and blocking palmitoylation often leads to increased ubiquitination and subsequent degradation (Valdez-Taubas and Pelham, 2005).

1.2 Enzymes regulating palmitoylation

The enzymes that regulate palmitoylation reactions are Protein Acyl-Transferases (PATs), which are responsible for catalyzing the addition of fatty acids to intracellular proteins, and Acyl Protein Thioesterases (APTs), which mediate deacylation reactions (Kang et al., 2008; Fukata & Fukata, 2010). Thioesterases were identified prior to the identification of PATs. APT1 and APT2 mediate depalmitoylation reactions in the cytoplasm, whereas Protein Palmitoyl Thioesterase 1 (PPT1) is localized to lysosomes and is thought to function in the depalmitoylation of proteins during their degradation (Camp et al., 1994; Duncan and Gilman, 1998).

PAT enzymes were identified initially in the yeast *Saccharomyces cerevisiae*. These enzymes, Erf2 (Effect on Ras Function 2) and Akr1p (ankyrin-repeat containing protein 1), were shown to mediate palmitoylation of yeast Ras and casein kinase proteins respectively (Lobo et al., 2002; Roth et al., 2002). Comparison of the amino acid sequences of these PAT enzymes revealed the presence of a shared 51 amino acid zinc finger DHHC (aspartate-histidine-histidine-cysteine)-cysteine-rich domain. This domain is critical for PAT activity of both enzymes and was used to search for similar PAT enzymes in mammalian cells. Subsequently, a family of 23 “zDHHC” enzymes was cloned from mammalian cells and some of these were shown to exhibit both PAT activity and substrate specificity (Fukata et al., 2004). All zDHHC enzymes are predicted to be polytopic membrane proteins and over-expression analyses have shown their association with different intracellular compartments but mainly the endoplasmic reticulum and Golgi (Ohno et al., 2006).

Palmitoylation mediated by zDHHC enzymes has been shown to follow a two-step process, where the enzyme undergoes “autopalmitoylation” followed by acyl chain transfer to the substrate protein (Mitchell et al., 2010; Jennings and Linder, 2012). Recent structural insight into zDHHC20 and zDHHC15 revealed the presence of a “pocket” between the transmembrane domains of these enzymes that

accommodates the acyl-CoA substrate and affects enzyme fatty acid selectivity (Greaves et al., 2017; Rana et al., 2018).

1.3 ZDHHC9 (Zinc Finger DHHC domain-containing protein 9)

1.3.1 The *ZDHHC9* gene and its transcripts

The *ZDHHC9* gene encodes the main part of a heterodimer that acts as a PAT enzyme (Swarthout et al., 2005). The gene is located on the long arm of the X chromosome in humans, and more specifically at the q26.1 chromosomal region.

The *ZDHHC9* gene consists of 10 exons in human and mouse. The first exon is untranslated as the ATG initiating codon is located on exon 2 and the stop codon is located at the beginning of exon 10. In both human and mouse there are 6 mRNA transcripts but only two of these encode for a protein. Mouse transcript 1 has a length of 2982 bp while transcript 2 is 2815 bp long (<http://www.ensembl.org>). Northern blot analysis identified a 2.3 kb *ZDHHC9* transcript in human tissues, which was highly expressed in brain, kidney, skeletal muscle, lung and liver. However, the tissue distribution of the endogenous protein has not been reported to-date (Swarthout et al., 2005).

1.3.2 *ZDHHC9* transcript expression in brain

According to a published atlas of the adult human brain transcriptome, *ZDHHC9* is highly expressed at the globus pallidus, ventral thalamus and white matter (mainly in corpus callosum) while it shows a low expression level at the cerebral cortex (Hawrylycz et al., 2012). In the developing human brain, *ZDHHC9* expression is regionally and temporally regulated (<http://brainspan.org/>). During the prenatal period *ZDHHC9* is expressed at low levels throughout the brain. In thalamus, it reaches its peak during the antenatal period while in striatum peak expression occurs during adulthood.

Based on Allen brain atlas for adult mouse brain, *Zdhhc9* is expressed mainly in the corpus callosum, piriform area, hippocampus (CA1 and CA3 pyramidal layers as well as the granule cell layer of the dentate gyrus). It is also expressed throughout the cerebellum.

1.3.3 Transcriptional regulation of *ZDHHC9*

A recent study reported that zDHHC9 expression is regulated by a micro RNA, miR-134. Although miR-134 has been proposed to affect all types of neurons, the study showed that functionally active miR-134 is produced in only a selected population of neurons, the cortical interneurons (Chai et al., 2013). It is known that synaptic activity stimulates miR-134 expression, which then regulates dendrite growth, spine formation and synaptic plasticity (Schratt et al., 2006; Gao et al., 2010). miR-134 interacted directly with the zDHHC9 mRNA in somatostatin positive (SST+) neurons and the zDHHC9 mRNA was down-regulated by neuronal activity through its interaction with miR-134 (Chai et al., 2013). The reduced expression of zDHHC9 had an effect on H- Ras localization which is a signalling molecule crucial for neuronal development and function and which was previously suggested to be palmitoylated by zDHHC9 (Swarthout et al., 2005).

Although some actions of miR-134 might be localized to the soma of the neuron, downstream effects could also impact synaptic regions *via* effects of zDHHC9 on synaptic targeting of H-Ras and other substrates of this enzyme. The involvement of the miR-134/zDHHC9/H-Ras pathway on dendritic growth could influence spine formation. Finally, the modulation of protein palmitoyltransferases by activity-regulated microRNAs could be a way of influencing synaptic function particularly in mature neurons. This has been the case for another microRNA, miR-138 that was shown to regulate expression of depalmitoylation enzyme APT1 in quiescent neurons, activating $G\alpha_{13}$ in synapses and causing spine shrinkage (Banerjee et al., 2009; Siegel et al., 2009). However, it is worth noting that miR-138

expression is repressed by neuronal activity in contrast to miR-134 (Banerjee et al., 2009; Siegel et al., 2009).

1.3.4 zDHHC9 structure and function

zDHHC9 is an integral membrane protein of 364 amino acids (aa) with a mass of 40,940 Da. It contains four predicted transmembrane regions, a proline-rich domain and a zinc-finger DHHC (aspartic acid–histidine–histidine–cysteine) cysteine-rich domain in the cytoplasmic loop (131–182 aa). A zinc finger is a structural motif of proteins, characterized by the coordination of zinc ions that help the stabilisation of the fold (Klug and Rhodes, 1987). The active site of the enzyme is believed to be centred at the conserved cysteine 169 of the DHHC motif as no enzymatic activity is observed when this residue is substituted by a serine (Swarthout et al., 2005).

Palmitoylation mediated by zDHHC9 occurs in two steps. During the first step, autopalmitoylation takes place and an enzyme–palmitoyl intermediate is formed. During the second step, the palmitoyl moiety is transferred to a protein substrate or if no substrate exists, hydrolysis of the thioester linkage produces the enzyme and free palmitate (Mitchell et al., 2014). The identified potential substrates of zDHHC9 to-date include H- and N-Ras, BK channels and the β 2 adrenergic receptor (Swarthout et al., 2005; Tian et al., 2010; Adachi et al., 2016). The lack of available zDHHC9 antibodies has prevented analysis of endogenous zDHHC9 localisation but epitope-tagged protein is localized at the endoplasmic reticulum (ER) and Golgi in mammalian cell lines (Swarthout et al., 2005) and the cell body and neurites in hippocampal neurons (Levy et al., 2011). In yeast, the homologue of zDHHC9, Erf2, requires association with a co-factor, Erf4 for PAT activity (Lobo et al., 2002) and initial work with zDHHC9 demonstrated that the protein alone could not act as a PAT, prompting a search for a human homologue of

yeast Erf4. This search led to the identification of GCP16 as a key protein required for zDHC9 function (Swarthout et al., 2005).

1.3.5 Protein alignment between human and mouse zDHC9

Mouse and human zDHC9 proteins consists of 364aa, and the proteins share a 99.2% similarity and 98.4% identity based on emboss water online program analysis (https://www.ebi.ac.uk/Tools/psa/emboss_water/, Figure 1.1).

```

# Length: 364
# Identity:   358/364 (98.4%)
# Similarity: 361/364 (99.2%)
# Gaps:      0/364 ( 0.0%)
# Score: 1920.0
#
#
#-----
EMBOSS_001      1 MSVMVVRKKVTRKWEKLPGRNTFCCDGRVMMARQKGI FYLTLFLILGICT      50
|||||
EMBOSS_001      1 MSVMVVRKKVTRKWEKLPGRNTFCCDGRVMMARQKGI FYLTLFLILGICT      50

EMBOSS_001     51 LFFAFECRYLAVQLSPAIPVFAAMLFLFSMATLLRTSFSDPGVI PRALPD     100
|||||
EMBOSS_001     51 LFFAFECRYLAVQLSPAIPVFAAMLFLFSMATLLRTSFSDPGVI PRALPD     100

EMBOSS_001    101 EAAFIEMEIEATNGAVPQGQRPPRIKNFQINNQIVKLYCYTCKIFRPP     150
|||||
EMBOSS_001    101 EAAFIEMEIEATNGAVPQGQRPPRIKNFQINNQIVKLYCYTCKIFRPP     150

EMBOSS_001    151 RASHCSICDNCVERFDHHC PWVGN CVGKRNYRYFYLFILSLSLLTIYVFA     200
|||||
EMBOSS_001    151 RASHCSICDNCVERFDHHC PWVGN CVGKRNYRYFYLFILSLSLLTIYVFA     200

EMBOSS_001    201 FNIVYVALKSLKIGFLEILKETPGTVLEV L ICFFTLWSVVGLIGFHTFLV     250
|||||
EMBOSS_001    201 FNIVYVALKSLKIGFLEILKETPGTVLEV L ICFFTLWSVVGLIGFHTFLV     250

EMBOSS_001    251 ALNQT TNEDIKGSWIGKNRVQNPYSHGNIVKNCCEVL CGPLPPSVLDRRG     300
|||||
EMBOSS_001    251 ALNQT TNEDIKGSWIGKNRVQNPYSHGNIVKNCCEVL CGPLPPSVLDRRG     300

EMBOSS_001    301 ILPLEESGSRPPSTQETSSSLLPQSPAPTEHLNSNEMPEDSSSTPEEMPPP     350
|||||
EMBOSS_001    301 ILPLEESGSRPPSTQETSSSLLPQSPASTE H MNSNEMAEDTSIPEEMPPP     350

EMBOSS_001    351 EPPEPPQEAAEAEK      364
|||||:||||
EMBOSS_001    351 EPPEPPQEASEAEK      364

```

Figure 1.1 Protein alignment between human (top sequence) and mouse (bottom sequence) zDHC9 using Emboss Water. The only amino acid differences are located in the cytosolic C-terminus of the protein.

1.4 GCP16 (Golgi Complex-Associated Protein of 16kDa)

By searching mammalian genomic databases for orthologues of *Schizosaccharomyces pombe Erf4*, researchers identified *GCP16*, also known as *GOLGA7 (Golgi Autoantigen Golgin subfamily a7)* (Swarthout et al., 2005). Northern blot analysis detected a 1.9-kb transcript in all human tissues examined except colon and thymus. *GCP16* is located on the short arm of chromosome 8 in humans, and more specifically on the p11.21 chromosomal region. *GCP16* has 137 amino acids and a molecular mass of 16 kDa. A similarity search revealed *GCP16* homologues in mouse, nematode, and fly, but not in yeast (*S.cerevisiae*) and plants (Ohta et al., 2003).

GCP16 was first identified in a yeast 2-hybrid screen searching for novel interactions with the N-terminal domain of *GCP170 (Golgi Complex-Associated Protein of 170 kDa)* (Ohta et al., 2003). *GCP16* is co-localized with *GCP170* and giantin at the Golgi and overexpression of *GCP16* in COS-1 cells inhibited protein transport from the Golgi to the cell surface (Ohta et al., 2003), implying a role for *GCP16* in secretory pathway function.

Labelling experiments with [³H] palmitic acid and mutational analysis demonstrated that *GCP16* is palmitoylated at Cys69 and Cys72 (Ohta et al., 2003). Mutant proteins lacking one or the other palmitoylation site retained Golgi membrane targeting, but a mutant lacking both sites dispersed to the cytoplasm, indicating that palmitoylation anchors *GCP16* to Golgi membranes (Ohta et al., 2003). In conclusion, *GCP16* is a palmitoylated membrane protein that is possibly involved in vesicular transport from the Golgi to the cell surface (Ohta et al., 2003).

1.5 zDHH9-GCP16 complex

Epitope-tagged *GCP16* colocalizes with zDHH9 (Figure 1.2) and the two proteins coimmunoprecipitated from transfected HEK293 cells (Swarthout et al.,

2005). zDHHC9 and GCP16 were also purified as a stoichiometric complex from insect cells infected with recombinant zDHHC9 and GCP16 baculoviruses (Swarthout et al., 2005). The purified zDHHC9/GCP16 complex displayed PAT activity towards both H-Ras and N-Ras in vitro. Similar to the Erf2–Erf4 complex, zDHHC9 required GCP16 to function as the PAT for H-Ras and was inactive in the absence of GCP16, thus showing that zDHHC9 and GCP16 are functional orthologues of Erf2 and Erf4 (Lobo et al., 2002; Swarthout et al., 2005). Both the autopalmitylation of zDHHC9 and the palmitoylation of H-Ras and N-Ras depends upon the presence of GCP16 (Swarthout et al., 2005). The exact role that GCP16 plays in zDHHC9-mediated palmitoylation reactions is not presently clear but zDHHC9 requires GCP16 for its stability (Swarthout et al., 2005).

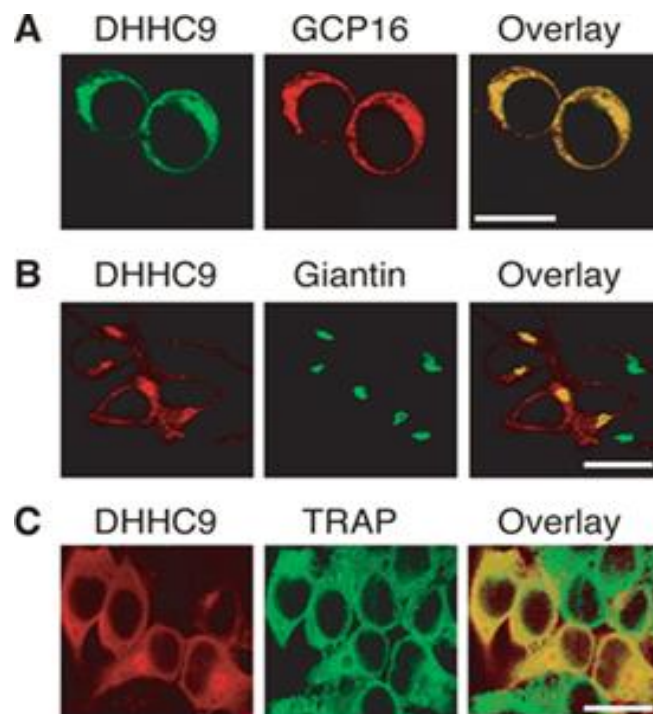


Figure 1.2 Subcellular distribution of zDHHC9 and GCP16 in HEK-293 cells (Swarthout et al., 2005). HEK-293 cells were transfected with zDHHC9-Myc-His and GFP-GCP16 cDNAs. A) GFP-GCP16 was visualized by epifluorescence, and zDHHC9-Myc-His was detected by indirect immunofluorescence using anti-Myc antibody. B) and C) to identify the cellular structures where zDHHC9 was localized, HEK-293 cells were transfected with zDHHC9-Myc-

His and FLAG-GCP16 cDNAs and processed for immunofluorescence with anti-Myc and anti-giantin or anti-TRAP- a antibodies. zDHHC9 codistributed with the Golgi marker giantin (B) and the ER marker TRAP-a (C). The cells were visualized by confocal microscopy.

1.6 A palmitoylation- depalmitoylation cycle regulates the subcellular trafficking of Ras family GTPases, substrates of zDHHC9

At present, only a small number of zDHHC9 substrates is known and among them are H-Ras and N-Ras (Apolloni et al., 2000; Swarthout et al., 2005; Chai et al., 2013). Ras is a protein family which is ubiquitously expressed in all cell lineages and organs. All Ras protein family members belong to a class of protein called small GTPases and their activity is regulated based on the presence of bound GTP or GDP. Ras proteins are involved in cellular signal transduction that regulates cell growth and differentiation and are activated by growth factors such as insulin and epidermal growth factor (Joneson & Bar-Sagi, 1997; Campbell et al., 1998).

Ras proteins must be localized to the inner surface of the plasma membrane (PM) to be biologically active (Willumsen et al., 1984). Ras polypeptides are synthesized on cytosolic ribosomes and undergo a complex series of post-translational modifications at their C- terminal CAAX motif: farnesylation of the cysteine, proteolytic removal of the AAX motif and carboxymethylation of the farnesylated cysteine (Casey et al., 1989; Gutierrez et al., 1989; Hancock et al., 1989). Farnesylation occurs in the cytoplasm, mediated by farnesyl transferase whereas proteolysis and carboxymethylation occur on the cytoplasmic face of the ER (Hancock et al., 1989; Resh, 2012). The farnesylated cysteine then operates with a second signal in the upstream hypervariable region to target Ras to the PM. This second signal in N-Ras and H-Ras is palmitoylation; H-Ras is palmitoylated at cysteines 181 and 184, whereas N-Ras is monopalmitoylated at Cys 181 (Hancock et al., 1989) early in the secretory pathway (at either the ER or Golgi), leading to Ras trafficking to the PM by vesicular transport.

In contrast to H- and N- Ras, K- Ras lacks palmitoylation sites and its second membrane attachment signal is a polybasic domain. This C- terminal lysine and arginine- rich region mediates the sorting of K- Ras out of the conventional exocytic pathway towards an undefined pathway to the cell surface that bypasses the Golgi (Apolloni et al., 2000). In contrast, H- and N- Ras are palmitoylated at the Golgi and traffic to the cell surface by the conventional secretory pathway (Apolloni et al., 2000).

Palmitoylation of Ras proteins is highly dynamic and palmitoylation turnover dictates the distribution of H- and N- Ras on the Golgi and at the PM. Work using semi-synthetic fluorescent Ras constructs microinjected into cells suggested that the half-life of palmitoylation was on the order of a few minutes and faster than that predicted by traditional ³H palmitate pulse-chase experiments (Magee et al., 1987; Rocks et al., 2005). Although these experiments examined localization of Ras as proxy for palmitoylation, they highlighted the importance of palmitoylation turnover in ensuring the correct distribution of the protein at Golgi and PM as a construct with a non-cleavable thioether linkage between the cysteine and acyl chain was mislocalised in cells (Rocks et al., 2005). Thus, a Ras cycle was proposed in which depalmitoylation releases Ras from membranes and subsequent palmitoylation resets its distribution at Golgi and PM (Figure 1.3).

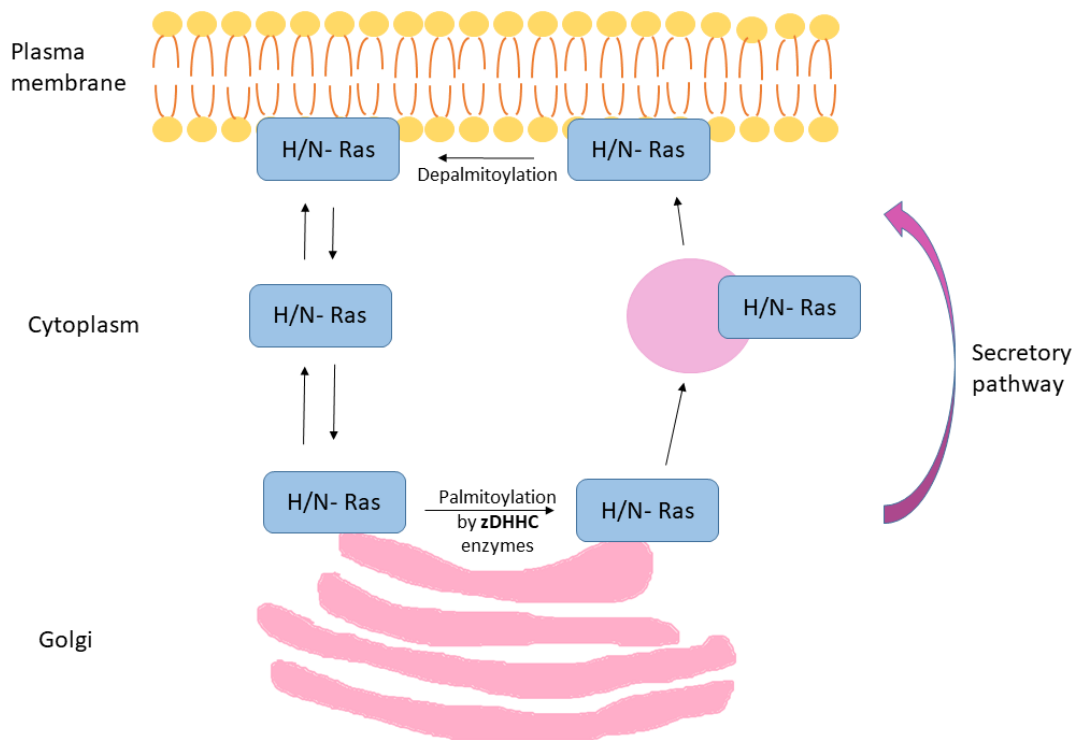


Figure 1.3 The Ras palmitoylation cycle. Schematic representation of the cycle where depalmitoylation releases farnesylated H-/N-Ras from the plasma membrane and facilitates their distribution to the Golgi where they can be palmitoylated by ZDHHC enzymes, leading to entry into budding vesicles that deliver H-/N-Ras back to the plasma membrane.

The removal of palmitate from PM-localized Ras is accelerated by binding of FKBP (FK506 Binding Protein) and can be catalyzed by APT1 (Lysophospholipase I) (Duncan and Gilman, 1998; Ahearn et al., 2011). Depalmitoylated Ras dissociates from the membrane and accumulates in the Golgi as a result of repalmitoylation. The degree of palmitoylation determines Ras temporal and spatial location, as the dually palmitoylated H- Ras accumulates to a greater extent at the PM than the monopalmitoylated N- Ras, which is more prominently distributed to the Golgi (Apolloni et al., 2000). It is important to note that Rocks et al. proposed that the palmitoylation of Ras proteins does not require specific recognition by any zDHHC enzyme, and indeed RNAi knockdown of zDHHC9 had no effect on the trafficking and localization of Ras constructs (Rocks et al., 2010).

1.7 Palmitoylation and nervous system function

Proteomic profiling has identified a large number of different classes of protein that are modified by palmitoylation (Figure 1.4). In particular, many regulators of neuronal excitability and function are known to be palmitoylated, such as the voltage-gated sodium channel (Schmidt & Catterall, 1987; Bosmans et al., 2011) and BK channels (Tian et al., 2008). Palmitoylation also controls cell surface expression and function of many ligand-gated ion channels, including α -amino-3-hydroxy-5-methyl-4-isoxazole-propionate (AMPA) receptors (Hayashi et al., 2005), *N*-methyl-D-aspartate (NMDA) receptors (Hayashi et al., 2009), Kainate receptors (Pickering et al., 1995), P2X7 receptors (Gonnord et al., 2009), and γ -aminobutyric acid (GABA) receptors (Keller et al., 2004; Rathenber et al., 2004; Fang et al., 2006). Furthermore, palmitoylation affects the function of voltage-gated calcium (Chien et al., 1996; Hurley et al., 2000; Chan et al., 2007) and potassium channels (Gubitosi-Klug et al., 2005; Jindal et al., 2008; Tian et al., 2008). Palmitoylation has a variety of effects on these different receptors, for example, regulating the trafficking of AMPA and NMDA glutamate receptors and the voltage dependence of Kv1.1 potassium channels (Gubitosi-Klug et al., 2005; Hayashi et al., 2005; Hayashi et al., 2009).

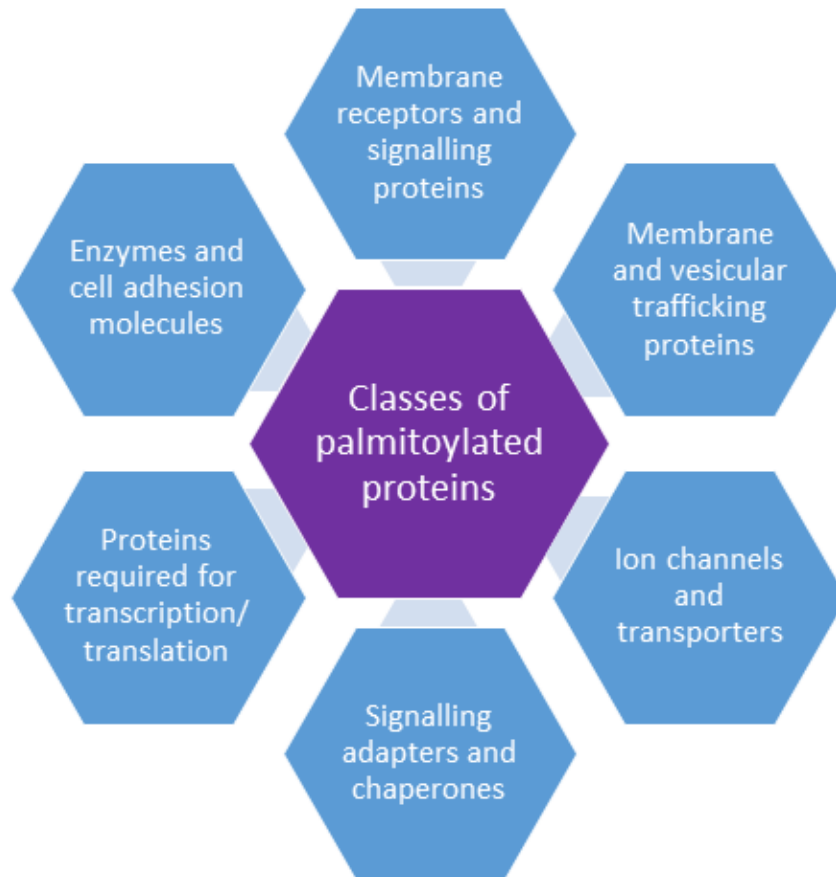


Figure 1.4 Schematic representation of the various classes of proteins that are palmitoylated.

Another important target of palmitoylation is PSD95, a key component of the postsynaptic scaffolding apparatus, which directly regulates NMDA receptor localization and indirectly affects AMPA receptor localization *via* interactions with stargazin (Noritake et al., 2009; Ho et al., 2011). Treatment of neurons with the non-specific palmitoylation inhibitor 2-bromopalmitate results in the dispersal of PSD95 and AMPA-type glutamate receptors from synaptic clusters and reduces the amplitude and frequency of AMPA-mediated miniature excitatory postsynaptic currents. Furthermore, glutamate-induced internalization of AMPA receptors requires palmitoylation of PSD95 and was enhanced with the overexpression of palmitoylated PSD95 (Noritake et al., 2009). The palmitoylation of PSD95 is dynamic and regulates synaptic targeting of PSD95, which in turn regulates synaptic strength

via effects on the synaptic localization of AMPA receptors (El- Hussein et al., 2002; Mitchell et al., 2006). In addition, AMPA receptor subunits are palmitoylated at two sites, which are proposed to regulate trafficking of the protein from the Golgi and cycling of the receptor at synapses *via* regulation of the interaction with the cytoskeletal protein 4.1N (Hayashi et al., 2005). Furthermore, palmitoylation of Grip1b (Glutamate receptor interacting protein 1) is proposed to also affect the localization of AMPA receptors by regulating the trafficking of AMPA receptor-containing vesicles (Thomas et al., 2012). Thus, the global effects of palmitoylation on AMPA receptor localization are complex and involve several palmitoylated proteins (including palmitoylation of AMPA receptors directly). NMDA receptors are also palmitoylated at two sites that regulate surface expression of the receptors albeit by different mechanisms to those reported for AMPA receptors (Hayashi et al., 2009).

Various members of the zDHC protein family are involved in important pathways for neuronal function. Apart from zDHC9 whose role will be discussed further in subsequent chapters, zDHC2, zDHC3, zDHC5, zDHC8, zDHC17 and zDHC23 are implicated in key pathways. Briefly, zDHC2 regulates activity-dependent palmitoylation of PSD95 (Noritake et al., 2009), which impacts AMPA receptor localization at synapses. AMPA receptor localization is also affected by zDHC5/8 via their effects on palmitoylation of GRIP1b (Thomas et al., 2012) and δ -catenin (Brigidi et al., 2014). zDHC3 is involved in neuronal regulation enhancing palmitoylation of the γ 2 subunit of the GABA_A receptor (Keller et al., 2004). zDHC17 is a neuronal protein that was first identified by its interaction with huntingtin (htt) (Singaraja et al., 2002) and which is thought to have many important neuronal substrate proteins including SNAP25 and cysteine-string protein (Ohyama et al., 2007). Neuronal nitric oxide synthase (nNOS) is an inducible, PDZ domain-containing protein that interacts with zDHC23, a protein expressed in the postsynaptic density fraction of neurons (Saitoh et al., 2004). Protein interactions with the PDZ domain of nNOS can target the enzyme to appropriate sites within the

cell and this process is very crucial for specifying the sites of generation of nitric oxide in the central nervous system (Saitoh et al., 2004).

In addition, a subset of zDHHC enzymes was identified that control the palmitoylation and function of the STREX (alternatively spliced stress-regulated exon) variant of the large conductance calcium and voltage-activated potassium (BK) channel (Tian et al., 2010). A dicysteine motif (Cys12-Cys13) within the alternatively spliced STREX insert in the C terminus of BK channels is palmitoylated by a subset of zDHHC enzymes (3, 5, 7, 9 and 17), which impacts the regulation of STREX channels by protein kinase A (Tian et al., 2008). Knockdown of any one of five zDHHCs (3, 5, 7, 9 or 17) had very similar effects on palmitoylation status, membrane association, and the ability to prevent PKA-mediated inhibition of STREX channels in HEK293 cells (Tian et al., 2008; 2010). It is not clear why knockdown of five different zDHHC enzymes affects STREX palmitoylation. Each zDHHC might have an effect in controlling palmitoylation and function because the normal cellular expression of each of these zDHHCs is required for efficient palmitoylation as the channel traffics to the PM. It may also reflect potential different localization of specific zDHHC-substrate interactions occurring within the trafficking pathway. This may be particularly important for tetrameric proteins like BK channels such that a combinatorial code of palmitoylation on multiple sites across multiple subunits is important for the overall palmitoylation status and effect on function. zDHHC9 among the other zDHHCs is an important determinant of STREX BK channel palmitoylation and STREX domain interaction with the PM and function.

In contrast to the emerging role of zDHHC enzymes in nervous system function, less is known about the role of depalmitoylation enzymes. Interestingly APT1 has been implicated in dendritic spine morphogenesis. Indeed, microRNA-138 was shown to negatively regulate the size of dendritic spines in hippocampal neurons, and APT1 was identified as a target of this miRNA (Siegel et al., 2009). It was proposed that the effects of APT1 knockdown on spines were via increased palmitoylation of $G\alpha_{13}$ (Siegel et al., 2009).

1.8 Other post-translational modifications important in nervous system function

In addition to palmitoylation, several other post-translational modifications play critical roles as regulators of synaptic transmission and plasticity, which is important for processes such as learning and memory. Phosphorylation plays a key role in regulating different forms of neural plasticity such as neurite outgrowth, and hippocampal Long-Term Potentiation (LTP), and plays a crucial role in the function of NMDA and AMPA subtypes of glutamate receptors (Pasinelli et al., 1995).

The cytosolic carboxyterminal regions of AMPAR GluR subunits act as substrates for various protein kinases, which regulate AMPAR endocytosis and channel conductance (Roche et al., 1996; Barria et al., 1997; Mammen et al., 1997; Derkach et al., 1999; Kristensen et al., 2011; Jenkins and Traynelis, 2012). All AMPAR subunits (GluR1 to GluR4) are targets of kinases such as CaMKII (Ca²⁺/calmodulin-dependent protein kinase II), Fyn (Fyn Proto-Oncogene, Src Family Tyrosine Kinase), JNK (JUN N-Terminal Kinase), PKA/C/G (protein kinase A/C/G) (Shepherd and Huganir, 2007; Lu and Roche, 2012).

GluR1 and GluR2 are widely found in brain tissue and their phosphorylation has been broadly studied. More specifically, GluR1 and 2 represent the vast majority of hippocampal AMPA receptors (Wenthold et al., 1996). The conductance of GluR1 is modulated by phosphorylation of Ser-831 by PKC/CaMKII enzymes, while its opening probability is regulated by phosphorylation of Ser-845 by PKA (Roche et al., 1996; Derkach et al., 1999). Phosphorylation of Ser-845 regulates recycling of the receptor and its dephosphorylation is associated with the regulation of Long-Term Depression (LTD) (Ehlers, 2000; Lee et al., 2003; Brown et al., 2005). Phosphorylation of Tyr-876 and Ser-880 on GluR2 subunits is important for receptor endocytosis (Chung et al., 2000, 2003; Hayashi and Huganir, 2004). More precisely, GRIP1/2 and PICK1 bind to the PDZ ligand in the carboxy-terminal tail of GluR2 and phosphorylation of Tyr-876 and Ser-880 selectively blocks the binding of GRIP1/2 but not PICK1, leading to enhanced endocytosis and LTD (Matsuda et al., 1999; Chung et al., 2000).

The NMDA receptor is phosphorylated on its GluN2B subunit at Ser-1166 by PKA, which affects Ca^{2+} permeation (Murphy et al., 2014). Phosphorylation also controls the surface and synaptic expression of NMDA receptors in a subunit-specific manner. For example, synaptic activity causes internalisation of GluN2B *via* a clathrin-dependent pathway, which is strictly regulated by GluN2B phosphorylation on Tyr-1472 site by Fyn/Src kinases. This specific residue belongs to the YEKL endocytic motif, recognized by the clathrin adaptor AP-2 and is essential for internalization of GluN2B to commence. Phosphorylation of Tyr-1472 inhibits the binding of AP-2, and as a result, endocytosis of the receptor is blocked and its surface expression is enhanced (Lavezzari et al., 2003; Prybylowski et al., 2005). Fyn/Src kinases are able to directly bind to membrane-associated guanylate kinase (MAGUK) proteins such as PSD95 (Tezuka et al., 1999). Therefore, phosphorylation of GluN2B on Tyr-1472 is enhanced by interaction of GluN2B with these scaffolding proteins and increased phosphorylation of GluN2B on this specific residue is associated with the presence of GluN2B in synapses.

In addition to phosphorylation, ubiquitination is another post-translational modification with an important role in nervous system function. It is known that the ubiquitin- proteasome pathway can alter neuronal activity and glutamatergic neurotransmission. Changes in ubiquitination can cause dynamic changes in the number and morphology of dendritic spines and as a result, it modifies synaptic plasticity and activity (DiAntonio et al., 2001; Mabb and Ehlers, 2010).

Several subunits of AMPA and NMDA receptors are ubiquitinated and proteomics conducted on rodent brain tissue highlighted GluN1, GluN2A/2B and GluR1–4 as being modified (Na et al., 2012; Wagner et al., 2012). The NMDA receptor subunits GluN1 and GluN2B are ubiquitinated in an activity-dependent manner by ubiquitin E3 ligases Fbx2 and Mind Bomb-2 (Jurd et al., 2008; Kato et al., 2010). Moreover, the ubiquitin E3 ligase Nedd4-1 ubiquitinates GluN2D (Gautam et al., 2013). In mammals, AMPA receptor subunits are also ubiquitinated by ubiquitin E3 ligases APCCdh1, Nedd4-1 and RNF167 (Schwarz et al., 2010; Fu et al., 2011; Lin

et al., 2011; Lussier et al., 2011, Lussier et al., 2012; Scudder et al., 2014; Widagdo et al., 2015). It was shown that GluR1 and GluN1 ubiquitination is upregulated by repetitive stress which modulates neuronal activity (Yuen et al., 2012).

Collectively, the large body of data on phosphorylation and ubiquitination highlights the prominent role played by post-translational modifications in nervous system function.

1.9 ZDHHC mutations and disease

Mutations in zDHHC enzyme family have been linked to different forms of cancer. Mutations in *ZDHHC9* were identified in leukaemia and colorectal cancer and will be further discussed in the next sections. Dysregulated expression (downregulation) of *ZDHHC2* has been found in colorectal cancer and gastric adenocarcinoma due to mutations (Oyama et al., 2000; Yan et al., 2013). Moreover, downregulation of *ZDHHC14* expression has been identified in testicular germ cell tumors and prostate cancer while overexpression has been found in gastric cancer and leukemia (Anami et al., 2010; Yu et al., 2011; Yeste-Velasco et al., 2014). An increase in copy number of *ZDHHC11* has been described in lung and bladder cancers (Yamamoto et al., 2007; Kang et al., 2008).

In addition to cancer, there are several links between palmitoylation enzymes and neurological disorders. A SNP in the *ZDHHC8* gene has been associated with an increased risk of schizophrenia in one study (Mukai et al., 2004). Two zDHHC enzymes have been linked to Huntington's disease (HD): zDHHC13 and zDHHC17. Although there is no direct clinical link between these enzymes and HD, an association has been suggested because the enzymes palmitoylate the huntingtin protein (HTT) (Yanai et al., 2006; Sanders & Hayden, 2015). It has also been suggested that HTT positively regulates zDHHC17 enzymatic activity, perhaps acting as a co-factor (Huang et al., 2011). The possibility that the zDHHC17/13:HTT interaction is relevant to HD is supported by the observation that pathogenic

expansion of the polyglutamine region of HTT leads to loss of palmitoylation of HTT and loss of HTT regulation of zDHHC17 (Yanai et al., 2006; Huang et al., 2011).

Mutations in *ZDHHC9* and *ZDHHC15* have been linked to intellectual disability. A chromosomal translocation containing *ZDHHC15* was identified in a single patient with severe ID (Mansouri et al., 2005), whereas the mutations identified in *ZDHHC9* create either truncated proteins that lack the catalytic domain of the enzyme or amino acid substitutions in the catalytic domain that decrease the steady state level of enzyme autoacylation, which is intimately linked with palmitoyltransferase activity (Raymond et al., 2007; Mitchell et al., 2010, 2014; Jennings and Linder, 2012). Therefore, it is likely that deficits caused by these mutations in the *ZDHHC9* gene arise due to a loss of palmitoylation of specific substrate proteins. The following table summarizes the links of zDHHC enzymes to disease.

Table 1.1 Links of zDHHC enzymes to disease.

Disorder	Enzymes	Summary on molecular data	References
X-linked ID	zDHHC9, zDHHC15	Mutations in <i>ZDHHC9</i> cause loss of function or reduced enzymatic function. Chromosomal translocation containing <i>ZDHHC15</i> .	Mansouri et al., 2005; Raymond et al., 2007; Mitchell et al., 2010, 2014; Jennings and Linder, 2012
Schizophrenia	zDHHC8	SNP in <i>ZDHHC8</i> associated with increased risk.	Mukai et al., 2004
Huntington's disease	zDHHC13, zDHHC17	The enzymes palmitoylate huntingtin protein (HTT), pathogenic expansion of	Yanai et al., 2006; Huang et al., 2011;

		polyglutamine region of HTT leads to loss of its palmitoylation and loss of HTT regulation of zDHHC17.	Sanders & Hayden, 2015
Infantile neuronal ceroid lipofuscinosis	PPT1	Mutations cause undetectable enzymatic activity.	Vesa et al., 1995
Colorectal cancer	zDHHC9, zDHHC2	Downregulation of <i>ZDHHC2</i> ; upregulation of <i>ZDHHC9</i> .	Oyama et al., 2000; Birkenkamp-Demtroder et al., 2002; Mansilla et al., 2007
Leukaemia	zDHHC9, zDHHC14	<i>ZDHHC14</i> overexpressed, <i>zDHHC9</i> inactivation slows down the development of myeloid leukaemia.	Yu et al., 2011; Liu et al., 2016
Testicular and prostate cancer	zDHHC14	Downregulation of expression in testicular germ cell tumours and prostate cancer.	Yeste-Velasco et al., 2014
Gastric cancer	zDHHC2, zDHHC14	Downregulation of <i>ZDHHC2</i> in gastric adenocarcinoma. Overexpression of <i>ZDHHC14</i> in gastric cancer.	Anami et al., 2010; Yan et al., 2013
Lung cancer	zDHHC11	Increase in copy number.	Kang et al., 2008
Bladder cancer	zDHHC11	Increase in copy number.	Yamamoto et al., 2007

Finally, mutations in PPT1 which encodes for palmitoyl-protein thioesterase 1 have been shown to cause infantile neuronal ceroid lipofuscinosis, a neurodegenerative lysosomal-storage disorder with early-onset (Vesa et al., 1995).

1.9.1 Intellectual disability

Intellectual disability (ID, formerly known as mental retardation), is a generalized neurodevelopmental disorder characterised by deficits in intellectual functions such as learning and problem solving, and in adaptive functions such as practical and social skills (San Martin and Pagani, 2014). More specifically, ID is characterized by intelligence quotient (IQ) score lower than 70 and by deficits in at least two adaptive functions that generally affect the every day life. The incidence of ID is 1.04 % according to a meta-analysis study (Maulik et al., 2011).

ID causes significant limitations both in intellectual functioning referring to general mental capacity (such as learning, reasoning, and problem solving) and in adaptive behaviour comprising conceptual, social and practical skills and originates before the age of 18. Adaptive behaviour is a type of behaviour that is used to adjust to another type of behaviour or situation. This is often characterized as a kind of behaviour that allows an individual to change a non-constructive or disruptive behaviour to something more constructive. These behaviours are most often social or personal behaviours. For example a constant repetitive action could be re-focused on something that creates or builds something.

ID is the most prevalent severe handicap in children and can be caused by environmental and/or genetic factors (Ropers, 2010). X-linked intellectual disability (XLID), which arises from mutations in genes on the X-chromosome accounts for about 10–12% of the ID seen in males (Ropers, 2010). It is a genetically heterogeneous disorder with more than 100 genes currently described. Most genes are responsible for a small proportion of patients only, which has hitherto hampered the systematic screening of large patient cohorts.

1.9.2 Effects of *ZDHHC9* mutations on the nervous system

Mutations in *ZDHHC9* have been shown to cause a number of symptoms, including XLID, epilepsy, and speech and attention deficits (Raymond et al., 2007; Baker et al., 2015). Furthermore, hypoplasia of the corpus callosum was identified together with a reduced volume of sub-cortical structures such as the thalamus and striatum. The first study that described subjects with *ZDHHC9* mutations identified inherited mutations in *ZDHHC9* in four of 250 families with XLID via a systematic Sanger re-sequencing screen of coding exons and splice junctions of all X chromosome genes (Raymond et al., 2007). In three of the families of the study, the ID phenotype was associated with a Marfanoid Habitus, but none of the affected individuals met the Ghent criteria for Marfan syndrome.

The identified mutations in *ZDHHC9* were one frame shift mutation, one splice site mutation and two missense mutations. All mutations affected highly conserved amino acid residues of zDHHC9 (Raymond et al., 2007). The two nonsense mutations create a truncation and a frame shift, both deleting the essential DHHC catalytic domain of zDHHC9. The two missense mutations led to single amino acid changes in the DHHC domain of zDHHC9 (R148W and P150S) and reduce the steady state level of autopalmitoylated zDHHC9 (Mitchell et al., 2014). Autopalmitoylation of zDHHC enzymes is essential for their subsequent palmitoylation of substrate proteins. In a later study, the coding exons of the X chromosome were sequenced in 208 families with XLID (Tarpey et al., 2010). One frameshift mutation and one splice site mutation in *ZDHHC9* were identified in 2 independent families. In addition to ID, the phenotype of the patients included Marfanoid Habitus.

Loss of function (or reduced function) mutations in *ZDHHC9* are likely to cause the reported symptoms due to reduced palmitoylation of specific substrate proteins. For example, this could alter the relative proportion of RAS proteins within the different compartments of nerve cells. Interestingly, mutations in H-Ras cause

Costello syndrome, which is characterized by ID (Aoki et al., 2005) and mutations in N-Ras cause Noonan syndrome which is also characterized by ID (Denayer et al., 2012).

1.9.2.1 *ZDHHC9 mutations and epilepsy*

Rolandic epilepsy (RE) also known as Benign Childhood Epilepsy with Centro-Temporal Spikes, (BECTS) is the most frequently diagnosed epilepsy syndrome of childhood (Panayiotopoulos et al., 2008). A recent study associated *ZDHHC9* mutations to this type of epilepsy (Baker et al., 2015). The study included all the known cases of XLID due to *ZDHHC9* mutations in the United Kingdom. The authors described neurological, cognitive and neuroanatomical characteristics of nine males from three families with loss-of-function mutations. Seven out of nine males with *ZDHHC9* mutations had been diagnosed with epilepsy. The prevalence of epileptic seizures in males with *ZDHHC9* mutations was at least triple that expected for patients with ID and seven times that expected for mild ID. *ZDHHC9* mutations correlate with susceptibility to focal seizures. Cognitive deficits in patients with *ZDHHC9* mutations were present either when there was an overt seizure history or not, were present before the overt seizures started, and were still obvious many years after seizure remission, characteristics reminiscent of idiopathic (mixed etiology) RE. In the idiopathic RE cohort, cognitive performance is variable and neuroanatomical abnormalities are very mild among patients, in contrast to the cohort of *ZDHHC9* mutation patients which is described by relatively homogenous cognitive and neuroanatomical abnormalities.

Cognitive deficits in patients with *ZDHHC9* mutations are associated with mild to moderate ID together with linguistic and non-linguistic deficits that are also present in idiopathic RE such as impaired oromotor control, reduced verbal fluency, and reduced inhibitory control on visual attention tasks (Baker et al., 2015). Verbal dyspraxia and speech processing deficit are often present in familial and sporadic RE (Lundberg et al., 2005). As regards the impairment in inhibitory control mechanisms,

children with RE have been also described presenting this deficit possibly suggesting that rolandic seizure activity affects the proper development of attentional control networks.

There is higher consistency in neurological and cognitive deficits than in physical deficits in patients with *ZDHHHC9* mutations as only in three out of the five families patients did present with Marfanoid Habitus, whereas all families include patients with epilepsy, oromotor deficits, ID, and shrunken corpus callosum (Baker et al., 2015). It is possible that characterization of neurological and cognitive functions could help interpretation of genomic test results more than the characterization of physical dysmorphology in neurodevelopmental disorders.

1.9.2.2 ZDHHHC9 mutations are associated with hypoplasia of corpus callosum

The first link between *ZDHHHC9* and the corpus callosum came from a study showing that a pathogenic *ZDHHHC9* mutation was associated with non-syndromic mild ID (Masurel-Paulet et al., 2014). The nonsense mutation (p.Arg298*) was identified in a family by parallel sequencing of all X chromosome exons. An 18-year-old patient and his 40-year old maternal uncle were characterized by lingual fasciculation, limited extension of the elbows and the joints of the hands. The patients did not have any facial dysmorphism or Marfanoid Habitus. Brain MRI revealed dysplasia of corpus callosum (Masurel-Paulet et al., 2014). Another interesting characteristic is that both patients exhibited anxiety disorder.

Hypoplasia of the corpus callosum (generalized or segmental) was subsequently shown to be a common neuroanatomical characteristic in *ZDHHHC9* patients, at ages from early childhood to mid-adulthood (Masurel-Paulet et al., 2014; Baker et al., 2015). Shrinkage of the corpus callosum and especially in its posterior connections between temporal cortices has been previously described in some neurodevelopmental disorders that are accompanied by expressive language deficit (Halgren et al., 2012; Northam et al., 2012). *ZDHHHC9* dysfunction could therefore

serve as a model to study the relationship between hypoplasia of corpus callosum, epilepsy, oromotor dysfunction and cognitive development.

The following table summarizes the key features of the zDHHHC9 enzyme and the effect of *ZDHHHC9* mutations.

Table 1.2 Key features of zDHHHC9.

	Summary	References
mRNA expression	Highly expressed in brain, kidney, skeletal muscle, lung and liver, lower expression in heart, colon, placenta, small intestine, peripheral blood leukocytes, spleen and thymus.	Swarthout et al., 2005
Localisation (for transfected epitope-tagged zDHHHC9)	Endoplasmic reticulum (ER) and Golgi in mammalian cell lines, the cell body and neurites in hippocampal neurons.	Swarthout et al., 2005; Levy et al., 2011
Potential substrates	H-Ras, N-Ras, STREX, beta 2-Adrenergic Receptor.	Swarthout et al., 2005; Tian et al., 2010; Adachi et al., 2016
Phenotypes of patients with <i>ZDHHHC9</i> mutations affecting the nervous system	ID, epilepsy, speech and attention deficits, corpus callosum shrinkage, reduced volume of thalamus and striatum, marfanoid habitus.	Raymond et al., 2007; Masurel-Paulet et al., 2014; Baker et al., 2015

Mutations identified affecting the nervous system	R148W, P150S, R298*, Y59Sfs*33, T11fs*33	Raymond et al., 2007; Masurel-Paulet et al., 2014; Baker et al., 2015
Known or predicted effect of mutations	Truncated proteins that lack the catalytic domain or a decrease of the steady state level of enzyme autopalmitylation.	Raymond et al., 2007; Mitchell et al., 2010, 2014; Jennings and Linder, 2012

1.9.3 ZDHHC9 dysfunction as a cause of other disorders

Differential expression of the *ZDHHC9* gene has been also implicated in colorectal cancer (Mansilla et al., 2007). Furthermore, zDHHC9 may be important in the development of leukaemia (Liu et al., 2016). A microarray study showed that *ZDHHC9* was upregulated in human colon adenocarcinoma samples compared to normal colon mucosa (Birkenkamp-Demtroder et al., 2002). Another study validated this result and also showed that *ZDHHC9* overexpression was specific for gastrointestinal tumours and its overexpression significantly decreased the proliferation of microsatellite stable cell lines (Mansilla et al., 2007). Thus, *ZDHHC9* is highly expressed in microsatellite stable colon tumours although its role is not yet characterised for this type of cancer (Mansilla et al., 2007).

zDHHC9 has also been suggested to have an important role in leukemogenesis induced by oncogenic N-Ras (Liu et al., 2016). It was demonstrated that zDHHC9 is a Ras palmitoyltransferase in vivo although knockout of this enzyme only partially affected Ras palmitoylation. zDHHC9 inactivation inhibited oncogenic N-Ras plasma membrane translocation and cellular transformation, significantly slowed down the development of myeloid leukaemia and led to an improvement in overall survival of mice. However, although zDHHC9 inactivation could delay the

leukaemia progress, it could not completely eliminate it (Liu et al., 2016). Nevertheless, this study highlights the potential of zDHHC9 inhibitors to be used in leukaemia treatment.

1.10 Genetic animal models of ID

1.10.1 Down syndrome

Down syndrome is the most common genetic cause of ID with an incidence of 1 in 733 live births, caused by trisomy of chromosome 21 (Lejeune et al., 1959; Canfield et al., 2006). This disorder is characterised by deficits in learning, memory and language skills (Nelson et al., 2005). Many patients with Down Syndrome also suffer from cardiovascular problems, a higher incidence of leukemia, immunological dysfunction, premature aging, hypotonia, and brain accumulation of plaques reminiscent of Alzheimer's disease plaques and neurofibrillary tangles during the third decade of life (Epstein, 1995; Roizen, 2001). Brains of Down syndrome patients show morphological changes such as cortical shrinkage, increased neuronal density, loss of basal forebrain cholinergic neurons, small cerebellum and dendritic spine changes in neocortex (Takashima et al., 1981; Scott et al., 1983; Epstein, 1995; Seidl et al., 2001).

Mouse models of Down syndrome have been developed that carry extra parts of mouse chromosome 16 (MMU16; named Ts65Dn, Ts1Cje and Ms1Ts65 mouse models) or of human chromosome 21 (HSA21).

Ts65Dn mice have an extra copy of about 104 mouse genes orthologous to those on HSA21 and therefore are considered partially trisomic. This animal model recapitulates most developmental and functional deficits of Down syndrome patients compared to the rest of the models developed to-date. To be more precise, the mice exhibit sensory-motor and behavioural developmental delay, hyperactivity and learning and memory deficits in adulthood (Davisson et al., 1993; Coussons-

Read & Crnic, 1996; Holtzman et al., 1996; Escorihuela et al., 1998). Neuroanatomical studies show that Ts65Dn mice have decreased volume of CA2 region and decreased neuronal number in the dentate gyrus of hippocampus (Insausti et al., 1998). Changes in the structure of dendritic spines in the cortex and hippocampus and dysfunction of hippocampal LTP have also been described (Escorihuela et al., 1995; Reeves et al., 1995, Escorihuela et al., 1998; Sago et al., 2000). Moreover, functional abnormalities have been found in the noradrenergic projections to the cerebral cortex and hippocampus, but not in the cerebellum (Dierssen et al., 1997). Based on those data, alterations in neurogenesis and/or neuronal migration are believed to cause those changes. Because of the loss of basal forebrain cholinergic neurons that is also described in this animal model, it also serves as a model for Alzheimer's disease (Holtzman et al., 1996).

Ts1Cje mice, which are trisomic for a shorter part of MMU16 (about 81 genes), show similar changes but with a less severe phenotype (Sago et al., 1998; Sago et al., 2000; Siarey et al., 2005; Belichenko et al., 2007; Belichenko et al., 2009). The mice have milder learning deficits than those of Ts65Dn, such as a slight impairment in spatial learning and mild hypoactivity and they do not show degeneration in basal forebrain cholinergic neurons (Sago et al., 1998, Sago et al., 2000). Ms1Ts65 mice, which are partially trisomic carrying an extra copy of a shorter MMU16 segment, show deficits in a spatial navigation task and have overall milder phenotypic deficits compared to Ts65Dn and Ts1Cje mouse models (Sago et al., 2000).

In addition to the already described trisomic mouse models, transgenic mice for Down syndrome have been developed by inserting yeast artificial chromosomes (YAC) into the murine genome. The YACs include Down syndrome Critical Region 1 (DCR-1) which is a part of the human chromosome 21. Two YAC lines, the 230E8 and 152F7 lines, show learning and memory impairments in the Morris water maze in adulthood (Smith et al., 1997). The 152F7 line does not show neuropathological

changes that could explain the learning and memory deficits. In contrast, the 230E8 line shows higher cortical neuronal density (Smith et al., 1997).

Apart from the above, a mouse line overexpressing the Down syndrome candidate gene *Dyrk1a*, a *Drosophila minibrain* homologue that plays an important role in brain development and function, is also a model of Down syndrome (Okui et al., 1999; Hammerle et al., 2002). DYRK1A protein which is a serine–threonine kinase, phosphorylates the microtubule-associated protein tau and the cyclic-AMP response element binding protein (CREB) among others (Woods et al., 2001; Yang et al., 2001). Transgenic mice overexpressing *Dyrk1a* in the forebrain exhibit delay in motor responses (Altafaj et al., 2001). Adult mice are hyperactive in an open field and show a deficit in learning and memory in Morris water maze (Altafaj et al., 2001). Loss of both *Dyrk1a* copies in mice is embryonic lethal, while heterozygous mice have decreased brain and body size and developmental delay (Fotaki et al., 2002).

1.10.2 Fragile X syndrome

X-linked intellectual disability accounts for 5% of all intellectual disability cases, with a 20–30% higher prevalence in males than females (Herbst and Miller, 1980). X-linked intellectual disability is categorised as either syndromal or non-specific (Branchi et al., 2003). In syndromal form of XLID, cognitive dysfunction is one part of a complex syndrome that is characterized by developmental abnormalities, such as changes in normal brain connectivity. Fragile X syndrome (FXS) is the most commonly inherited form of syndromal XLID as it represents 15–20% of all XLID cases (Turner et al., 1996). FXS affects 1 in 1400 males and 1 in 2500 females (Scorza and Cavalheiro, 2011), and is caused by an unstable DNA region on the X chromosome that becomes highly expanded when inherited. At the molecular level, an increase in the number of repeats of a CGG trinucleotide at the 5' untranslated region of *FMR1* gene causes the disorder. The healthy population has between 6–50 CGG trinucleotides, while FXS patients have more than 230 (Pieretti

et al., 1991). Hypermethylation of the trinucleotide area and the promoter area takes place, inhibiting expression of the *FMR1* gene and the production of the Fragile X Mental Retardation Protein (FMRP) (Verheij et al., 1993). This protein is a RNA-binding protein involved in brain development and, more specifically, in synaptogenesis (Khandjian et al., 1999).

FXS patients exhibit attention deficit, hyperactivity, autism and epilepsy (Bakker & Oostra, 2003). These phenotypes are recapitulated in *Fmr1* KO mice that have abnormal expression of GABA receptor subunits (Bakker et al., 1994; Curia et al., 2009). *Fmr1* KO mice display impaired flexibility in spatial learning during the reversal phase of Morris water maze (Bakker et al., 1994; D'Hooge et al., 1997). Moreover they exhibit increased exploratory activity. Histological studies show abnormalities in dendritic spines and higher spine density in pyramidal cells of occipital cortex in *Fmr1* KO mice (Comery et al., 1997). These findings, which are similar to abnormalities observed in FXS patients, show that FMRP plays an important role in synaptic maturation and pruning.

1.10.3 Rett syndrome

Rett syndrome (RTT) is a neurodevelopmental disorder affecting mostly females, with a prevalence of 1:10,000–20,000 (Branchi et al., 2003). Affected girls exhibit abnormal motor gait, stereotypic hand movements and autistic-like behaviour. Moreover, most patients show speech abnormalities and severe cognitive deficits with low IQ (Dunn and MacLeod, 2001). One striking fact about RTT is that patients look normal at birth, but when they reach 6 to 18 months of life, they show regression of some acquired skills, such as speech, communication and motor coordination. Mutations in the *MECP2* gene located on the X chromosome cause the disease in most of the cases. The gene encodes for MeCP2 (methyl-CpG binding protein 2), a protein that binds specifically to methylated CpG DNA sequences and along with histone deacetylases, condenses chromatin structure making DNA inaccessible to transcriptional factors thus suppressing the expression

of various genes. *MECP2* is ubiquitously expressed, suggesting that MeCP2 protein is a global regulator of DNA expression in various tissues. MeCP2 binds to intergenic and intronic and sparsely methylated promoters of active genes, suppressing their expression (LaSalle and Yasui, 2009).

Various mouse models have been developed for the study of RTT providing valuable information about the pathophysiology of the disease. A mouse model was created that expresses a truncated MeCP2 protein and recapitulates many behavioural aspects of the disorder (Shahbazian et al., 2002). More precisely, the mice do not differ from their wild type littermates until 6 weeks of age, but after that age they progressively show motor deficits and anxiety-like phenotypes. Moreover, during a tail suspension test, they show stereotypic forelimb movements. However, the mice producing the truncated MeCP2 protein do not exhibit severe cognitive deficits when tested in a water maze or a contextual fear conditioning task, thus not recapitulating the severe ID of RTT patients.

A second mouse model of RTT (*Mecp2*-null mice) does not show any abnormal characteristics at birth, and only starts to display motor deficits and an abnormal increase in body weight at 5 weeks of age which is not related to the syndrome (Chen et al., 2001). Male mice are hemizygous for the *MECP2* mutation, and do not produce a functional protein, which causes a high mortality by 10 weeks of age (Chen et al., 2001). Female mice which are heterozygous produce varying amounts of functional protein and exhibit a less severe phenotype (Stearns et al., 2007). The mice display some cognitive abnormalities in fear conditioning and object recognition memory (Stearns et al., 2007).

A third mouse model with mice lacking *Mecp2* using Cre-loxP technology, starts showing motor deficits, breathing difficulties (which are also present in patients with RTT), and weight gain between 3 and 8 weeks of age (Guy et al., 2001).

RTT syndrome shows a broad range of variant forms with different severity (Webb and Latif, 2001). The different mouse models that have been characterised recapitulate different aspects of this syndrome and are probably relevant for the

study of those specific aspects. As this syndrome is caused by dysfunction of a crucial protein for gene expression regulation, it is highly possible that various neurotransmitters, different brain regions and behavioural processes are disrupted, affecting different developmental time points (Berger-Sweeney, 2003). RTT is a disorder that affects neuronal development and early brain growth as pre- and post-synaptic components of synapses are affected (Johnston et al., 1995; Naidu, 1997). A hypothesis for the regressive nature of this disorder is that MeCP2 mutations could disrupt synaptic proliferation and pruning at a developmental period where most of the synaptic proliferation is taking place in cerebral cortex (7–18 months in humans, and first weeks of life in mice) (Johnston et al., 2001). This would suggest that abnormalities in neuronal maturation are a main cause of the behavioural manifestations in RTT.

1.10.4 Non-syndromic XLID

In contrast to syndromal XLID where intellectual disability is a secondary characteristic of serious brain dysfunction with a developmental cause, non-specific XLID can offer useful information about the dysregulation of biological pathways as a cause of developmental delay. For this reason, non-syndromic forms of XLID provide an important way to characterise genes, molecular pathways and cellular processes underlying cognition, providing a deeper understanding of cognition from a biological perspective (Chelly, 1999; Toniolo, 2000; Toniolo and D’Adamo, 2000).

Many genes have been implicated in non-syndromic XLID including *GDI1* (GDP Dissociation Inhibitor 1) (Branchi et al., 2003). This gene encodes for a rabGDP-dissociation inhibitor that mediates vesicle fusion and intracellular trafficking (Bienvenu et al., 1998), crucial for axonal and dendritic outgrowth during neuronal maturation (D’Adamo et al., 1998). Knock out mice for *Gdi1* do not exhibit any gross behavioural abnormalities in a variety of tasks, nevertheless they show a deficit in hippocampal-dependent tasks that test short-term memory. Moreover the KO mice have abnormal sociability, showing lower aggression levels than normal

mice (D'Adamo et al., 1998; D'Adamo et al., 2002). Experiments utilising electrophysiology showed that *Gdi1* KO mice exhibit a specific synaptic plasticity impairment implying that abnormal neuronal activity may cause the behavioural deficits that were revealed (D'Adamo et al., 2002).

Apart from *GDI1*, most of the other genes identified as responsible for non-syndromal XLID, encode for regulators of the Ras superfamily of small GTPases or their effectors (Chelly, 1999; Toniolo, 2000).

1.11 Molecular and cellular mechanisms implicated in ID

Disruption of several cellular processes and pathways has been linked to development of ID, as already shown by the various animal models of ID. Mutations in genes can cause ID because of abnormalities in neurodevelopment and brain formation or because of dysfunction of molecular mechanisms involved in plasticity and organisation of synapses (Vaillend et al., 2008).

Brain plasticity is a fundamental property of the nervous system at a functional and structural level and it is involved in various processes from memory storage to nervous system development and regeneration after injury (Vaillend et al., 2008). Disruption of this brain plasticity is established as a cause of ID. Plasticity related genes when mutated, cause ID as they normally play an important role in activity-dependent processes, such as synaptic organization at a molecular level, intracellular signalling regulating gene expression, and neuronal cytoskeleton remodelling during learning and memory formation. The role of some of these genes is cell-type or brain-region-specific or even time-specific during lifespan (Vaillend et al., 2008), therefore when it is disturbed, it can cause severe phenotypes.

Although mechanisms of neurogenesis and neuronal migration during development are not normally defined as processes of plasticity, those mechanisms are affected in most of inherited disorders of nervous system and sometimes genes

involved in neurodevelopment are also involved in adult neurogenesis and plasticity (Esposito et al., 2005; Hevner et al., 2006). Therefore we cannot refer to neurodevelopment and plasticity as two totally different processes. Genes that are involved in mechanisms of neurogenesis and neuronal migration, such as actin and microtubule-cytoskeletal associated proteins and proteins that are involved in signal transduction pathways, when mutated cause severe behavioural deficits.

The cause of ID can be related to both neuronal and glial abnormalities, and in case of affected membrane or cytoskeletal stability, glycosylation or mitochondrial processes, muscle dysfunction is also present along with ID.

Studies of ID like the current one, could provide us with valuable information about brain plasticity mechanisms. At the same time, studying brain plasticity could open new roads in the identification of new genes, mutations in which can cause ID.

1.12 Metabolic biomarkers of intellectual disability

A predictive biomarker is a biomarker that can be used to estimate the likelihood of a particular future event (Baum, 2016). The first metabolic biomarker of intellectual disability that was identified was for phenylketonuria, and elevated blood phenylalanine levels can be used as a predictive biomarker of this disorder (Baum, 2016).

Most people with high levels of blood phenylalanine have polymorphisms or mutations in the phenylalanine hydroxylase gene that leads to an inability to metabolize phenylalanine (Scriver & Waters, 1999). This defect in phenylalanine hydroxylase activity causes a build-up of phenylalanine and, subsequently, progressive and severe brain damage. Therefore, high blood phenylalanine levels are a causal predictive biomarker of severe ID.

Asbjørn Følling first discovered the metabolic dysfunction in phenylketonuria through a urine biomarker called phenylpyruvic acid rather than a blood biomarker

(Centerwall & Centerwall, 2000). When there is dysfunction of normal phenylalanine metabolism, phenylalanine is processed through other pathways, which leads to secretion of phenylpyruvic acid in urine. Therefore, high urine concentration of phenylpyruvic acid is also a predictive biomarker of ID, but not causative of this disorder. A diet low in phenylalanine can also decrease blood phenylalanine and phenylpyruvic acid in urine.

Studies have suggested a role for an altered inflammatory response in ID in patients with Down Syndrome (DS). Serum levels of a number of inflammatory biomarkers were assessed such as serum amyloid A (SAA), C-reactive protein (C-RP), and high mobility group box-1 (HMGB1) in DS patients and cognitively healthy controls. SAA, C-RP and HMGB1 were significantly higher in DS patients compared to healthy controls (Manti et al., 2018). Moreover, serum C-RP was inversely correlated with IQ in DS patients (Manti et al., 2018).

Moreover, in a family study of ID, serum levels of Interleukin 1 beta (IL1 β) and Interleukin 6 (IL6) were significantly different between the family members with ID and controls (Aureli, 2014). In this study, the patients had a positive association of ID with polymorphisms in brain derived neurotrophic factor (BDNF), IL6 and interleukin 1 receptor antagonist (IL1RA) genes.

Overall, a small amount of research has been conducted in order to discover metabolic biomarkers for ID but hopefully future studies will highlight new molecules involved.

1.13 Aims of this thesis

In humans, mutations in *ZDHH9* cause XLID with Rolandic epilepsy, and speech and attention problems. Moreover in most of the patients described to-date, hypoplasia of corpus callosum is a common characteristic. The aim of this study is to examine how the knockout of *Zdhc9* in mice affects the brain, cognitive processing, and underlying cell pathways. Specifically, I will:

- (i) Characterise zDHHC9 expression in a new *Zdhhc9* knockout mouse line using quantitative polymerase chain reaction (qPCR) and immunoblotting.
- (ii) Examine how knockout of *Zdhhc9* affects behaviour. These tasks will include learning and memory tests such as pair-wise visual discrimination and reversal learning, and spatial learning in the Morris water maze. In addition, other characteristics of patients with *ZDHHC9* mutations or phenotypes seen in other mouse models of ID will be investigated, such as hypotonia and anxiety.
- (iii) Determine if *Zdhhc9* knockout mice display the same defect in corpus callosum as seen in patients with *ZDHHC9* mutations.
- (iv) Identify molecular changes that occur in *Zdhhc9* knockout mice, focusing on alterations in the cellular profile of palmitoylated proteins. Acyl resin-assisted capture (Acyl-RAC) will be used to purify palmitoylated proteins from the brains of wild-type and knockout mice, followed by comparative proteomic analysis using mass spectrometry and immunoblotting. Any proteins displaying reduced palmitoylation will be further investigated as zDHHC9 substrates using cell-based assays and techniques including click chemistry.
- (v) Identify any metabolic changes in *Zdhhc9* knockout mice using metabolomics that will be undertaken on mouse urine samples.

These analyses will determine if this KO mouse line is a good model with which to dissect the molecular and cellular basis of the neurological impairments in humans with *ZDHHC9* mutations, and will identify novel changes in the mutant mice that may underlie observed behavioural and anatomical deficits.

CHAPTER 2

2 Materials and Methods

All animal procedures were conducted in the Biological Procedures Unit of the University of Strathclyde in accordance with Home Office procedures (under a personal, a project and an establishment licence for animal work). Except otherwise indicated, all chemicals were purchased from Sigma-Aldrich (Poole, UK).

2.1 *Zdhhc9* knock-out mice

Zdhhc9 knock- out (KO) mice were purchased from Mutant Mouse Regional Resource Centers (MMRRC, USA). The strategy of KO resulted in the disruption of the first coding exon of the *Zdhhc9* gene, whereby a genomic region of 207 bp including most of the first coding exon (exon 2) of *Zdhhc9* was deleted. The selection cassette that was used for the KO strategy contained both Neomycin (Neo) and LacZ and is 5,288 bp long, according to the sequence in the genotyping protocol given by Lexicon Genetics Incorporated, who produced the KO line (<http://mmrrc.mousebiology.org>).

2.2 Mouse colony and genotyping

In order to have the *Zdhhc9* mutation in a C57BL/6 genetic background, backcrossing was performed for at least 6 generations. In each backcross, mouse breeding used heterozygous (HET) female mice at least seven weeks old and C57BL/6 wild type (WT) male mice that were not from the colony. In some cases, KO male mice were paired with C57BL/6 WT female mice in order to achieve larger numbers of HET female mice for use in subsequent backcrosses. In each cage, one male was put with two females during the breeding period, which lasted for two

weeks, after which male mice were removed from the cages. When the newborns reached three weeks of age, a small part of ear tissue was collected and sent for genotyping to Transnetyx, Inc (Cordova, USA). On the same day, mice were weaned and ear tagged for identification purposes. On receipt of genotyping results, HET female and KO male newborns were kept in order to be used in the next breeding cycle when they reached the age of seven weeks. For the final backcrosses (≥ 6), HET females were caged with C57BL/6 WT males in order to give birth to KO and WT male mice which were used as experimental mice for behavioural testing when they reached adulthood (8-10 weeks old).

2.3 Behavioural tests

2.3.1 SHIRPA

SHIRPA stands for **S**mithKline Beecham, **H**arwell, **I**mperial College, **R**oyal London Hospital, **P**henotype **A**ssessment and as the name describes, it is a general phenotypic assessment of genetically modified mice (Masuya et al., 2005). It is the first test that was conducted in the mice of this study and allows the identification of any physical gross abnormalities focusing mostly on nervous system and motor function.

Each adult animal (8 to 10 weeks old) was first placed in a Plexiglas box with small holes that allow the mouse to breathe. The researcher then scored a list of behaviours of the animal during a 5-minute period (Table 2.1) inside the box. Consequently, the animal was hand-restrained by the researcher in order to score some more behavioural characteristics such as pinna and cornea reflexes (Table 2.1) with paying attention to minimise the stress of the animal during handling.

Table 2.1 List of behaviours that were scored for each animal. The animal was in the arena for a 5 minute period or restrained. Y stands for yes, n stands for no.

<i>Location</i>	<i>Measure</i>	<i>Score scale</i>	<i>Range of scores</i>
<i>In arena (in the box)</i>	body position	0-5	lying flat to vertical leaping
	spontaneous activity	0-4	none to extreme rapid dart
	tremor	0-2	none to marked
	urination	y/n	yes/no
	defecation	y/n	yes/no
	bizarre behaviours	y/n	yes/no
	convulsions	y/n	yes/no
	palebral closure	0-2	eyes wide open to eyes completely closed
	piloerection	0-1	none to fur standing on end
	gait	0-3	normal to incapacity
	pelvic elevation	0-2	markedly flattened to elevated
	tail elevation	0-2	dragging to straub tail
	evidence of grooming	y/n	yes/no
whiskers	Intact (I), malformed/ no whiskers		
<i>Restrained</i>	pinna reflex	0-2	none to hyperactive (repetitive)
	cornea reflex	0-2	none to hyperactive (repetitive)
	lacrimation	y/n	yes/no
	provoked biting	y/n	yes/no
	trunk curl	y/n	yes/no

	visual placing	0-4	none to early vigorous extension
	righting reflex	0-3	no impairment to complete failure to right

2.3.2 Hanging wire task

The day following the physical gross examination, each animal was first weighed and then tested in the hanging wire test in order to assess grip strength. The animal was placed on a cage lid and given a small shake so that it would grab the lid and then the lid was flipped upside down with the animal hanging approximately 25 cm above a safe surface (benchtop). The time that the animal spent hanging was noted. Mice were given 3 trials of 2 minutes maximum and the average time was used. The animals were given a 2 minute rest between trials.

2.3.3 Rotarod task

The day following the hanging wire task, the animals were tested on an accelerating rotarod in order to measure motor coordination and balance (Ugo Basile/Stoelting rotarod). The animals were initially placed onto the rotarod, which was rotating at 3 rpm and accelerated up to 21 rpm within a period of 5 minutes. The animals were left for a maximum of 8 minutes on the rotarod. The animals completed 3 trials with a 10 minute rest between the trials, and the average time that they spent on the rotarod was used.

2.3.4 Open field test

The animals were tested in the open field test (OFT) in order to evaluate locomotor activity and anxiety. Each mouse was placed into a 40 cm x 40 cm x 40 cm open-top box for a 15 minute habituation period followed by a 30 minute test

period. The animals were tracked throughout the whole 45 minute task using Noldus Ethovision Tracking package (version 8.5). The main measures produced were locomotor output (distance travelled) and thigmotaxis (time in outer edge of the box).

2.3.5 Elevated plus maze

The animals were further tested on the elevated plus maze (EPM) to examine anxiety levels. The maze consists of two closed and two open arms (each arm is 30 cm long) raised above the floor by 80 cm. Each animal was placed on the centre of the maze and left to explore it for a single trial of 10 minutes. Noldus Ethovision Tracking package (version 8.5) was used to track the animals during the task. The main measures taken were distance travelled and time spent in open and in closed arms of the maze.

2.3.6 Startle curve

The startle curve is a measure of startle reactivity (and hearing ability). The animals were exposed to a range of volumes from 65dB (background level of volume) to 120dB for 20 minutes and their startle reactivity was measured as displacement of an accelerometer attached to the restrainer. Emotional and motor components also play a role in the startle reflex. The instrument used was the SR Lab apparatus from San Diego Instruments.

2.3.7 Pre-pulse inhibition

Two days after the startle curve task, mice were tested in the pre-pulse inhibition task. Pre-pulse inhibition (PPI) measures sensorimotor gating which is partly controlled through the cortico-striatal pathway (Graybiel, 2000). The pre-pulse inhibition also provides an even more sensitive measure of hearing. During the task which lasts for 20 minutes, animals were exposed to 120dB startle trials which were preceded with a range of pre-pulses above the background level of

65dB. The pre-pulse levels were 4, 8 and 16dB above the background level of 65dB. Normally, the preceding stimulus attenuates the startle response. It has been shown that animal models of schizophrenia have dysregulated pre-pulse inhibition (Powell et al., 2009). Decreased PPI is observed in Huntington's disease patients (Swerdlow et al., 1995). Moreover, the *Zdhhc17* KO mice have decreased pre-pulse inhibition (Singaraja et al., 2011). The instrument used was the SR Lab apparatus from San Diego Instruments.

2.3.8 Morris water maze

The animals were tested in the Morris water maze in order to assess spatial learning and reference memory which is dependent on hippocampal NMDA-receptor function (Morris, 1989; Tsien et al., 1996).

Based on external cues on the walls of the room, the animals needed to orientate themselves in order to find a submerged platform positioned either on the North (N) or South (S) area of a water maze.

For the purposes of the task, a round black IR-translucent Perspex tank 98 cm diameter stood on an IR lightbox and was filled with tap water and left overnight to reach room temperature (21°C). Then, a round 10 cm transparent platform was submerged 1 cm below the water surface of the maze.

During the first day of the task, a habituation period of 60 seconds took place where the platform was placed at the centre of the round water maze. Each mouse was placed on the platform and was given a small boost to start swimming and explore the maze. If the animal did not return to the platform within the 60 seconds of the habituation, the researcher placed it on the platform for 5 seconds. The animal was then removed from the maze and dried out under a heat bulb.

Following the habituation period and for 5 subsequent days, 4 acquisition trials of 60 seconds maximum took place each day using pseudorandomly various release

points that are not close to the platform (Figure 2.1). The platform was placed at a distance of 20 cm from the maze wall towards the centre of the maze for the acquisition trials.

More precisely, when the platform was placed on the N of the maze, the release points of East (E), Southeast (SE), South (S), Southwest (SW) and West (W) were used and not the N, Northwest (NW) and Northeast (NE) release points as they were very close to the submerged platform and thus it is very easy for the mouse to find the platform by chance (Figure 2.1). If the mouse did not locate the platform within 60 seconds, it was placed on the platform for 5 seconds. The animal was always given 10 minutes rest between trials in order to avoid hypothermia.

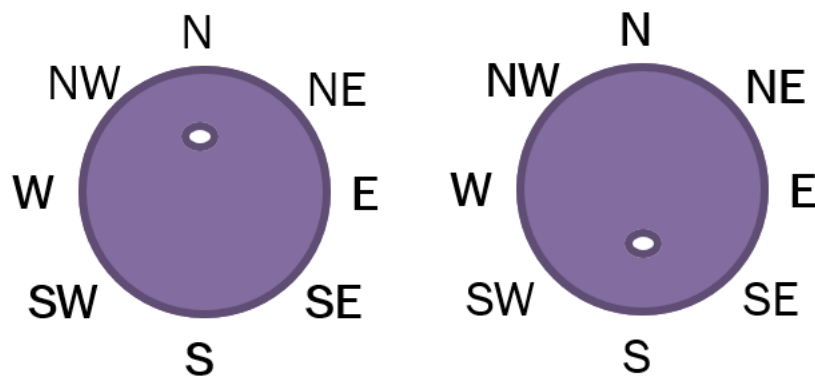


Figure 2.1 Map of the Morris water maze, the submerged platform (white circle) and the various release points. With bold letters, the release points that are actually used are depicted depending on the place of the submerged platform. When the platform was placed on the north (N) of the water maze, the release points of N, NE and NW were not used because of their proximity to the platform. Respectively, when the platform was placed on the south (S) of the water maze, the release points of S, SW and SE were not used.

Half of the animals were trained to find a N hidden platform and the other half were trained to find a S hidden platform in order to exclude any possibility of

preference for a specific location. Floaters (not common in this study) were excluded from the experiment. The Ethovision tracking software version 8.5 was used throughout the experiment and the main measures taken were duration to find the platform (latency), distance moved and mean velocity.

Probe trial

On the 6th day, a single probe trial of 60 seconds took place where the platform was removed and the time the animal spent swimming in the quadrant where the platform was *versus* the opposite quadrant was measured in order to assess reference memory.

Visual cue test

On the 7th day of the experiment a visual cue test of 60 seconds maximum duration was conducted to exclude any visual problems, motivation differences or motor dysfunction. Before the visual cue test, all the external cues were covered as a white curtain was placed around the water maze hanging from the wall. The platform was this time positioned 2 cm above the water level and a yellow flag was placed on it to make it easily visible. The animal was put in the water maze near the maze wall and the time the animal spent to reach the platform was noted.

2.3.8.1 Reversal learning version of Morris water maze

For the reverse learning version of the Morris water maze, on the 8th day the platform position was reversed and the animals were tested for another week using the new platform position. On the 13th day, a probe trial took place and on the 14th day a visual cue trial was conducted.

2.3.8.2 Working memory version of Morris water maze

Mice were initially tested in the original water maze protocol and then beginning 3 days after the last reference memory session, mice were tested for 3

consecutive days in the water maze with a different platform position each day. For these tests the platform was smaller (7 cm diameter) to increase difficulty. On each day, mice were allowed up to 7 trials and given a score which was the number of trials required to reach a criterion of reaching the platform in 10 seconds or less for two consecutive trials. If the criterion was not reached by the 7th trial, a score of 8 was given if it would be possible to reach criterion on the next trial, otherwise a score of 9 was given. Their score indicated the number of trials they needed in order to reach the criterion.

2.3.9 Three-chamber apparatus for sociability and social novelty

In order to assess sociability and social novelty the Ugo Basile/Stoelting 3-chamber apparatus was used. The apparatus is a clear Perspex box separated into 3 chambers (each chamber 40 cm x 20 cm). The partitions have openings (10 cm x 6 cm) that allowed the mouse to move freely from chamber to chamber. Two cylindrical wire cages (16 cm in height; 9 cm diameter) were used to contain the stranger mice and were placed in the side chambers.

Each animal was placed in the middle chamber and left to explore the whole apparatus for a 5-minute habituation period. Then a novel C57BL/6 adult male mouse was used as stranger mouse and placed in one of the cages. The experimental animal was then left to explore the apparatus for a 10-minute period which assesses sociability based on the time the experimental animal spent in the chamber where the novel mouse was versus the empty chamber. Then another novel mouse was introduced in the other cage and the experimental animal was left for 10 additional minutes to explore the apparatus in order to assess social novelty based on the time the experimental animal spent in the chamber where the new mouse was put *versus* the chamber with the first stranger mouse. Noldus Ethovision tracking package (version 8.5) was used to track the animals during the task. The main measures taken were distance travelled and time spent in the chamber where the first or second stranger mouse was placed.

2.3.10 Sucrose preference task

During the sucrose preference task, the preference of mice for a 1% w/v sucrose solution *versus* water was studied. 24-hour water/sucrose consumption was measured for a period of 5 days in order to determine if the mice experienced anhedonia which is the core symptom of depression based on their preference for sucrose *versus* water and in the event of anhedonia their preference for sucrose is low. For this study, the animals were housed in separate cages and weighed every day.

2.3.11 Pairwise discrimination task

The Pairwise discrimination task was conducted using the touchscreen testing method 89540- Pairwise Discrimination Task for Mouse by Campden Instruments Ltd. This is a computer-automated behavioural testing method that allows computer graphic visual stimuli to be presented to rodents and the rodents to respond to the stimulus on the computer screen via a nose-poke (Bussey et al., 2008).

The pairwise discrimination task and the reversal learning mode of it were used to identify memory or cognitive flexibility deficits. During the pairwise discrimination touchscreen task, the mice must learn that of two visual stimuli, only one is associated with a reward (strawberry flavoured milk). When the mice learned which stimulus was associated with a reward, the contingencies were reversed.

Before conducting the task, mice were habituated to being picked up and handled for 5 min per day for 5 days. Mice were also food-restricted to 85-90% of their free feeding weight according to a normal growth curve to provide an incentive to work in the task. Food restriction started 5 days before the initial training period.

The mice then underwent a training period for 10 days, which involved habituation in the touch screen apparatus (day 1) and initial touch training (day 2) where mice learned that only by nose poking the touchscreen (without any specific stimulus displayed), they could get a reward. Then, on day 3 and day 4 the mice gained a reward only after touching the screen when a stimulus was presented ('must touch training'). Finally, during the 'punish incorrect training' (from day 5 to day 10) the light of the apparatus was turned on after touching the blank screen instead of the stimulus presented and no reward was given in this case and the animals received a time out period in illuminated apparatus.

The visual discrimination task was then performed for a period of 15 days, followed by the same period of testing after reversal of the contingencies. Each day of testing involved the completion of 30 trials in less than 60 minutes. A trial starts with the presentation of two novel objects on the screen; one was set as being correct and the other one as incorrect. The mouse must nose poke the correct object in order to get the liquid reward. When it exits the food tray, the next trial starts. If the mouse pokes the incorrect object, no reward is given and the light of the apparatus turns on for 5 seconds before a correction trial starts. The correction trial consists of presentation of the same objects at the same position. Correction trials continue until the correct object is chosen.

2.3.12 Same paired associated learning (sPAL)

The same paired associate learning (sPAL) is a variant of the pairwise discrimination task. In the sPAL task, mice learn and remember which of three objects goes in which of three spatial locations. On a given trial, two identical objects are presented; one in its correct location; the other in an incorrect location. The rodent must choose which stimulus is in the correct location.

The first five days of testing in the touch screen boxes involved initial training, after which the mice started training in the full task.

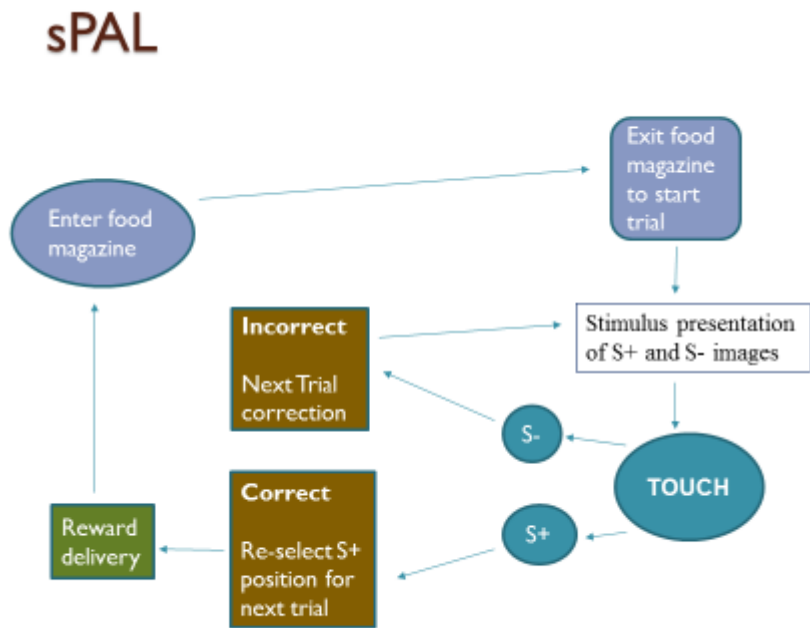


Figure 2.2 Illustration of the sPAL task (details in the text).

A trial begins with the presentation of two novel stimuli on the screen; one is programmed as being correct (S+) and one as being incorrect (S-) (Figure 2.2). Whether the S+ is on the right or left is determined pseudorandomly. The mouse must nose-poke the correct stimulus to elicit a food delivery response. If the mouse nose-pokes the incorrect stimulus, no reward is delivered and a time out period follows before the mouse is given the opportunity to complete a correction trial. Correction trials ensue until the correct stimulus is chosen. A correction trial consists of re-presentation of the stimulus array in the same Left-Right configuration.

PAL assesses visual memory and new learning, and is an essential tool for accurately assessing individuals with possible dementia, mild cognitive impairment, Alzheimer's disease, and age-related memory loss.

2.3.13 Five Choice Serial Reaction Time Test

The Five Choice Serial Reaction Time Test (5CSRTT) is designed to allow mice to associate light with a reward after nose-poking the location where the light appears. The test measures visuospatial attention and motor impulsivity.

This task was conducted by a Master's student in our group (Lee Wheeler). For this task, 9-hole operant boxes (Cambridge Cognition) were used after blocking four of the holes, giving five sites where a nose-poke can be registered by a mouse (holes 1, 3, 5, 7, 9). Lights that can illuminate above each hole signify the hole that the mouse is expected to nose-poke to receive the reward. On the reverse side of the box, an opening with a reward tray can pump a liquid reward into a small trough with a light to illuminate the area of the reward in the event of a correct response. The liquid reward used was a strawberry milkshake (Yazoo). The testing boxes were connected to a camera to allow visualisation of the animals during the task as well as a computer running a specialised software designed for use with the boxes (CCL control data handling software from CeNeS Cognition).

To motivate the mice to work for a reward, animals were food restricted to 90% of their free feeding weight (as ascertained by a growth curve for the control and background strain of the C57BL/6). Access to free feeding was removed a week before the habituation period to ensure that the animals would be motivated to receive the liquid reward and during that week the animals were offered small amounts of the milkshake to ensure that they were familiarized to consume it. The animals were weighed on a daily basis, after the trial and at around the same time each day.

During habituation and test period, each animal was tested for 30 min unless completing 100 trials in less time. During habituation in the box which lasted for a week, there was an illumination period of 32 sec and then the mouse would get a reward only after nose-poking the correct hole.

The habituation week was followed by the test period: the illumination was reduced to 16 sec and once the majority of the group reached more than 80 trials, the group was moved to the next level with further decreased illumination time (8, 4, 2 and 1 sec) over a 12 week period. The final week of testing included illumination for 0.8 sec.

After the final week of testing, two variations were run for an additional week. The first variation included randomisation of inter-trial intervals on a per trial basis between four different settings (4.5, 6, 7.5 and 9 sec). In the second variation the illumination period was similarly randomised among four periods shorter than 0.8 sec.

2.4 Mouse transcardial perfusion for ex vivo MRI

In order to perform *ex vivo* MRI scan of mouse brain, transcardial perfusion was performed. Initially, the animal was weighed and then put under deep anaesthesia by injecting intraperitoneally a mixture of lidocaine and pentobarbital in a 1:1 ratio (v/v) depending on the body weight. The dose of the mixture used was 0.008 ml/g of body weight. Then, the thoracic cavity was opened with scissors. The right atrium of the heart was cut and then the left ventricle was slowly and steadily injected with 20 ml of PBS to flush out the blood. An indication of the blood being flushed out was the colour change of the liver from dark red to light red. Then, 20 ml of 4% PFA in PBS (v/v) was steadily injected into the left ventricle.

Afterwards, the head was isolated from the rest of the body for brain extraction. For imaging the brain at high resolution, the brain was removed from the skull. This allows the brain to be perfused with gadolinium contrast agent evenly and to have a smaller field of view when the MRI is acquired, so the resolution is increased in a shorter time with better SNR (Signal to noise ratio). The midline of the skull was cut up, from the foramen magnum toward the frontal bone along the sagittal suture. Each side of the skull was then carefully peeled off, taking care that the meninges

did not pull parts of the cerebral hemispheres off with them. The brain was subsequently scooped out and kept in 4% PFA in PBS along with the medulla and olfactory bulbs at 4°C.

2.5 Fast low angle shot magnetic resonance imaging (FLASH MRI) and analysis

Brains were stored at 4°C for 7 days in order to then perform T1 weighted imaging and was sent to the University of Liverpool where the MRI scanning was performed in the laboratory of Professor Harish Poptani. The brain was initially incubated in 1.5% MultiHance contrast agent by Bracco Diagnostics containing 5.0 mM of Gadobenate Dimeglumine in 4% Paraformaldehyde in PBS at 4°C for 4 days prior to imaging. Gadolinium is the main chemical agent contained in Multihance that reduces the T1 relaxation time (Raymond and Pierre, 2005).

For imaging, the brain was placed into a pool of fluorinated oil within a holder before being put into the magnet. Adjusting the brain in the right position within the magnet took place before scanning. A 28mm resonator coil was used and all images were acquired at RT. The acquisition time was 2 hours and 3 minutes in a 9.4 Tesla pre-clinical horizontal bore Bruker magnet and a resolution of 41 µm. Images were preliminarily reconstructed using Paravision 6.0.1.

For analysis, manual morphometry was used. Manual image segmentation and structural volumetric analysis were carried out in Amira™6.01 software. The whole brain, corpus callosum and hippocampus were segmented using a number of semi-automatic segmentation tools within the software. A surface generate module was attached to each of the segmentation labels and a surface view module was then used to obtain a 3D reconstruction. Material statistics were used to evaluate the number of voxels contributing to each of the segmented structures.

2.6 Mouse brain isolation and storage for non-MRI experiments

Adult male mice (8-10 weeks old) were humanely killed by cervical dislocation. Brains were isolated and kept for protein analysis, DNA and RNA extraction. For protein assays, immediately after dissection, the brain was put in cold falcon tubes and stored at -80 °C. For DNA extraction, part of tissue stored at -80°C was used.

For RNA extraction, the frontal cortex and the hippocampus were dissected and kept separately from the rest of the brain. For RNA stabilization, 10 µl of RNA Later solution (Qiagen, East Sussex UK) was added per 1 mg of tissue. Firstly, the tissue was cut into slices less than 0.5 cm thick and put into RNA Later solution, followed by overnight incubation at 4°C. Brain tissue was then removed from the solution and kept at -80°C for long-term storage.

2.7 Molecular Biology

2.7.1 DNA extraction from mouse brain tissue

DNA extraction from mouse brain tissue was conducted using the Isolate Genomic DNA Mini kit (Bioline, London UK) according to the instructions of the supplier. For all centrifugations, the Eppendorf centrifuge 5415 R (Fisher Scientific) was used.

Briefly, up to 40 mg brain tissue was cut into small pieces and placed in a 1.5 ml polypropylene tube. 400 µl lysis buffer and 25 µl proteinase K were added to the sample and mixed by vortexing. The sample was incubated at 50°C with intermittent vortexing until lysis was optimal. The sample was then centrifuged at 10,000 x g for 2 min, followed by transfer of the supernatant to a 1.5 ml tube. 200 µl binding buffer was then added followed by vortexing for 15 sec. The sample was transferred to a spin column that was placed in a collection tube and centrifuged at 10,000 x g for 1 min. The spin column was then placed in a new collection tube.

700µl wash buffer was then added to the column and centrifuged at 10,000 x g for 1 min. The flow-through was then discarded. This washing step with centrifugation was repeated and the sample was then centrifuged again at 14,000 x g for 2 min. The collection tube was then discarded and the spin column was placed in a new 1.5 ml elution tube. 200 µl elution buffer was added directly to the spin column membrane which was then incubated for 1 min at room temperature (RT). A final spin of 6,000 x g for 1 min was sufficient to elute the DNA which was kept at 4°C for short-term storage or at -20°C for long term storage after determining its concentration.

2.7.2 RNA isolation from mouse brain tissue

For RNA isolation, all pipettes and surfaces were cleaned with RNase Zap. Sterile, RNase-free pipette tips and Eppendorf 1.5 ml tubes were also used. The RNeasy Lipid Tissue Mini Kit (Qiagen, East Sussex UK) was used for RNA extraction according to the instructions of the supplier. For centrifugations at RT, the Eppendorf centrifuge 5415 R (Fisher Scientific, Loughborough UK) was used while at 4°C, the Heraeus multifuge 3 S-R (DJB Labcare, Milton Keynes UK) was used.

A maximum of 500 mg mouse brain tissue was processed in the first steps of the procedure. The brain tissue was removed from storage and its weight was determined. Disruption and homogenization of the tissue was conducted using a Polytron homogenizer (T25 basic, IKA Labortechnik): the tissue was placed in a suitably sized vessel (according to the instructions of the homogenizer) containing 5 ml QIAzol Lysis Reagent (Qiagen, East Sussex UK) and the homogenizer was operated at full speed until the lysate was uniformly homogeneous (30–60 s). The tube containing the homogenate was then placed at RT for 5 min. This step promotes dissociation of nucleoprotein complexes.

1 ml chloroform was then added, and the tube was shaken vigorously for 15 s for subsequent phase separation and incubated at RT for 2–3 min. Then a centrifugation at 5,000 x g for 15 min at 4°C took place and the sample separated into 3 phases: an upper, colourless, aqueous phase containing RNA; a white interphase; and a lower, red, organic phase. The upper, aqueous phase was transferred to a fresh tube. Only 600 µl of this phase was used and the rest of the sample was kept at -80°C. Then, one volume of 70% ethanol was added to the upper phase and the tube was mixed thoroughly by vortexing. Up to 700 µl of the sample was transferred to an RNeasy Mini spin column placed in a 2 ml collection tube (supplied by the kit), and centrifuged for 15 s at 9,000 x g at RT. The flow-through was discarded, and the remainder of the sample was transferred to the RNeasy Mini spin column and the same centrifugation step was repeated. The flow-through was discarded again.

The following steps included on-column DNase digestion with the RNase-Free DNase Set (Qiagen, East Sussex UK). Firstly, 350 µl Buffer RW1 (supplied) was added to the RNeasy spin column which was then centrifuged for 15 s at 9,000 x g to wash the membrane. The flow-through was discarded. 15 µl DNase I stock solution was added to 105 µl of Buffer RDD, mixed by gently inverting the tube and added directly to the RNeasy spin column membrane. The spin column was then placed on the benchtop for 30 min. Following this, 350 µl Buffer RW1 was added to the RNeasy spin column, which was then centrifuged for 15 s at 9,000 x g, and the flow-through discarded. 500 µl Buffer RPE was added to the RNeasy spin column and then centrifuged for 15 s at 9,000 x g to wash the membrane. The flow-through was discarded and 500 µl Buffer RPE was again added to the RNeasy spin column and centrifuged for 2 min at 9,000 x g to ensure that no ethanol was carried over during RNA elution.

The RNeasy spin column was placed in a new 2 ml collection tube (supplied with the kit) and the old collection tube with the flow-through was discarded. A

centrifugation step was conducted at full speed for 1 min to eliminate any possible carryover of Buffer RPE or residual flow-through. The RNeasy spin column was placed in a new 1.5 ml collection tube and 50 µl RNase-free H₂O were finally added directly to the spin column membrane. Then the sample was incubated for 1 min at RT and a centrifugation for 1 min at 9,000 x g eluted the RNA which was subsequently stored at -80°C after determining its concentration.

2.7.3 Spectrophotometric quantification of DNA and RNA

The concentration of isolated DNA and RNA as well as their purity were measured using the Nanodrop 2000c spectrophotometer (Thermo Scientific, Loughborough UK) at 260nm. 2 µL of each sample was sufficient for analysis.

2.7.4 End-point polymerase chain reaction (PCR)

End-point polymerase chain reaction (PCR) was used to amplify specific *Zdhhc9* DNA and cDNA sequences. The PCR reaction mix was prepared at RT and contained half the final volume of 2x GoTaq Hot Start Green Master Mix (Promega, Southampton UK), 0.5 µM of each primer (Forward and Reverse), 1 µl of cDNA and H₂O to a final volume of 20 µl.

For cloning *Zdhhc9* KO transcript cDNA, KOD Hot Start DNA polymerase was used (Novagen, Livingston UK). The PCR reaction mix was prepared at RT and contained 1/10 of the final volume of 10x Buffer for KOD Hot Start DNA Polymerase, 0.02 U/µl of KOD Hot Start DNA Polymerase, 0.3 µM of each primer (forward and reverse), dNTPs (0.2 mM each), 2.5 mM of MgSO₄, 2 µl of DMSO, 50 ng of plasmid DNA template and H₂O up to a final volume of 50 µl.

The sequences for all the primers used in this study are shown in the following table.

Table 2.2 DNA sequences for all the primers used in this study (shown in 5' to 3' orientation).

Primer name	Primer Sequence (5'-3')
Primers for genotyping	
DNA196-5	GAAAGAAGGTGACACGGAAATG
DNA196-6	CAAATGCCCAGGAGGTACTGT
Neo3a	GCAGCGCATCGCCTTCTATC
Primers for end-point PCR and qPCR	
MA1 F	AAAGCCCATCTTGGACCAGGAAC
MA1 R	TCAACAGCGTGGCCATGGAG
MA2 F	GTGATGGCCGCGTCATGATG
MA2 R	AAGAGCATAGCGGCAAACACAGG
z9v1 F	ATCGTCTATGTGGCCCTCAAATCC
z9v1 R	GGAATGTGTGAAATCCAGTCAGCC
z9v2 F	ATCGTCTATGTGGCCCTCAAATCC
z9v2 R	AGACGGCTTCACACGGACGAAC
PPIA F	TATCTGCACTGCCAAGACTGAATG
PPIA R	CTTCTTGCTGGTCTTGCCATTCC
HPRT1 F	CTCATGGACTGATTATGGACAGGAC
HPRT1 R	GCAGGTCAGCAAAGAACTTATAGCC
TBP F	CCGTGAATCTTGGCTGTAACTTG

TBP R	GTTGTCCGTGGCTCTTATTCTC
MAO F	TCAGGGAGAAGTCGCTACCACC
MAO (B) F	CCGAGTTCAGTGTCCCTTGTTCA
3UTR R	TGGCATCTTCTGCCACTGTCTTAA
3UTR (B) R	AAAGTTTGCAGCAAGAAGATGCC
Primers for sequencing	
3UTR R s	CATCTTCTGCCACTGTCT
3UTR (B) R s	GCAAGAAGATGCCGGTAA
MAO F s	GAAGTCGCTACCACCTCT
Primers for cloning	
BAM ZD9 F	GATCGGATCCATGCTCTTTCTTTTCTCCA
BAM ZD9 R	GATCGGATCCCTACTTCTCAGCTTCGGA

The Veriti 96 well thermal cycler (Applied Biosystems, Loughborough UK) was used for the PCR reaction which consisted of an initial polymerase activation step of 2 min at 95°C, followed by 30 cycles of a denaturation step of 30 sec at 95°C, an annealing step for 30 sec at 54-58°C depending on the primers used each time, and an extension step at 72°C for 30 sec-5 min depending on the length of the expected product. A final extension step for 5 min at 72°C was also included.

For cloning, an initial polymerase activation step of 2 min at 95°C was used, followed by 30 cycles of a denaturation step of 20 sec at 95°C, an annealing step for 10 sec at 63°C and an extension step at 68°C for 1 min.

PCR products were stored at 4°C before agarose gel electrophoresis was used to determine their quality.

2.7.5 Agarose gel electrophoresis

Separation and analysis of DNA fragments was performed by agarose gel electrophoresis. In this method, an electric field is applied to move the negatively charged DNA through a matrix of agarose. Shorter molecules move faster than longer ones because they migrate more easily through the pores of the gel. The electrophoresis tank was purchased from Thermo Fisher Scientific (Loughborough UK). A concentration of either 1 or 2 % (w/v) agarose (Bio-Rad, Herts UK) was used to make gels, supplemented with Sybr Safe® (Life Technologies) at a 1:10,000 dilution. The gel was submerged in TAE buffer (0.04 M Tris, 1 mM EDTA, acetic acid to pH 8) and 10 µl of DNA sample were loaded onto the gel in 2.5 µl of sample loading buffer supplied with the marker of molecular weight. The HyperLadder 1 kb and the HyperLadder 100 bp (Bioline, London UK) were used as markers of DNA size. After electrophoresis at 80 V, the gel with the DNA samples was observed under ultraviolet light.

2.7.6 Reverse transcription PCR

Reverse transcription of RNA was conducted using the Tetro cDNA synthesis kit (Bioline, London UK). Firstly, all pipettes and surfaces were cleaned with RNase Zap (Sigma Aldrich). Sterile, RNase-free pipette tips and Eppendorf tubes were also used. The reaction was prepared on ice and contained 1/20 the final volume of oligo (dT)₁₈ primers (supplied with kit), dNTP mix (final concentration of 0.5 mM), Reverse transcription buffer (supplied with kit), RNase inhibitor (final concentration of 0.5 U/µl), Tetro Reverse Transcriptase (final concentration of 10 U/µl), up to 5µg RNA and DEPC-treated H₂O to a final volume of 20 µl. The samples were then incubated

at 45°C for 30 min in a Veriti 96 well thermal cycler (Applied Biosystems, Loughborough UK); the reaction was terminated by heating at 85°C for 5 min and the samples were then put on ice. The cDNA was stored at -20°C until further use.

2.7.7 Quantitative PCR (qPCR)

Quantitative (formerly real time) PCR (qPCR) was performed in AB Applied Biosystems Step One Plus Real Time PCR System, using the SYBRR Select Master Mix (Life Technologies, Paisley UK). The main component of the Master Mix is the SYBRR GreenER™ dye which detects PCR products by binding to double stranded DNA formed during PCR. Other components of the Master Mix are AmpliTaqR DNA Polymerase Ultra Pure (UP) with a hot start mechanism, Heat-labile Uracil-DNA Glycosylase (UDG), ROX™ dye Passive Reference and dNTP blend containing dUTP/dTTP.

Before preparing the reaction, all pipettes and surfaces were cleaned with RNase Zap (Sigma Aldrich). Sterile, RNase-free pipette tips and Eppendorf tubes (fast reaction tubes with cap by AB Applied Biosystems) were also used. The reaction was prepared at RT and contained half the final volume of 2x SYBRR Select Master Mix, 1µl cDNA, 0.1 µM of each primer (forward and reverse) and DEPC-treated H₂O to a final volume of 20 µl.

The PCR reaction consisted of an initial polymerase activation step of 2 min at 95°C, followed by 40 cycles of a denaturing stage of 15 sec at 95°C and an annealing and extension step at 60°C for 1 min. A melting curve analysis was included consisting of 95°C for 15 sec, 60°C for 1 min and 95°C for 15 sec.

2.7.8 Plasmids

Mouse HA tagged- Zdhhc9 construct in pEF-BOS vector was provided by Professor Masaki Fukata (Fukata et al., 2004).

2.7.9 Sequencing

Samples and primers were sent to the GATC Company (Konstanz, Germany), who undertook sequencing using an ABI automated Sanger sequencer (primer sequences shown in Table 2.2). The results were analysed either with Geneious 8.0.4 program or with EMBOSS Water for Pairwise Sequence Alignment (free available online).

2.7.10 Cloning of Zdhhc9 KO cDNA into the pEF-BOS-HA plasmid

After amplification of the mutant cDNA using primers that contain BamH1 sites (Table 2.2), agarose gel electrophoresis was conducted in order to assess the amplified product. Then the Invitrogen™ PureLink™ Quick Gel Extraction Kit (Thermo Fisher Scientific) was used to isolate the amplified DNA following the instructions of the supplier.

The pEF-BOS-HA plasmid vector that contains a BamH1 site and encodes a triple HA-tag at the N-terminus (total vector size 5.4 kb) was digested by BamH1 enzyme. Specifically, 2 µl of FastDigest BamH1 was used along with 2µl of 10x FastDigest Green Buffer, 2µl of Fast AP (alkaline phosphatase; all three components from Thermo Scientific, Loughborough UK), 1 µg plasmid DNA and H₂O up to a final volume of 20 µl. The reaction mix was incubated in water bath for 50 min at 37°C. Then, denaturation of the phosphatase at 65 °C for 15 min followed. In order to assess the digestion, 5µl of digested pEF-BOS-HA was used for 1% agarose gel electrophoresis. The amplified mutant DNA was also digested as described for the plasmid. Using again the same gel extraction kit as above, the insert was isolated.

Then ligation reaction took place at RT using 2 µl of T4 DNA ligase (Promega), half the final volume of 2X Rapid Ligation Buffer (Promega), 1 µl of the digested

vector, 2 μ l of the insert (PCR product) and H₂O up to a final volume of 12 μ l. The reaction mix was left at RT for 1.5 h.

For transformation, half of the ligation mix was added to One Shot® TOP10 Chemically Competent *E. Coli* cells (Life Technologies) and incubated on ice for 15-30 min. Afterwards, cells were transferred for 30 sec into a 42 °C water bath and then returned to ice for 2 min. 250 μ l of autoclaved Lysogeny Broth (LB, 10 g/l NaCl, 10 g/l tryptone, 5 g/l yeast extract medium) was added on cells under sterile conditions (near flame). Cells were then incubated for 1 h at 42°C with constant shaking before being plated on LB agar (15 g/l agar in LB) plates containing ampicillin (100 μ g/ml) as selective antibiotic under sterile conditions and placed for overnight incubation at 37 °C .

Small-scale plasmid purifications (Minipreps) were prepared from the plates that had bacterial growth. Each bacterial colony was placed in 5ml LB medium that contained ampicillin (100 μ g/ml) and incubated overnight with shaking at 200 rpm at 37 °C. The following day, cultures were placed at 4 °C till plasmid DNA extraction was conducted using the PureLink™ Quick Plasmid Miniprep Kit (Life Technologies) following the instructions of the supplier.

After isolating the plasmid DNA, digestion with BamH1 was conducted in order to assess if the cloning was successful based on the observation of the insert after agarose gel electrophoresis (insert size~ 1,000bp). Then samples that had the insert were sent for sequencing to confirm that the insert had the correct orientation.

After receipt of the sequencing results, some of the Miniprep colony was put in 100ml LB medium with 100 μ g/ml ampicillin and incubated with rocking overnight at 37 °C in order to create a large-scale plasmid purification preparation (Midiprep). Then the Plasmid DNA purification NucleoBond Xtra Midi kit (Macherey-Nagel, Duren Germany) was used in order to extract the DNA plasmid following the

instructions of the supplier. The isolated DNA plasmid was then used for transfection of HEK293T cells after determining its concentration.

The remaining Miniprep colony was kept to create a glycerol stock under sterile conditions (50% glycerol v/v) which was snap-frozen and then stored at -80 °C.

2.7.11 Plating HEK293T cells

For cell culture, 0.05 % Trypsin-EDTA and heat inactivated foetal bovine serum (FBS) were purchased from Life Technologies. 75 cm² flasks and BioCoat Poly-D-Lysine 24-well plates were obtained from Corning Incorporated. Cellcoat® Poly-D-Lysine 6-well plates were purchased from Greiner Bio-One.

Human Embryonic Kidney 293 cells that express a mutant of the SV40 large T antigen (HEK293T) were purchased from ATCC. Cells were grown in Dulbecco's Modified Eagle Medium (DMEM, Life Technologies) with 10% FBS and maintained at a humidified atmosphere of 37°C/ 5% CO₂. Cells growing in a 75 cm² flask were plated after briefly being washed in 3 ml of Trypsin (pre-heated at 37°C) and then incubated for 3 min at 37°C in 3 ml Trypsin. Cells were detached from the flask by gentle agitation and pipetting and plated at a dilution of 1:10 for 6-well plates and 1:6 for 24-well plates.

2.7.12 Transfection of HEK293T cells

Cells were transfected 24 hours after being plated. Lipofectamine2000 reagent (Invitrogen) was used for all transfections. For double transfections, 0.5 µg of each plasmid was added to 50 µl of serum-free DMEM in a sterile 1.5 ml tube. For immunofluorescence, 2 µg of plasmid was used for single transfection. Then, Lipofectamine 2000 was added into 50 µl of serum-free DMEM at a 2µl/µg DNA

ratio. The mixes were then incubated for 5 min at RT, and subsequently combined and incubated at RT for 20 min. The final mix was then added to cells, which were returned to the incubator. Cells were analysed 24 hours post-transfection.

2.8 Biochemistry

2.8.1 HEK293T cell lysates

24 hours after transfection, HEK293T cells were briefly washed twice with ice-cold phosphate-buffered saline (PBS, 136.89 mM NaCl, 2.68 mM KCl, 10.14 mM Na₂HPO₄, 1.76 mM KH₂PO₄, pH 7.4) and then lysed in 100µl of Laemmli sample buffer [50 mM Tris (pH 6.8), 0.1 % (w/v) bromophenol blue, 10 % (v/v) glycerol, 2 % (w/v) sodium dodecyl sulphate (SDS), 25 mM dithiothreitol (DTT)]. Samples were then incubated at 95°C for 5 min and analysed by SDS-PAGE.

2.8.2 Determination of protein concentration

To determine total protein concentration in samples, Thermo Scientific™ Pierce™ BCA Protein Assay kit was used. The assay is a detergent-compatible formulation based on bicinchoninic acid (BCA) for the colorimetric detection and quantitation of total protein.

Firstly, protein standards of various known concentrations were prepared from bovine serum albumin (BSA) following the manufacturer's instructions. Briefly, the contents of a BSA ampule provided by the kit were diluted into several Eppendorfs, using the same diluent as the sample of interest (PBS). The sample of interest was also diluted in ratios of 1:10 and 1:20 to ensure that its absorbance would fall within the range of the BSA standards.

50 parts of BCA Reagent A were mixed with 1 part of BCA Reagent B (ratio 50:1). Then 0.05mL of each standard and unknown sample was transferred into test tubes

and 1mL of the BCA reagent was added to each tube and mixed by vortexing. The tubes were covered and incubated at 37°C for 30 minutes in a water bath and then put on the benchtop to reach RT. The absorbance of each sample at 562 nm was measured using a Pharmacia Biotech Ultrospec 2000 UV/Visible spectrophotometer. A standard curve was prepared by plotting the absorbance of each BSA standard versus its known concentration in µg/mL. This standard curve was used to determine the protein concentration of the unknown samples.

2.8.3 Polyacrylamide gel electrophoresis and Western blot equipment

Gel plates, combs, casting stand and frame, electrophoresis chambers, transfer tanks, power supplies and nitrocellulose membranes were purchased from Bio-Rad.

2.8.4 Sodium dodecyl sulphate (SDS) - polyacrylamide gel electrophoresis (PAGE)

SDS-PAGE is a widely used technique for the separation of proteins according to their molecular weight. SDS is an anionic detergent that binds non-covalently to proteins, causing their denaturation and imparting a negative charge. Thus, when an electric field is applied, proteins migrate towards the anode through a polyacrylamide gel.

The gel was made by pouring two polyacrylamide solutions (one for the resolving gel and one for the stacking gel) between a glass cassette assembled in a casting stand and frame. Firstly, the solution for the resolving gel which is responsible for protein separation was made containing a 12% polyacrylamide concentration by mixing 5 ml of 2x resolving buffer (0.2% (w/v) SDS, 4 mM EDTA, 750 mM Tris, pH 8.9), 4 ml 30% acrylamide/bis-acrylamide (Sigma), 0.8 ml distilled H₂O (dH₂O), 8 µl N,N,N',N'-tetramethyl-ethane-1,2-diamine (TEMED, from Sigma), and 200 µl of 10% ammonium persulfate (APS) solution. TEMED polymerises acrylamide and bis-acrylamide and APS acts as a catalyst. The stacking gel had a polyacrylamide concentration of 4.5% and was used to improve the resolution of

the electrophoresis. It was prepared by mixing 3 ml of 2x stacking buffer (0.2 % (w/v) SDS, 4 mM EDTA, 250 mM Tris, pH 6.8), 0.9 ml 30 % acrylamide/bis-acrylamide, 1.95 ml dH₂O, 7.5 µl TEMED and 150 µl 10 % APS. A comb put in the gel creates wells for sample loading and is removed when the gel is polymerized.

The protein samples were prepared in Laemmli sample buffer and denatured at 95°C for 5 min. Afterwards, samples were loaded into the gel wells in a tank filled with running buffer [25 mM Tris, 192 mM Glycine (Fisher Scientific) and 0.1 % SDS (w/v)]. Prestained Protein Marker from New England Biolabs (7-175 KDa) or Ez-Run markers from Fisher (Loughborough UK, size range 20-118 KDa) was also loaded into the gel as marker of molecular weight. For sample migration through the stacking gel, 90 V were applied while through the resolving gel, 150 V were applied.

2.8.5 Antibodies

The following primary and secondary antibodies were used for Western blotting and immunofluorescence (Table 2.3).

Table 2.3 Primary and secondary antibodies used in this study for Western blotting or immunofluorescence.

Primary antibodies	Dilution	Technique
mouse Syntaxin (HPC-1, Sigma)	1:1,000	Western blotting
rabbit Csp-a (100 µg 1 mg/ml, EnzoLife Sciences)	1:5,000	Western blotting
mouse Snap25 (SMI 81, Covance)	1:5,000	Western blotting
rabbit H-Ras (C-20 SC-520, Santa Cruz)	1:300	Western blotting
mouse N-Ras (IgG1 F155 SC-31, Santa Cruz)	1:500	Western blotting
mouse β-actin (ab 8226, 100 µl 1.0 mg/ml, Abcam)	1:3,000	Western blotting
rat HA (High Affinity, Roche Diagnostics)	1:1,000	Western blotting

rabbit GAPDH (14C10, Cell Signaling Technology)	1:1,000	Western blotting
mouse VAMP1/2 (MAB 333, Chemicon International)	1:1,000	Western blotting
mouse VAMP2 (Synaptic Systems)	1:5,000	Western blotting
rabbit VAMP3 (Synaptic Systems)	1:1,000	Western blotting
mouse Synaptotagmin 1 (105011, Synaptic Systems)	1:1,000	Western blotting
mouse Vglut1 (Neuromab)	1:2,000	Western blotting
rabbit Vglut2 (ab84103, Abcam)	1:250	Western blotting
rabbit Flotillin 2 (Cell Signaling Technology)	1:1,000	Western blotting
mouse GluR1 (N355/1, Neuromab)	1:1,000	Western blotting
rabbit phospho-GluR1 (S845, Abcam)	1:1,000	Western blotting
mouse GluR2 (21/32, Neuromab)	1:500	Western blotting
rabbit PSD95 (Cell Signaling Technology)	1:1,000	Western blotting
mouse NR2b (N59/20, Neuromab)	1:500	Western blotting
rat CCR5 (MAB 6138, R&D Systems)	1:500	Western blotting
rabbit Pde10a (GTX118886, Genetex)	1:3,000	Western blotting
mouse Synaptophysin (MAB 368, Millipore)	1:20,000	Western blotting
mouse Calnexin (C45520 BD 610524, Transduction Laboratories)	1:1,000	Western blotting
mouse HA (16B12, Covance)	1:50	Immunofluorescence
rabbit GM130 (ab52649, Abcam)	1:50	Immunofluorescence

Secondary antibodies	Dilution	Technique
donkey anti-mouse, anti-rabbit or anti-rat IRDye 680RD (LI-COR)	1:10,000	Western blotting
donkey anti-mouse, anti-rabbit or anti-rat IRDye 800CW (LI-COR)	1:10,000	Western blotting
anti-mouse IgG, Peroxidase and anti-rat IgG, Peroxidase (GE, Healthcare) linked to horseradish peroxidase (HRP) enzyme	1:2,000	Western blotting
donkey anti-mouse AlexaFluor 488 IgG (H+L, Invitrogen)	1:400	Immunofluorescence
donkey anti-rabbit AlexaFluor 647 IgG (H+L, Life Technologies)	1:400	Immunofluorescence

2.8.6 Western blotting

After SDS-PAGE, proteins from the gel were transferred onto a nitrocellulose membrane (0.45 μm pore, Bio-Rad) for subsequent antibody detection. The membrane and 2 sheets of Whatman paper were soaked in transfer buffer (48 mM Tris, 39 mM Glycine, 1.3 mM SDS, 20 % methanol) and then the membrane was placed on the gel in a cassette between the two sheets of Whatman paper. The cassette was firmly closed and put into a Bio-Rad Trans-Blot Cell filled with transfer buffer before applying a constant current of 120 mA overnight. The gel was placed next to the cathode so that the proteins could migrate towards the membrane.

The membrane was then briefly washed in PBS-Tween [PBS plus 0.02 % (v/v) Tween 20] and incubated in 5 % (w/v) non-fat milk in PBS-T for 1 h to prevent non-specific binding of antibodies. The membrane was then briefly washed with PBS-T

and incubated with the primary antibody against the protein of interest for 1 h at RT or overnight at 4°C with constant agitation.

The membrane was then washed 4 times in PBS-T for 5 min per time and probed with the secondary antibody (1:10,000 dilution) for 50 min at RT with constant agitation. Finally the membrane was washed again 4 times in PBS-T and observed after being scanned in a LI-COR® Odyssey infrared Imaging System (LI-COR® Biosciences).

2.8.7 Cell fractionation and Resin-Assisted Capture of S-acylated proteins (Acyl-RAC)

Purification of S-acylated proteins using acyl resin-assisted capture (Acyl-RAC) was conducted in order to study palmitoylation in mouse brain tissue. This technique allows analysis of the level of palmitoylation of known palmitoylated proteins, or identification of novel palmitoylated proteins.

As the majority of palmitoylated proteins are membrane-associated, a membrane fraction was the starting material for this assay. In order to separate proteins associated to membranes from proteins localised in the cytosol or nucleus, differential centrifugation was applied during the first steps of the protocol. For cell fractionation analysis of Ras distribution between cytosol and membrane, cytosolic fractions were also collected.

Proteins which do not undergo S-acylation or other cysteine modifications contain unmodified cysteine residues with free Sulfhydryl (SH) groups. As the generation of free SH groups is a key step in the Acyl-RAC protocol to purify palmitoylated proteins, free SH groups are modified with S-methyl methanethiosulfonate (MMTS). This reagent blocks free SH-groups by adding a thiomethyl group via formation of a mixed disulfide bond.

In a subsequent step, S-acyl chains are cleaved by hydroxylamine (HA) treatment. HA reduces the thioester bond of proteins resulting in free SH-groups, which can then bind to Thiopropyl Sepharose® beads forming disulphide bonds, and allowing separation of proteins that were originally acylated from non-acylated proteins.

For the first steps of the protocol, buffer A (25 mM HEPES, 25 mM NaCl, 1 mM EDTA, pH 7.4) was prepared fresh the day before the experiment and kept at 4°C. Protease inhibitor cocktail was added to the buffer just before the experiment. Blocking buffer (100 mM HEPES, 1.0 mM EDTA, 2.5% SDS and 1.25% MMTS) and binding buffer (100 mM HEPES, 1.0 mM EDTA, 1% SDS) were also prepared fresh the day before the experiment. Blocking buffer was kept at 4°C while binding buffer was kept at RT.

Whole mouse brain was initially cut into pieces with a scalpel in order to facilitate homogenization; this step was not necessary when the starting material was isolated hippocampi. The tissue was then placed in a Dounce homogenizer with Buffer A, homogenized by 20 strokes and then passed at least 5 times through a syringe with a 26G needle (BD Microlance). The homogenate was centrifuged at 800 xg for 5 min at 4°C in order to pellet the nuclei. Then a differential centrifugation was conducted: the supernatant was centrifuged at 16, 100 xg for 50 min at 4°C in a TLA-55 Rotor. The supernatant of this centrifugation which is the cytosolic fraction was removed and kept for analysis in the case of cell fractionation experiment. The pellet which is the membrane fraction was re-suspended in 200µl buffer A containing 0.5% Triton X-100 (v/v). Total protein concentration was determined using the BCA protein assay kit in order to determine the amount of protein that would be used for the rest of the experiment.

Only part of the membrane fraction (100 µl) was used for Acyl-RAC and the remainder was stored at -80°C. In order to block free SH groups with MMTS, 200 µl

of blocking buffer was added to the membrane fraction and incubated for 1.5 h at 40°C in a dry bath with frequent vortexing every 15 min.

3 volumes of ice-cold 100% acetone were added to the mixture and incubated for 20 min at -20°C for protein precipitation. The mixture was then centrifuged at 5000 xg for 10 min at 4°C. The supernatant was removed and the pellet was air-dried and then washed five times by re-suspension in 1 ml of 70 % (v/v) ice-cold acetone by vortexing and then centrifugation at 5, 000 xg for 10 min at 4°C. The washed pellet was finally re-suspended in 400 µl binding buffer.

For the resin capture, the Thiopropyl Sepharose® beads were activated: 0.2 g of beads were put into a 15 ml falcon tube, which was then filled with dH₂O to the top and rotated for 15 min on a benchtop rotator (Blood tube rotator SBI by BIBBY Stuart Scientific). Then, the beads were pelleted by centrifugation at 1, 000 xg for 5 min. The excess water was removed and the activated beads were resuspended in appropriate binding buffer (0.1 g beads/ml binding buffer).

200 µl of the beads-binding buffer mixture was aliquoted into 1.5 ml Eppendorf tubes and centrifuged for 3 min at 800 xg. The binding buffer was carefully removed and the protein sample was split in 160 µl into reaction tubes which contained the previously activated beads (one for HA and one for Tris as a control). The remaining 80 µl was kept as total input control and stored at -80°C until further use. For treatment with HA, 2M HA at pH 7.2, which was prepared just before the experiment, was added to a final concentration of 0.5M. For negative control treatment, HA was replaced with the same concentration of Tris (Trizma base, Sigma), also prepared just before the experiment.

These samples were then incubated overnight at RT with end-over-end mixing on the benchtop rotator. In order to separate the beads from the unbound proteins, the samples were centrifuged at 800 x g for 5 minutes at RT. The supernatant was removed and retained as the unbound fraction.

The remaining beads were washed 5 times with 1 ml binding buffer by vortexing and pelleting the beads by centrifugation at 1, 000 xg for 30 sec. Subsequently, the proteins were eluted from the beads by incubations in 100 µl 1x Laemmli buffer containing 50 mM DTT for 15 minutes at RT and then 5 minutes at 95 °C. Then another centrifugation at 1, 000 xg for 30 sec was performed and the supernatant was retained. The eluted proteins represented the bound fraction. Before subjecting all samples to SDS-PAGE. The final volumes of the bound and unbound fractions were then equalised to 300 µl and the unbound and total input were mixed with Laemmli buffer containing 50 mM DTT for 5 minutes at 95 °C.

2.9 Immunofluorescence and confocal microscopy

HEK293T cells were plated in 6-well plates after putting two 12 mm pre-coated Poly-D-Lysine coverslips (Vitrocam, Surrey UK) per well. 24 hours later, cells were transfected using 2 µg plasmid DNA per well. The following day, the coverslips were washed x3 in PBS, and fixed in 4% Formaldehyde (16% Formaldehyde methanol-free from Thermo Scientific was diluted in PBS) for 20 min at RT. Then coverslips were washed twice in PBS containing 0.3% Bovine Serum Albumin (BSA, Fisher Scientific) and cells were permeabilized for 6 min in PBS containing 0.3% BSA and 0.25% Triton X-100. Then the coverslips were washed in PBS containing 0.3% BSA and the primary antibodies were added on for 1 h. Three washes with PBS-BSA followed before the secondary Alexa Fluor-conjugated antibodies were added for 1h (1:1,000 dilution in PBS/BSA). The coverslips were again washed 3 times with PBS-BSA and once with dH₂O before being air-dried for 30 min. The coverslips were then mounted on slides using Mowiol mounting agent. The next day, cells were observed under an SP5 confocal microscope (Leica Microsystems) using two different channels based on the secondary antibodies used.

2.10 Data analysis

The density of protein bands on immunoblots was quantified and background density of the same gel lane subtracted in order to measure relative protein expression. The software Image Studio™ Lite V3.1 (LI-COR Biosciences, Lincoln, NE, USA) was used for quantification of immunoblots visualised by the Odyssey® infrared imaging system (LI-COR). The relative protein levels were calculated using Excel software (Microsoft® Office system). The mean of the measured values was presented with the standard error of the mean (SEM). The results were plotted using GraphPad Prism® software or Excel.

Statistical analysis was conducted using either SPSS version 22 or Minitab version 17 software packages. For parametric data analysis, unpaired t-tests in Minitab or general linear model repeated measures (ANOVA) in SPSS were used as appropriate. For non-parametric data analysis, Mann-Whitney U test was used in SPSS.

2.11 Omics approaches

2.11.1 Proteomics

Proteomic profiling was conducted in collaboration with Dr M. Collins (University of Sheffield) using samples enriched for palmitoylated proteins by acyl-RAC. Bound fractions from KO and WT whole mouse brains (n=2) were sent for analysis (HA and Tris treated samples). The preparation of the samples followed the described method (Chandran et al., 2017).

Briefly, samples were alkylated, separated using SDS-PAGE with a 4–20% precast TGX mini-gel (Biorad) and visualized with Instant Blue (Expedeon). Each gel lane was divided into 5 sections. In-gel digestion was performed as previously described (Bayés et al., 2011) and extracted peptides were analysed in a 60 min nanoflow Liquid Chromatography–Mass Spectrometry/Mass Spectrometry (LC-MS/MS)

experiment on an Orbitrap Elite (from Thermo Fisher) hybrid mass spectrometer with a nanospray source, attached to an Ultimate RSLCnano LC System (Dionex). Data were processed with MaxQuant version 1.5.2.8 (quantitative proteomics software package) and were searched against mouse UniProt sequence databases (downloaded June 2015). Label free quantification was performed using MaxQuant calculated protein intensities in order to find the relative levels of proteins in each purification (Cox et al., 2014).

In order to look for important changes between KO and WT mouse brain palmitoylation, firstly proteins with a ratio of HA/Tris < 5 were removed from the dataset to focus on proteins that are more likely to be palmitoylated and then KO HA/WT HA ratios were calculated. At the end, proteins that present a fold change ≥ 2 and ≤ 0.5 were selected for further analysis.

2.11.2 Metabolomics

Metabolomic profiling from urine samples of 3 WT and 3 KO adult male mice was conducted in collaboration with Dr David Watson at the University of Strathclyde. The protocol was based on previously published work by Dr Watson's group (Ali et al., 2016). Briefly, 100 μ l of urine was collected in Eppendorf tube from each mouse by being scruffed by the neck. The mice tend to urinate while being scruffed as they are stressed. The samples were then prepared for LC-MS analysis.

LC-MS data were acquired on a Dionex 3000 HPLC (Thermo Fisher Scientific) coupled to an Exactive Orbitrap (Thermo Fisher Scientific) in both positive and negative mode set. A p value <0.05 for negative and positive ion data was applied for filtering in order to identify significant changes between WT and KO animal metabolome.

MetaboAnalyst was used for Pathway Analysis (free available online tool). The analysis included all metabolites with p value <0.05 . The pathway analysis included an Overrepresentation analysis using Hypergeometric Test and Pathway topology analysis using Relative-betweenness Centrality. Betweenness Centrality measures the number of shortest paths from all nodes to all the others that pass through a given node within a pathway. Pathways with a p value <0.05 were considered significantly changed in KO animals.

2.11.3 Integrated metabolomic and transcriptomic analysis

MetaboAnalyst offers the option of integrated metabolomic and transcriptomic analysis. Transcriptomic data were previously acquired in our lab by Professor Luke Chamberlain in collaboration with the DNA Microarray Facility in Max-Planck-Institute for Molecular Biology and Genetics in Germany. Whole brain tissue was used from 3 WT and 3 KO adult male mice for RNA extraction and transcriptomics. An unpaired t test was conducted to identify statistically significant changes in gene expression between WT and KO mouse brain. A p value <0.05 and a fold change of >1.5 in upregulation/downregulation was used to filter the results. Initially, transcriptomic pathway analysis was conducted for the molecules meeting those criteria using g:Profiler which is free available online tool (<https://biit.cs.ut.ee/gprofiler/>).

For the integrated pathway analysis, all metabolites with a p value <0.05 were included along with the transcriptomic data. This type of pathway analysis contains enrichment analysis which aims to evaluate whether the observed genes and metabolites in a particular pathway are significantly enriched (appear more than expected by random chance) within the dataset. For this, the over-representation analysis (ORA) was used based on hypergeometric test.

Apart from enrichment analysis, the integrated pathway analysis contains topology analysis which aims to evaluate whether a given gene or metabolite plays

an important role in a biological response based on its position within a pathway. For this, the Degree Centrality option was used which measures the number of links that connect to a node (representing either a gene or metabolite) within a pathway.

Moreover, the gene-metabolite mode allows joint-analysis and visualization of both significant genes and metabolites.

CHAPTER 3

3 Initial characterisation of the *Zdhhc9* mouse line

3.1 Introduction

The zDHHC9 enzyme is an integral membrane protein of 41 kDa containing four transmembrane domains. The DHHC catalytic domain is located in the cytoplasmic loop between the 2nd and 3rd transmembrane domains (Swarthout et al., 2005). In the Golgi, along with GCP16 (Golgi Complex associated protein of 16 kDa), it forms a complex that palmitoylates H-Ras and N-Ras (Swarthout et al., 2005).

Differential expression or disruption of the *ZDHHC9* gene which is located on X-chromosome in human and mouse, has been implicated so far in human colorectal cancer (Mansilla et al., 2007), leukaemia (Liu et al., 2016), and various neurological defects including intellectual disability, epilepsy, and speech and attention deficits (Raymond et al., 2007; Baker et al., 2015). However, it is currently unknown what molecular and cellular changes underlie these neurological impairments caused by *ZDHHC9* mutations. In addition to H- and N-Ras, the β 2-Adrenergic Receptor (Adachi et al., 2016) and BK potassium channels (Tian et al., 2010) are the only known substrates of this enzyme.

Zdhhc9 is highly expressed in mouse brain (<http://mouse.brain-map.org/>). The mouse protein also shows a high similarity of 99.2% to the human zDHHC9 protein (found using EMBOSS water), therefore a *Zdhhc9* knockout (KO) mouse model would be ideal to investigate how disruption of *ZDHHC9* affects molecular and cellular pathways linked to behaviour. A study published in 2010 reported the generation of approximately 400 KO mouse lines, which included a *Zdhhc9* line (Tang et al., 2010). However, to-date there has been no significant analysis of this novel KO line and specifically whether it might represent a useful model system to

investigate zDHHC9 function and how dysfunction of this enzyme leads to neurological impairments.

The aim of this chapter was to investigate the expression of *Zdhhc9* mRNA transcripts in the *Zdhhc9* mouse line and to determine if it represents a true KO model.

3.2 Results

3.2.1 *Zdhhc9* KO mice are born at a lower frequency than WT mice

After genotyping weaned mice back- crossed for at least 6 generations gathering data from 7 breeding cycles we observed that the average ratio of KO mice versus WT males that were born and weaned was 0.35 ± 0.08 , while the respective ratio for HET females versus WT females is 0.96 ± 0.15 . The ratio of KO to WT animals was significantly different from the expected ratio of 1. Therefore, the disruption of *Zdhhc9* causes some lethality in male animals. In contrast to the KO animals, the mutation does not seem to disrupt the number of HET animals born and weaned (Figure 3.1) compared to WT animals.

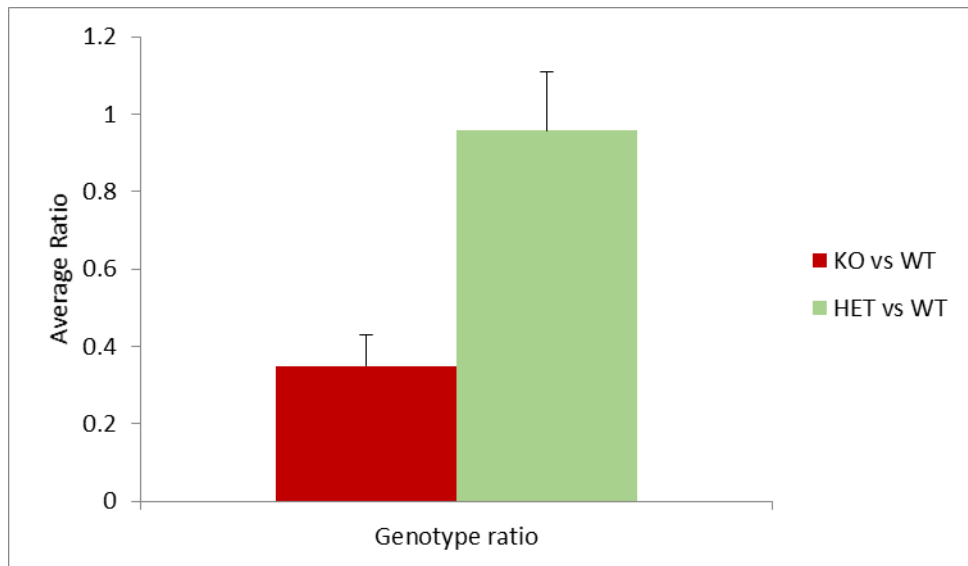


Figure 3.1 Average ratios of numbers of *Zdhhc9* KO versus WT male animals weaned and HET versus WT female animals weaned. The animals included were back- crossed for at least 6 generations. Data gathered from 7 breeding cycles. Error bars represent standard error of the mean (SEM).

3.2.2 Qualitative analysis of *Zdhhc9* expression in brain samples from WT and *Zdhhc9* KO mice

At the time of undertaking this analysis, a number of commercial antibodies against zDHHC9 were tested. However, I did not identify an antibody that specifically recognized the zDHHC9 protein. Therefore, in order to study the expression of *Zdhhc9* in mouse brain, RNA was extracted from WT and KO brain samples and cDNA was synthesized. The RNA was reverse transcribed to cDNA, which was then used in end-point PCR reactions with primers designed to amplify specific regions of *Zdhhc9* and of reference genes. cDNA synthesis and successful amplification of target DNA was initially tested by end-point PCR (Figure 3.2).

To be more precise, the *Zdhhc9* cDNA region from the 5'UTR to Exon 2 was amplified in the mRNA Confirmation assay 1 (MA1) and the *Zdhhc9* cDNA region from Exon 2 to Exon 3 was amplified in the mRNA Confirmation assay 2 (MA2). Moreover, the region of *Zdhhc9* transcript 1 from exon 5 to exon 7 was amplified (z9v1).

The reference genes peptidylprolyl isomerase A (PPIA), TATA box binding protein (TBP) and hypoxanthine guanine phosphoribosyl transferase (HPRT1) were selected based on a previous study conducted in mouse brain (Pernot et al., 2010) showing that they have ubiquitous expression and their transcripts were amplified. Negative controls for the PCR were included for each primer pair in which cDNA was not added. Negative reverse transcription controls were also used (no reverse transcriptase enzyme added) which are control reactions that test for amplification of contaminating genomic DNA.

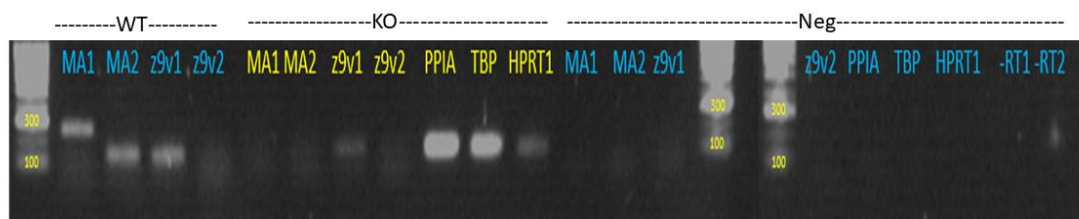


Figure 3.2 Agarose gel electrophoresis of end-point PCR products from WT and KO brain cDNA samples. mRNA Confirmation assay 1 (MA1) amplified a *Zdhhc9* mRNA region of 283 bp from the 5'UTR to Exon 2 in the WT mouse but not in the KO confirming that exon 2 is deleted. mRNA Confirmation assay 2 (MA2) amplified a *Zdhhc9* mRNA region of 154 bp from Exon 2 to Exon 3 at the WT mouse but not in the KO as exon 2 is deleted. z9v1 and z9v2 stand for *Zdhhc9* transcript 1 and 2 respectively. z9v1 amplifies a *Zdhhc9* mRNA region of 139 bp from exon 5 to exon 7. z9v2 was designed to amplify a *Zdhhc9* mRNA region of 106 bp from exon 5 to exon 7 but was not amplified under these PCR conditions. Reference genes amplified were PPIA, TBP and HPRT1. Negative (Neg) controls for each primer pair are reactions where the reaction mix did not include cDNA. -RT1 stands for negative Reverse Transcription control with MA1 primers. -RT2 is negative Reverse Transcription control with PPIA primers. The HyperLadder 100 bp was used as marker of DNA size.

To sum up, the above results confirm that exon 2 (coding exon 1) of *Zdhhc9* is deleted in the KO mouse brain as the strategy of KO was targeting the deletion of this genomic region. However, it seems that there is a transcript that is produced in the KO mouse using the z9v1 primers, which therefore requires further investigation.

3.2.3 Quantitative analysis of *Zdhhc9* expression in brain samples from WT and *Zdhhc9* KO mice

To investigate the relative levels of *Zdhhc9* mRNA between WT and KO mouse brain, qPCR was conducted with cDNA from 3 KO and 3 WT mouse brain samples. Using the cycle threshold (Ct) values, normalisation against the two reference genes was conducted based on the following equation for each brain sample:

$$\Delta Ct = Ct (\text{target gene}) - Ct (\text{reference gene})$$

Then the average ΔCt was calculated (Figure 3.3) for the KO and WT group and statistical analysis revealed significant differences in expression of MA2 between WT and KO groups when normalised against the two reference genes. Moreover, a significant difference in expression of z9v1 when normalised against HPRT1 was noted.

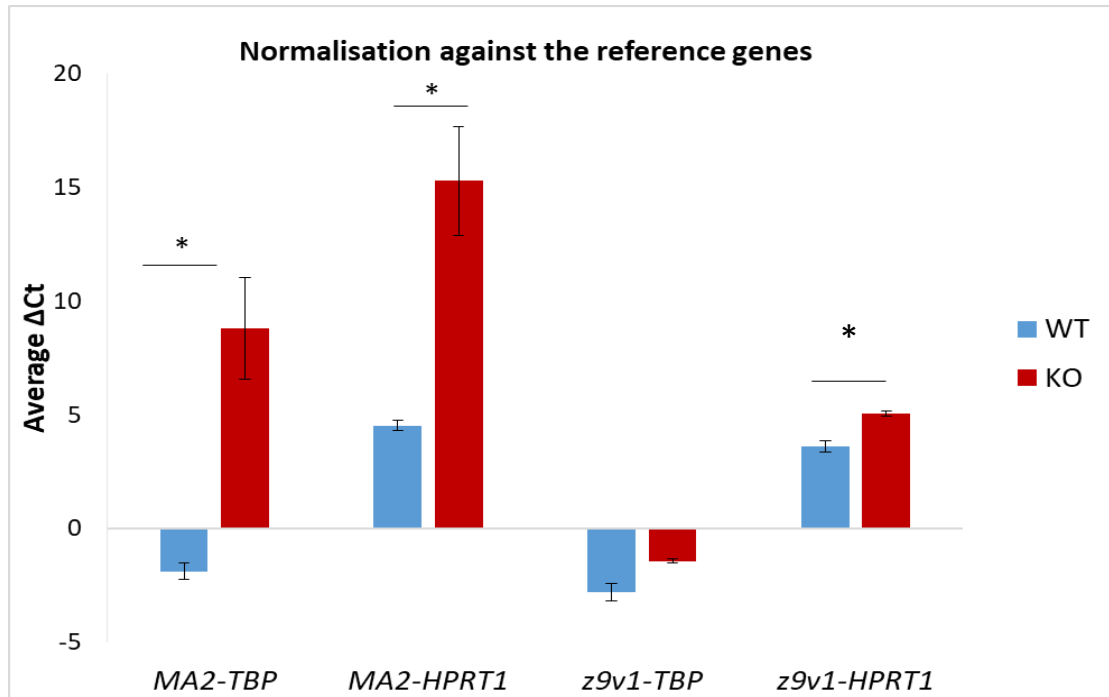


Figure 3.3 Comparison of the average ΔC_t values of WT and KO mouse brain samples (n=3 WT, 3 KO) for MA2 and z9v1 after normalisation against TBP and HPRT1. cDNA from WT and KO mouse brain was amplified for 40 cycles using specific primers for the different targets (MA2, z9v1, TBP and HPRT1) and SYBRR Select Master Mix. Statistical analysis (unpaired t-test, Minitab) revealed a significant effect of genotype in MA2-TBP ($p=0.042$), MA2-HPRT1 ($p=0.046$) and z9v1-HPRT1 ($p=0.037$). p value for z9v1-TBP was 0.075.

Then, the expression fold change (EFC) of each gene was calculated following the equation:

$$EFC = 2^{-\Delta\Delta C_t}$$

where $\Delta\Delta C_t = \text{average } \Delta C_t(\text{KO}) - \text{average } \Delta C_t(\text{WT})$

When $EFC > 1$, then the target gene is upregulated in KO where $EFC < 1$ the target gene is downregulated in KO (Figure 3.4).

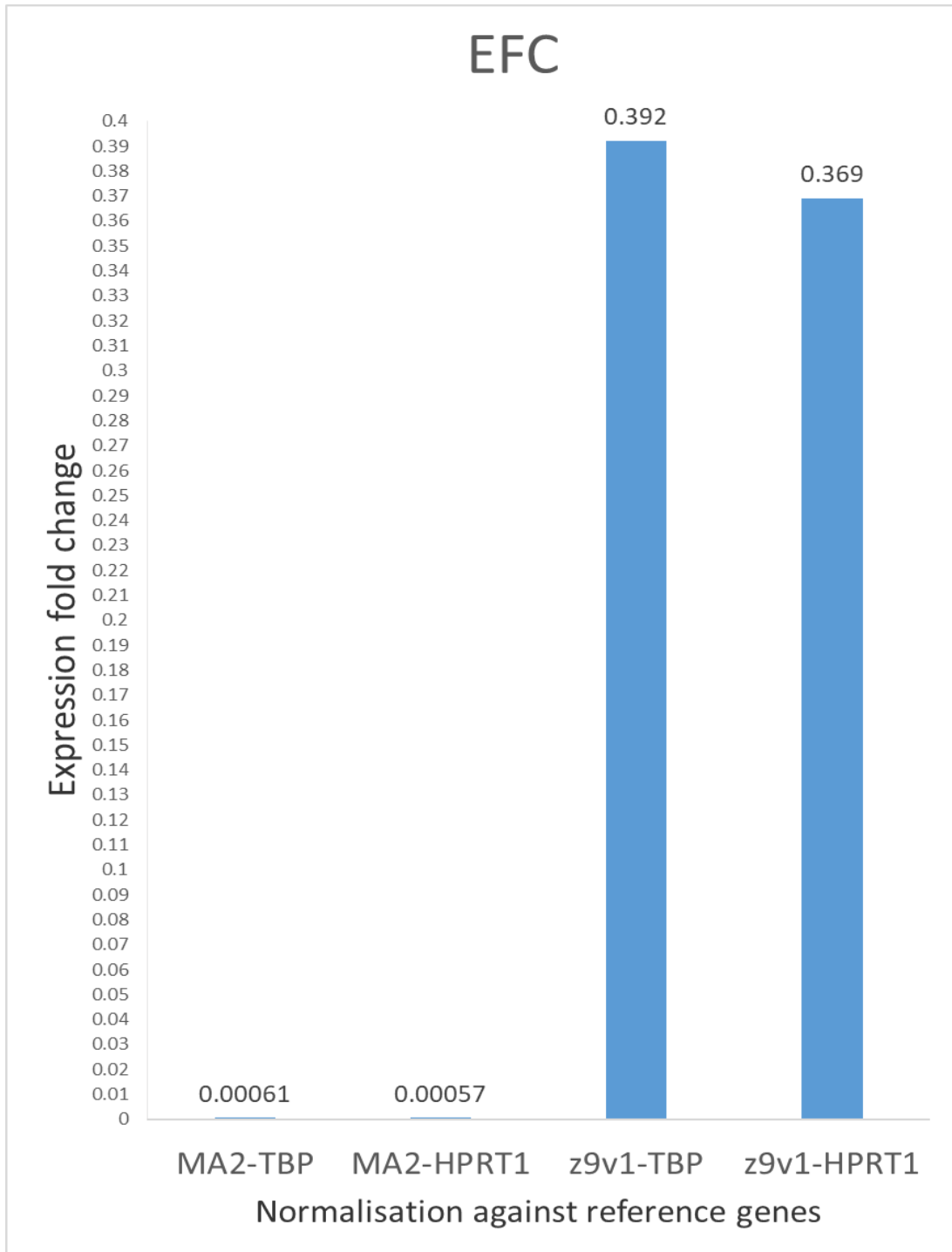


Figure 3.4 Expression fold change (EFC) for MA2 and z9v1 target genes after normalisation against reference genes TBP and HPRT1. In all cases, $EFC < 1$ which means that MA2 and z9v1 are downregulated in Zdhhc9 KO mouse brain.

Based on the mRNA confirmation assay 2 (MA2), there is a large difference in expression between WT and KO mice (1639-fold when the normalisation is against *TBP* and 1754-fold against *HPRT1*), which effectively shows that a *Zdhhc9* transcript containing this region is not present in the *Zdhhc9* KO mice, as expected (Figure 3.4). In contrast transcript 1 (z9v1) in KO brain was calculated to be present at 39.2 % of the WT level when normalised against *TBP* and 36.9% when normalised against *HPRT1* (Figure 3.4). These results confirm that although the targeted exon is removed in KO mice, there are still low levels of a transcript produced.

Based on previous microarray data from our group from mouse brain samples, using two different probes complementary to the 3'UTR of the *Zdhhc9* mRNA (probe sequences 5'GGGAGGGGTGCAAACCACGACTTTTAATCTATTTGAAGGCGATTAACTGTGTCTAATGC3' and 5'TAAAAGTCTGCACTTTGCTGGTTTCTTTTCCTCAGGGGAAGCCTGAGTGCTCACTTAAAC3') *Zdhhc9* expression was down-regulated 2.88 times and 1.77 times respectively in KO mouse. These microarray results are similar to the difference in expression of transcript 1 (z9v1) that we detected by qPCR (Table 3.1).

Table 3.1 Difference in expression of *Zdhhc9* between KO and WT mouse brain normalised against two reference genes. Using the MA2 primers, an almost 1700-fold lower expression was detected in the *Zdhhc9* KO mouse brain versus WT. Using z9v1 primers, an almost 2.6-fold reduction was detected in the KO mouse brain, which is a 38% down-regulation of expression.

	<i>Fold difference in zDHHC9 transcript between WT and Zdhhc9 KO mice</i>	
	<i>Normalisation against TBP</i>	<i>Normalisation against HPRT1</i>
mRNA confirmation assay 2 (MA2)	1639	1754
transcript 1 (z9v1)	2.55	2.71

3.2.4 Analysis of the mRNA transcript detected in *Zdhhc9* KO mouse brain

To investigate the *Zdhhc9* transcript that was detected in KO mouse brain, primers complementary to Exon 1 (untranslated) and the 3' UTR of *Zdhhc9* were designed in order to amplify the full coding sequence contained in this transcript. Amplification of cDNA from WT and KO brain using two different 3' UTR (untranslated region) primers showed that a shorter transcript is present in KO samples compared to WT (Figure 3.5). The PCR products were then sequenced, which revealed that the transcript that was identified in the KO brain lacks 290 nucleotides compared to the WT *Zdhhc9* transcript (Figure 3.6). The correct translation initiation codon is missing in this transcript but it is possible that translation could start from a different position (e.g. from the next available ATG).

However, at present it is not known if any protein is produced from this mutant transcript.

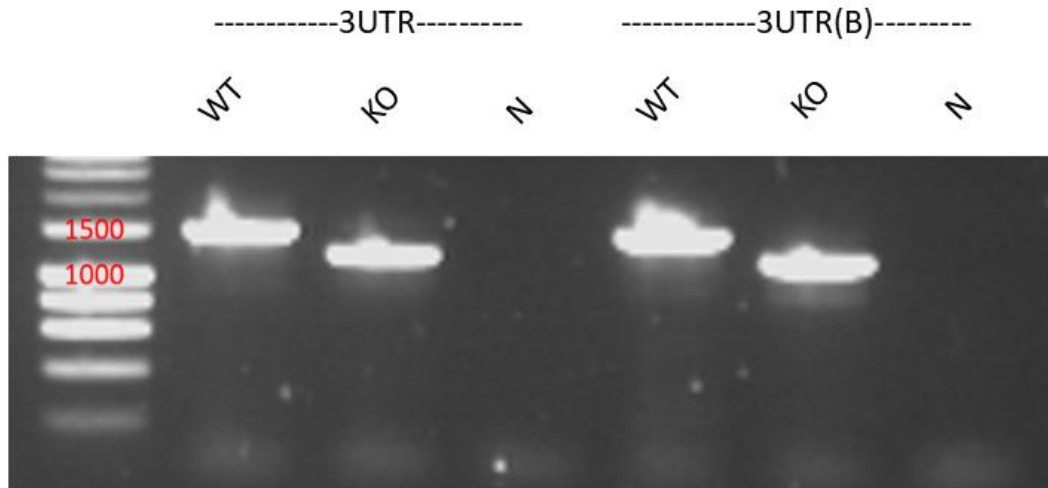


Figure 3.5 Agarose gel electrophoresis of end-point PCR products from WT and KO mouse brain cDNA samples. The following primers were used for PCR: 3UTR amplifying a 1524 bp region in the WT mouse brain and 3UTR(B) amplifying a 1481 bp region in the WT mouse brain. N: negative control for PCR. The HyperLadder 1 kb was loaded as marker of DNA size (first lane).

EMBOSS_001	165	TTTCTGCCCCAGTTGCC -GGCCGAGTTCAGTGTCCCTTGTTCAGGGCTC	213
EMBOSS_001	1	TTTCTGCCNCCAGTTGCCGGGCCGAGTTCAGTGTCCCTTGTTCAG-----	45
EMBOSS_001	214	TTGATAATGTTTGACCCAGTGGCAACACTAGTAGACGACCTGATTTTAAA	263
EMBOSS_001	46	-----	45
EMBOSS_001	264	GCTGACCTCAGCCTCTGCATCTTCTCTCGAGTAGTCCCAAAGCCCATCTT	313
EMBOSS_001	46	-----	45
EMBOSS_001	314	GGACCAAGAACTGTAATCATGTCTGTGTATGTTGTTAAGAAAGAAAGTGAAC	363
EMBOSS_001	46	-----	45
EMBOSS_001	364	ACGSAATGAGAGAACTCCCAAGCAAGAACACCTTCTGCTGTGATGACC	413
EMBOSS_001	46	-----	45
EMBOSS_001	414	GCCTCATGATGCCCCGCAAAAGGGCATCTTCTACCTGACCCCTCTTCCTC	463
EMBOSS_001	46	-----	45
EMBOSS_001	464	ATCCTGAGGACATGTACACTCTTCTTTCCTTCGATGTCTGCTACCTGAC	513
EMBOSS_001	46	-----GTCTGCTACCTGAC	60
EMBOSS_001	514	TGTTCAAGCTGTCTCCTGCCATTCTGTGTTTGCCTATGCTCTTCTTT	563
EMBOSS_001	61	TGTTCAAGCTGTCTCCTGCCATTCTGTGTTTGCCTATGCTCTTCTTT	110
EMBOSS_001	564	TCTCCATGGCCACGCTGTTGAGGACAAAGTTTCAAGTACCCTGGAGTGATT	613
EMBOSS_001	111	TCTCCATGGCCACGCTGTTGAGGACAAAGTTTCAAGTACCCTGGAGTGATT	160
EMBOSS_001	614	CCTCGAGCACTACCAGATGAAGCAGCTTTCATAGAAATGAAATAGAAAC	663
EMBOSS_001	161	CCTCGAGCACTACCAGATGAAGCAGCTTTCATAGAAATGAAATAGAAAC	210
EMBOSS_001	664	CACCAATGTTGCCGTGCCACAGGGCCAGCAGCCACCTCCTCGATTAAAG	713
EMBOSS_001	211	CACCAATGTTGCCGTGCCACAGGGCCAGCAGCCACCTCCTCGATTAAAG	260
EMBOSS_001	714	ATTTCCAGATAAACAACCAGATTGTGAAACTGAAATACTGTTATACATGC	763
EMBOSS_001	261	ATTTCCAGATAAACAACCAGATTGTGAAACTGAAATACTGTTATACATGC	310
EMBOSS_001	764	AAGATCTTCCGGCCTCCCAAGGCTCCCAATTGTAGCATCTGTGACAACGT	813
EMBOSS_001	311	AAGATCTTCCGGCCTCCCAAGGCTCCCAATTGTAGCATCTGTGACAACGT	360
EMBOSS_001	814	TGTGGAGCGCTTCGACCATCACTGCCCTGGGTGGGAAACTGTGTTGGAA	863
EMBOSS_001	361	TGTGGAGCGCTTCGACCATCACTGCCCTGGGTGGGAAACTGTGTTGGAA	410
EMBOSS_001	864	AGAGGAACTACCGCTACTTCACTCTTCACTCTCTCTCTCCCTCCTC	913
EMBOSS_001	411	AGAGGAACTACCGCTACTTCACTCTTCACTCTCTCTCTCTCCCTCCTC	460
EMBOSS_001	914	ACAATTTATGTCTTCGCCTTTAACATCGTCTATGTGGCCCTCAAATCCTT	963
EMBOSS_001	461	ACAATTTATGTCTTCGCCTTTAACATCGTCTATGTGGCCCTCAAATCCTT	510
EMBOSS_001	964	GAAAATTGGCTTCTGGAGACTGAAAGAAACGCCTGGAACTGTTCTGG	1013
EMBOSS_001	511	GAAAATTGGCTTCTGGAGACTGAAAGAAACGCCTGGAACTGTTCTGG	560
EMBOSS_001	1014	AAGTACTCATTGCTTCTTCACTCTCTGGTCTGTTGTGGGGCTGACTGGA	1063
EMBOSS_001	561	AAGTACTCATTGCTTCTTCACTCTCTGGTCTGTTGTGGGGCTGACTGGA	610
EMBOSS_001	1064	TTTACACATTCTTGTGGCTTCAATCAGACCACCAATGAAGACATCAA	1113
EMBOSS_001	611	TTTACACATTCTTGTGGCTTCAATCAGACCACCAATGAAGACATCAA	660
EMBOSS_001	1114	AGGATCATGGACAGGGAAGAAATCGTGTGCAGAAATCCGTACAGCCACGGCA	1163
EMBOSS_001	661	AGGATCATGGACAGGGAAGAAATCGTGTGCAGAAATCCGTACAGCCACGGCA	710
EMBOSS_001	1164	ACATTGTGAAGAACTGCTGTGAAGTGTCTTGTGGCCCTTGGCCCCAGT	1213
EMBOSS_001	711	ACATTGTGAAGAACTGCTGTGAAGTGTCTTGTGGCCCTTGGCCCCAGT	760

```

EMBOSS_001      1214 GTCCTGGATCGAAGGGGTATTTTGCCACTGGAGGAAAGTGGAAAGTCGACC 1263
      |||||||||||||||||||||||||||||||||||||||||||||
EMBOSS_001      761 GTCCTGGATCGAAGGGGTATTTTGCCACTGGAGGAAAGTGNAAGTCGACC 810

EMBOSS_001      1264 TCCAAGTACTCAAGAGACCAGCAGTAGCCTGTTGCCACAGAGCCCAGCCT 1313
      |||||||||||||||||||||||||||||||||||||||||||||
EMBOSS_001      811 TCCAAGTACTCAAGAGACCAGCAGTAGCCTGTTGCCACAGANCCCAGCCT 860

EMBOSS_001      1314 CCACAGAGCATATGAACTCTAATGAGATGGCAGAGGACACCAGCATTTCCT 1363
      |||||||||||||||||||||||||||||||||||||||||.|||||.|||.|||||
EMBOSS_001      861 CCACAGAGCATATGAACTCTAATGAGATGGCAGANGACACCNCGCNTTCCT 910

EMBOSS_001      1364 GAAGAGATGCCACCTCCAGAACCCCCAGAGCCACCACAGGAGGCATCCGA 1413
      ||..|||||||||||||||.|||||||.|||||||.|||||||||||||||
EMBOSS_001      911 GANNAGATGCCACCTCCANAACCCCCANAGCCACCNCAGGAGGCATCCGA 960

EMBOSS_001      1414 AGCTGAGAAG 1423
      |||||..||
EMBOSS_001      961 AGCTGANNAG 970

```

Figure 3.6 Nucleotide alignment between the *Zdhhc9* transcript 1 (top sequence) and the transcript isolated from the KO mouse brain (bottom sequence) using EMBOSS Water. The sequence that is lacking from the transcript amplified from KO mouse brain is highlighted in blue. The ATG initiation codon is situated in position 332 of the *Zdhhc9* transcript 1 and indicated in yellow star (region missing in the transcript isolated from the KO mouse brain). The red star shows a potential initiation codon in the *Zdhhc9* transcript from KO brain (ATG in position 98).

3.2.5 Analysis of expression of mutant *Zdhhc9* in HEK293T cells

Due to lack of specific zDHHC9 antibodies at the time of undertaking this analysis, we were unsure about the exact protein that is expressed (if any) in KO mouse brain. If translation started from the next available ATG in the shorter mRNA fragment present in KO mice (red star in Figure 3.6), then this would produce an N-terminally truncated protein that includes the DHHC catalytic domain. This DNA fragment was therefore cloned into the pEF-BOS-HA plasmid using BamH1 sites that were introduced in the primers used for PCR amplification. The pEF-BOS-HA plasmid encodes an N-terminal triple HA tag. HEK293T cells were transfected with this plasmid and protein expression in cell lysates was analysed by SDS-PAGE and Western Blotting using an HA antibody (Figure 3.7, upper panel). A shorter zDHHC9

protein is produced from the mutant construct and expressed at similar levels to full-length zDHC9 in HEK293T cells.

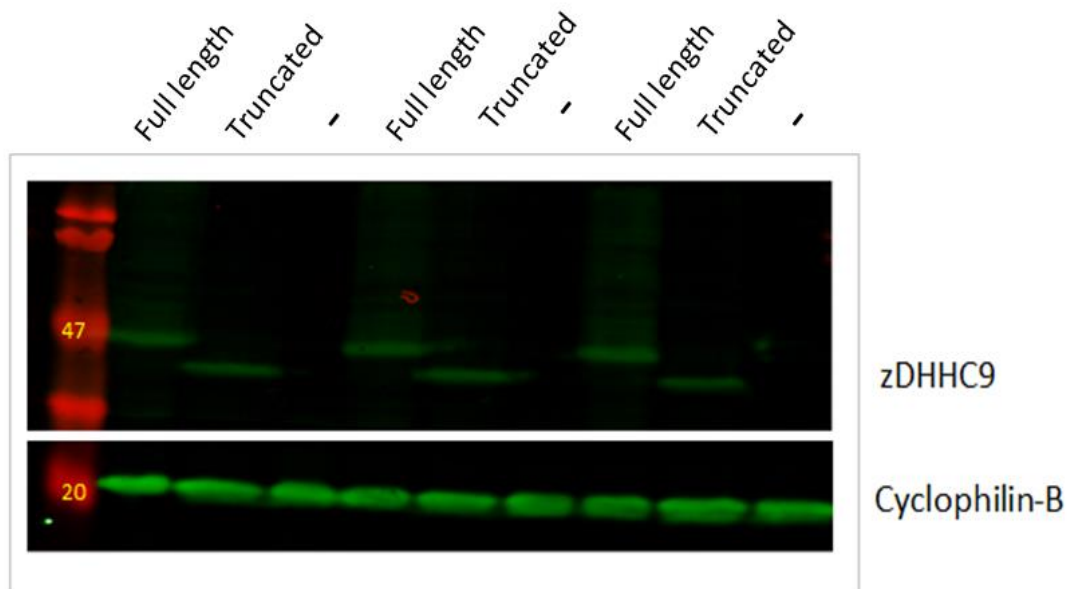


Figure 3.7 Expression of full-length and truncated zDHC9 in HEK293T cells. Cells were transfected with plasmids encoding HA-zDHC9 (full length and mutant construct) and cell lysates were analysed by SDS-PAGE and immunoblotting. “-” represents cells transfected with empty pEF-BOS. The membrane was incubated overnight with antibody against HA in order to detect HA tagged-zDHC9 (upper part of figure). The membrane was also incubated overnight with antibody against Cyclophilin-B as loading control (lower part of figure). Position of molecular weight markers are shown on the left.

3.2.6 Localisation of mutant zDHC9 in HEK293T cells

In order to further investigate the truncated zDHC9 protein, HEK293T cells on coverslips were transfected with either full-length HA-zDHC9 plasmid or with

mutant HA-zDHHc9. Slides were stained with HA antibody and an antibody against the Golgi protein, GM130, and then observed under a confocal microscope. While WT zDHHc9 was localised mainly in Golgi and showed co-localisation with the Golgi marker GM130 (Figure 3.8A-C), mutant zDHHc9 showed a dispersed localisation similar to that expected of endoplasmic reticulum and showed very little overlap with the GM130 Golgi marker (Figure 3.8D-F).

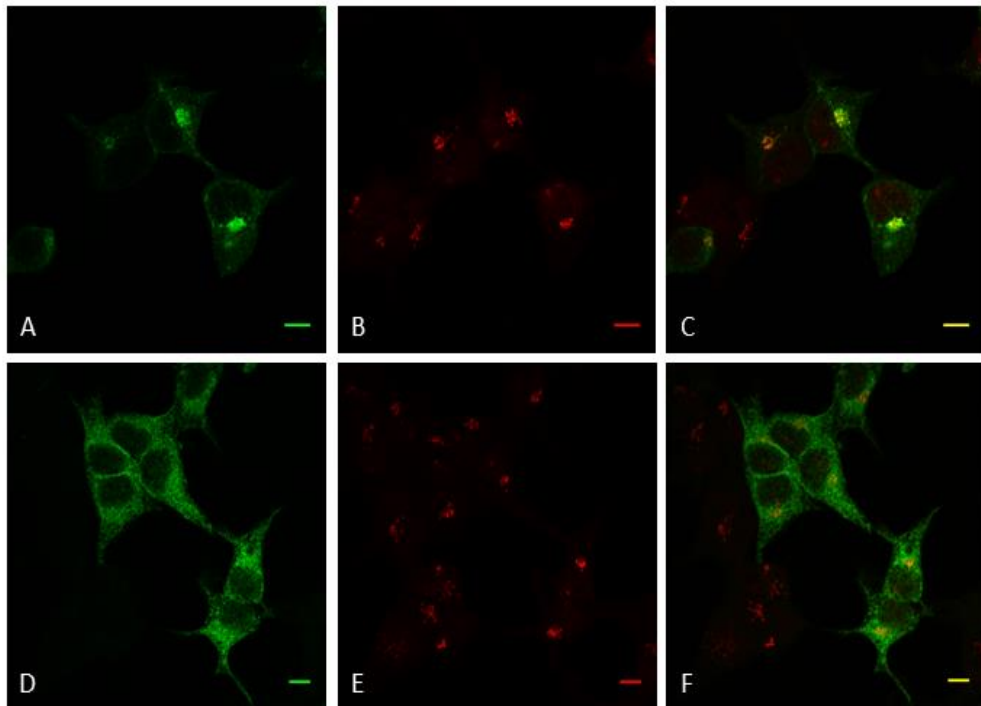


Figure 3.8 Localisation of full-length and mutant zDHHc9 in HEK293T cells. Antibodies against HA and GM130 (cis-Golgi marker) were used to study the localisation of the proteins using 488 (for HA) and 633 (for GM130) channels (Leica Microsystems). Panels A,B,C show cells transfected with full-length HA-zDHHc9 plasmid. Panel A shows the localisation of zDHHc9 in the 488 channel. Panel B shows the same cells as panel A using the 633 channel for the detection of GM130 which is localised in cis-Golgi. Panel C is merge of panels A and B. Panels D,E,F show cells transfected with mutant HA-zDhhc9 plasmid. Panel D shows the localisation of mutant zDHHc9 in the 488 channel. Panel E shows the same cells as panel D using the 633 channel for the detection of Golgi marker GM130. Panel

F is merge of panels D and E. Scale bars on the bottom right of each panel correspond to 10 μm .

3.2.7 A new antibody against zDHHC9 confirms KO of zDHHC9 expression and the absence of a truncated zDHHC9 protein in KO brain

At the end of this PhD project, work performed by Professor Luke Chamberlain identified a commercial zDHHC9 antibody that specifically recognises this zDHHC enzyme isoform but not zDHHC-3, -7, -15, or -17 in transfected HEK293T cells (Figure 3.9 left panel). Although this antibody recognised multiple protein bands in brain lysates there was clear loss of an immunoreactive band in KO brain samples at the size expected of zDHHC9 (Figure 3.9). Furthermore, KO samples did not contain an additional lower molecular weight immunoreactive band (compared to WT samples) (Figure 3.9 right panel). These analyses suggest that the mouse line is a true KO model and that the smaller mRNA fragment present in *Zdhhc9* KO mice does not produce detectable levels of a corresponding protein.

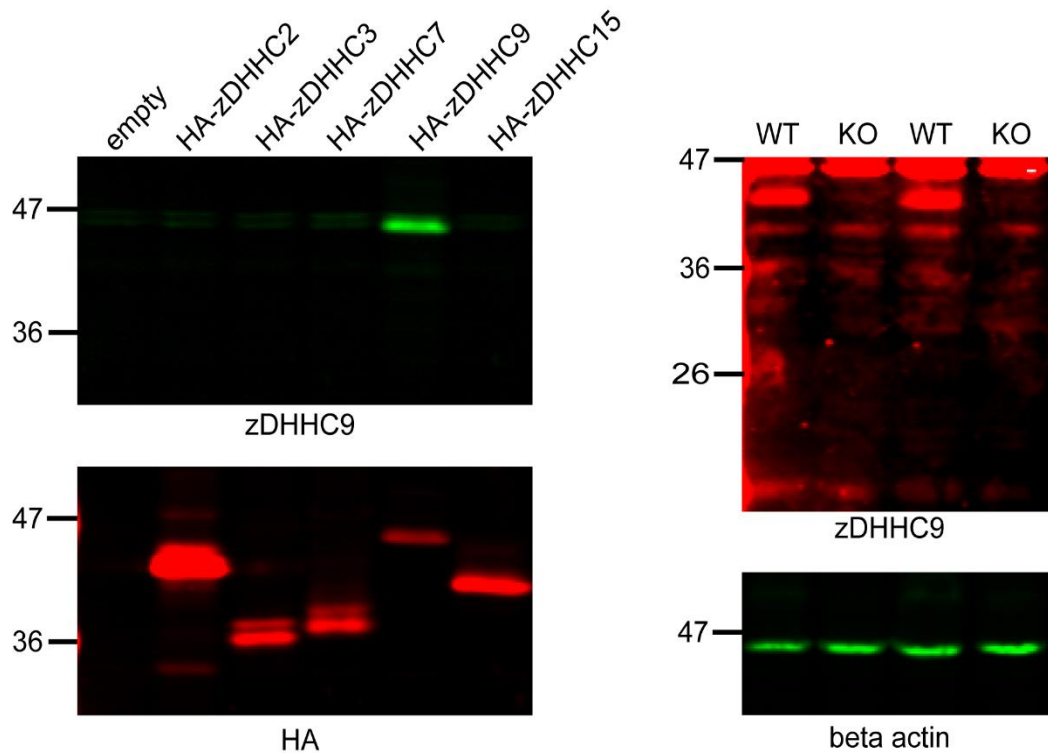


Figure 3.9 Confirmation of the KO of zDHHc9 expression in protein level. Lysates from HEK293T cells transfected with HA-tagged zDHHcs were probed with antibodies against zDHHc9 (top left) and HA (bottom left). Brain lysates from WT and mutant mice were probed with antibodies against zDHHc9 (top right) and beta actin (bottom right). Position of molecular weight markers is shown on the left of all immunoblots.

3.3 Discussion

Gene targeting techniques have been available for over 30 years and have been widely used to disrupt genes of interest in order to delineate their function (Mansour et al., 1988; Hall et al., 2009). Mice serve as good experimental animal species in order to study biological processes because they share around 99% of the same genes with humans (Capecchi, 1994). KO mice have been generated for thousands of mouse genes and they have contributed valuable insight into gene

function and molecular and cellular mechanisms underlying disease (Hall et al., 2009).

When working with a knockout mouse model, it is important to investigate that the gene is indeed knocked out. There are various studies published where the researchers do not investigate the presence of other mRNA fragments produced from the disrupted gene. This chapter emphasises the importance of confirming the knock out of a gene and characterising the transcripts produced (if any). This is particularly important if protein detection is not easy for example due to the lack of commercially useful antibodies. I confirmed that exon 2 of *Zdhhc9* is deleted in KO mice as expected from the strategy of creating the KO line. However, a shorter transcript that lacks exon 2 was detected in KO mouse brain albeit at statistically lower levels than the WT transcript. Sequence analysis of the cloned fragment showed that it lacked the initiating methionine of zDHC9 although an in-frame ATG codon was present downstream, suggesting that a shorter zDHC9 protein construct might be produced from this mRNA species. Although a shorter transcript was expressed at roughly one third of the levels of the WT transcript, immunoblotting failed to detect a corresponding protein fragment. Importantly, the antibody used was generated against a C-terminal peptide of zDHC9 that is encoded by the short mRNA species. It is possible that no protein is produced from the shorter mRNA because it is not efficiently processed by the translation machinery or alternatively a protein might be made but rapidly degraded.

The *Zdhhc9* transcript that we identified in the KO brain lacks 290 nucleotides compared to the WT transcript due to disruption of exon 2 (coding exon 1) in *Zdhhc9* DNA sequence. Some of this missing region in the mutant transcript belongs to the untranslated part of the gene. If translation starts at the first ATG within the undisrupted open reading frame, then the protein that would be produced from this transcript would lack transmembrane domain 1 and part of 2 but not the catalytic region. Overall, the protein would lack 73 aa. After cloning this mutant transcript

and expressing it in HEK293T cells, we identified a shorter zDHHC9 tagged protein (Figure 3.7). Subcellular localisation of the mutant zDHHC9 is different from the wild-type protein (Figure 3.8). Normally, zDHHC9 is localised in endoplasmic reticulum (ER) and Golgi (Swarthout et al., 2005). In the Golgi apparatus, it forms a complex with GCP16, which stabilises and activates the enzyme. Retention of the mutant zDHHC9 in the ER is likely due to absence of the first and part of second transmembrane domain, which may interfere with protein assembly and folding. In addition, recent work has suggested that the transmembrane domains of zDHHC enzymes may be important for palmitoylation activity/specificity (Greaves et al., 2017) and therefore removal of the transmembrane domains in the mutant protein may perturb enzyme activity and possibly also substrate recognition.

Although it appears that the shorter *Zdhhc9* transcript in KO animals does not produce corresponding protein. Other studies have highlighted the importance of undertaking a rigorous assessment of KO models. A vitamin D receptor knockout mouse line was found to express a shorter mRNA fragment that lacked the targeted exon 2 but contained exons 3-9 and two 5' untranslated exons (Bula et al., 2005). Like our study, this transcript was expressed at lower levels than the WT transcript but in this case it produced a protein fragment that was identified in western blots and thought to originate due to translational initiation at the codon for Met-52. Furthermore, this truncated receptor retained full binding for 1,25-dihydroxyvitamin D3 (Bula et al., 2005). This study further highlights the potential for expression of altered and potentially dominant-negative protein fragments that may exert a major contribution on the reported phenotypes of certain mouse models. Although most studies reporting novel KO mouse lines examine expression of the protein in WT versus KO samples, it is important that care is taken to probe for the presence of lower molecular weight fragments and to use different antibodies to confirm true knockout (e.g. antibodies against both the N- and C-termini of the protein of interest).

Another finding made was that disruption of *Zdhhc9* causes a semi-lethal phenotype, which is similar to what has been reported for the disruption of *Zdhhc5* (Li et al., 2010). Mice homozygous for disruption of this gene were born at a ratio of 0.5 compared to WT animals (Li et al., 2010). In contrast to the *Zdhhc9* KO mouse line, the *Zdhhc5* line is a genetrapped model that still expresses zDHHC5 protein at 10% of the level of WT mice. Despite this residual expression, the genetrapped mutations are semi-lethal similar to *Zdhhc9* KO mice. Although *Zdhhc9* male KO mice are born at a frequency of 0.3 compared to male WT mice, the *Zdhhc9* KO males that are born are otherwise healthy and fertile. The low ratio of KO/WT male animals may suggest that *Zdhhc9* is important for embryonic development but not crucial, and thus perhaps some KO embryos are re-absorbed at an early stage. The ratio of HET versus WT female animals is close to 1, showing that one WT allele is sufficient for normal embryonic survival and that disruption of the second allele in the case of heterozygous animals does not lead to any lethality.

In humans, there are seven allelic variants of *ZDHHC9* that have been associated to ID. Three of them are caused by nonsense mutations, three by missense mutations and one by deletion of exons. The first nonsense mutation is a 4-bp duplication in exon 3 that causes a truncated protein lacking the catalytic domain (Raymond et al., 2007). The second nonsense mutation is on a splice site resulting in a frameshift and subsequent truncation and removal of the catalytic domain (Raymond et al., 2007). Those mutations are loss-of-function. A nonsense mutation in exon 9 of the gene creates a stop codon: c.892C > T; p.Arg298* (Masurel-Paulet et al., 2014). The mutant protein does not lack the catalytic domain as the mutation is situated in exon downstream of the catalytic domain. Indeed the protein is predicted to contain all four TMDs but to lack the C-terminal tail. It will be interesting to determine how this C-terminal region contributes to zDHHC9 function. One possibility is that it plays a role in substrate recognition.

The two missense mutations are within the catalytic domain of the protein (442C-T and 448C-T transitions) that cause amino acid substitutions (Raymond et al., 2007). These mutations reduce the steady state level of autopalmitoylated zDHHC9 enzyme (Mitchell et al., 2014). As autopalmitoylation precedes substrate palmitoylation, these mutations thus directly perturb zDHHC9 enzymatic function.

A *de novo* missense mutation was recently described in exon 3 of the gene, a single nucleotide substitution, c.286C > T; p.Arg96Trp (Han et al., 2017) which has been already described in a family (Tzschach et al., 2015). It is not within the catalytic domain but upstream of it, nevertheless it is pathogenic. Again, it will be interesting to determine how this mutation affects zDHHC9 function.

Deletion of exons 9 and 10 which are downstream of the catalytic domain, causes a pathologic phenotype with mild developmental delay and behaviour disorder (Boone et al., 2010). Thus, it is clear that in humans, even when the catalytic domain of zDHHC9 is not directly affected, mutations upstream or downstream of it are enough to cause ID.

CHAPTER 4

4 Behavioural and anatomical investigation of the effect of *Zdhhc9* KO in mouse brain

4.1 Introduction

Intellectual disability (ID, formerly known as mental retardation) is a generalised neurodevelopmental disorder occurring in 1% of the total population (Maulik et al., 2011). It is a world- wide disorder with similar prevalence to schizophrenia and depression and although it has been studied for decades, its pathophysiology is not yet fully understood.

ID is characterised by deficits in intellectual functions such as learning and problem solving and in adaptive functions such as practical and social skills. Genetic factors can cause ID i.e. mutations in genes or chromosomal abnormalities that are inherited however ID can also be acquired before or after birth because of infections, environmental factors or brain trauma (Moeschler et al., 2014).

Many genetic factors are known to cause ID, including mutations in the *ZDHHC9* gene (Raymond et al., 2007). In addition, while this study was ongoing, further analysis of patients with *ZDHHC9* mutations uncovered epilepsy, hypotonia, and speech and attention deficits in these individuals. In addition, another prominent feature was hypoplasia of the corpus callosum (Baker et al., 2015).

At present, there is essentially no information available on how *ZDHHC9* mutations actually cause these neurological deficits. The novel *Zdhhc9* KO mouse line that was characterised (at mRNA and protein level) in chapter 3 may offer a valuable resource to delineate the links between palmitoylation and ID, epilepsy and other neurological deficits.

In this chapter, I report the first behavioural characterization of *Zdhhc9* KO mice in order to delineate the role of zDHHC9 in behaviour and nervous system function, and determine if these mice exhibit similar features to humans with *ZDHHC9* mutations. A range of behavioural tests were conducted in adult male *Zdhhc9* KO mice, with a particular focus on learning and memory tests, and test of anxiety, which is commonly affected in other ID mouse models. In addition, I explored if the most prominent brain structure change in patients with *ZDHHC9* mutations- hypoplasia of the corpus callosum- is also observed in this model.

4.2 Results

4.2.1 Physical gross examination of *Zdhhc9* KO mice

In order to identify any gross physical abnormalities caused by disruption of the *Zdhhc9* gene, the SHIRPA protocol was conducted on 24 WT and 18 KO littermates at 8-10 weeks old. The results of this analysis are presented in Table 4.1.

Physical examination showed that only 1 of the 18 KO mice had very small, almost non-existent whiskers on one side. Statistical analysis for non-parametric data using a Mann-Whitney test in SPSS version 22 revealed no significant differences for the morphology of the whiskers between WT and KO animals. As regards provoked biting, the Mann-Whitney test showed a p value of 0.051 close to significance for the effect of genotype. For visual placing behaviour, the Mann-Whitney test revealed a significant difference between WT and KO animals ($p=0.001$), with the KO animals extending earlier their paws when reaching a surface. Other than this, no other gross physical deficits were readily visible on KO mice.

Table 4.1 List of behaviours that were scored for each animal while the animal was in the arena for a 5 minute period or restrained. Y stands for yes while n stands for no. The number of animals that presented this behaviour out of the total number of animals is noted in parenthesis.

<i>Location</i>	<i>Measure</i>	<i>Score scale</i>	<i>Range of scores</i>	<i>WT</i>	<i>KO</i>
<i>In arena (in the box)</i>	body position	0-5	lying flat to vertical leaping	3	3
	spontaneous activity	0-4	none to extreme rapid dart	2	2
	tremor	0-2	none to marked	0	0
	urination	y/n	yes/no	y	y
	defecation	y/n	yes/no	y	y
	bizarre behaviours	y/n	yes/no	y	y
	convulsions	y/n	yes/no	n	n
	palebral closure	0-2	eyes wide open to eyes completely closed	0	0
	piloerection	0-1	none to fur standing on end	0	0
	gait	0-3	normal to incapacity	0	0
	pelvic elevation	0-2	markedly flattened to elevated	1	1
tail elevation	0-2	dragging to straub tail	1	1	

	evidence of grooming	y/n	yes/no	y	y
	whiskers	Intact (I), malformed (M)/ no whiskers		I (24/24)	I (17/18) M (1/18)
<i>Restrained</i>	pinna reflex	0-2	none to hyperactive (repetitive)	1	1
	cornea reflex	0-2	none to hyperactive (repetitive)	1	1
	lacrimation	y/n	yes/no	n	n
	provoked biting	y/n	yes/no	y (20/24) n (4/24)	y (10/18) n (8/18)
	trunk curl	y/n	yes/no	y	y
	visual placing	0-4	none to early vigorous extension	1	1 (11/18) 2 (5/18) 3 (2/18)
	righting reflex	0-3	no impairment to complete failure to right	0	0

The weight of the animals before conducting the SHIRPA was also measured (Figure 4.1) identifying a significant difference between WT and KO animals with the KO animals being significantly lighter (average WT weight: 27.58 g, average KO weight: 25.36 g, $p=0.002$).

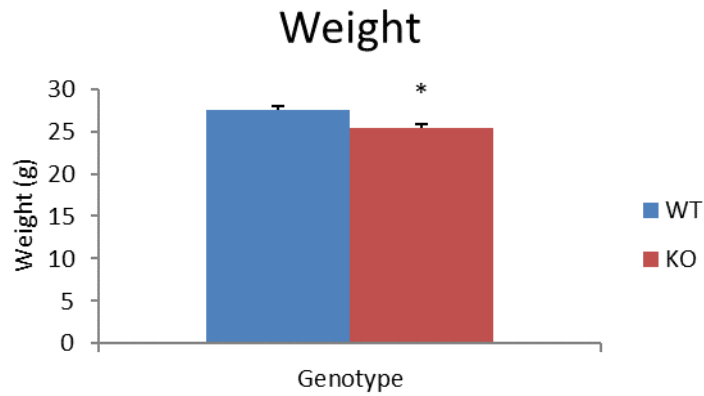


Figure 4.1 Weight of male *Zdhhc9* KO and WT animals before conducting the SHIRPA task (n=18 KO, 24 WT). Average weight (g) is shown; error bars show SEM. Statistics were conducted using unpaired t test in Minitab version 17 (p=0.002 for effect of genotype).

4.2.2 *Zdhhc9* KO mice exhibit hypotonia in the hanging wire

In order to compare the grip strength of *Zdhhc9* KO mice to WT littermates the hanging wire task was conducted in 14 KO and 20 WT mice that were 8-9 weeks old. Prior to conducting the task, the weight of each animal was noted as heavier animals tend to spend less time hanging on the wire.

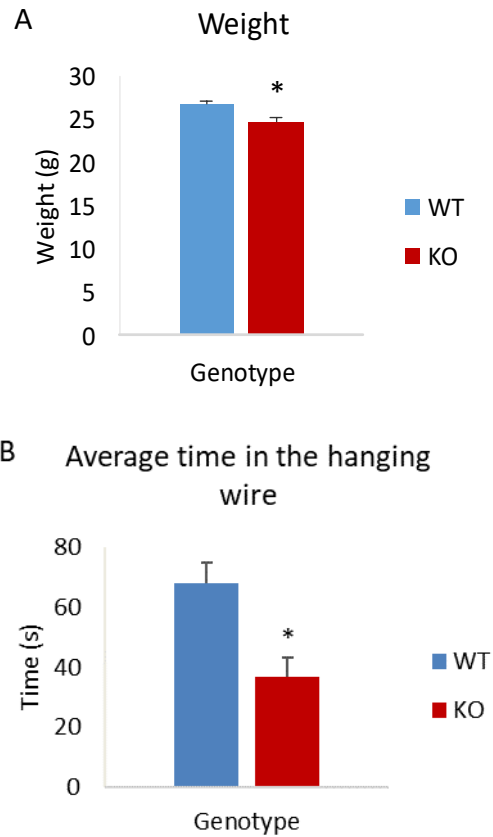


Figure 4.2 Comparison of wild- type and Zdhhc9 KO mice in the Hanging Wire test. (A) Weight of Zdhhc9 KO and WT animals before conducting the hanging wire task (n=14 KO, 20 WT); and (B) average time spent on the wire; error bars show SEM. Statistics were conducted using unpaired t test in Minitab version 17, $p=0.002$ for effect of genotype in weight and in time spent in the wire.

Zdhhc9 KO mice were found to be significantly lighter (average weight for WT: 26.81 gr, for KO: 24.72 gr) and also spent significantly less time hanging on the wire (average time for WT: 68.03 s, for KO: 36.59 s), which may indicate lower grip strength ($p=0.002$ for effect of genotype on weight and on performance in the wire, using unpaired t test with Minitab version 17, Figure 4.2).

4.2.3 Zdhhc9 KO mice show normal motor coordination on the rotarod

In order to examine the motor coordination and balance of the Zdhhc9 KO mice, the rotarod task was conducted on the same mice (n=14 KO and 20 WT, 8-9 weeks old).

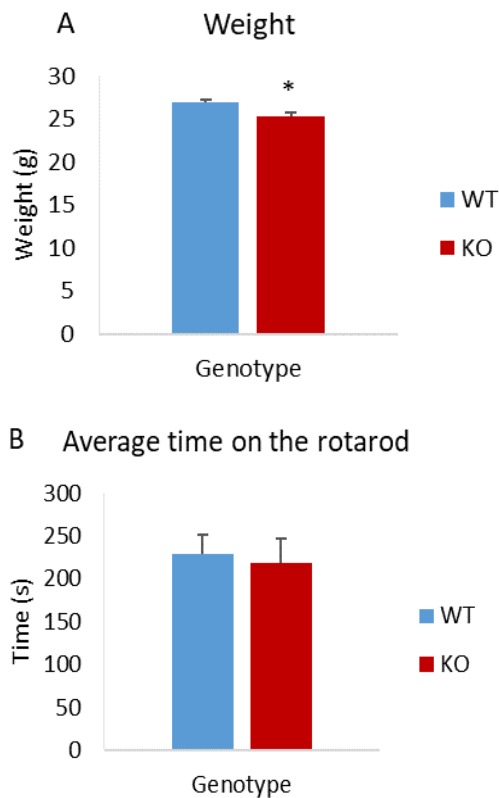


Figure 4.3 Comparison of wild- type and Zdhhc9 KO mice on a rotarod. (A) Weight of Zdhhc9 KO and WT animals before conducting the rotarod task (n=14 KO, 20 WT); and (B) average time spent on the rotarod ; error bars show SEM. Statistics were conducted using unpaired t test in Minitab version 17, $p=0.017$ for effect of genotype on weight.

The weight of the animals was significantly different on the day of the experiment with the KO mice being significantly lighter (average weight for WT:

26.92 g, for KO: 25.23 g, $p=0.017$ for effect of genotype using unpaired t test with Minitab version 17, Figure 4.3A). As regards their performance on the rotarod, both groups performed in a similar manner, indicating normal motor coordination and balance (Figure 4.3B).

4.2.4 Effect of age on hanging wire and rotarod task

In order to examine if there is any deterioration of the deficit of the *Zdhhc9* KO mice in the hanging wire test with age or if there is any deficit in rotarod performance with older mice, animals were tested on both tasks when they were 8 weeks old and again at 16 weeks old ($n=10$ KO, 12 WT).

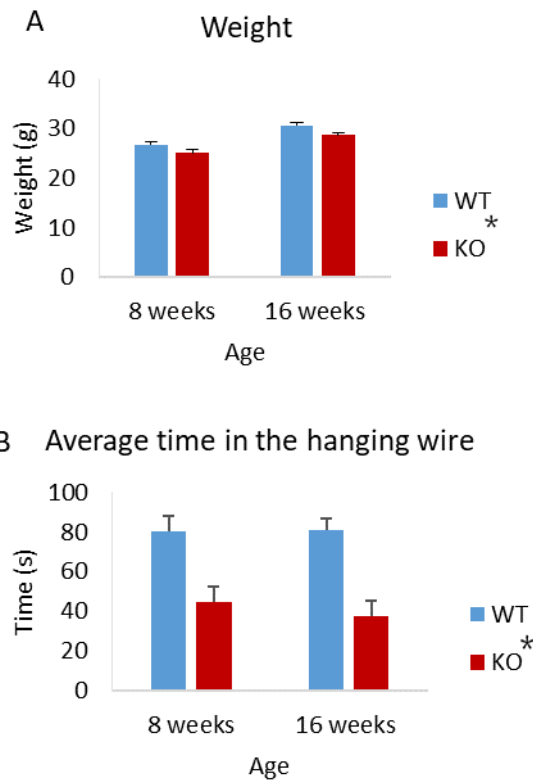


Figure 4.4 Effect of age on the hanging wire task. (A) Weight of *Zdhhc9* KO and WT animals before conducting the hanging wire ($n=10$ KO, 12 WT) at 8 and 16 weeks of age; and (B) average time spent on the hanging wire at 8 and 16 weeks of age; error bars show SEM. Statistics were conducted using general linear model, repeated measures in SPSS version 22

($p=0.045$ for effect of genotype on weight and $p<0.001$ for effect of genotype on time spent on the wire).

There was a significant effect of genotype on weight ($p=0.045$, however close to non-significance) and on performance on the hanging wire ($p<0.001$) using a general linear model, repeated measures in SPSS version 22 (Figure 4.4). However, there was no effect of age on performance showing that there is no deterioration or amelioration of the deficit of KO mice in the hanging wire with age (Figure 4.4B).

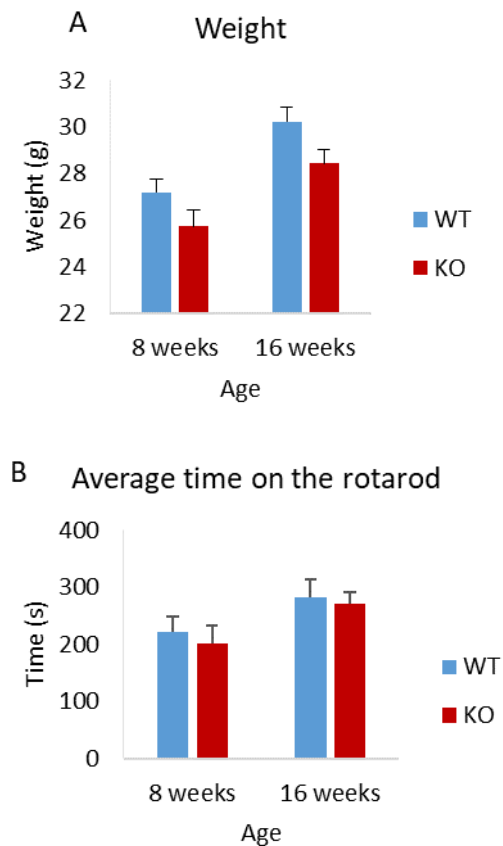


Figure 4.5 Effect of age on rotarod performance. (A) Weight of *Zdhhc9* KO and WT animals before conducting the rotarod ($n=10$ KO, 12 WT) at 8 and 16 weeks of age; and (B) time

spent on the rotarod at 8 and 16 weeks of age; error bars show SEM. Statistics were conducted using general linear model, repeated measures in SPSS version 22, ($p=0.07$ for effect of genotype on weight and $p>0.05$ for effect of genotype on time spent on the rotarod).

Regarding the rotarod task, there was no effect of genotype on weight ($p=0.07$, general linear model, repeated measures using SPSS version 22) or performance indicating that the performance of the mice remained unchanged with age and that there was no deficit in *Zdhhc9* KO mice in this test (Figure 4.5).

4.2.5 *Zdhhc9* KO mice exhibit normal locomotor activity in the open field test but different thigmotactic behaviour during the habituation period compared to WT mice

In order to assess the locomotor activity of *Zdhhc9* KO mice, the open field test (OFT) was conducted in 14 KO and 20 WT adult mice. For this, the mice were placed individually in the testing arena and their motion was recorded over a period of 15 minutes, which is the habituation period followed by a 30 minute-test period. The results are presented in time bins of 5 minutes.

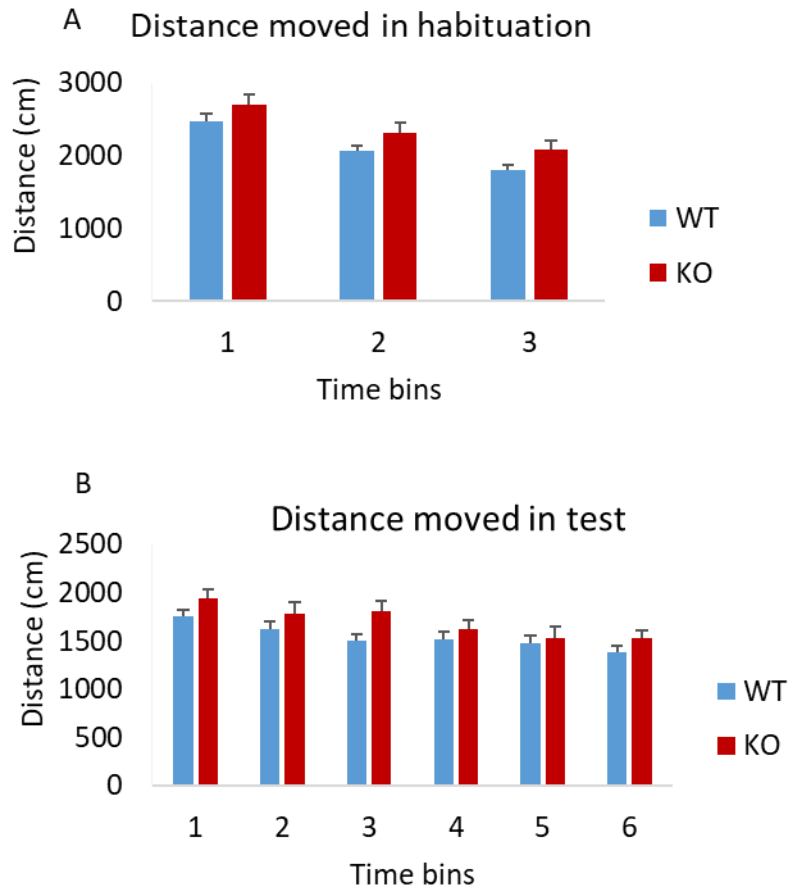
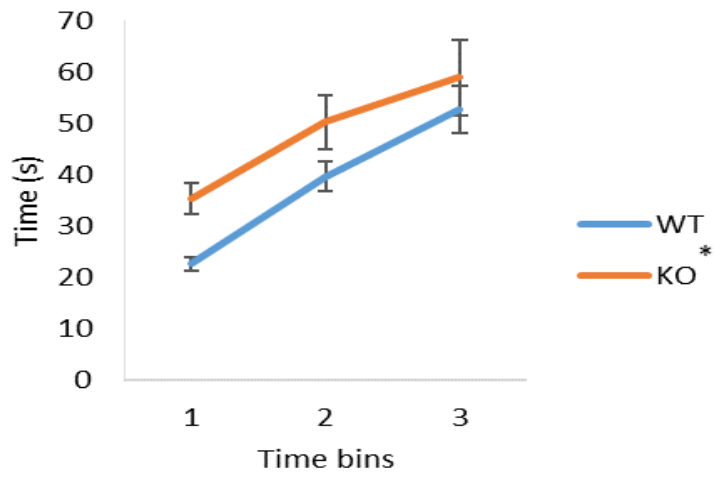


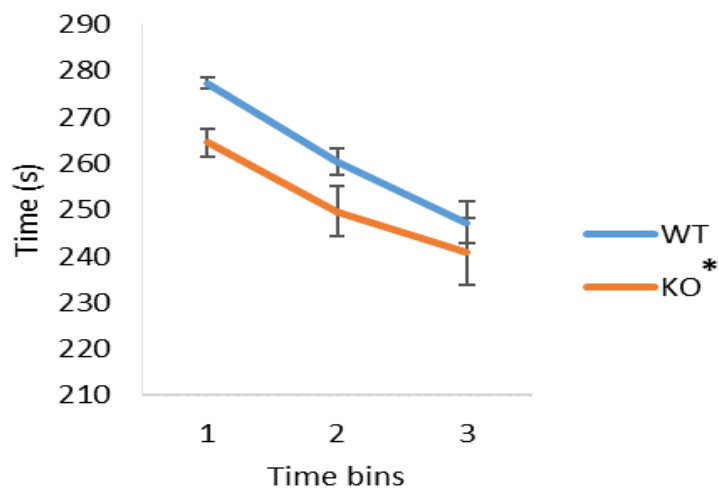
Figure 4.6 Distance moved in open field test for Zdhhc9 KO and WT mice. Distance moved in habituation period (A) and in test period (B) (n=14 KO, 20 WT) are depicted; error bars show SEM. Statistics were conducted using general linear model, repeated measures in SPSS version 22 ($p=0.073$ for effect of genotype during habituation and $p=0.105$ for effect of genotype during test period). Each time bin represents a period of 5 min.

There was no significant difference in habituation ($p=0.073$) or test period ($p=0.105$) in distance moved between the two groups (general linear model, repeated measures using SPSS version 22), however there was a trend for hyperactivity in the KO group throughout the experiment (Figure 4.6).

A Time in inner zone during habituation



B Time in outer zone during habituation



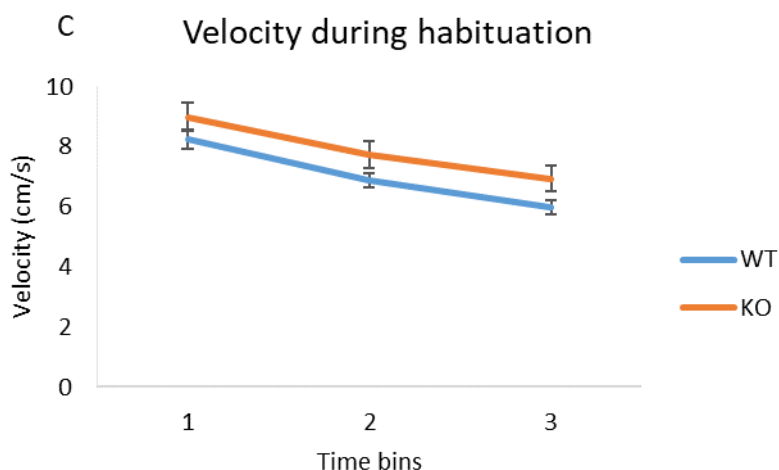
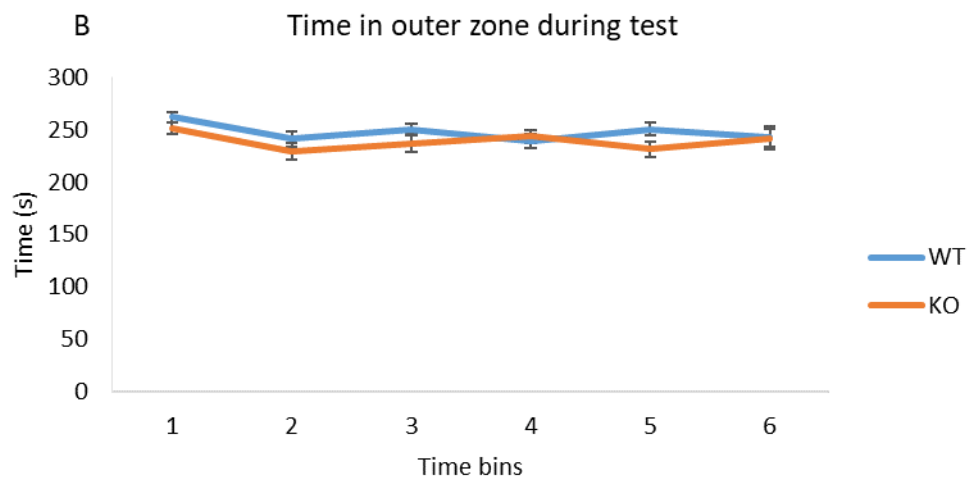
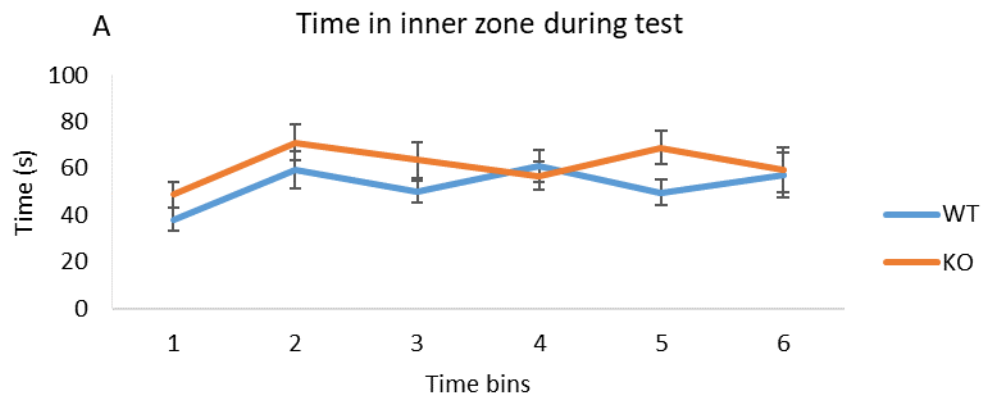


Figure 4.7 Thygmotactic behaviour and velocity of *Zdhhc9* KO and WT mice during the habituation period of open field test. Time spent in inner zone of the open field (A), time spent in outer zone (B) and mean velocity during habituation (C) are shown (n=14 KO, 20 WT; error bars show SEM). Statistics were conducted using general linear model, repeated measures in SPSS version 22 (p=0.039 for effect of genotype in time spent in inner and outer zones and p=0.073 for effect of genotype on velocity). Each time bin represents a period of 5 min.

Although there was no significant difference in locomotor activity, there was a difference in thygmotactic behaviour between KO and WT animals during the habituation period with KO mice spending significantly more time in the inner zone of the open field and subsequently less time near the walls of the open top box (p=0.039 for effect of genotype on time spent in inner and outer zone during habituation, Figure 4.7A,B). The velocity of the animals during this period was not significantly different (p=0.073, Figure 4.7C). This result possibly indicates lower anxiety levels of the KO mice during the habituation.

As regards the test period, there was no significant difference in time spent in inner and outer zones or in velocity of the two groups (Figure 4.8).



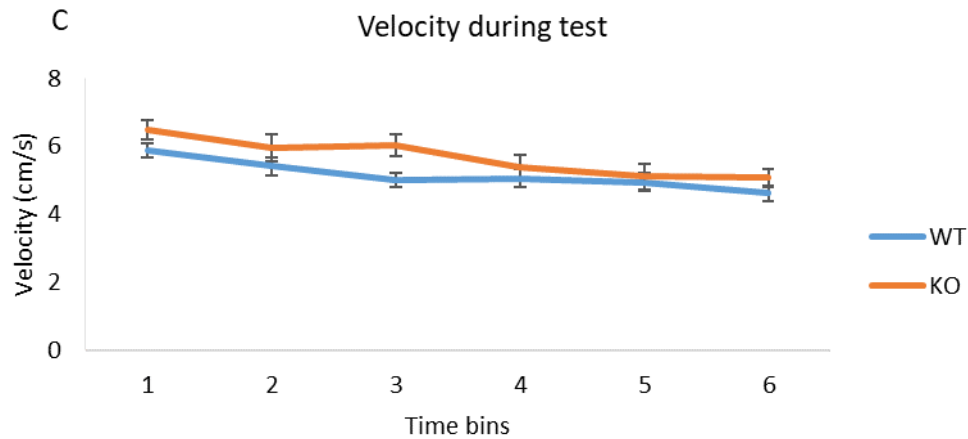


Figure 4.8 Thygmotactic behaviour and velocity of Zdhhc9 KO and WT mice during the test period of open field test. Time spent in inner zone of the open field (A), time spent in outer zone (B) and mean velocity during test (C) are shown (n=14 KO, 20 WT; error bars show SEM). Statistics were conducted using general linear model, repeated measures in SPSS version 22 ($p > 0.05$ for effect of genotype in time spent in inner and outer zones and in velocity). Each time bin represents a period of 5 min.

4.2.6 Zdhhc9 KO mice exhibit reduced anxiety levels in the elevated plus maze

The performance of the Zdhhc9 KO mice in the habituation period of the OFT suggested a possible change in anxiety levels. To examine this further, the 14 KO and 20 WT adult male mice were subsequently tested in the elevated plus maze (Figure 4.9). The time spent between open and closed arms of this apparatus is used as a measure of anxiety in rodents.

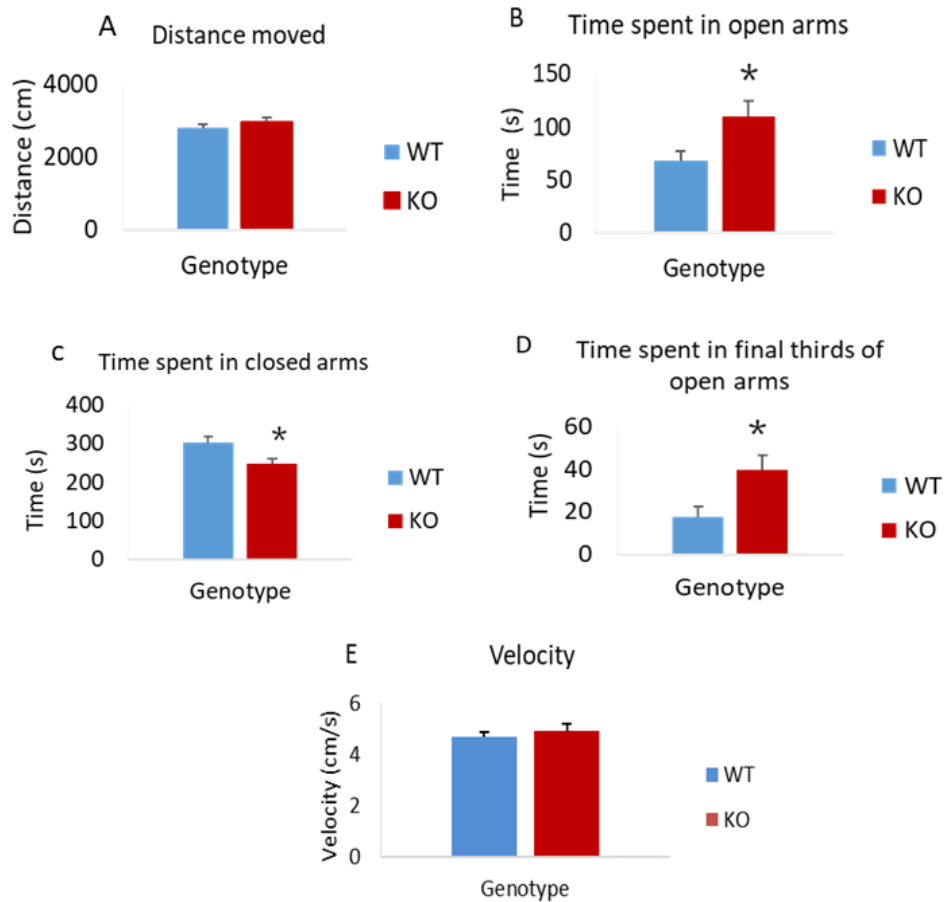


Figure 4.9 Performance of Zdhhc9 KO and WT mice in the elevated plus maze. Distance moved (A), time spent in open arms (B), time spent in closed arms (C), time spent in final third of open arms (D) and mean velocity during test (E) are shown (n=14 KO, 20 WT) ; error bars show SEM. Statistics were conducted using unpaired t test in Minitab version 17 ($p=0.021$ for effect of genotype on time spent in the open arms, $p=0.008$ for effect of genotype on time spent in closed arms and $p=0.011$ for effect of genotype on time spent in the final thirds of open arms).

Both groups moved a similar distance during the test period and had similar velocity but they differed significantly in time spent in the open arms ($p=0.021$), closed arms ($p=0.008$) and final thirds of open arms ($p=0.011$) suggesting that the KO mice do indeed have lower anxiety levels than WT mice. Statistics were conducted using unpaired t test in Minitab version 17.

4.2.7 Zdhhc9 KO mice exhibit reduced startle reactivity in the startle curve

Startle reactivity is a measure of the startle reflex but emotional and motor components play a role in this response (Crawley, 2006). It is interesting that startle reactivity has been associated to anxiety levels as anxiolytic drugs have been found to reduce this response (Walker and Davis, 1997). Moreover, children with anxiety disorder show increased startle reactivity (Bakker et al., 2009).

In order to assess startle reactivity in the Zdhhc9 KO animals, the startle curve task was conducted in 22 KO and 24 WT animals that were exposed to a range of volumes and their startle reactivity was measured as displacement of an accelerometer attached to the restrainer.

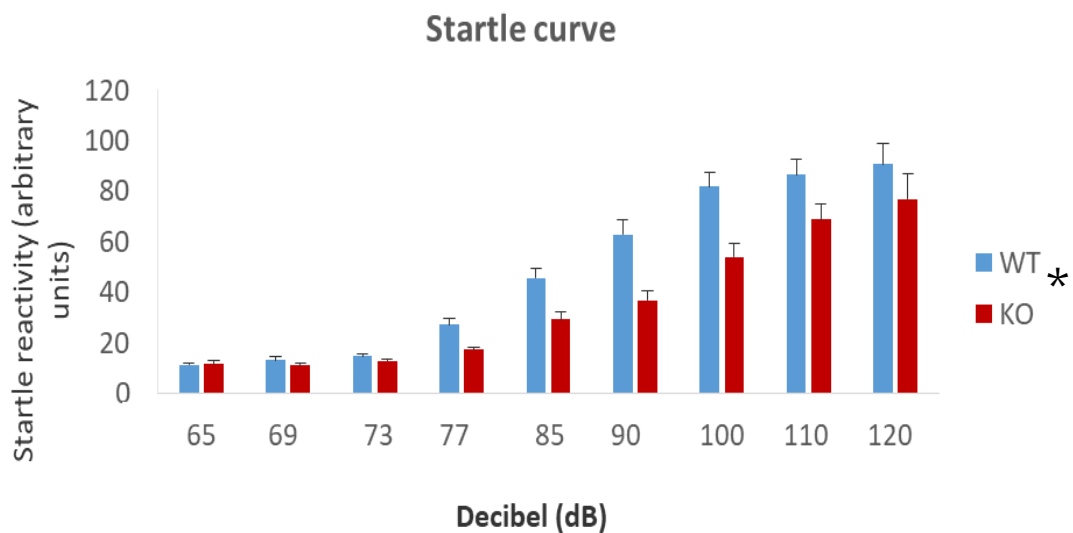


Figure 4.10 Startle reactivity of Zdhhc9 KO and WT mice. The startle response to a sound at a range of levels (dB) was measured; error bars show SEM. Statistics were conducted using general linear model, repeated measures in SPSS version 22 (n=22 KO, 24 WT, $p=0.001$ for effect of genotype).

There was a significant effect of genotype in startle reactivity ($p=0.001$, general linear model, repeated measures, SPSS version 22,

Figure 4.10). The results indicate that the *Zdhhc9* KO animals begin to exhibit a startle response at higher decibel levels (85dB and above) compared to WT animals (77 dB), which is overall consistent with the lower anxiety levels of KO animals indicated from the previous tasks.

4.2.8 *Zdhhc9* KO mice exhibit normal pre-pulse inhibition

2 days after the startle curve task, the same animals (n=22 KO, 24 WT) were tested in pre-pulse inhibition task to assess sensorimotor gating. This task also provides a sensitive measure of hearing. Animals were exposed to 120dB startle trials which were preceded with a range of pre-pulses above the background level of 65dB. The pre-pulse levels were 4, 8 and 16dB above the background level of 65dB (so 69, 73 and 81dB).

The results are presented as % of pre-pulse inhibition which is calculated as $100 \times \frac{\text{startle reactivity at 120dB} - \text{startle reactivity at prepulse level}}{\text{startle reactivity at 120dB}}$

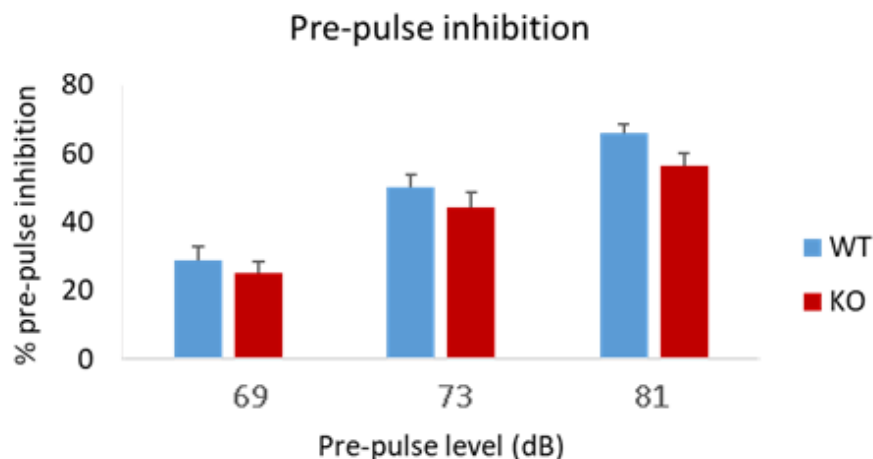


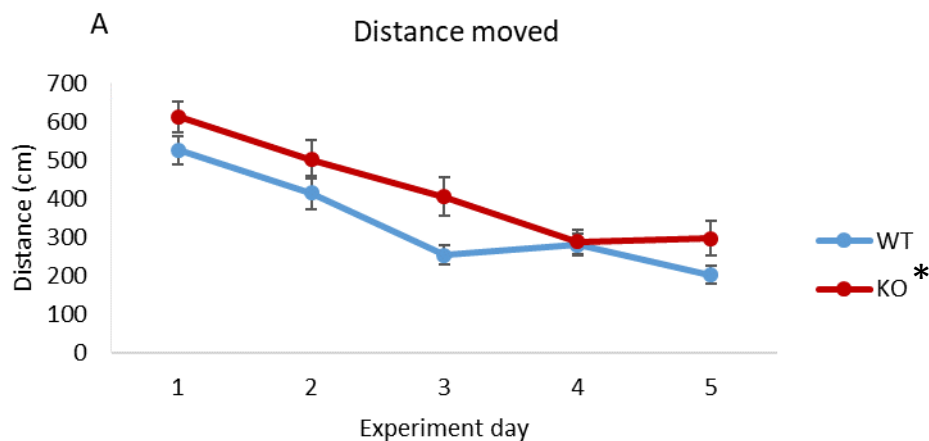
Figure 4.11 Analysis of pre-pulse inhibition of *Zdhhc9* KO and WT mice. Mice received a pre-pulse at the levels (dB) shown. Following this, the startle response to a 120 dB sound was measured. Results are presented as % pre-pulse inhibition; error bars show SEM.

Statistics were conducted using general linear model, repeated measures in SPSS version 22 (n=22 KO, 24 WT, $p>0.05$ for effect of genotype).

The *Zdhhc9* KO animals showed a similar pattern of pre-pulse inhibition to WT animals indicating that they have normal sensorimotor gating and hearing ability (Figure 4.11).

4.2.9 *Zdhhc9* KO mice exhibit a different pattern of spatial learning in the Morris water maze

The results presented thus far suggested that *Zdhhc9* KO mice have reduced anxiety levels, lower grip strength and possibly also hyperactivity. Disruption of the *ZDHHC9* gene in humans is associated with intellectual disability (ID), and thus to identify any learning and memory deficits in the mouse model (that may have relevance to ID), 20 KO and 26 WT mice were tested in the Morris water maze. The distance travelled and the time spent by WT and KO mice to find a submerged platform in the water tank was measured over five consecutive days.



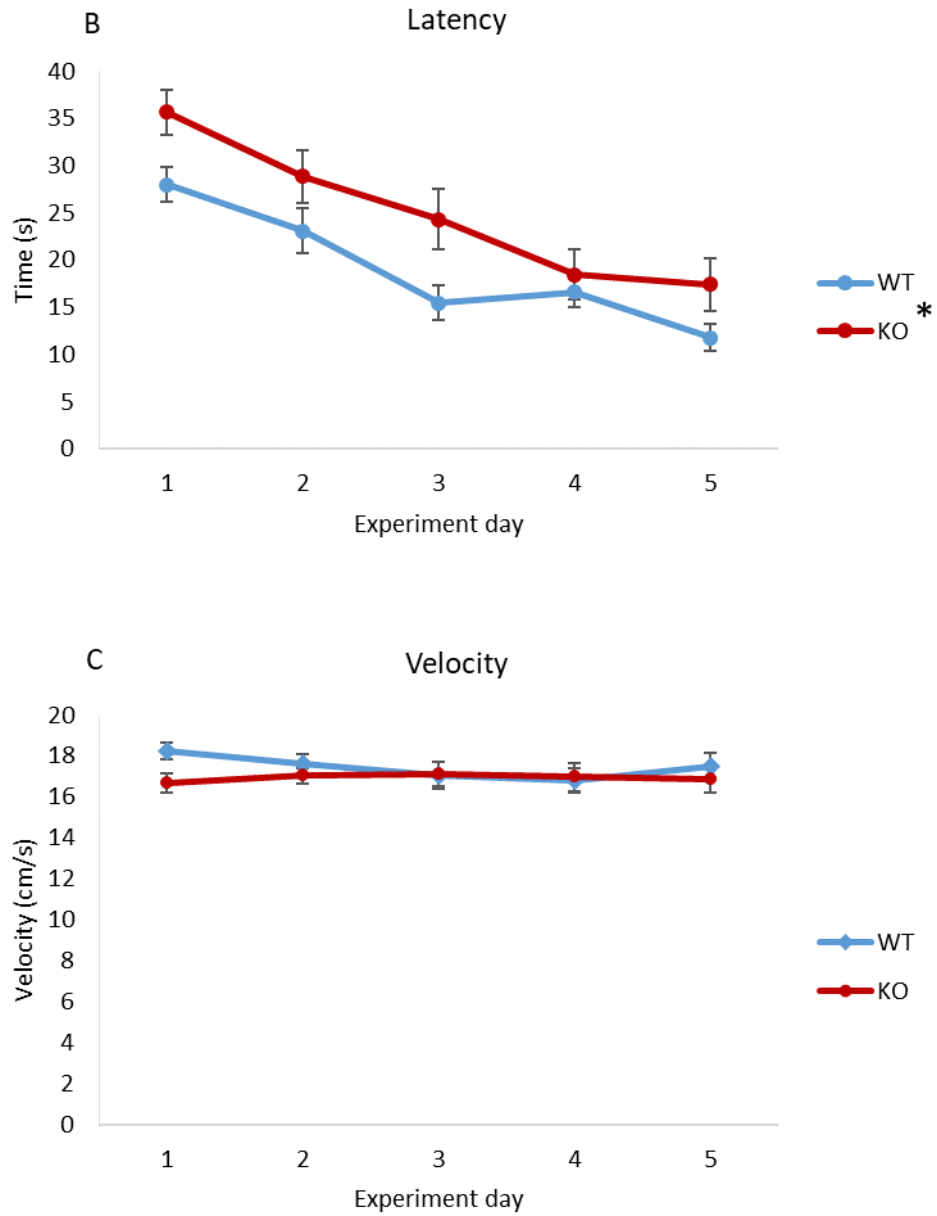


Figure 4.12 Performance of Zdhhc9 KO and WT mice in the Morris water maze. Distance moved (A), latency (B) and mean velocity (C) during the 5 days of the experiment are shown (n=20 KO, 26 WT) ; error bars show SEM. Statistics were conducted using general linear model, repeated measures in SPSS version 22 (p=0.005 for effect of genotype on distance moved and p=0.003 on latency).

The KO mice displayed a different pattern of spatial learning showing a learning deficiency (Figure 4.12). There was an overall effect of genotype on distance moved ($p=0.005$) and latency (duration to complete the task, $p=0.003$) but not in velocity suggesting that the observed deficit is not related to swimming ability.

Following the water maze experiment, a probe trial took place in order to assess reference memory on the same animals (20 KO, 26 WT) where the platform was removed and the time spent in the quadrant where the platform was versus the opposite quadrant was measured.

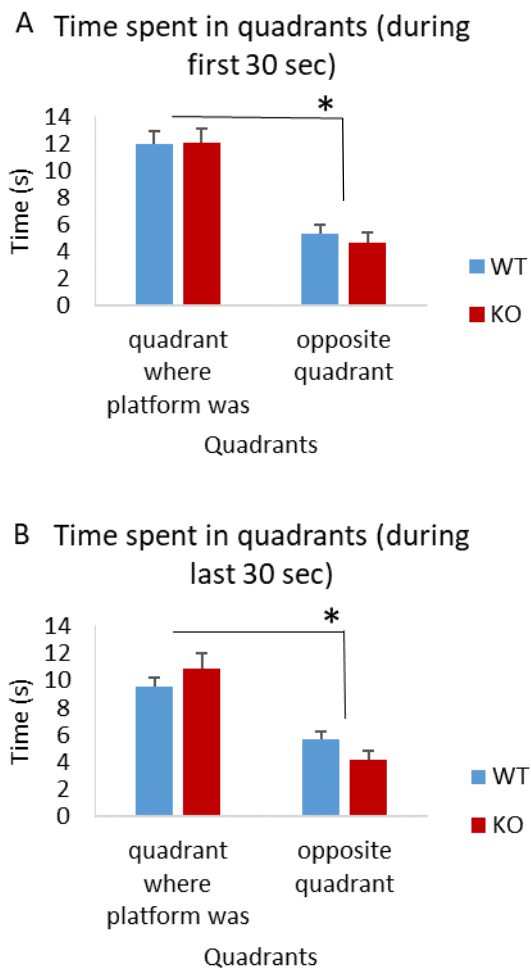


Figure 4.13 Performance of Zdhhc9 KO and WT mice in the probe trial of Morris water maze. Time spent in quadrants during the first 30 seconds of the trial (A) and during the last

30 seconds of the trial (B) are shown (n=20 KO, 26 WT); error bars show SEM. Statistics were conducted using general linear model, repeated measures in SPSS version 22 ($p < 0.001$ for effect of quadrant during the first and last 30 seconds).

There was a significant effect of quadrant but not genotype on performance indicating that both groups learned where the platform was by the end of the task (general linear model, repeated measures, $p < 0.001$ for effect of quadrant) as they spent significantly more time in the quadrant where the platform was during the 60 seconds of the probe trial (Figure 4.13).

After the probe trial, a visual cue test was conducted on the same animals (20 KO, 26 WT) in order to exclude the possibility of any motivation differences or visual deficits. Both groups reached the platform in a similar time indicating that Zdhhc9 KO mice were as motivated to complete the task as WT animals and they were able to see the platform (Figure 4.14).

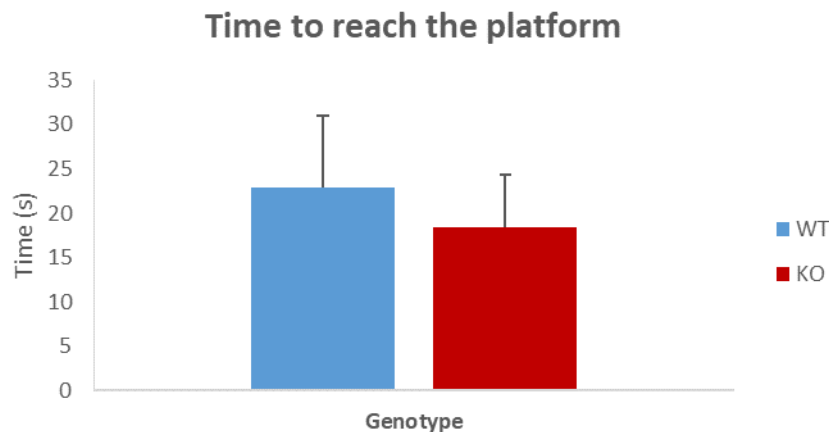
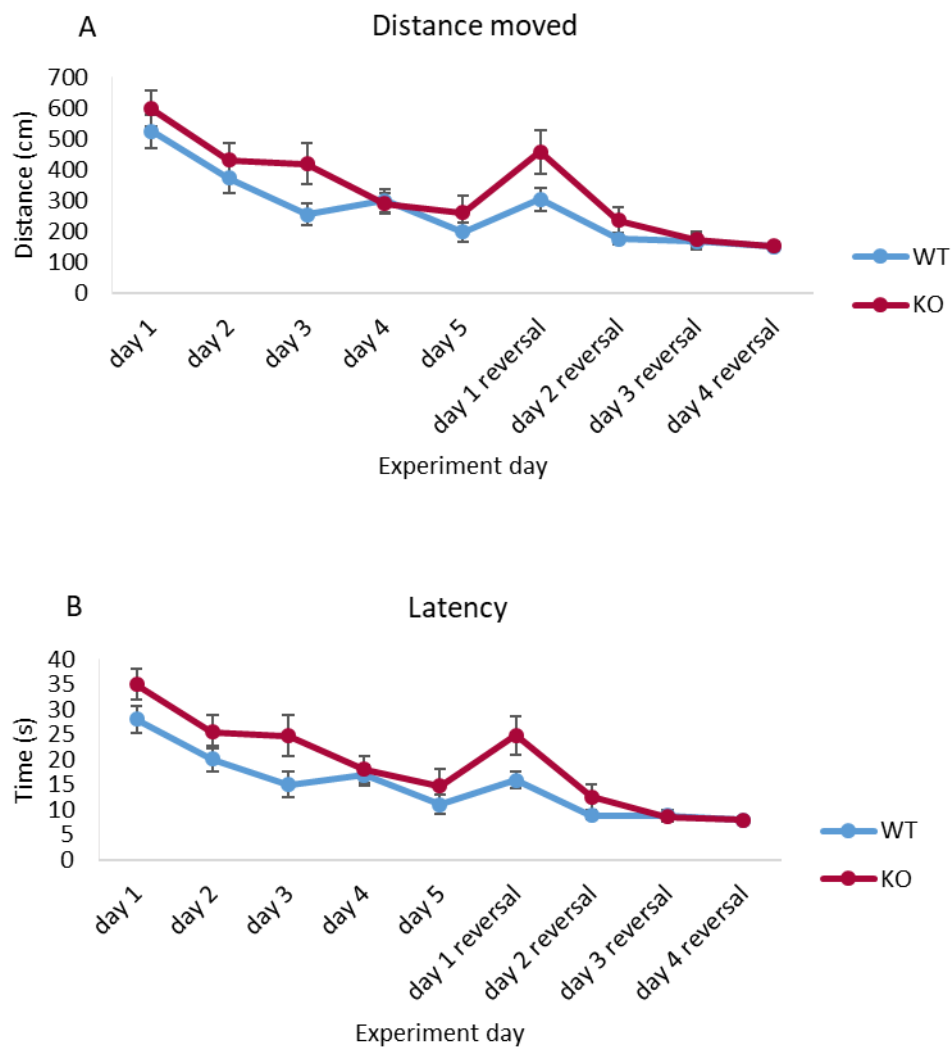


Figure 4.14 Comparison of Zdhhc9 KO and wild- type mice in the visual cue trial of the Morris Water Maze. Time spent to reach the visible platform for Zdhhc9 KO and WT mice during the visual cue trial of Morris water maze; error bars show SEM. Statistics were conducted using unpaired t test in Minitab version 17 (n=20 KO, 26 WT, $p > 0.05$ for effect of genotype).

4.2.10 Zdhhc9 KO mice exhibit a different pattern of reversal learning in Morris water maze

It was subsequently tested if changing the position of the platform (reversal learning) led to a different response from WT and KO mice. 13 KO and 16 WT mice were tested in the Morris water maze, where the mice learned platform position over an initial 5 days (as above) followed by a learning period in which the position of the platform was moved.



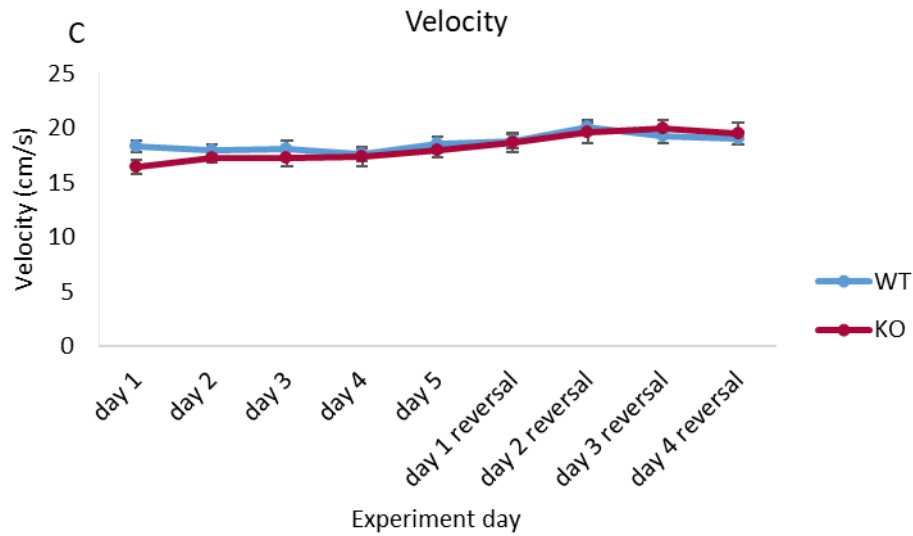


Figure 4.15 Performance of *Zdhhc9* KO and WT mice in Morris water maze and reversal learning test. Distance moved (A), latency (B) and mean velocity (C) during the 9 days of the experiment are shown (n=13 KO, 16 WT); error bars show SEM. Statistics were conducted using general linear model, repeated measures in SPSS version 22. For the first 5 days: p=0.024 for effect of genotype in latency, p=0.057 in distance moved and p>0.05 in velocity. For the first 2 days of reversal learning: p=0.049 for effect of genotype in distance moved, p=0.026 for latency and p>0.05 in velocity.

For the first 5 days of the experiment there was an effect of genotype in latency (p=0.024) but not in distance moved (p=0.057, however close to significance) or velocity (p=0.197) (Figure 4.15). For the first 2 days of the reversal learning there was an effect of genotype in both distance moved (p=0.049) and latency (p=0.026) without a difference in velocity between the two groups. On days 3 and 4 of the reversal learning, the two groups had similar performance (Figure 4.15).

At the end of the traditional task and before the reversal learning task started, a probe trial was conducted on the same animals in order to assess reference memory (13 KO, 16 WT). There was a significant effect of quadrant (p<0.001) but not genotype on performance indicating that both groups learned

where the platform was by the end of the task (general linear model, repeated measures) as they spent significantly more time in the quadrant where the platform was during the 60 seconds of the probe trial (Figure 4.16).

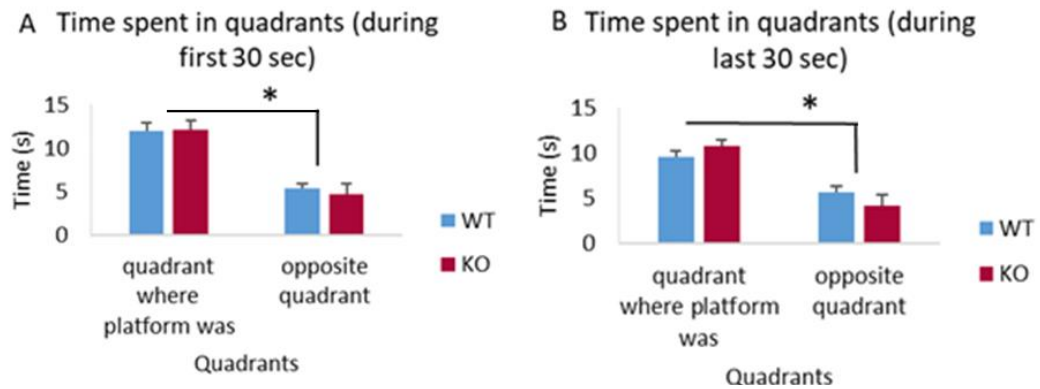


Figure 4.16 Performance of *Zdhhc9* KO and WT mice in the probe trial of Morris water maze. Time spent in quadrants during the first 30 seconds of the trial (A) and during the last 30 seconds of the trial (B) are shown (n=13 KO, 16 WT); error bars show SEM. Statistics were conducted using general linear model, repeated measures in SPSS version 22 ($p < 0.001$ for effect of quadrant during the first and last 30 seconds).

After the probe trial and before the reversal learning, a visual cue test was also conducted on the same animals (13 KO, 16 WT) in order to exclude the possibility of any motivation differences or visual deficits and both groups reached the platform on a similar time indicating that they were both motivated to complete the task and able to see the platform (Figure 4.17).

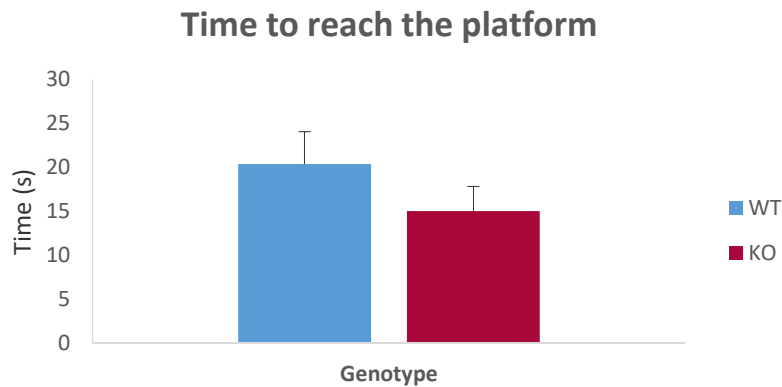
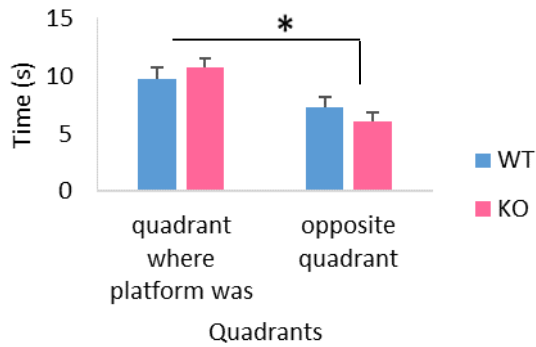


Figure 4.17 Comparison of Zdhhc9 KO and wild- type mice in the visual cue trial of the Morris Water Maze. Time spent to reach the visible platform for Zdhhc9 KO and WT mice during the visual cue trial of Morris water maze; error bars show SEM. Statistics were conducted using unpaired t test in Minitab version 17 (n=13 KO, 16 WT, $p>0.05$ for effect of genotype).

At the end of the reversal learning task, a probe trial was conducted on the same animals in order to assess reference memory (13 KO, 16 WT). There was a significant effect of quadrant ($p=0.010$) but not genotype on performance during the first 30 seconds of the probe trial indicating that both groups learned where the platform was by the end of the task (general linear model, repeated measures) as they spent significantly more time in the quadrant where the platform was (Figure 4.18A).

During the last 30 seconds of the probe trial, there was no significant effect of quadrant but genotype ($p=0.043$, general linear model, repeated measures) indicating that the animals not being able to find the platform, started looking for the platform in other locations including the opposite quadrant (Figure 4.18B).

A Time spent in quadrants during first 30 sec



B Time spent in quadrants during last 30 sec

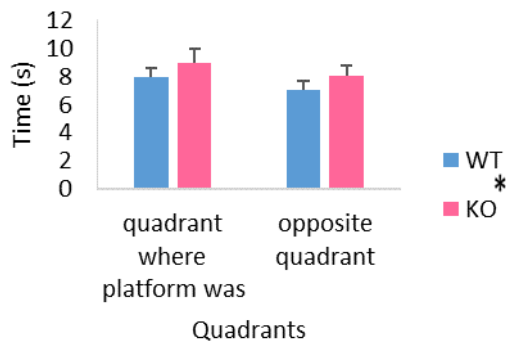


Figure 4.18 Performance of Zdhc9 KO and WT mice in the probe trial of Morris water maze after reversal learning. Time spent in quadrants during the first 30 seconds of the trial (A) and during the last 30 seconds of the trial (B) are shown; error bars show SEM (n=13 KO, 16 WT). Statistics were conducted using general linear model, repeated measures in SPSS version 22 (p=0.01 for effect of quadrant during the first 30 seconds and p=0.043 for effect of genotype during the last 30 seconds).

After the probe trial of the reversal learning, a visual cue test was conducted on the same animals (13 KO, 16 WT) in order to ensure that there were no motivation differences at this stage of the experiment or any visual deficits and

both groups reached the platform on a similar time indicating that they were both motivated to complete the task and able to see the platform (Figure 4.19).

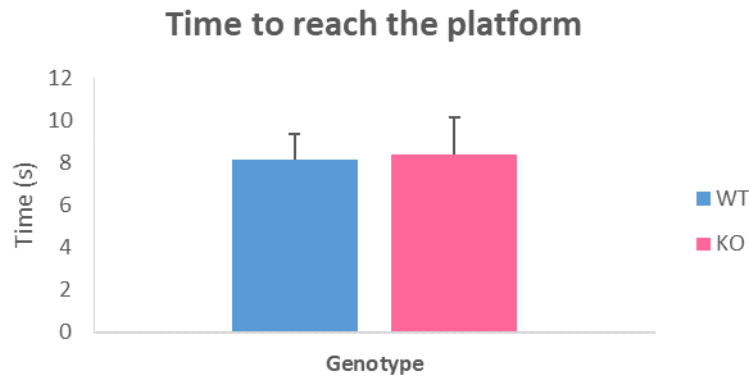


Figure 4.19 Comparison of Zdhhc9 KO and wild- type mice in the visual cue trial of Morris water maze after reversal learning. Average time taken to reach the visible platform is shown and error bars show SEM. Statistics were conducted using unpaired t test in Minitab version 17 (n=13 KO, 16 WT, $p>0.05$ for effect of genotype).

4.2.11 Zdhhc9 KO mice show normal working memory in Morris water maze

In order to examine if the Zdhhc9 KO animals exhibit a deficit in working memory, the working memory version of the Morris water maze was conducted in 7 KO and 10 WT animals after the traditional task. During the first 5 days of the traditional task, there was an overall effect of genotype on distance moved ($p=0.033$) but not on latency ($p=0.057$, however close to significance) or velocity ($p=0.914$) (Figure 4.20).

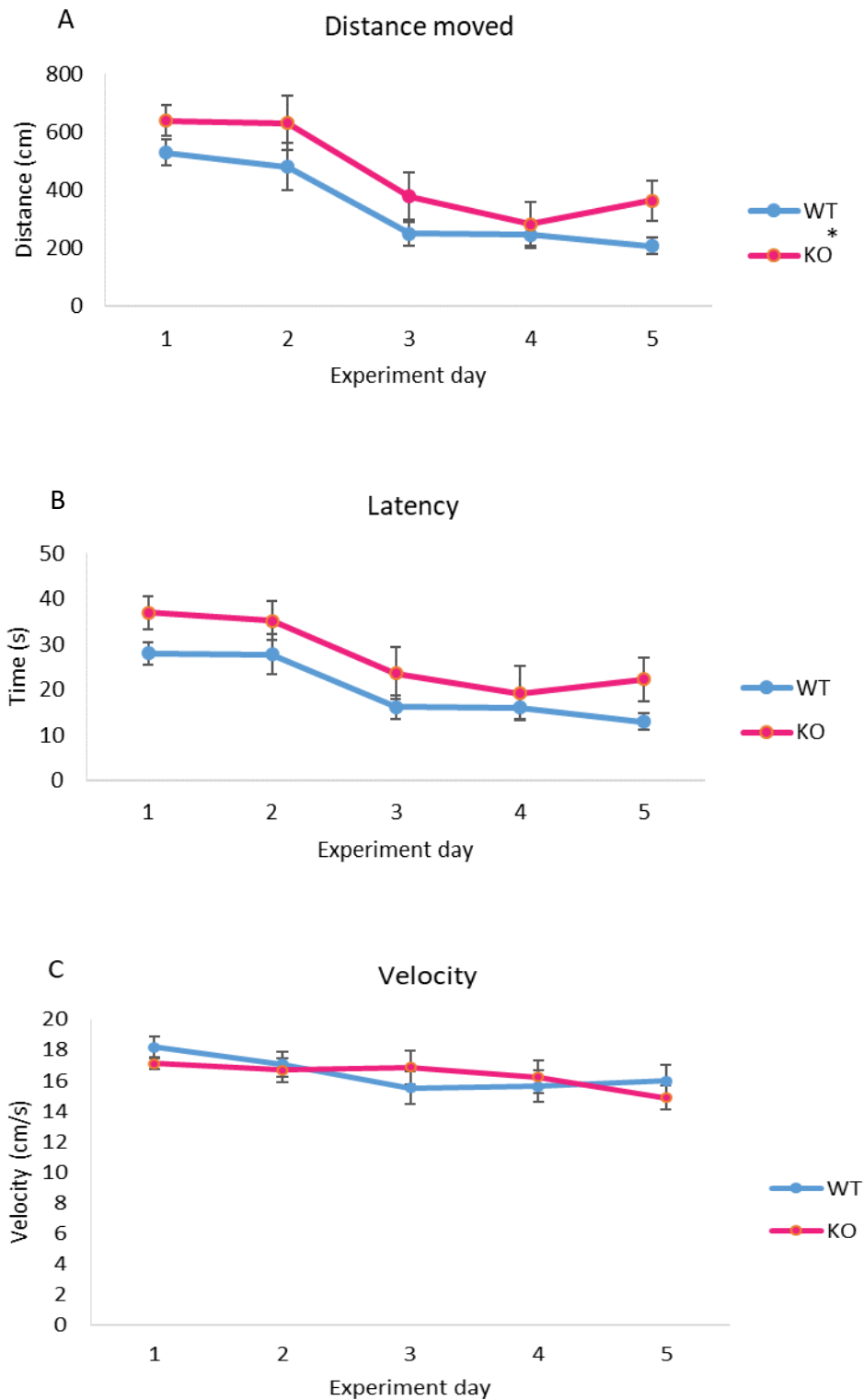


Figure 4.20 Performance of Zdhhc9 KO and WT mice in Morris water maze. Distance moved (A), latency (B) and mean velocity (C) during the 5 days of the experiment are shown

(n=7 KO, 10 WT); error bars show SEM. Statistics were conducted using general linear model, repeated measures in SPSS version 22 ($p=0.033$ for effect of genotype on distance moved, $p=0.057$ on latency and $p=0.914$ on velocity).

At the end of the traditional task and before the working memory task started, a probe trial was conducted on the same animals in order to assess reference memory (7 KO, 10 WT). There was a significant effect of quadrant ($p<0.001$) but not genotype on performance indicating that both groups learned where the platform was by the end of the task (general linear model, repeated measures) as they spent significantly more time in the quadrant where the platform was during the 60 seconds of the probe trial (Figure 4.21).

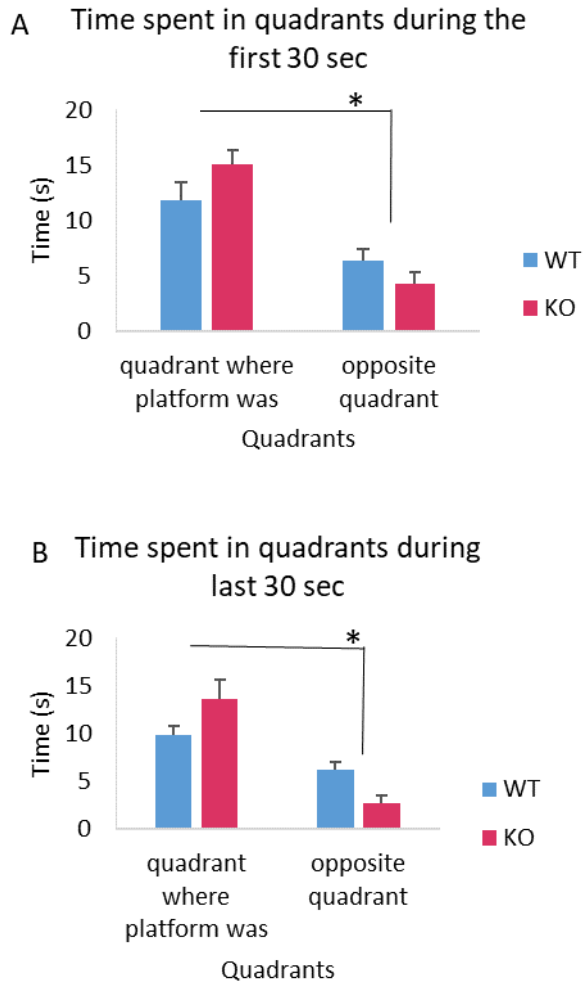


Figure 4.21 Performance of Zdhhc9 KO and WT mice in the probe trial of Morris water maze. Time spent in quadrants during the first 30 seconds of the trial (A) and during the last 30 seconds of the trial (B) are shown (n=7 KO, 10 WT); error bars show SEM. Statistics were conducted using general linear model, repeated measures in SPSS version 22 ($p < 0.001$ for effect of quadrant during the first and last 30 seconds).

After the probe trial, a visual cue test was conducted on the same animals (7 KO, 10 WT) in order to ensure that there were no motivation differences or visual deficits and both groups reached the platform in a similar time indicating that they

were both motivated to complete the task and able to see the platform (Figure 4.22).

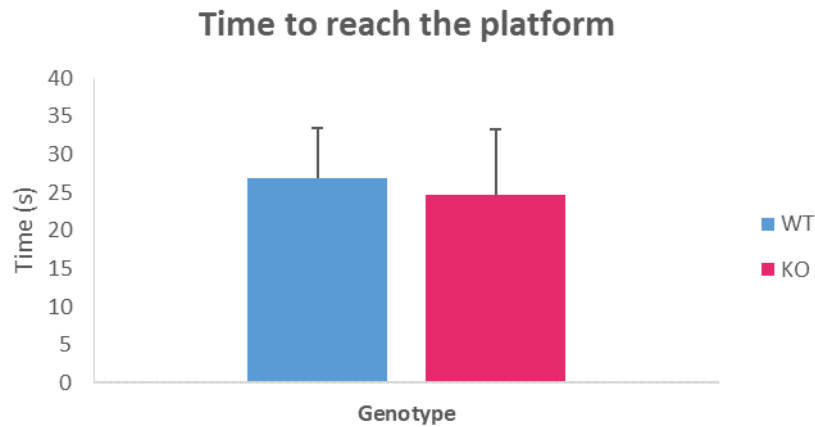


Figure 4.22 Performance of *Zdhhc9* KO and wild- type mice in the visual cue trial of Morris Water Maze. Average time spent to reach the visible platform is shown; error bars show SEM. Statistics were conducted using unpaired t test in Minitab version 17 (n=7 KO, 10 WT, $p>0.05$ for effect of genotype).

During the working memory task which lasted for 3 days and assesses how fast animals learn where the platform is within a day with the position of the platform changing every day, both groups performed in a similar manner indicating that the KO mice do not have a spatial working memory deficit (Figure 4.23).

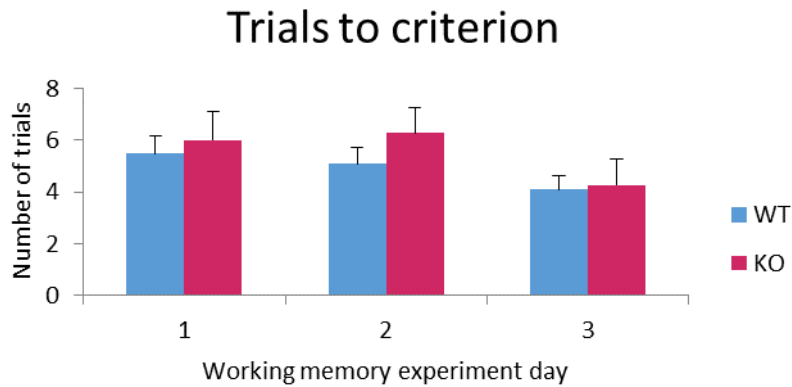


Figure 4.23 Performance of *Zdhhc9* KO and WT mice during the working memory experiment of Morris water maze. The number of trials to reach criterion is shown for each day of the experiment (n=7 KO, 10 WT); error bars show SEM. Statistics were conducted using general linear model, repeated measures in SPSS version 22 ($p > 0.05$ for effect of genotype).

4.2.12 *Zdhhc9* KO mice show normal sociability and social novelty

In order to assess social interactions in the *Zdhhc9* KO mice, 14 KO and 20 WT mice were tested in the 3 chamber apparatus for sociability and social novelty measuring the time each animal spent in the chamber where the stranger mouse 1 was put *versus* the empty chamber and then in the chamber where the stranger mouse 2 was put *versus* the chamber with the stranger mouse 1. Both groups spent similar time in the chamber where the stranger mouse 1 was, indicating that the KO mice show normal sociability (Figure 4.24A). Moreover, during the social novelty session, both groups spent similar time in the chamber where the stranger mouse 1 and 2 was, with both groups showing a preference for stranger mouse 2 as expected, indicating that the KO mice show normal behaviour during this task (Figure 4.24B).

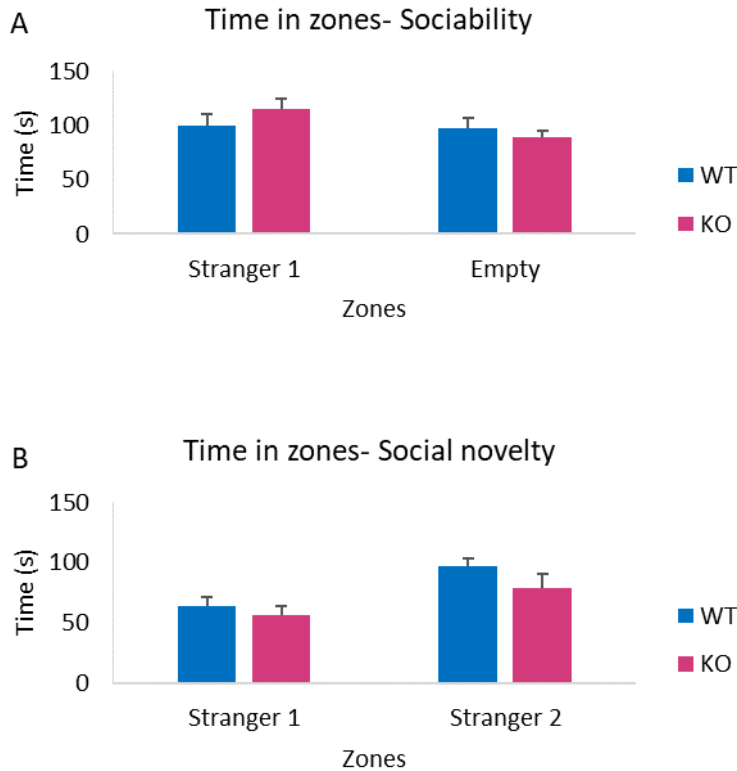


Figure 4.24 Residence time of *Zdhhc9* KO and wild- type mice in zones of the sociability and social novelty tests. Average time spent in different zones of the 3 chamber apparatus for sociability (A) and social novelty (B) for *Zdhhc9* KO and WT mice; error bars show SEM. The zone called 'stranger 1' represents the chamber where the 1st stranger mouse was placed while the zone called 'stranger 2' stands for where the 2nd stranger mouse was placed. Statistics were conducted using general linear model, repeated measures in SPSS version 22 (n=14 KO, 20 WT, $p > 0.05$ for effect of genotype).

As regards the distance moved, both groups travelled similar distance during the sociability ($p=0.053$, however close to significance) and social novelty ($p=0.188$) part of the task (Figure 4.25A, B). Their velocity was also similar ($p=0.059$ for sociability and $p=0.17$ for social novelty, Figure 4.25C, D).

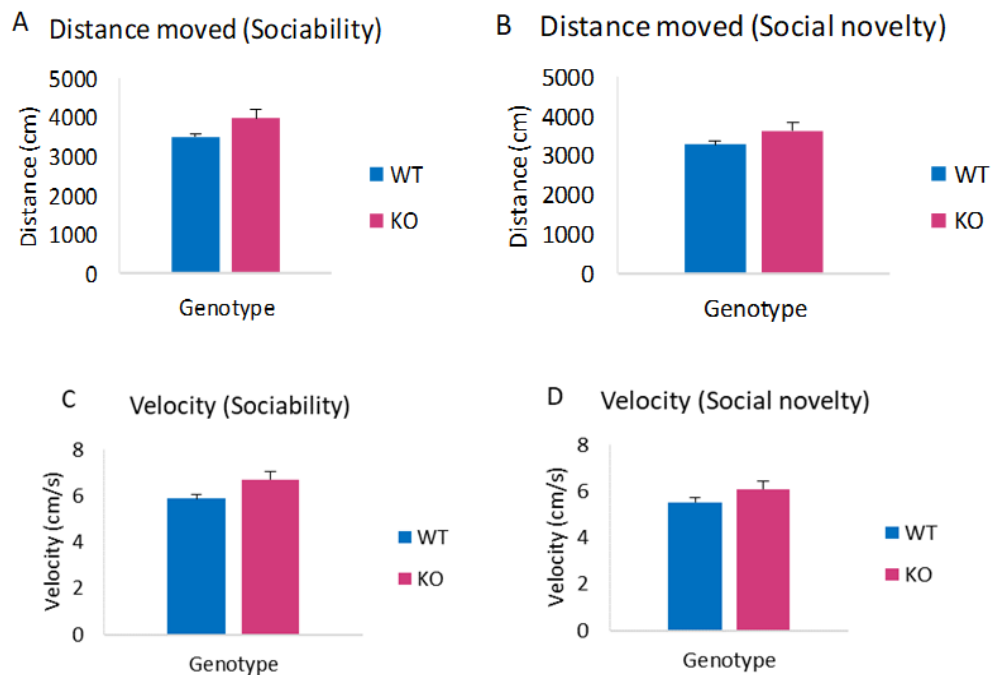


Figure 4.25 Distance moved and mean velocities for Zdhhc9 KO and WT mice in the 3 chamber apparatus for sociability and social novelty. Average distance moved during sociability (A) and social novelty (B) part of the experiment are presented as well as mean velocities during sociability (C) and social novelty (D) ; error bars show SEM. Statistics were conducted using unpaired t test in Minitab version 17 (n=14 KO, 20 WT, $p=0.053$ for effect of genotype on distance moved during sociability and $p=0.188$ for effect of genotype on distance moved during social novelty while $p=0.059$ for effect of genotype on velocity during sociability and $p=0.17$ for effect of genotype on velocity during social novelty).

4.2.13 Zdhhc9 KO mice show normal sucrose and water intake

In order to assess if Zdhhc9 KO animals experience any anhedonia, their preference for sucrose solution *versus* water was compared to the WT animals; 4 KO and 8 WT animals were studied for a period of 5 days. The sucrose and water intake are presented as a percentage of the total body weight in order to exclude the factor of possible intake differences based on body weight (Figure 4.26).

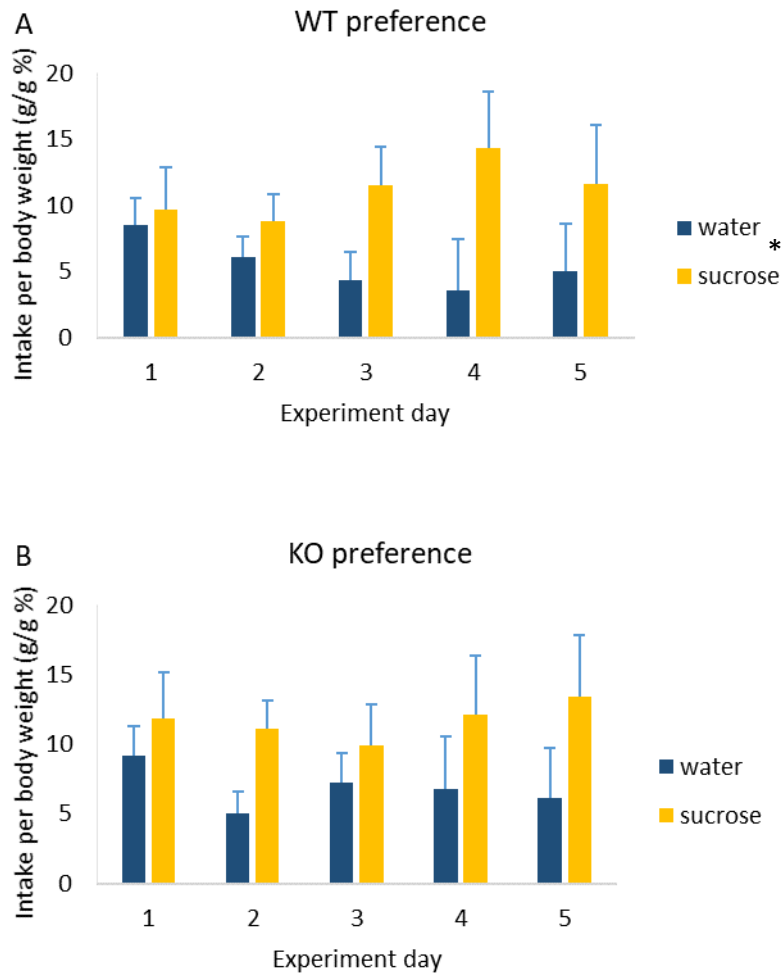


Figure 4.26 Preference of Zdhhc9 KO and wild-type mice for sucrose and water. WT (A) and Zdhhc9 KO (B) mice preference for sucrose solution versus water was measured over a period of 5 days. Results are expressed as intake per body weight; error bars show SEM. Statistics were conducted using general linear model, repeated measures in SPSS version 22 (n= 4 KO, 8 WT, $p=0.02$ for effect of solution in WT group while $p>0.05$ for effect of solution in KO group).

A similar trend of preference for sucrose *versus* water for both WT and KO groups was noticed (Figure 4.26). There was a significant preference for sucrose

versus water for the WT group ($p=0.020$ for effect of solution, Figure 4.26A). There was a similar trend for sucrose preference in the KO group but this was not statistically significant, possibly due to the small sample size ($n= 4$ for KO animals, Figure 4.26B).

4.2.14 Zdhhc9 KO mice show normal learning and cognitive flexibility in the pairwise discrimination task

In order to assess memory and cognitive flexibility that mainly involves the prefrontal cortex, the pairwise discrimination task was conducted in 12 KO and 12 WT mouse littermates. During the pairwise discrimination touchscreen task, the mice must learn that of two visual stimuli, only one is associated with a reward. The trial is completed for 15 days and the mice are tested each day. Following this period, the contingencies were then reversed to examine cognitive flexibility in the animals.

Both experimental groups completed similar number of trials and correction trials during the task and the reversal learning part of the task (Figure 4.27A, B). Moreover, both groups showed a similar pattern of correct responses during the task indicating that the Zdhhc9 KO animals perform normally in this task which mainly involves the prefrontal cortex (Figure 4.27C). The percentage of correct responses does not include correction trials.

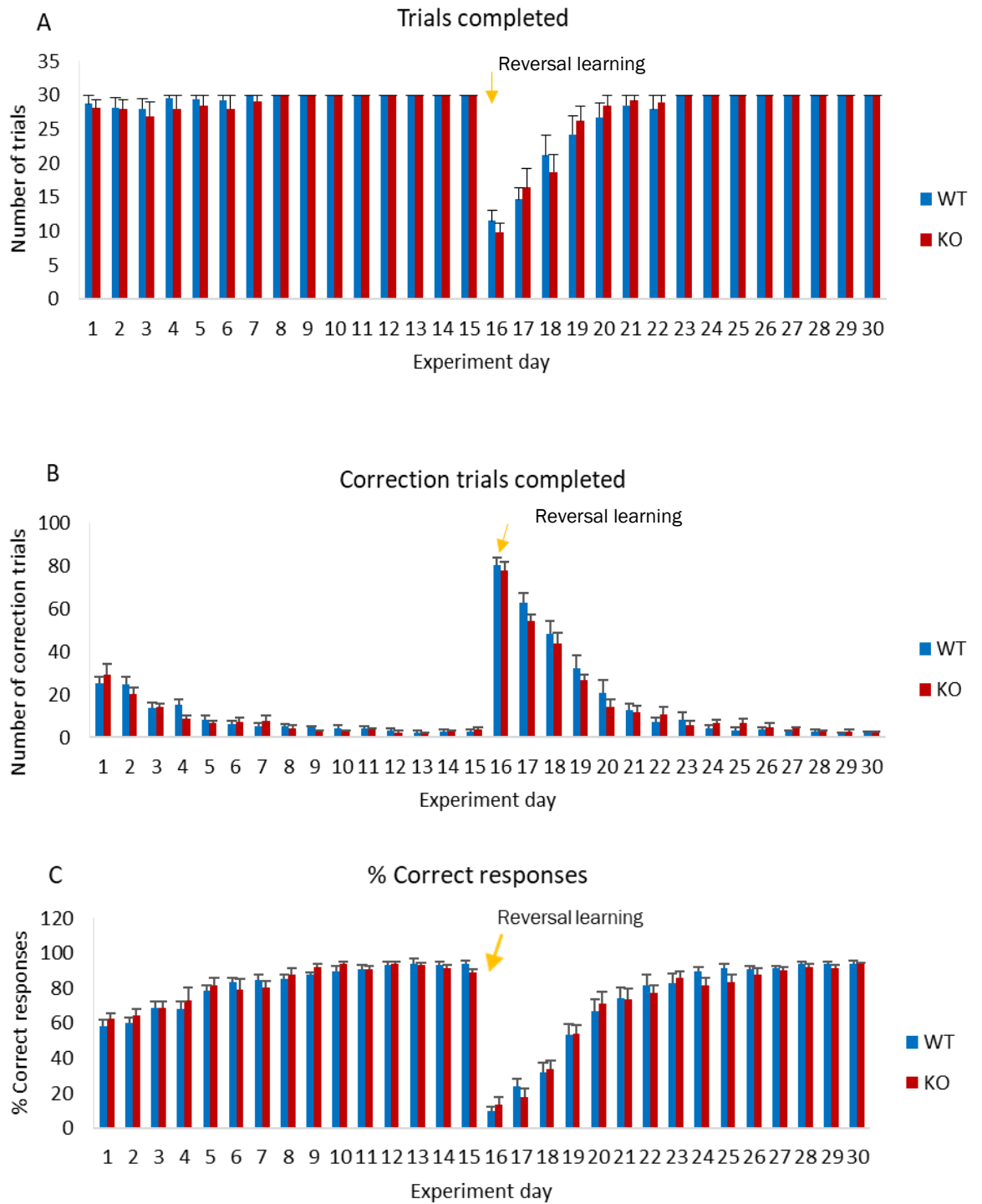


Figure 4.27 Performance of WT and Zdhhc9 KO mice in pairwise discrimination task and reversal learning. Number of trials completed (A), correction trials completed (B) and percentage of correct responses (C) are presented for a period of 30 days. On day 16, the

contingencies were reversed. Error bars show SEM. Statistics were conducted using general linear model, repeated measures in SPSS version 22 (n= 12 KO, 12 WT, $p>0.05$ for effect of genotype).

4.2.15 Analysis of the performance of Zdhhc9 KO mice in same paired associated learning (sPAL)

In order to further examine the behaviour of Zdhhc9 KO mice in learning and memory tasks, we used a variant of the pairwise discrimination task, sPAL in which rodents must learn and remember which of three objects goes in which of three spatial locations. sPAL assesses visual memory and new learning. 8 KO and 8 WT adult male mice that were backcrossed for less than 6 generations were used for this experiment.

No statistically significant effect of prior exposure to this task for either WT or KO mice was observed for time to complete the task (latency), trials completed, number of correction trials or percentage of correct responses (Figure 4.28). This suggests that the task is probably too complex to assess learning in mice.

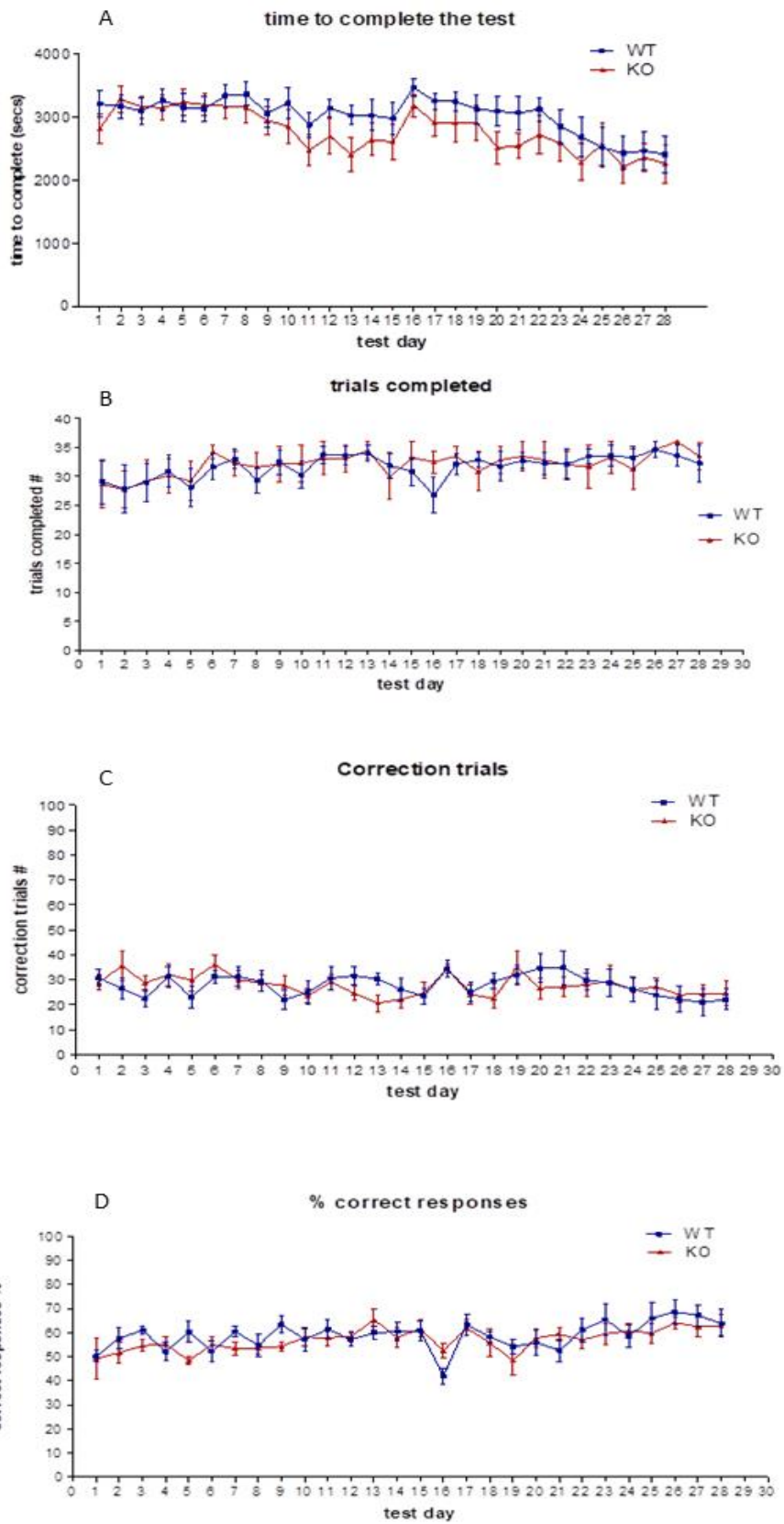


Figure 4.28 Performance of WT and Zdhhc9 KO mice in sPAL task. Time taken for mice to complete the task (A), number of trials completed (B), number of correction trials completed (C) and percentage of correct responses (D) are presented over a period of 28 days; error bars show SEM. Statistics were conducted using general linear model, repeated measures in SPSS version 22 (n= 8 KO, 8 WT, $p>0.05$ for effect of experiment day).

4.2.16 Zdhhc9 KO mice complete more trials than the WT mice but they have similar correct responses to the WT animals in the Five Choice Serial Reaction Time Task (5CSRTT)

In order to assess visuospatial attention and motor impulsivity, 10 KO and 10 WT mice were trained in the 5CSRTT for a period of 45 days.

The 5CSRTT was initially designed by Trevor Robbins and colleagues in the early 1980s as an analogue of the human continuous performance task. Because the 5CSRTT has separate measures of attention, impulsivity, and reaction times, it has proven useful in the pre-clinical study of the treatment of diagnoses such as attention-deficit/hyperactivity disorder and is also a precursor to modern rodent models of gambling and decision-making.

The 5CSRTT is designed to allow mice to associate light with a reward after nose- poking the location where the light appears. If they do not nose-poke the correct location (hole), no reward is given.

Zdhhc9 KO mice completed significantly more trials during the experiment compared to the WT animals ($p<0.001$ for effect of genotype) but the percentage of correct responses did not differ from the WT animals (Figure 4.29).

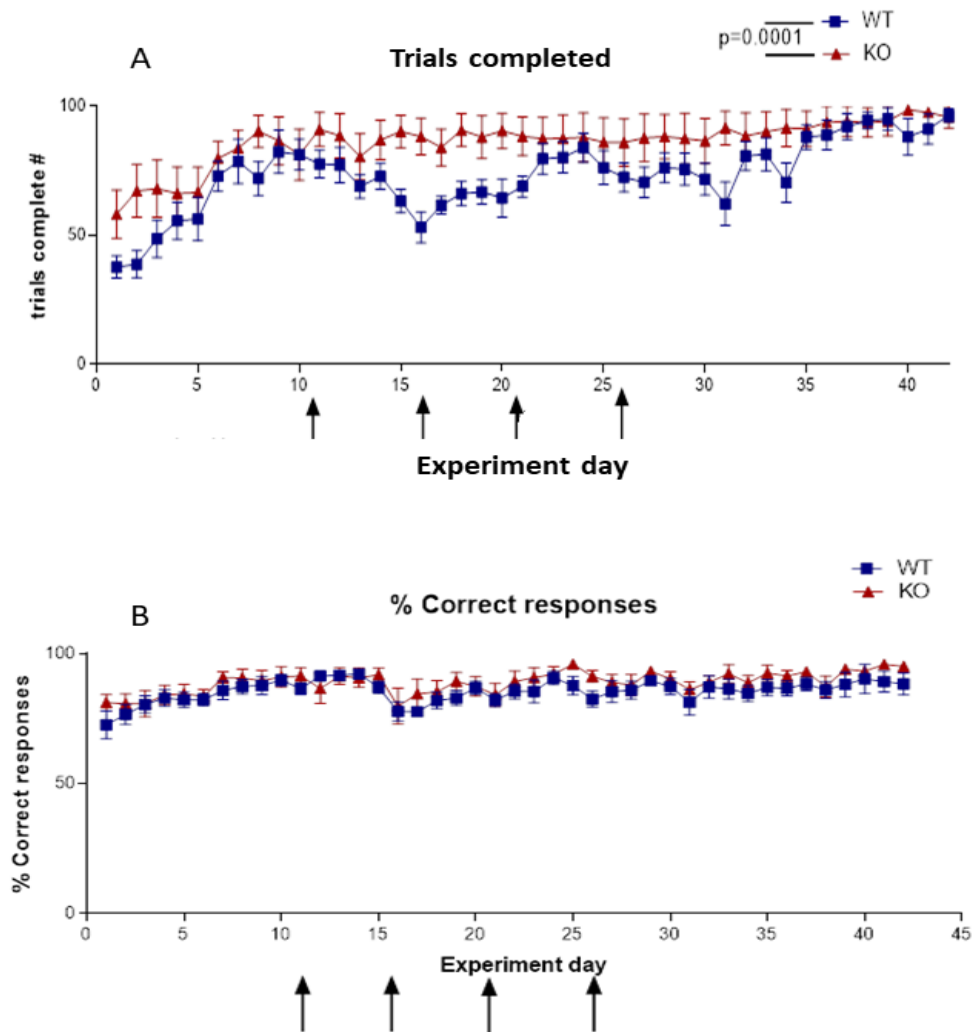


Figure 4.29 Performance of WT and Zdhhc9 KO mice in the test period of the Five Choice Serial Reaction Time Task. Number of trials completed (A) and percentage of correct responses (B) are presented over a period of 42 days; error bars show SEM. The arrows represent the days during which the difficulty was increased – each level increase decreased the stimulus duration time further. Statistical analysis was conducted using general linear model, repeated measures in SPSS version 22 (n=10 KO, 10 WT, $p = 0.0001$ for effect of genotype in trials completed and $p > 0.05$ for effect of genotype in percentage of correct responses).

4.2.17 Zdhhc9 KO mice react faster when responding correctly while they have similar percentage of correct responses and they complete similar number of trials to the WT mice in the final week of the 5CSRTT

During the final week of the 5CSRTT, a very short illumination period (0.8 s) was used to assess the performance of the animals. During this difficult task, Zdhhc9 KO mice completed a similar number of trials and had similar percentage of correct responses to the WT animals (n=10 KO, 10 WT, Figure 4.30A, B). However, their reaction time to a correct response was significantly lower indicating that the KO mice react faster (p=0.02 for effect of genotype, Figure 4.30C).

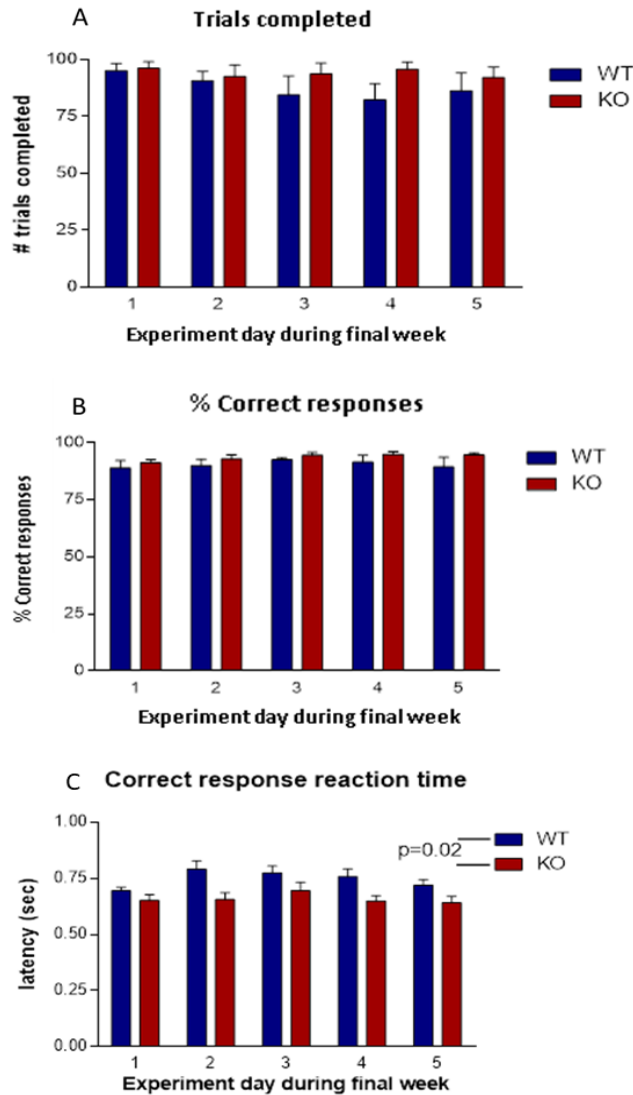


Figure 4.30 Performance of WT and Zdhhc9 KO mice in the final segment of the Five Choice Serial Reaction Time Task. Number of trials completed (A), percentage of correct responses (B) and correct response reaction time (C) are presented over the final week of the experiment, during which the stimulus duration was 0.8 sec; error bars show SEM. Statistical analysis was conducted using general linear model, repeated measures in SPSS version 22 (n=10 KO, 10 WT, $p > 0.05$ for effect of genotype in trials completed and percentage of correct responses while $p = 0.02$ for effect of genotype in correct response reaction time).

4.2.18 Zdhhc9 KO mice register more beam breaks while they have similar number of premature responses to the WT mice in the final week of the 5CSRTT

Measuring premature responses allows an insight into impulsivity and whether an animal is able to refrain from nose- poking at random in hope of a reward. A response would be considered premature when there has been a nose-poke which has come before a signal.

There was a low number of premature responses over the course of the five days of the final segment of 5CSRTT with exception of the first day, however this pattern was similar for both groups of mice and no significant effect of genotype was seen overall (Figure 4.31A).

In order to investigate the activity of Zdhhc9 KO mice during the training period, the number of beam breaks was examined. Inside each testing chamber, two beams register the movement of the animal; one placed at the front of the chamber near the nose-poke holes and another one on the opposite side next to the reward hopper. Each time the mouse passes through the beam, a beam break is registered. Zdhhc9 KO mice registered a higher number of beam breaks than the WT mice ($p=0.001$ for effect of genotype, Figure 4.31B) during the final week of the experiment.

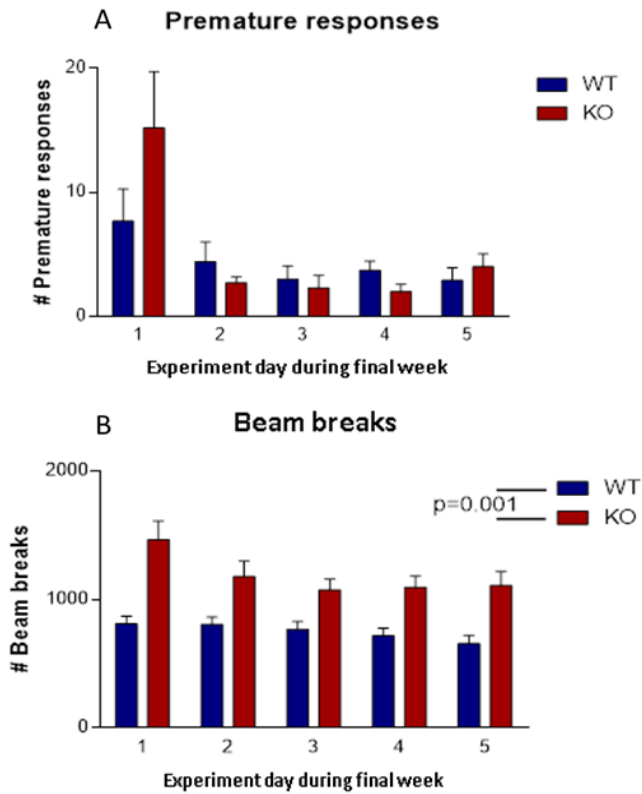


Figure 4.31 Number of premature responses (A) and beam breaks (B) of WT and *Zdhhc9* KO mice in the final segment of the Five Choice Serial Reaction Time Task. During the final week of the experiment, the stimulus duration was 0.8 sec. Error bars show SEM. Statistical analysis was conducted using general linear model, repeated measures in SPSS version 22 (n=10 KO, 10 WT, $p>0.05$ for effect of genotype in number of premature responses while $p=0.001$ for effect of genotype in number of beam breaks registered).

4.2.19 *Zdhhc9* KO mice have decreased volume of corpus callosum but not of hippocampus

In order to examine if the *Zdhhc9* KO mice exhibit shrinkage of corpus callosum, similarly to patients with mutations in this gene (Baker et al., 2015), *ex vivo* MRI scanning of 3 KO and 3 WT mouse brains was performed. The hippocampus was also examined due to the importance of this brain structure for learning and

memory and for successful completion of the Morris Water Maze task in which *Zdhhc9* KO mice were shown to have a deficit.

Coronal, transverse plane and sagittal images (Figure 4.32, Figure 4.33, Figure 4.34 respectively) showed a reduced corpus callosum area in KO mouse brain while no differences were observed in area of hippocampus between WT and KO mice.

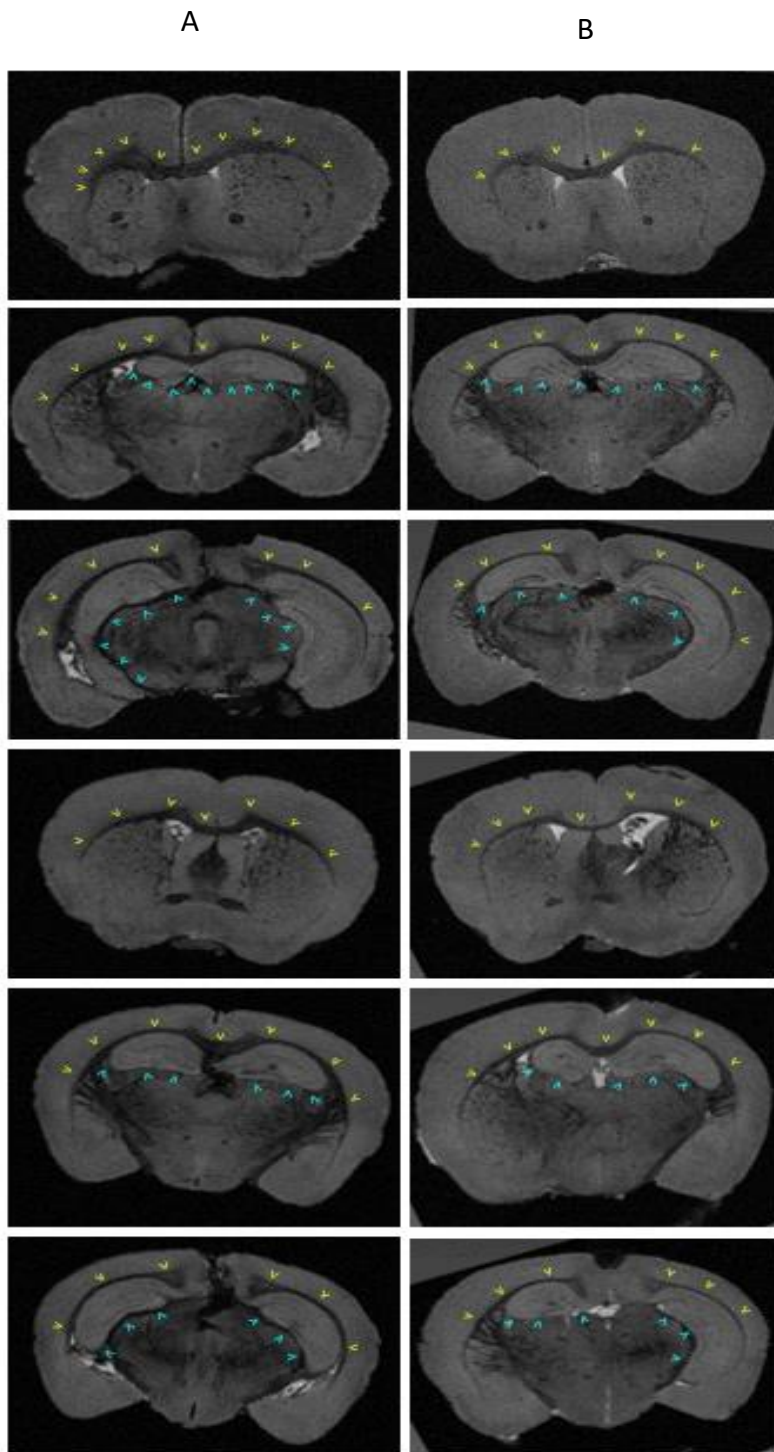


Figure 4.32 Coronal images from WT (A) and KO (B) mouse brains after ex vivo MRI scan in a 9.4 Tesla magnet. The yellow arrowheads point at corpus callosum while the light blue arrowheads point at the hippocampi.

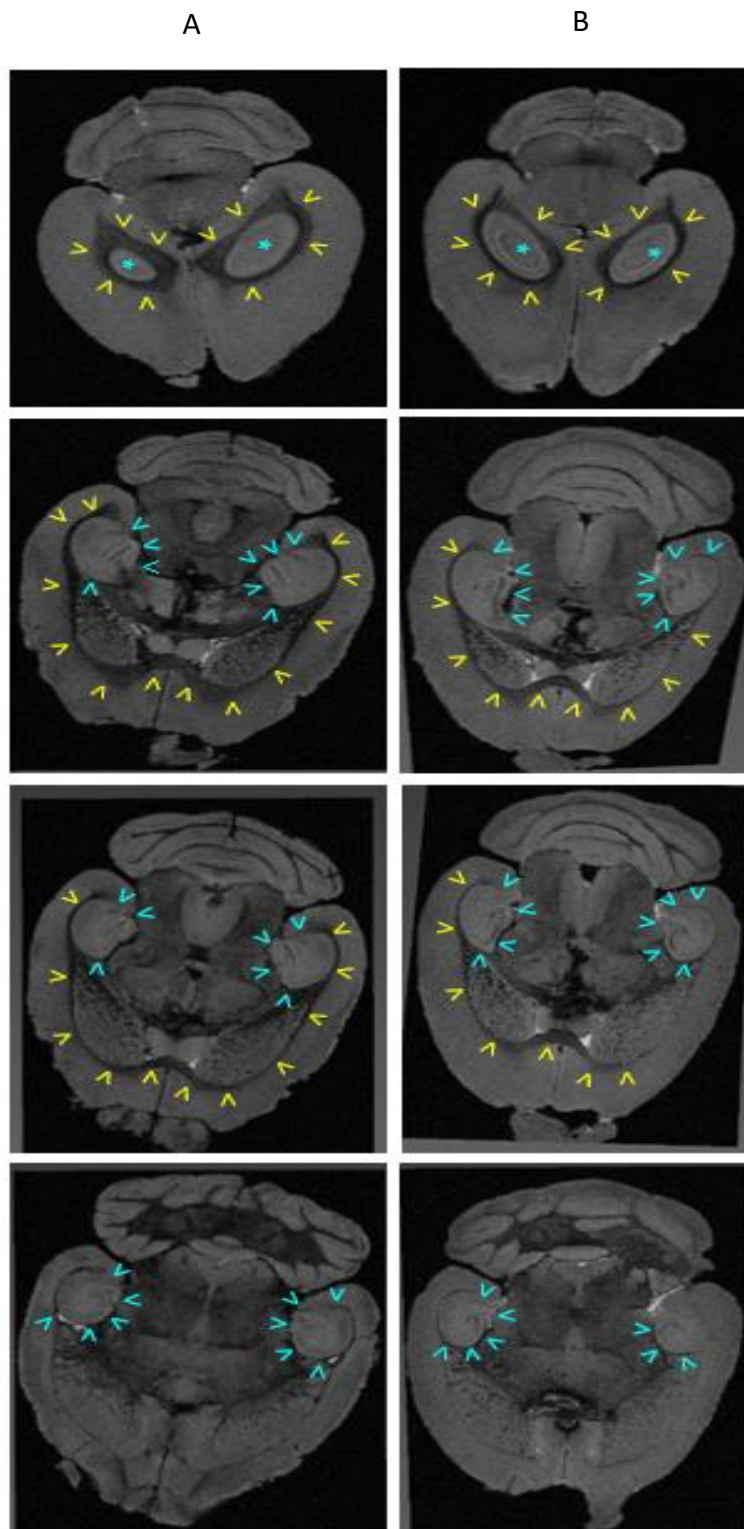


Figure 4.33 Transverse plane images from WT (A) and KO (B) mouse brains after *ex vivo* MRI scan in a 9.4 Tesla magnet. The yellow arrowheads point at corpus callosum while the light blue arrowheads point at the hippocampi. The light blue asterisks also depict the area of hippocampi (light area enclosed by the corpus callosum).

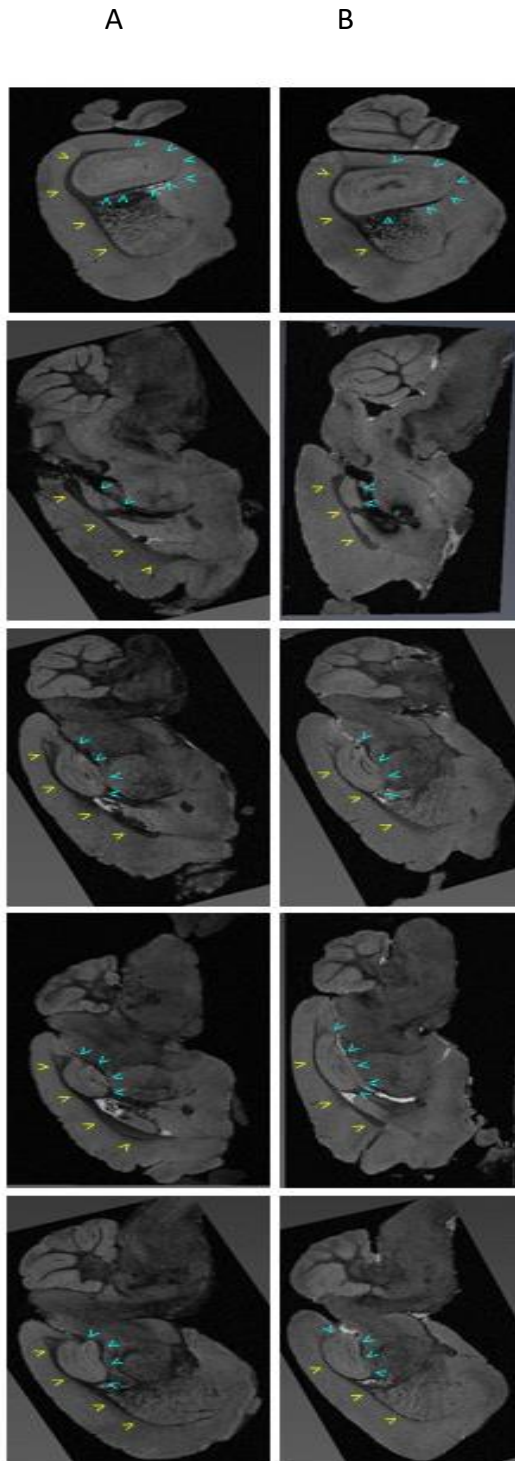


Figure 4.34 Sagittal images from WT (A) and KO (B) mouse brains after ex vivo MRI scan in a 9.4 Tesla magnet. The yellow arrowheads point at corpus callosum while the light blue arrowheads point at the hippocampus.

To further investigate the reduction in corpus callosum area and to confirm that the hippocampus remains unaffected, 3D whole brain reconstruction (Figure 4.35) and volumetric quantification of these brain regions (Figure 4.36) were conducted using Amira software.

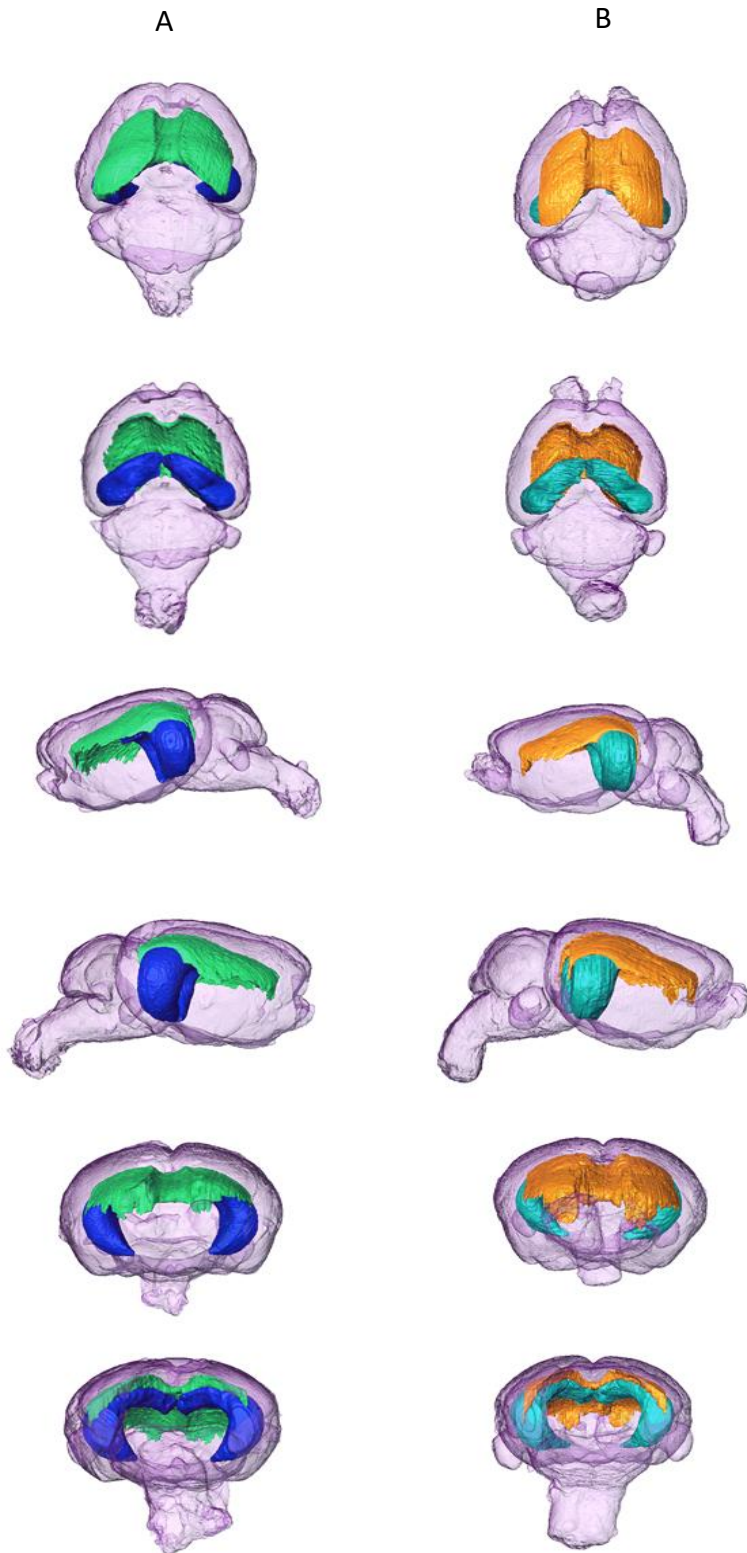
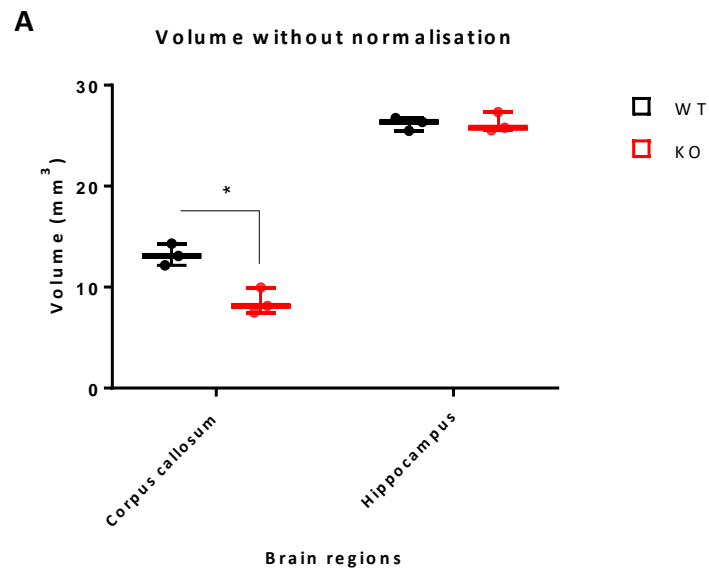


Figure 4.35 3D reconstruction of a WT (A) and KO (B) mouse brain using Amira 6.01 software after ex vivo MRI scan. Volumetric analysis was conducted for hippocampus (dark

blue in panel A and turquoise in panel B), corpus callosum (green in panel A and orange in panel B) and whole brain (light purple in both panels).

Volumetric analysis of regions of interest was performed with or without normalisation against the whole brain volume in order to examine if normalisation had an impact on the result. Analysis without normalisation indicated that the KO animals showed an average 35% reduction in the total volume of corpus callosum but not in hippocampus (Figure 4.36A). This reduction was statistically significant (average volume 8.5 mm³ for KO and 13.2 mm³ for WT, unpaired t test, p=0.017).



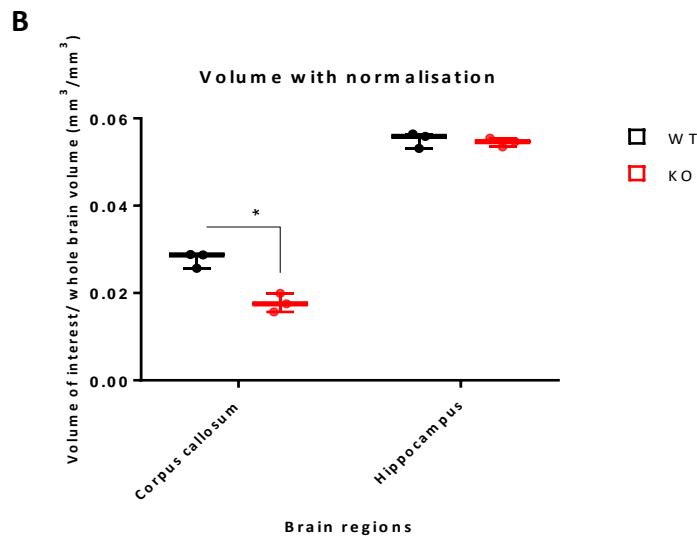


Figure 4.36 Box and whiskers graphs showing the various data points for the volume of corpus callosum and hippocampus made using GraphPad Prism7. Panel A shows volumes without normalisation while panel B shows volumes normalised against the total volume of each brain. The whiskers indicate the maximum and minimum data points while the thick horizontal line indicates the median. Statistics were conducted using an unpaired t-test ($n=3$ WT, 3 KO).

Analysis with normalisation against the total brain volume of each sample showed similar results with the analysis without normalisation. KO animals showed an average 36% reduction in the total volume of corpus callosum (Figure 4.36 B) but not in hippocampus. This reduction was statistically significant (unpaired t test, $p=0.008$).

4.3 Discussion

This chapter describes the first behavioural characterization of *Zdhhc9* KO mice. The KO mice have been subjected to a variety of behavioural tasks in order to test motor coordination and balance, locomotor activity and anxiety, sensorimotor gating, anhedonia, sociability and social novelty, learning and memory and

visuospatial attention. In most of the behavioural tasks conducted, *Zdhhc9* KO mice showed similar performance to their WT littermates. However, there were some important deficits noted in some tests that are worthy of further discussion.

Zdhhc9 KO mice show altered visual acuity in the visual placing test, which is manifested by an early extension of their paws before they reach a surface. However, the KO mice did not exhibit any differences in some tests that heavily rely on the visual system such as the visual cue trial of the Morris water maze and all the stages of the pairwise discrimination task and the paired associated learning task. A diminished visual placing reflex could imply retinal degeneration (Rogers et al., 1999) therefore an increased visual placing reflex as in the case of *Zdhhc9* KO mice could imply higher visual acuity.

Moreover the KO mice show lower grip strength in the hanging wire, reduced anxiety levels in the elevated plus maze and in the habituation of the OFT and reduced startle reactivity in the startle curve. Moreover, they show a deficit in spatial learning and a reversal learning deficit in the Morris water maze (MWM). In the 5CSRTT, they work harder completing more trials than the WT animals while achieving similar percentage of correct responses. They also have shorter correct reaction time and show hyperactivity registering more beam breaks in the final part of the 5CSRTT when the stimulus duration is very short.

Some of those interesting behavioural deficits are present in other well characterised murine models of ID such as Down syndrome, Fragile X syndrome and Rett syndrome as it will be discussed in this section.

Hypotonia in *Zdhhc9* KO mice and other animal models or human disorders

Lower grip strength of the *Zdhhc9* KO mice in the hanging wire possibly indicates hypotonia. A motor coordination or balance deficit could be excluded based on the fact that the KO mice perform normally on the rotarod. Moreover, the KO mice have normal swimming ability based on their velocity in the MWM. Their

velocity in the OFT is also similar to their WT littermates with a trend of KO mice being slightly faster so this excludes a motor deficit. In addition, the KO mice tend to be lighter than their WT littermates so this gives them an advantage in the hanging wire task however their performance indicates the opposite. This result could be explained by deficit at the neuromuscular junction.

Hypotonia is defined as low muscular tone and is a characteristic noted in other mouse models of brain dysfunction as well as human conditions including patients with *ZDHHC9* mutations as it will be discussed.

KO mice for *Ptchd1* (Patched Domain Containing 1) show hypotonia in the hanging wire but normal motor coordination on the rotarod similar to the *Zdhhc9* KO mice (Wells et al., 2016). *PTCHD1* is located on the long arm of the X chromosome and is mutated in about 1% of all patients with Autism Spectrum Disorders (ASD) and ID (Wells et al., 2016). The encoded protein is similar to *Drosophila* proteins that act as receptors for the morphogen sonic hedgehog. *PTCHD1* is required for the development and function of the thalamic reticular nucleus (TRN), a group of GABAergic neurons that regulate thalamocortical transmission, sleep rhythms, sensorimotor processing and attention. Patients with Attention Deficit Hyperactivity Disorder (ADHD) and ID caused by deletion of *PTCHD1* also suffer from hypotonia (Chaudhry et al., 2015).

Hypotonia is a core characteristic of Down Syndrome (DS), the most common genetic cause of ID. Lower grip force has been described in a mouse model of DS (Costa et al., 1999) resembling the muscular hypotonia found in patients with DS (Roizen, 2001; Scorza & Cavalheiro, 2011). *DYRK1A* located on 21 chromosome, is the human homologue of *Drosophila* minibrain gene, over-expressed in DS fetal brain. It encodes a serine-threonine kinase, probably involved in neuroblast proliferation. Transgenic mice overexpressing *Dyrk1A* exhibited hypotonia in the coat hanger test (Altafaj et al., 2001).

Rett syndrome, an X-linked neurodevelopmental disorder that affects mostly women is characterized by regression of language and hand use, ID and seizures among other symptoms. Most of the cases occur due to mutations in *MECP2* (Methyl-CpG Binding Protein 2). In a mouse model of the disease, where *Mecp2* is produced at 50% of the WT level, male mice show hypotonia in the hanging wire (Samaco et al., 2008). Hypotonia has also been described in patients with *MECP2* mutations or duplications (Heilstedt et al., 2002; Friez et al., 2006).

Hypotonia is also present in patients with *ZDHHC9* mutations (Raymond et al., 2007; Masurel-Paulet et al., 2014; Han et al., 2017) possibly indicating that the *Zdhhc9* KO mouse could serve as a model of the human condition. Moreover, hypotonia has been described in a patient with loss of *ZDHHC15* expression and severe ID due to a balanced chromosomal translocation (Mansouri et al., 2005).

Generalized hypotonia is among the characteristics of the Lujan-Fryns syndrome (LJS) which affects predominately males and is accompanied by mild to moderate ID with behavioural abnormalities, that could include emotional instability or even psychotic disturbances (Van Buggenhout and Fryns, 2006). Patients with LJS have also Marfanoid Habitus (long, hyperlax fingers and toes, tall stature, dolichostenomelia) like some patients with *ZDHHC9* mutations along with facial dysmorphism (prominent forehead contrasting with a long, narrow face) (Van Buggenhout and Fryns, 2006). Mutations in *MED12* (Mediator Complex Subunit 12) cause this syndrome (Schwartz et al., 2007).

Muscular hypotonia has also been found in male patients with Fragile X syndrome which is the most common inherited form of ID (Vieregge & Frosterl-Iskenius, 1989). Patients with Fragile X syndrome lack FMR1 protein due to silencing of *FMR1* gene caused by amplification of a CGG repeat and subsequent methylation of the gene promoter (Bakker et al., 1994).

Hypotonia has also been described in patients with mutations in genes such as *EEF1A2* (*Eukaryotic elongation factor 1, alpha-2*), *TUBB3* (Tubulin Beta 3 Class III), *STXBP1* (Syntaxin-binding protein 1, also known as Munc18-1) and *ARID1B* (AT-Rich Interaction Domain 1B). Neonatal hypotonia has been described in patients with *EEF1A2* mutations that also have ID, autistic behaviours and epilepsy (Nakajima et al., 2015). *EEF1A2* is highly expressed in the central nervous system and *EEF1A2* protein is involved in protein synthesis, suppression of apoptosis, and regulation of actin function and cytoskeletal structure (Nakajima et al., 2015). Mutations in the *TUBB3* result in malformation of cortical development and neuronal migration defects with the patients exhibiting axial hypotonia (Poirier et al., 2010). *De novo* *STXBP1* mutations have been found in patients with hypotonia, severe ID and non-syndromic epilepsy (Hamdan et al., 2009). *STXBP1* plays a role in release of neurotransmitters via regulation of syntaxin (Pevsner et al., 1994). Last but not least, hypotonia along with corpus callosum abnormalities, ID, speech impairment, and autism have been described in patients with haploinsufficiency of *ARID1B* which encodes for a component of the SWI/SNF chromatin remodelling complex (Halgren et al., 2012).

Reduced anxiety levels and startle reactivity in *Zdhhc9* KO mice and other animal models

Zdhhc9 KO mice exhibit reduced anxiety levels in the EPM spending more time in the open arms compared to the WT animals. Moreover, they show reduced anxiety in the habituation period of the OFT based on their lower thigmotaxis. They also show reduced startle reactivity in the startle curve which could also be explained by reduced anxiety.

The acoustic startle reflex is based on the observation that animals flinch immediately following a sudden stimulus such as a loud noise, and this test can be used as a behavioural tool to assess brain mechanisms of sensorimotor integration.

The startle response itself is mediated by neurons in the lower brainstem, whereas prepulse inhibition is dependent on a more complex forebrain circuitry (Koch, 1999).

Children with anxiety disorders show an increased acoustic startle reflex (Bakker et al., 2009). In accordance with that, in rats the amplitude of acoustic startle can be decreased by anxiolytic drugs (Walker and Davis, 1997) showing a link between anxiety and startle reactivity. The amygdala is a brain formation that is responsible for processing emotional reactions such as anxiety and fear (Davis, 2006) and these results suggest it could be possibly affected by the KO of *Zdhhc9*.

Fmr1-KO mice show reduced anxiety indicated by reduced thymotaxis in the OFT and in the light-dark exploration test (Peier et al., 2000) as well as reduced startle reactivity in high decibel levels (120 dB) of white noise (Nielsen et al., 2002). Another mouse model of Fragile X-syndrome, mice that have the I304N mutation in *Fmr1* show decreased anxiety in OFT and decreased acoustic startle response (Zang et al., 2009). The reduced anxiety of the mouse model may appear as contradictory compared to the anxiety presented by FXS patients but it is important to note that patients' anxiety disorder is predominately observed in social settings (Hagerman and Hagerman, 2002). *ZDHHC9* patients showed significantly stronger social and practical skills compared to an X-linked ID control group (Baker et al., 2015). This comes in accordance with the sociability and social novelty experiment we conducted with the KO mice performing similar to WT.

In a mouse model of Rett syndrome where *Mecp2* is produced at 50% of the WT level, male mice show decreased anxiety in the OFT (Samaco et al., 2008). As regards Down syndrome models, transgenic mice overexpressing *Dyrk1A* exhibited reduced anxiety in the OFT and EPM (Altafaj et al., 2001). In another DS model, Ts65Dn mice (partially trisomic) show reduced anxiety in the EPM (Escorihuela et al., 1998).

IL1RAPL1 (IL-1 receptor accessory protein-like 1) KO mice show reduced open-space and height anxiety in the OFT and EPM just like the *Zdhhc9* KO mice (Yasumura et al., 2014). *IL1RAPL1* is responsible for non-syndromic ID, is associated with autism and mediates excitatory synapse formation through interaction with presynaptic protein tyrosine phosphatase (PTP)d.

Finally, TLR (Toll-like receptor) 3-deficient mice demonstrate decreased anxiety in the OFT and EPM (Okun et al., 2010). TLRs are innate immune receptors that have emerged as regulators of neuronal survival and developmental neuroplasticity (Okun et al., 2010).

Hyperactivity in *Zdhhc9* KO mice and other animal models or human conditions

The attribute of hyperactivity in *Zdhhc9* KO mice was significantly noticed in the 5CSRTT. Based on the number of beam breaks registered, the KO mice show hyperlocomotion, breaking the beams almost twice as much as the WT animals to achieve the same result. The KO mice also complete significantly more trials during the training phase of the 5CSRTT and the percentage of correct responses for both animal groups is very similar. This could be an explanation about the trend of lower body weight for the KO animals, they work more completing more trials and they move more registering more beam breaks so they consume more energy and they tend to be lighter.

As regards the correct response time during the final phase of the 5CSRTT, the KO animals react faster having better performance than their WT counterparts which can be attributed to hyperactivity noted in this test that fits with the trend of hyperactivity noted in the OFT.

ZDHHC9 patients have impaired inhibitory control whilst completing visual attention tasks (Baker et al., 2015) having fewer omissions and higher commissions than the X-linked ID control group. In a go/no-go task where inhibitory responses can be tested, the *ZDHHC9* group performed better at the “go” stimuli than the X-

linked ID control group but they had problem inhibiting responses to the “no-go” stimuli. This response is of great interest and may explain why the *Zdhhc9* KO mice have deficit in tasks that involve many visual cues such as the MWM as it will be discussed. Moreover, this could even explain why the KO animals register more beam breaks. In a novel environment, they may be unable to concentrate on the task due to other visual cues.

Fmr1-KO mice also show hyperactivity in the two chambered light-dark transition test and in the OFT (Bakker et al., 1994; Peier et al., 2000; Mineur et al., 2002; Spencer et al., 2005). Another mouse model of Fragile X-syndrome, mice that have the I304N mutation in *Fmr1* show hyperactivity and higher exploratory behaviour in the OFT (Nielsen et al., 2002; Zang et al., 2009). As regards Down syndrome, transgenic mice overexpressing *Dyrk1A* exhibited mild hyperactivity in the OFT (Altafaj et al., 2001). *Zdhhc17*-KO mice also show hyperactivity in the OFT when tested in the dark (Singaraja et al., 2011).

Moreover, *PTCHD1* KO mice show hyperactivity in the OFT (Wells et al., 2016) and *IL1RAPL1* KO mice show hyperactivity in a variety of tasks including OFT (Yasumura et al., 2014).

Spatial learning and reversal learning deficit in Zdhhc9 KO mice and other animal models

Zdhhc9 KO mice also show a deficit in spatial learning in MWM indicating a hippocampal deficit. Aberrations in spatial learning are generally attributed to hippocampal defects (Logue et al., Wehner, 1997). Changes in hippocampus can affect the amygdala based on the fact that the two brain regions receive and send information to each other (Bast et al., 2001). Moreover, *Zdhhc9* KO mice have a deficit in the reversal learning of the MWM. The KO mice do not seem to be impaired in the retrieval of spatial information in training and reversal trials once this information has been learned, but they are significantly impaired in the

acquisition of the initial and reversal task. This does not appear to be caused by impairment in their ability to change their nonspatial information scheme, since there was no difference between KO and WT in the visible condition of the task. The latter also suggests that the increased latency of KO animals in the hidden platform condition is not caused by some underlying motivational, motor, or sensory deficit. Hence, the observed impairment appears to be limited to the spatial abilities of the mouse. This might be connected to the trend of hyperactivity and increased exploratory behaviour that might be responsible for excessive early search behaviour or interfering intertrial hyperactivity.

The reversal learning deficit could indicate that the KO animals have impaired cognitive flexibility. The reversal learning requires that the animal does not persevere in choosing the wrong solution and adapts to the new task and this attribute has been generally ascribed to the correct functioning of the prefrontal cortex (Eichenbaum et al., 1983; Abel & Lattal, 2001; Murray et al., 2015). However when the KO mice were tested in the pairwise discrimination touchscreen task, their performance in the reversal learning was similar to the WT animals. This indicates a deficit that is specific to the MWM task rather than a general cognitive flexibility deficit. The KO mice have difficulty in orientating themselves based on the extra maze cues.

Fmr1-KO mice also show a reversal learning deficit in MWM (Bakker et al., 1994). Interestingly this impairment in the reversal learning is not accompanied by deficit in probe or visual cue trials (Bakker et al., 1994) which is similar to the behavioural deficit found in *Zdhhc9* KO mice. Another study found similar deficit in reversal learning for the *Fmr1*-KO mice (D'Hooge et al., 1997) indicating perseverance which is also present in autism patients (Bernardet and Crusio, 2006).

In a model of DS where transgenic mice are overexpressing *Dyrk1A*, some deficits in the MWM were observed. The mice learned to reach the platform during acquisition, but the learning curve was significantly different from the WT mice

(Altafaj et al., 2001), similar to the learning curve of *Zdhhc9* KO mice. WT animals acquired this task faster than *Dyrk1A* transgenic mice, which showed significantly longer escape latencies in the first acquisition sessions just like the *Zdhhc9* KO mice. In the reverse platform test, *Dyrk1A* transgenic mice were poor in learning the new location of the platform. Moreover, they persisted in searching in the wrong quadrant, indicating a poor cognitive flexibility (Altafaj et al., 2001).

In another DS model, *Ts65Dn* mice (partially trisomic) show deficit in spatial learning in MWM (Escorihuela et al., 1998). A third DS mouse model with a smaller partial trisomy, the *Ts1Cje* mouse shows a spatial learning deficit in the MWM and deficit in cognitive flexibility in reversal learning of the MWM (Sago et al., 1998).

In the zDHHC family of protein acyl-transferases, except for zDHHC9 two other members have been implicated in playing a role in learning and memory processes in mice; zDHHC17 and zDHHC5. zDHHC17 is implicated in Huntington's disease with *Zdhhc17*-KO mice showing impaired hippocampal-dependent memory in a spatial test of novel- object location memory (Milnerwood et al., 2013). Moreover mice homozygous for a hypomorphic allele of *ZDHH5*, are born at half the expected rate, and survivors show a marked deficit in contextual fear conditioning, an indicator of defective hippocampal-dependent learning (Li et al., 2010). zDHHC5 is highly enriched in post-synaptic density and coimmunoprecipitates with post-synaptic density protein-95 (PSD95), and *ZDHH5* is expressed in the CA3 and dentate gyrus of hippocampus (Li et al., 2010).

Deficiency in synaptic proteins and regulators of neuroplasticity can cause behavioural characteristics similar to the ones presented in *Zdhhc9* KO animals. *IL1RAPL1* KO mice have mildly impaired spatial reference and working memories and decreased spine density (Yasumura et al., 2014). Mitogen-activated protein kinase phosphatase (MKP)-2 KO mice have impaired spatial learning in the MWM showing that MKP-2 plays a role in regulating hippocampal function (Rahman et al., 2016). In the reversal test of MWM, heterozygous *Ric-8* mutant mice exhibited

significant delay to find the hidden platform compared to WT littermates (Tõnissoo et al., 2006). Ric-8 is a guanine nucleotide exchange factor for a subset of G α proteins and is expressed in regions involved in the regulation of behaviour (neocortex, cingulate cortex and hippocampus).

Most patients with *ZDHHC9* mutations have mild to moderate rather than severe ID (Baker et al., 2015). If the ID is presented as a mild/moderate impairment then simple learning and memory tasks may not be challenging enough to create a significant difference between KO and WT mice. Our data show that the KO mice are not severely impaired in learning and memory tasks, resembling the human phenotype.

Learning, memory and behaviour are complex processes involving different brain regions and many specific proteins. Targeted disruption of specific genes is a powerful tool in the elucidation of the specific role of these genes in brain functioning. The KO model for *Zdhhc9* presented here is a potentially valid model to provide insight into the physiological function of zDHHHC9 and the pathophysiology of zDHHHC9 dysfunction in humans, as the genetically modified mice show abnormalities comparable to human *ZDHHC9* patients such as hypotonia and mild to moderate ID. Therefore, these mutant mice offer a good animal model to study the mechanisms leading to hypotonia and ID. Furthermore, experimental designs can be made to introduce *Zdhhc9* into the KO mice in a first step towards gene therapy for humans with dysfunctional zDHHHC9. Moreover, delineating the mechanism that is responsible for zDHHHC9 dysfunction can lead to a step towards understanding of other disorders that share ID as common characteristic.

The behavioural experimental data suggest that knockout of *Zdhhc9* disturbs processes that involve the hippocampus, the amygdala and the prefrontal cortex. Disruption of corpus callosum cannot be excluded as *Zdhhc9* is normally highly expressed in this region and disruption of corpus callosum function could affect the interhemispheric communication (Luders et al., 2010).

Interpretation of MRI analysis

MRI data suggested that *Zdhhc9* KO mice exhibit shrinkage of corpus callosum which is the biggest white matter tract in the human brain (Luders et al., 2010). Volumetric reduction of this area could be explained by reduced white matter in the KO mouse brain. Diffusion tensor imaging would be interesting to further investigate this hypothesis. This imaging technique is useful when white matter tracts need to be studied as it can estimate their location, orientation and anisotropy (Alexander et al., 2007).

Baker et al., (2015) described that a consistent finding for patients with *ZDHHC9* mutations was shrinkage of corpus callosum, with its cross-sectional area being reduced by 52% in *ZDHHC9* patients compared to people with X-linked ID which served as control for the study (n= 7 patients, 7 controls). Our findings correlate with the patient data indicating that *Zdhhc9* KO mice can serve as a model of the human condition.

Hippocampal volume was also examined in our study due to the importance of this brain region for learning and memory and based on our behavioural results showing that the KO mice have impaired spatial learning in the Morris water maze. Hippocampal volume was not impaired in KO mice. Interestingly, hippocampal volume reduction has not been found in *ZDHHC9* patients, in accordance with the data from the KO mice. Thus, changes in hippocampal-dependent function might be linked to changes in neuronal connectivity, as changes in dendritic spine number or morphology in the hippocampus has been reported in other ID mouse models (Kooy, 2003; Iwase et al., 2016).

Corpus callosum abnormalities have been described in a variety of syndromes and genetic disorders. Children with Down Syndrome have reduced volume of corpus callosum compared to healthy controls (Gunbey et al., 2017). Thinning of corpus callosum has also been described as a consistent finding in

adolescents with intellectual disability (Spencer et al., 2005). Another study concluded that adults with ID show abnormal white matter integrity (Yu et al., 2008). Moreover, hypoplasia of corpus callosum has been described in ADHD and autism (Paul, 2011).

Last but not least, decreased white matter volume has been found by MRI in *Zdhhc17*-KO mice that is not caused by changes in astrocyte or microglial cell numbers but by neuronal cell loss (Singaraja et al., 2011).

Further investigation is needed in order to delineate what causes the shrinkage of corpus callosum in *Zdhhc9* KO mice, in order to help us understand better the role of zDHC9 enzyme in brain function. Based on our behavioural and neuroanatomical data, *Zdhhc9* KO mouse can be a valuable model of the human condition.

CHAPTER 5

5 Biochemical and proteomic investigation of the effect of *Zdhhc9* KO in mouse brain

5.1 Introduction

Results of the previous chapter uncovered important behavioural deficits in *Zdhhc9* KO mice as well as shrinkage of corpus callosum. To shed light on how these behavioural and anatomical changes might occur, it is important to investigate underlying molecular changes in the *Zdhhc9* KO mice. Although previous work has suggested that H- and N- Ras may be major targets of zDHHC9 (Swarthout et al., 2005; Chai et al., 2013), there is currently no evidence that palmitoylation of these proteins is perturbed in the brain of *Zdhhc9* KO mice and it is also likely that other substrates of this enzyme exist, which may contribute to the changes observed in the previous chapter.

The zDHHC9 enzyme has previously been shown to be localised to the somatic Golgi apparatus in hippocampal neurons (Levy et al., 2011). This localisation would allow access of the enzyme to both pre- and post-synaptic proteins, suggesting that zDHHC9 could palmitoylate proteins targeted to either of these locations. Prominent palmitoylated presynaptic proteins include Cysteine-string protein, Synaptotagmin, Synaptobrevins and Snap25, while key palmitoylated postsynaptic proteins include GluR1 and GluR2 subunits of AMPA receptors, the NR2b subunit of NMDA receptors and PSD95 (Fukata and Fukata, 2010).

It is likely that KO of *Zdhhc9* causes dysregulation of palmitoylation in neurons. However, this does not rule out the possibility of the zDHHC9 enzyme also having important functions in other molecular mechanisms that are not related to palmitoylation *per se*. Such palmitoylation-independent protein interactions have

been reported for other enzyme isoforms, including zDHHC13 and zDHHC17 (Yang & Cynader, 2011; Lemonidis et al., 2014).

A useful strategy for the identification of dysregulated protein palmitoylation is isolation of palmitoylated proteins by approaches such as Acyl-RAC and subsequent analysis of proteins of interest by immunoblotting. Moreover, untargeted strategies can also be used such as 'palmitoylomics', which involves isolation of palmitoylated proteins and their subsequent analysis by Mass Spectrometry (MS). Validation of omics approaches is always desirable in order to eliminate any false positive results which may occur from untargeted approaches (De Bin et al., 2014).

In this chapter, protein expression and palmitoylation changes in synaptic proteins was investigated by isolation of the palmitoylome from WT and Zdhhc9 KO mouse brain and subsequent immunoblotting and MS analyses. The aim was to identify proteins with perturbed palmitoylation that might underlie the neurological deficits in Zdhhc9 KO mice.

5.2 Results

5.2.1 H-Ras and N-Ras protein levels are not affected in whole brain homogenates of Zdhhc9 KO mice.

As H-Ras and N-Ras are known substrates of the zDHHC9 enzyme, it was important to examine their protein levels in whole brain homogenates (n=3 KO, 3 WT). Band intensities on Western blots were quantified for the proteins of interest. β -actin was used as a loading control and was also included in quantification for normalisation of the band intensity of the protein of interest. There was a trend towards a decrease of H-Ras in KO mouse brains (Figure 5.1) but this was not statistically significant (2 sample t-test).

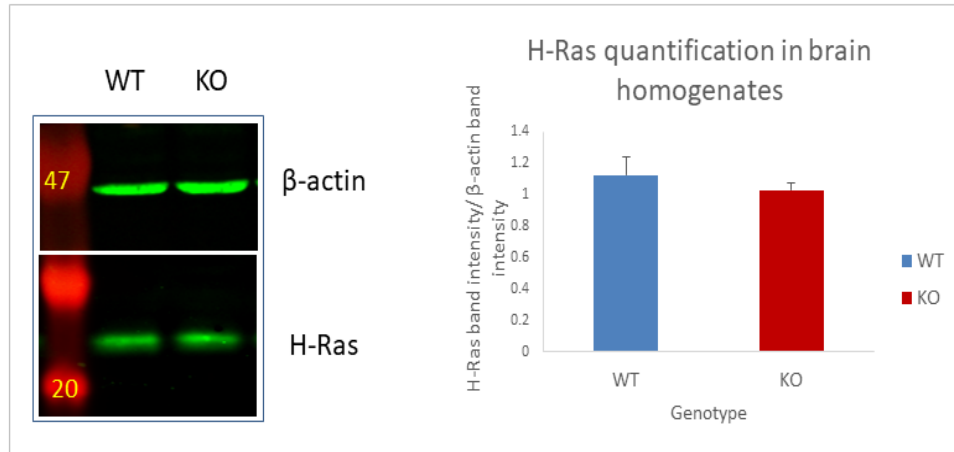


Figure 5.1 Quantification of H-Ras protein level in brain homogenates. Whole brain homogenates (13 μ g) were resolved by SDS-PAGE and transferred to nitrocellulose, and subsequently probed with β -actin and H-Ras antibodies. The left panel shows representative western blots (position of molecular weight markers is shown on the left), whereas the right panel shows quantified data from 3 KO and 3 WT mouse whole brain homogenates. Statistical analysis using an unpaired t-test indicated that there was no significant difference in H-Ras expression between WT and KO samples ($p > 0.05$).

As regards N-Ras protein level, there was also no significant difference in immunoreactive band intensity between WT and KO samples (Figure 5.2).

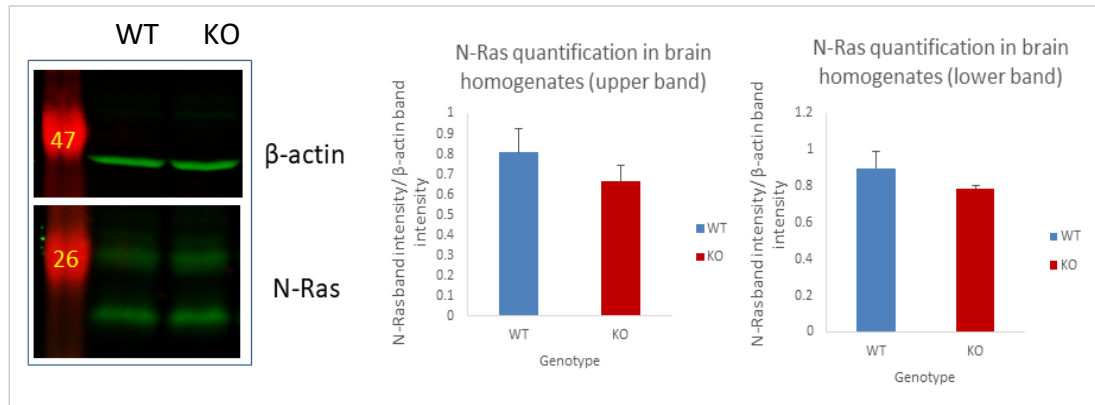


Figure 5.2 Quantification of N-Ras protein level in brain homogenates. Whole brain homogenates (40 μ g) were resolved by SDS-PAGE and transferred to nitrocellulose, and subsequently probed with β -actin and N-Ras antibodies. The left panel shows representative western blots (position of molecular weight markers is shown on the left), whereas the bar graphs on the right show quantified data from 3 KO and 3 WT mouse whole brain homogenates). Statistical analysis using an unpaired t-test indicated that there was no significant difference in N-Ras expression between WT and KO samples for the upper and lower band ($p > 0.05$).

5.2.2 H-Ras and N-Ras levels in membrane fractions are not affected in whole brain homogenates of *Zdhhc9* KO mice.

As H-Ras and N-Ras palmitoylation mediates stable membrane association, it was important to study the levels of those proteins in membrane fractions from WT and KO mouse brains ($n=3$ KO, 3 WT). As positive controls to show successful cell fractionation, the samples were probed with antibodies against Syntaxin, which is exclusively membrane-associated (Bennett et al., 1993) and GAPDH which is predominantly cytosolic (Tristan et al., 2011). The Syntaxin and GAPDH immunoblots in Figure 5.3 show that the fractionation procedure used successfully isolated samples enriched in membrane and cytosolic proteins. H-Ras was predominantly found in the membrane fraction, similar to Syntaxin. For

quantification of western blot band intensities, the membrane fraction band intensities were expressed as a percentage of total protein (membrane and cytosolic fractions band intensities). There was no significant difference in H-Ras levels in membrane fractions from WT and KO mice ($p=0.07$, 2 sample t-test, Figure 5.3).

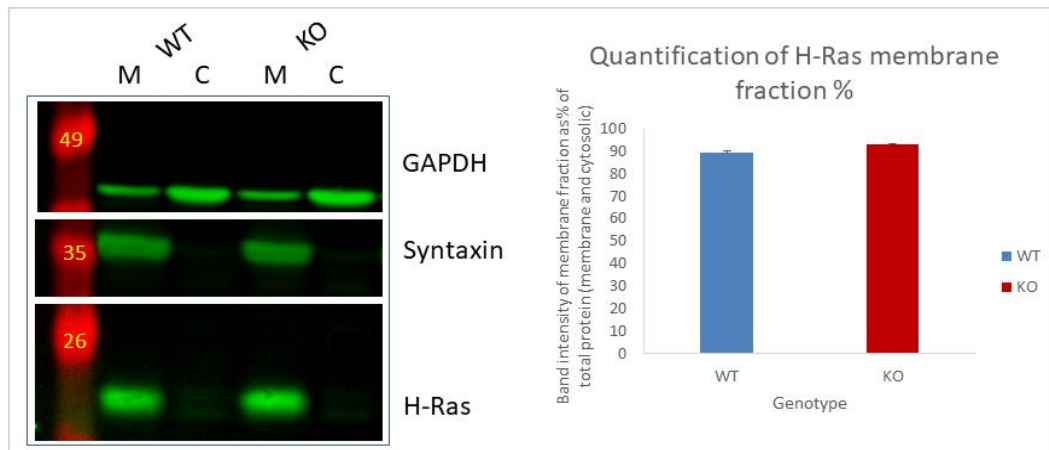


Figure 5.3 Quantification of H-Ras protein level in membrane fractions from brain homogenates. Membrane fractions from whole brain homogenates (20 μ g) were resolved by SDS-PAGE and transferred to nitrocellulose, and subsequently probed with GAPDH, Syntaxin and H-Ras antibodies. The left panel shows representative western blots (position of molecular weight markers is shown on the left), whereas the right panel shows quantified data from 3 KO and 3 WT membrane fractions. Statistical analysis using an unpaired t-test indicated that there was no significant difference in H-Ras expression between WT and KO samples ($p>0.05$). M: membrane fraction, C: cytosolic fraction.

N-Ras only has one palmitoylation site in contrast to the two sites in H-Ras, and N-Ras also displays a more rapid turnover of palmitoylation (Magee et al., 1987). As a result, N-Ras is also found in the cytosolic fraction (Figure 5.4). Quantification of the membrane association of N-Ras in WT and KO samples also revealed no significant difference (Figure 5.4).

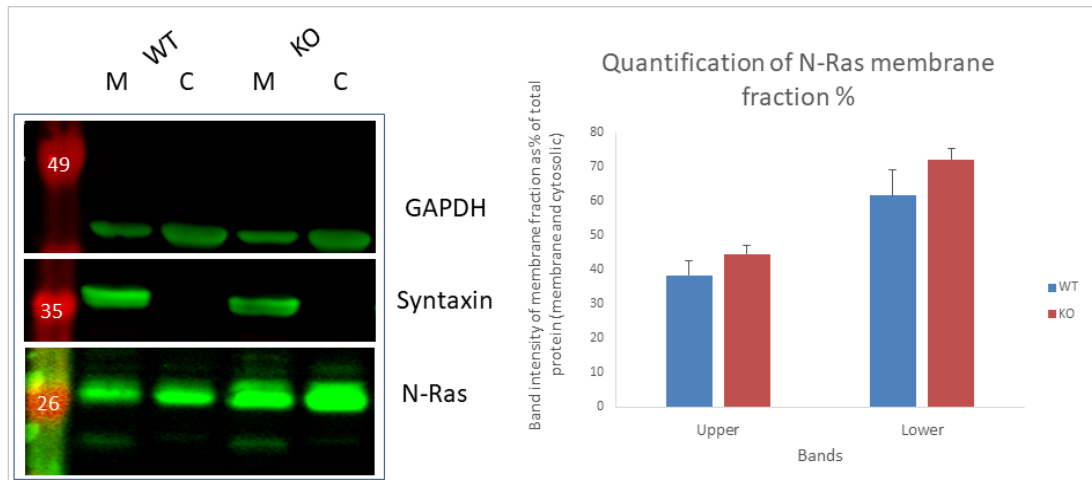


Figure 5.4 Quantification of N-Ras protein level in membrane fractions from brain homogenates. Membrane fractions from whole brain homogenates (20 μ g) were resolved by SDS-PAGE and transferred to nitrocellulose, and subsequently probed with GAPDH, Syntaxin and N-Ras antibodies. The left panel shows representative western blots (position of molecular weight markers is shown on the left), whereas the right panel shows quantified data from 3 KO and 3 WT membrane fractions. Quantification was conducted for upper and lower band of N-Ras. Statistical analysis using an unpaired t-test indicated that there was no significant difference in N-Ras expression between WT and KO samples ($p > 0.05$). M: membrane fraction, C: cytosolic fraction.

5.2.3 H-Ras palmitoylation is not affected in whole brain or hippocampus of Zdhhc9 KO mice.

Palmitoylation mediates membrane association of N-Ras and H-Ras (Hancock et al., 1989) and thus the results in Figures 5.3 and 5.4 imply that palmitoylation of these proteins is likely to be unaffected in KO mice. To test this directly, palmitoylated proteins were isolated by Acyl-RAC of whole brain and hippocampi of WT and KO mice (n=3 WT, 3 KO). Isolated hippocampi were included in this analysis as a deficit in hippocampal-dependent learning and memory was previously

recorded in the Morris water maze (see Chapter 4). Immunoreactivity of palmitoylated H-Ras (present in the Bound HA treated fraction) was expressed as a percentage of total H-Ras (Unbound and bound HA treated fractions) and was found to be unaffected in both whole brain and hippocampus of *Zdhhc9* KO mice (Figure 5.5).

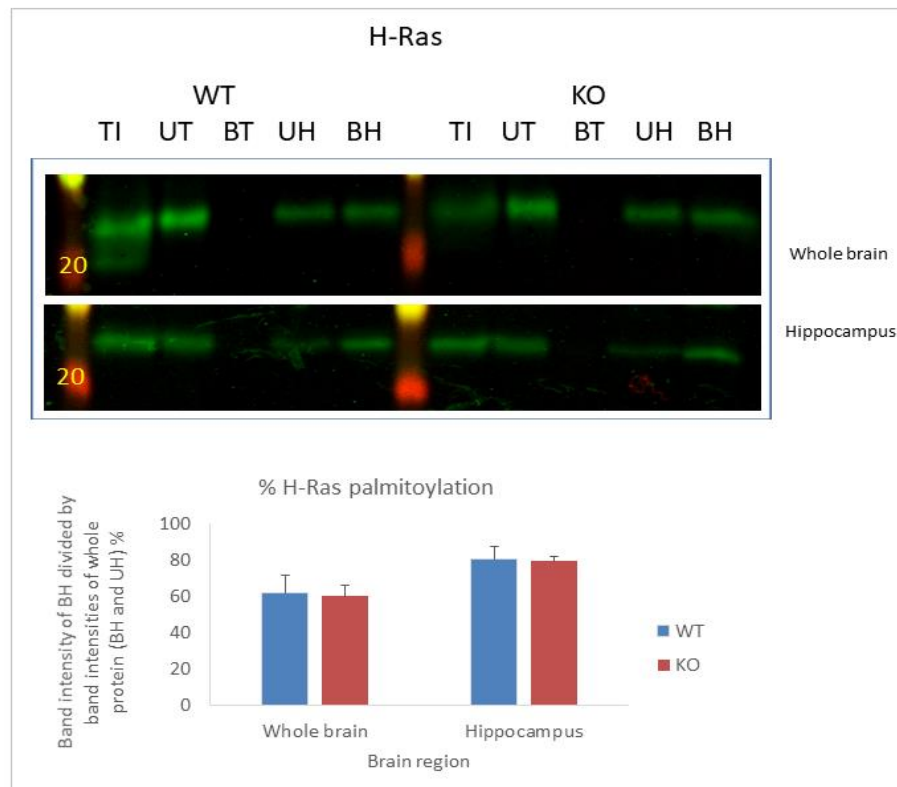


Figure 5.5 Quantification of H-Ras palmitoylation in whole brain and hippocampi of WT and *Zdhhc9* KO mice. Acyl-RAC samples from whole brain or hippocampi were resolved by SDS-PAGE and transferred to nitrocellulose, and subsequently probed with H-Ras antibody. The upper panel shows representative western blots (position of molecular weight markers is shown on the left), whereas the lower panel shows quantified data from whole brain or hippocampi of 3 KO and 3 WT mice. Statistical analysis using an unpaired t-test indicated that there was no significant difference in H-Ras palmitoylation between WT and KO samples ($p > 0.05$). TI: total input, UT: Unbound Tris treated fraction, BT: Bound Tris treated fraction, UH: Unbound HA treated fraction, BH: Bound HA treated fraction.

For all the Acyl-RAC experiments, β -actin was used as a negative control. As expected, this non-palmitoylated protein was completely excluded from the palmitoylated fraction (lanes BH in Figure 5.6).

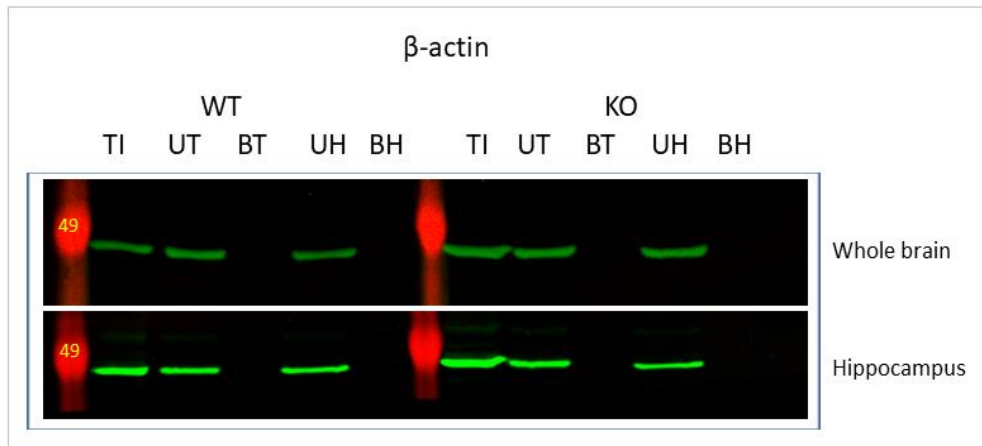


Figure 5.6 Western blots of β -actin as a negative control for Acyl-RAC in whole brain and hippocampi of WT and *Zdhhc9* KO mice. Acyl-RAC samples from whole brain or hippocampi were resolved by SDS-PAGE and transferred to nitrocellulose, and subsequently probed with β -actin antibody. Representative western blots (position of molecular weight markers is shown on the left) are shown from whole brain or hippocampi of 3 KO and 3 WT mice. β -actin is not palmitoylated as there is not a band in BH fraction. TI: total input, UT: Unbound Tris treated fraction, BT: Bound Tris treated fraction, UH: Unbound HA treated fraction, BH: Bound HA treated fraction.

5.2.4 Analysis of palmitoylated pre-synaptic proteins in *Zdhhc9* KO brain

In order to identify new substrates of the zDHHC9 enzyme, the major presynaptic proteins that have been reported to be palmitoylated were studied. Cysteine string protein (Csp) is a highly palmitoylated (14 palmitoylation sites) synaptic vesicle protein (Gundersen et al., 1994). Expression levels of Csp in whole brain homogenates (n=3 KO, 3 WT) were not significantly different between WT and KO animals (Figure 5.7).

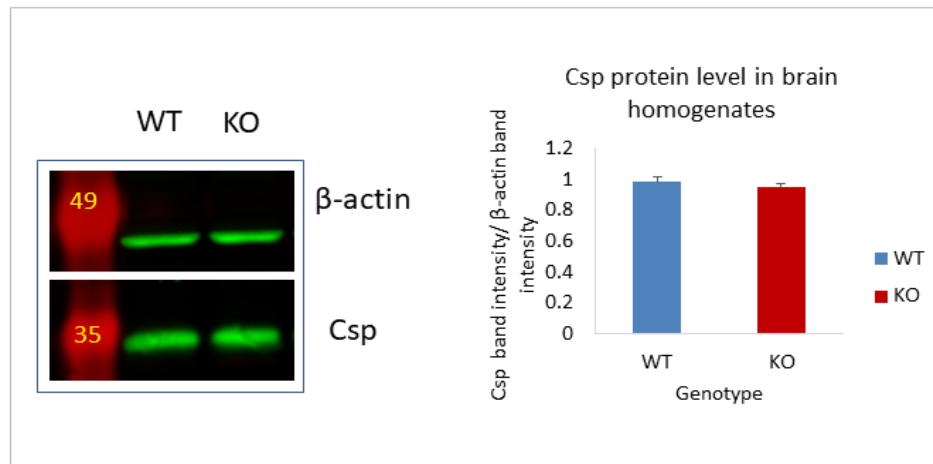


Figure 5.7 Quantification of Csp protein level in brain homogenates. Whole brain homogenates (13 μ g) were resolved by SDS-PAGE and transferred to nitrocellulose, and subsequently probed with β -actin and Csp antibodies. The left panel shows representative western blots (position of molecular weight markers is shown on the left), whereas the right panel shows quantified data from 3 KO and 3 WT mouse whole brain homogenates. Statistical analysis using an unpaired t-test indicated that there was no significant difference in Csp expression between WT and KO samples ($p > 0.05$).

Moreover, when Csp palmitoylation was studied by Acyl-RAC in whole brain and hippocampus of WT and *Zdhhc9* KO mice ($n=3$ WT, 3 KO), there was not a significant difference between the two genotypes of mice (Figure 5.8). It is important to note that the extensive palmitoylation of Csp results in a marked band-shift on SDS gels as evident from the hydroxylamine-treated samples in Figure 5.8 (Chamberlain and Burgoyne, 1996).

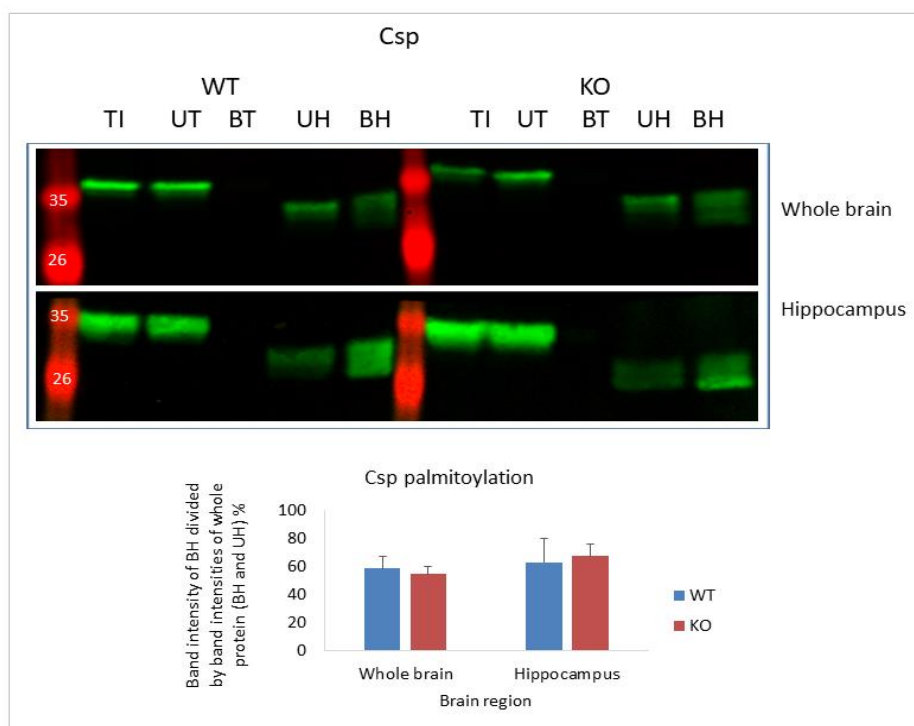


Figure 5.8 Quantification of Csp palmitoylation in whole brain and hippocampi of WT and Zdhhc9 KO mice. Acyl-RAC samples from whole brain or hippocampi were resolved by SDS-PAGE and transferred to nitrocellulose, and subsequently probed with Csp antibody. The upper panel shows representative western blots (position of molecular weight markers is shown on the left), whereas the lower panel shows quantified data from whole brain or hippocampi of 3 KO and 3 WT mice. Statistical analysis using an unpaired t-test indicated that there was no significant difference in Csp palmitoylation between WT and KO samples ($p > 0.05$). TI: total input, UT: Unbound Tris treated fraction, BT: Bound Tris treated fraction, UH: Unbound HA treated fraction, BH: Bound HA treated fraction.

Another important presynaptic protein which is known to be palmitoylated is Synaptosomal-associated protein of 25kDa (Snap25), a plasma membrane SNARE protein that mediates synaptic vesicle fusion (Hess et al., 1992). Initially, Snap25 protein levels were studied in whole brain homogenates (n=3 KO, 3 WT) and there was not a significant difference between WT and KO animals (Figure 5.9).



Figure 5.9 Quantification of Snap25 protein level in brain homogenates. Whole brain homogenates (13 μ g) were resolved by SDS-PAGE and transferred to nitrocellulose, and subsequently probed with β -actin and Snap25 antibodies. The left panel shows representative western blots (position of molecular weight markers is shown on the left), whereas the right panel shows quantified data from 3 KO and 3 WT mouse whole brain homogenates. Statistical analysis using an unpaired t-test indicated that there was no significant difference in Snap25 expression between WT and KO samples ($p > 0.05$).

Moreover, when Snap25 palmitoylation was studied by Acyl-RAC in whole brain and hippocampus of WT and *Zdhhc9* KO mice ($n=3$ WT, 3 KO), there was no significant difference detected between the two genotypes of mice (Figure 5.10).

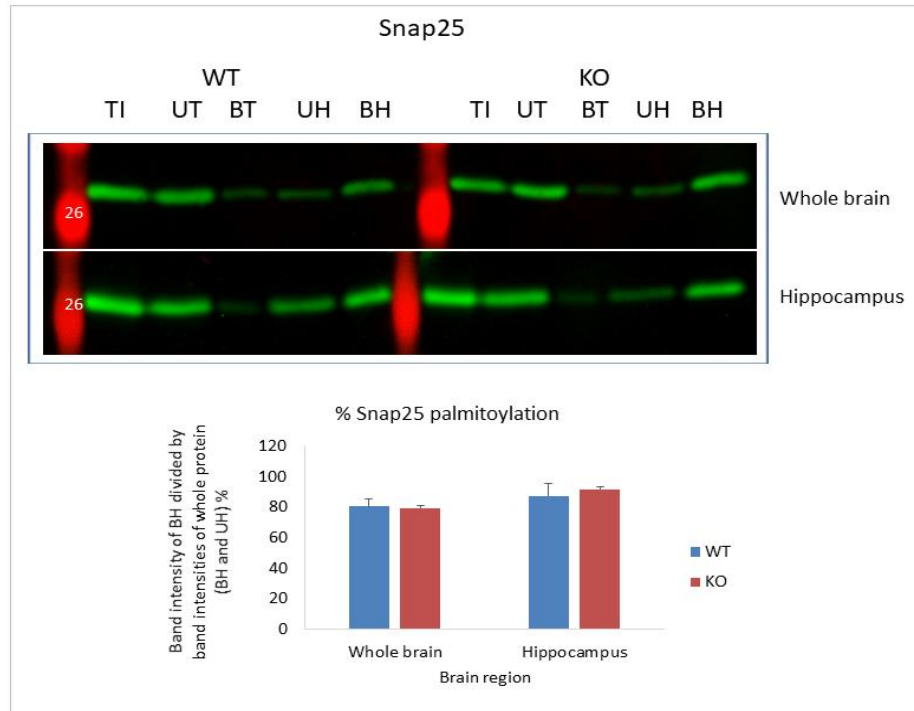


Figure 5.10 Quantification of Snap25 palmitoylation in whole brain and hippocampi of WT and *Zdhhc9* KO mice. Acyl-RAC samples from whole brain or hippocampi were resolved by SDS-PAGE and transferred to nitrocellulose, and subsequently probed with Snap25 antibody. The upper panel shows representative western blots (position of molecular weight markers is shown on the left), whereas the lower panel shows quantified data from whole brain or hippocampi of 3 KO and 3 WT mice. Statistical analysis using an unpaired t-test indicated that there was no significant difference in Snap25 palmitoylation between WT and KO samples ($p > 0.05$). TI: total input, UT: Unbound Tris treated fraction, BT: Bound Tris treated fraction, UH: Unbound HA treated fraction, BH: Bound HA treated fraction.

The vesicle-associated membrane protein (VAMP) family are synaptic vesicle SNARE proteins that are essential for neurotransmitter release (Bhattacharya et al., 2002) and that are known to be palmitoylated (Veit et al., 2000). Initially, an antibody was used that recognises VAMP1 and VAMP2. Analysis of whole brain homogenates ($n=3$ KO, 3 WT), showed that there was no overall difference in VAMP1/2 expression between WT and KO animals (Figure 5.11).

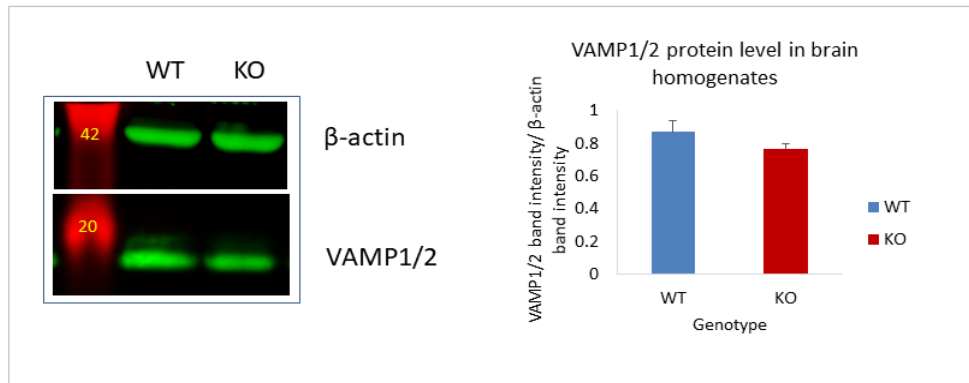


Figure 5.11 Quantification of VAMP1/2 protein level in brain homogenates. Whole brain homogenates (13 μ g) were resolved by SDS-PAGE and transferred to nitrocellulose, and subsequently probed with β -actin and VAMP1/2 antibodies. The left panel shows representative western blots (position of molecular weight markers is shown on the left), whereas the right panel shows quantified data from 3 KO and 3 WT mouse whole brain homogenates. Statistical analysis using an unpaired t-test indicated that there was no significant difference in VAMP1/2 expression between WT and KO samples ($p > 0.05$).

Moreover, when VAMP1/2 palmitoylation was studied by Acyl-RAC in whole brain and hippocampus of WT and *Zdhhc9* KO mice ($n=3$ WT, 3 KO), there was not a significant difference between the two genotypes of mice (Figure 5.12).

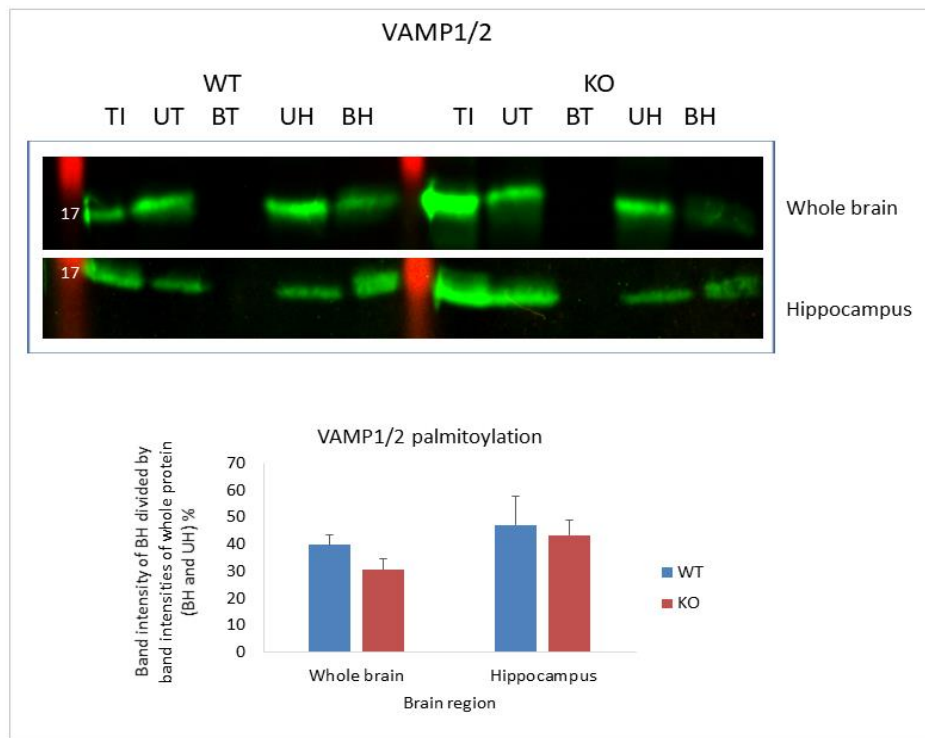


Figure 5.12 Quantification of VAMP1/2 palmitoylation in whole brain and hippocampi of WT and *Zdhhc9* KO mice. Acyl-RAC samples from whole brain or hippocampi were resolved by SDS-PAGE and transferred to nitrocellulose, and subsequently probed with VAMP1/2 antibody. The upper panel shows representative western blots (position of molecular weight markers is shown on the left), whereas the lower panel shows quantified data from whole brain or hippocampi of 3 KO and 3 WT mice. Statistical analysis using an unpaired t-test indicated that there was no significant difference in VAMP1/2 palmitoylation between WT and KO samples ($p > 0.05$). TI: total input, UT: Unbound Tris treated fraction, BT: Bound Tris treated fraction, UH: Unbound HA treated fraction, BH: Bound HA treated fraction.

To specifically study VAMP2, an isoform-selective antibody was used. A statistically significant decrease in VAMP2 expression was observed in KO mouse brain homogenates ($p = 0.04$, 2 sample t-test, Figure 5.13). Although this was a significant difference, the extent of the change was very small.

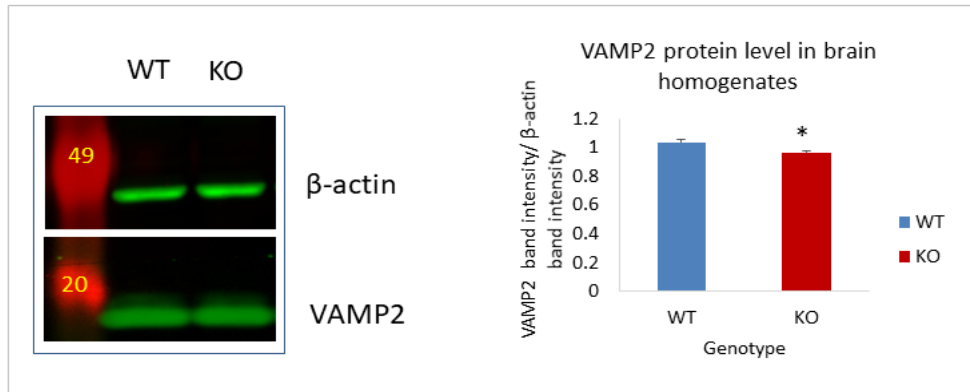


Figure 5.13 Quantification of VAMP2 protein level in brain homogenates. Whole brain homogenates (13 μ g) were resolved by SDS-PAGE and transferred to nitrocellulose, and subsequently probed with β -actin and VAMP2 antibodies. The left panel shows representative western blots (position of molecular weight markers is shown on the left), whereas the right panel shows quantified data from 3 KO and 3 WT mouse whole brain homogenates. Statistical analysis using an unpaired t-test indicated that there was a significant difference in VAMP2 expression between WT and KO samples ($p=0.04$).

When the same antibody was used in order to study palmitoylation of VAMP2 in whole brain of *Zdhhc9* KO mice, no significant change was observed between WT and KO animals (Figure 5.14), consistent with the results using the antibody that recognises both VAMP1 and VAMP2 (Figure 5.12).

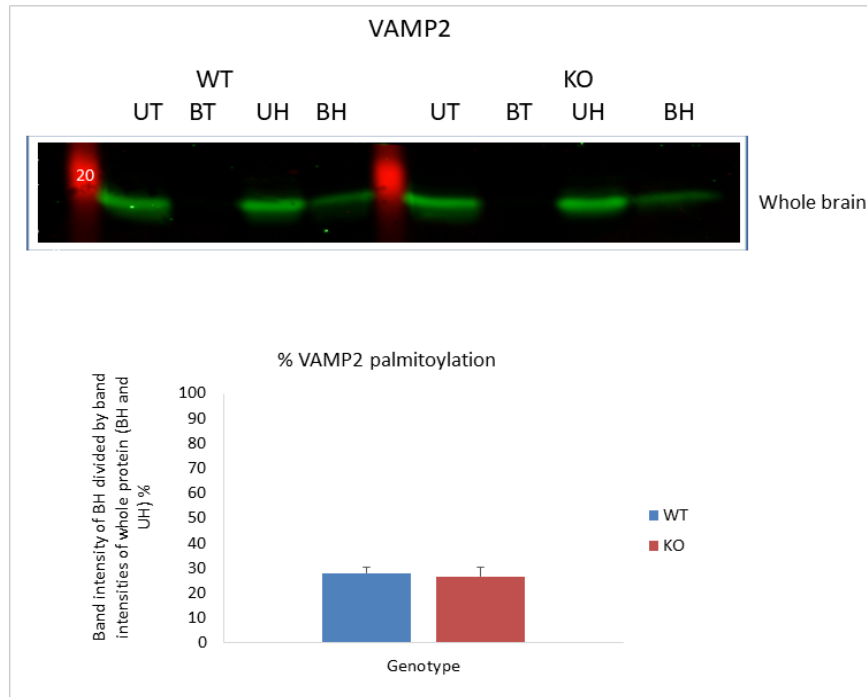


Figure 5.14 Quantification of VAMP2 palmitoylation in whole brain of WT and Zdhhc9 KO mice. Acyl-RAC samples from whole brain were resolved by SDS-PAGE and transferred to nitrocellulose, and subsequently probed with VAMP2 antibody. The upper panel shows representative western blot (position of molecular weight markers is shown on the left), whereas the lower panel shows quantified data from whole brain of 3 KO and 3 WT mice. Statistical analysis using an unpaired t-test indicated that there was no significant difference in VAMP2 palmitoylation between WT and KO samples ($p > 0.05$). UT: Unbound Tris treated fraction, BT: Bound Tris treated fraction, UH: Unbound HA treated fraction, BH: Bound HA treated fraction.

A third VAMP isoform was also studied (VAMP3), and there was no significant change in expression of this protein in whole brain homogenates of KO mice ($n=3$ KO, 3 WT) (Figure 5.15).

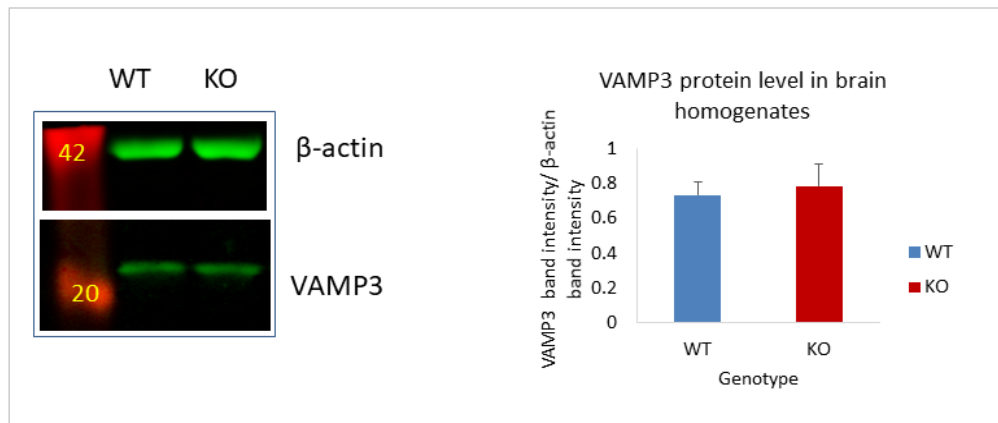


Figure 5.15 Quantification of VAMP3 protein level in brain homogenates. Whole brain homogenates (13 μ g) were resolved by SDS-PAGE and transferred to nitrocellulose, and subsequently probed with β -actin and VAMP3 antibodies. The left panel shows representative western blots (position of molecular weight markers is shown on the left), whereas the right panel shows quantified data from 3 KO and 3 WT mouse whole brain homogenates. Statistical analysis using an unpaired t-test indicated that there was no significant difference in VAMP3 expression between WT and KO samples ($p > 0.05$).

Synaptotagmin-1 is a presynaptic vesicle protein known to be palmitoylated (Chapman et al., 1996). The levels of this protein were unchanged in whole brain homogenates (n=3 KO, 3 WT) from KO animals (Figure 5.16).

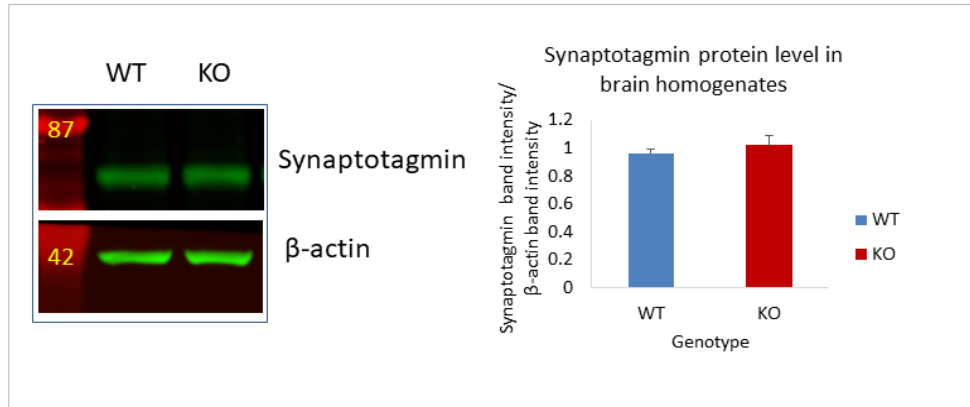


Figure 5.16 Quantification of Synaptotagmin 1 protein level in brain homogenates. Whole brain homogenates (13 μ g) were resolved by SDS-PAGE and transferred to nitrocellulose and subsequently probed with β -actin and Synaptotagmin 1 antibodies. The left panel shows representative western blots (position of molecular weight markers is shown on the left), whereas the right panel shows quantified data from 3 KO and 3 WT mouse whole brain homogenates. Statistical analysis using an unpaired t-test indicated that there was no significant difference in Synaptotagmin 1 expression between WT and KO samples ($p > 0.05$).

In addition, when Synaptotagmin 1 palmitoylation was studied by Acyl-RAC in whole brain and hippocampus of WT and *Zdhhc9* KO mice ($n=3$ WT, 3 KO), there was not a significant difference between the two genotypes of mice (Figure 5.17).

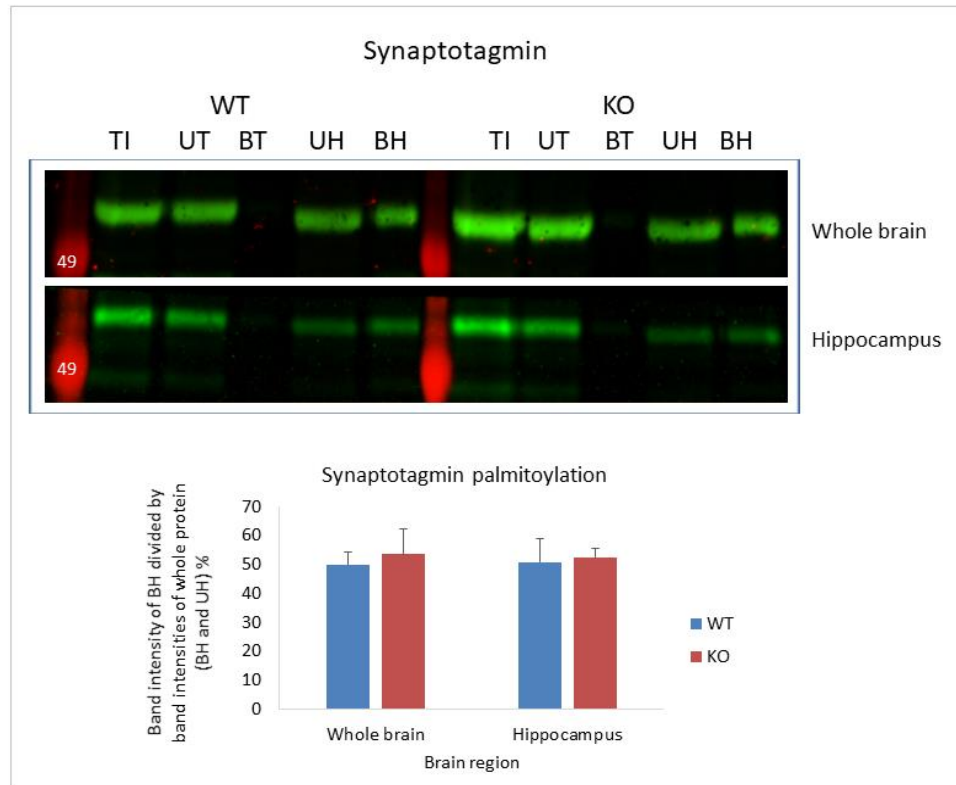


Figure 5.17 Quantification of Synaptotagmin 1 palmitoylation in whole brain and hippocampi of WT and *Zdhhc9* KO mice. Acyl-RAC samples from whole brain or hippocampi were resolved by SDS-PAGE and transferred to nitrocellulose, and subsequently probed with Synaptotagmin 1 antibody. The upper panel shows representative western blots (position of molecular weight markers is shown on the left), whereas the lower panel shows quantified data from whole brain or hippocampi of 3 KO and 3 WT mice. Statistical analysis using an unpaired t-test indicated that there was no significant difference in Synaptotagmin 1 palmitoylation between WT and KO samples ($p > 0.05$). TI: total input, UT: Unbound Tris treated fraction, BT: Bound Tris treated fraction, UH: Unbound HA treated fraction, BH: Bound HA treated fraction.

Finally, the expression and palmitoylation of Vesicular glutamate transporters (VGLUTs) was studied. These proteins transport glutamate from the cell cytoplasm into synaptic vesicles (Shigeri et al., 2004). VGLUT1 and VGLUT2

levels were examined in whole brain homogenates from WT and KO mice but no difference was noticed between the two groups (Figure 5.18).

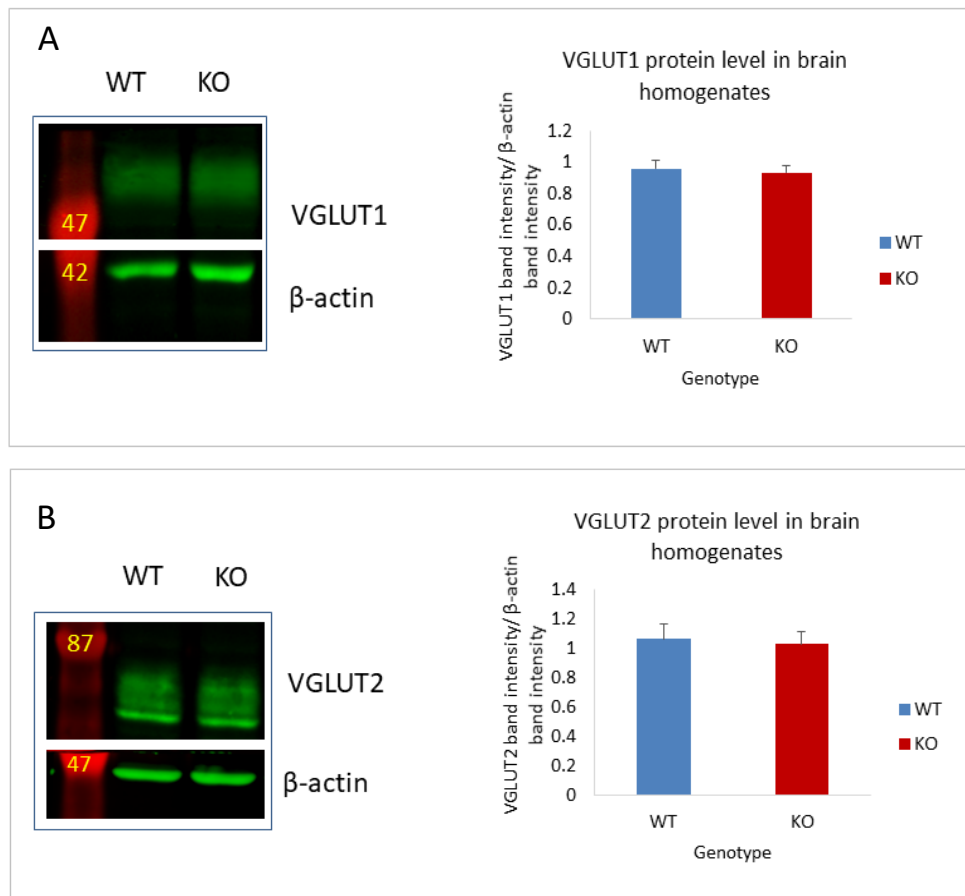


Figure 5.18 Quantification of VGLUT1 and VGLUT2 protein level in brain homogenates. Whole brain homogenates (13 μ g) were resolved by SDS-PAGE and transferred to nitrocellulose and subsequently probed with β -actin and VGLUT1 and VGLUT2 antibodies. The left parts of panels A and B show representative western blots (position of molecular weight markers is shown on the left), whereas the right parts of panels show quantified data from 3 KO and 3 WT mouse whole brain homogenates. Statistical analysis using an unpaired t-test indicated that there was no significant difference in VGLU1 and VGLUT2 expression between WT and KO samples ($p > 0.05$).

In order to examine if VGLUT1 and VGLUT2 palmitoylation is affected, Acyl-RAC in whole brain of WT and *Zdhhc9* KO mice (n=3 WT, 3 KO) was conducted but there was not a significant difference between the two genotypes of mice for VGLUT1 (Figure 5.19) or VGLUT2 (Figure 5.20).

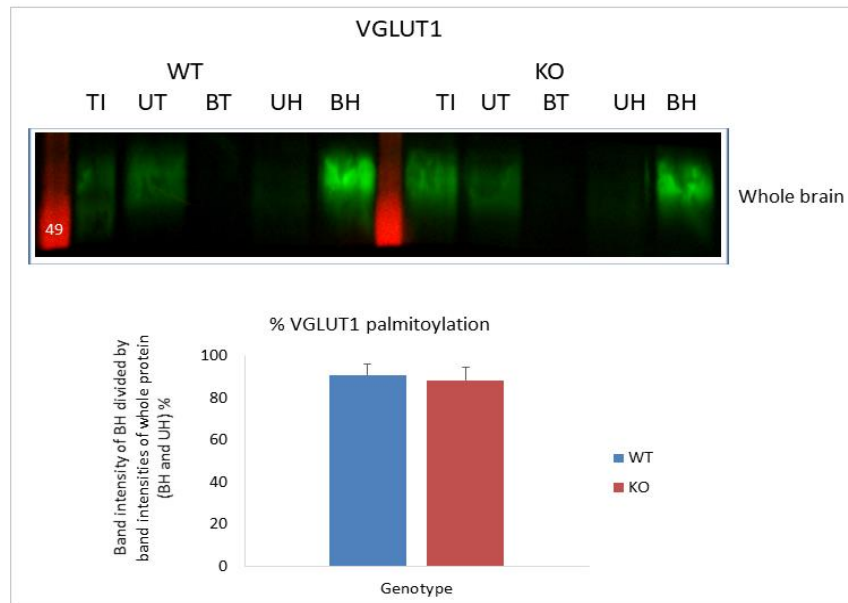


Figure 5.19 Quantification of VGLUT1 palmitoylation in whole brain of WT and *Zdhhc9* KO mice. Acyl-RAC samples from whole brain were resolved by SDS-PAGE and transferred to nitrocellulose and subsequently probed with VGLUT1 antibody. The upper panel shows representative western blot (position of molecular weight markers is shown on the left), whereas the lower panel shows quantified data from whole brain of 3 KO and 3 WT mice. Statistical analysis using an unpaired t-test indicated that there was no significant difference in VGLUT1 palmitoylation between WT and KO samples ($p > 0.05$). TI: total input, UT: Unbound Tris treated fraction, BT: Bound Tris treated fraction, UH: Unbound HA treated fraction, BH: Bound HA treated fraction.

Moreover, Acyl-RAC in hippocampi of WT and *Zdhhc9* KO mice (n=3 WT, 3 KO) was conducted but there was also no significant difference between the two genotypes of mice for VGLUT2 (Figure 5.20).

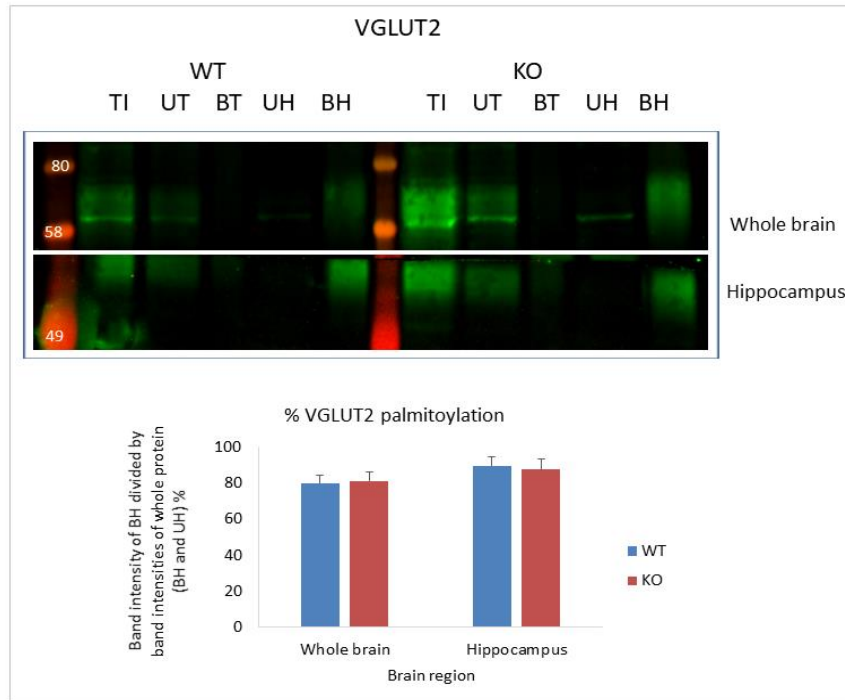


Figure 5.20 Quantification of VGLUT2 palmitoylation in whole brain and hippocampi of WT and *Zdhhc9* KO mice. Acyl-RAC samples from whole brain or hippocampi were resolved by SDS-PAGE and transferred to nitrocellulose, and subsequently probed with VGLUT2 antibody. The upper panel shows representative western blots (position of molecular weight markers is shown on the left), whereas the lower panel shows quantified data from whole brain or hippocampi of 3 KO and 3 WT mice. Statistical analysis using an unpaired t-test indicated that there was no significant difference in VGLUT2 palmitoylation between WT and KO samples ($p > 0.05$). TI: total input, UT: Unbound Tris treated fraction, BT: Bound Tris treated fraction, UH: Unbound HA treated fraction, BH: Bound HA treated fraction.

5.2.5 Analysis of palmitoylated post-synaptic proteins in *Zdhhc9* KO brain

It is clear from the preceding analyses that KO of *Zdhhc9* has little effect on the expression and palmitoylation of pre-synaptic proteins. To investigate if zDHHC9 function is more important in post-synaptic function, the expression and palmitoylation of a number of important post-synaptic proteins was investigated.

Initially, GluR1 and GluR2 subunits of AMPA receptors were studied as these are known to be regulated by palmitoylation (Hayashi et al., 2005). There was no change in expression of GluR1 protein level in whole brain homogenates of KO mice (Figure 5.21).

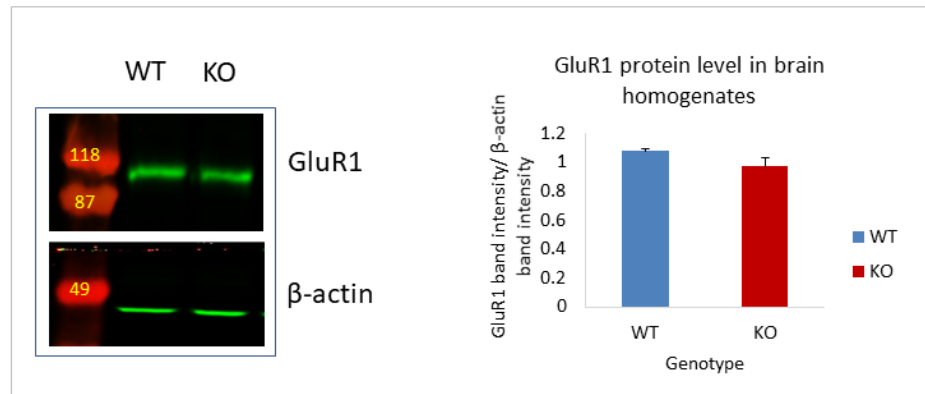


Figure 5.21 Quantification of GluR1 protein level in brain homogenates. Whole brain homogenates (13 μ g) were resolved by SDS-PAGE and transferred to nitrocellulose, and subsequently probed with β -actin and GluR1 antibodies. The left panel shows representative western blots (position of molecular weight markers is shown on the left), whereas the right panel shows quantified data from 4 KO and 4 WT mouse whole brain homogenates. Statistical analysis using an unpaired t-test indicated that there was no significant difference in GluR1 expression between WT and KO samples ($p > 0.05$).

Moreover the level of Phospho-GluR1 (Ser845) was studied as phosphorylation of GluR1 is essential for synaptic plasticity and promotes rapid excitatory transmission in the brain (Lee et al., 2003). The internalization and recycling of AMPA receptors depends on changes in phosphorylation of Ser845 (Ehlers, 2000). However, no difference was observed between WT and KO brain homogenates (Figure 5.22).

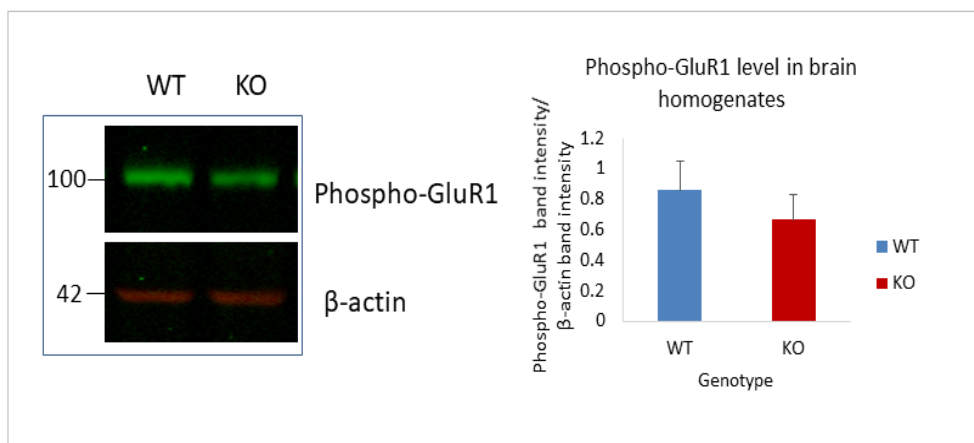


Figure 5.22 Quantification of phospho-GluR1 (Ser845) protein level in brain homogenates.

Whole brain homogenates (13 μ g) were resolved by SDS-PAGE and transferred to nitrocellulose, and subsequently probed with β -actin and phospho-GluR1 antibodies. The left panel shows representative western blots (position of molecular weight markers is shown on the left), whereas the right panel shows quantified data from 3 KO and 3 WT mouse whole brain homogenates. Statistical analysis using an unpaired t-test indicated that there was no significant difference in phospho-GluR1 expression between WT and KO samples ($p > 0.05$).

GluR1 and GluR2 palmitoylation is essential for the regulation of intracellular trafficking of the receptors (Yang et al., 2009). Therefore, GluR1 palmitoylation was studied by Acyl-RAC and there was no significant change in GluR1 palmitoylation in whole brain (Figure 5.23). Also, no change in palmitoylation was observed in the hippocampus of KO animals (Figure 5.23).

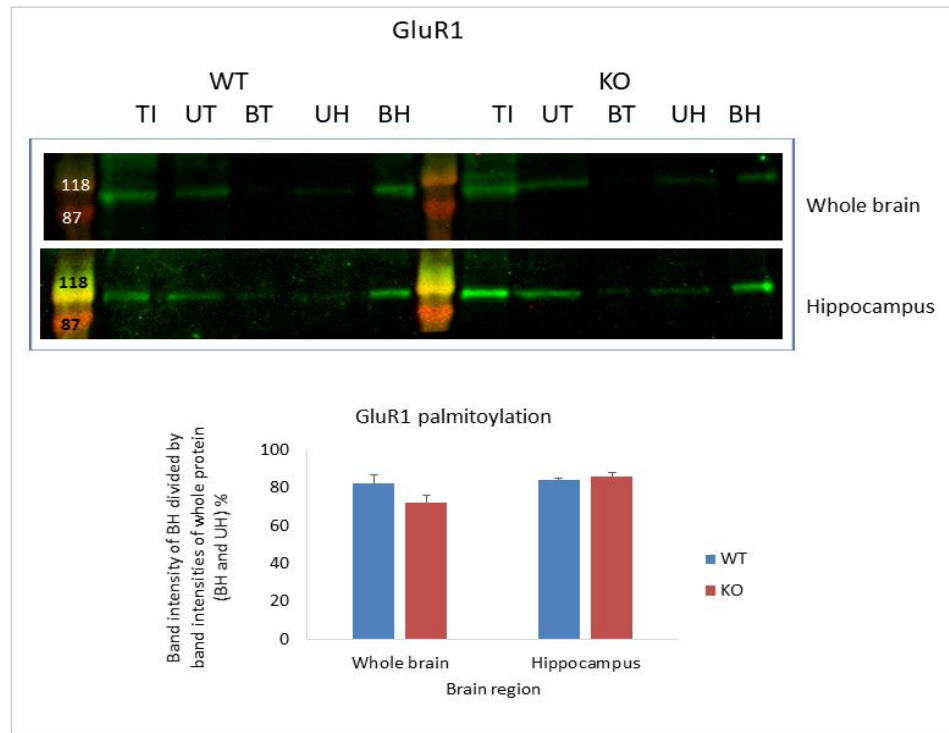


Figure 5.23 Quantification of GluR1 palmitoylation in whole brain and hippocampi of WT and *Zdhhc9* KO mice. Acyl-RAC samples from whole brain or hippocampi were resolved by SDS-PAGE and transferred to nitrocellulose and subsequently probed with GluR1 antibody. The upper panel shows representative western blots (position of molecular weight markers is shown on the left), whereas the lower panel shows quantified data from whole mouse brain (n=4KO, 4WT) or hippocampi (n=3KO, 3WT). Statistical analysis using an unpaired t-test indicated that there was no significant difference in GluR1 palmitoylation between WT and KO samples ($p>0.05$). TI: total input, UT: Unbound Tris treated fraction, BT: Bound Tris treated fraction, UH: Unbound HA treated fraction, BH: Bound HA treated fraction.

GluR2 levels were also studied in whole brain homogenates but no change was observed between WT and KO animals (Figure 5.24).

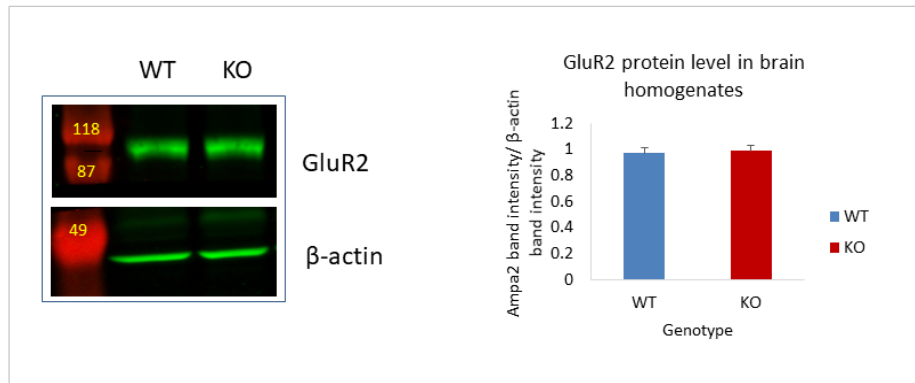


Figure 5.24 Quantification of GluR2 protein level in brain homogenates. Whole brain homogenates (13 μ g) were resolved by SDS-PAGE and transferred to nitrocellulose, and subsequently probed with β -actin and GluR2 antibodies. The left panel shows representative western blots (position of molecular weight markers is shown on the left), whereas the right panel shows quantified data from 3 KO and 3 WT mouse whole brain homogenates. Statistical analysis using an unpaired t-test indicated that there was no significant difference in GluR2 expression between WT and KO samples ($p > 0.05$).

Moreover, GluR2 palmitoylation that was studied by Acyl-RAC in whole brain did not show any significant difference between the two genotypes (Figure 5.25). Thus, there was no overall change in expression or palmitoylation of GluR1 and GluR2 AMPA receptor subunits.

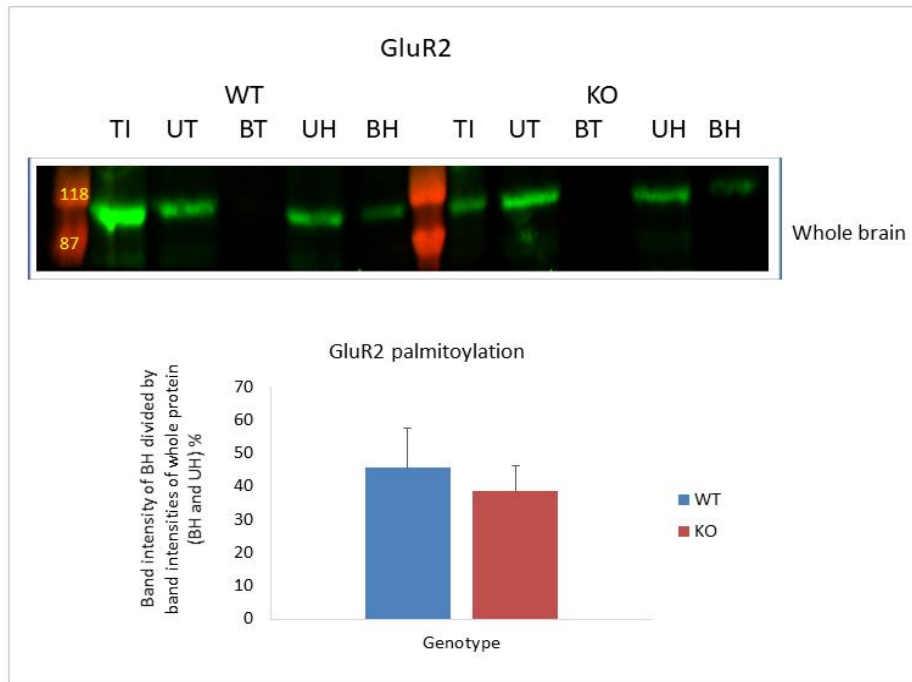


Figure 5.25 Quantification of GluR2 palmitoylation in whole brain of WT and Zdhhc9 KO mice. Acyl-RAC samples from whole brain were resolved by SDS-PAGE and transferred to nitrocellulose, and subsequently probed with GluR2 antibody. The upper panel shows representative western blot (position of molecular weight markers is shown on the left), whereas the lower panel shows quantified data from whole brain of 3 KO and 3 WT mice. Statistical analysis using an unpaired t-test indicated that there was no significant difference in GluR2 palmitoylation between WT and KO samples ($p > 0.05$). TI: total input, UT: Unbound Tris treated fraction, BT: Bound Tris treated fraction, UH: Unbound HA treated fraction, BH: Bound HA treated fraction.

Postsynaptic density protein 95 (PSD95) is a synaptic scaffolding protein that plays a key role in the clustering of AMPA and NMDA receptors (Yudowski et al., 2013; Bustos et al., 2014). When PSD95 protein level was examined in brain homogenates, there was not a significant change identified between WT and KO animals (Figure 5.26).

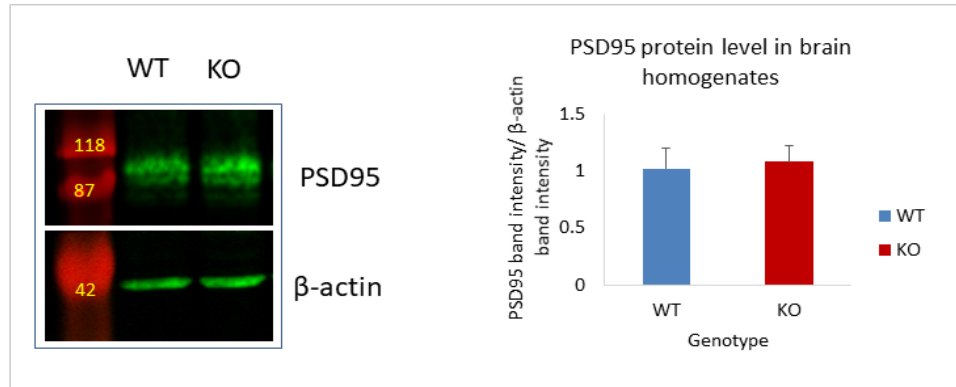


Figure 5.26 Quantification of PSD95 protein level in brain homogenates. Whole brain homogenates (13 μ g) were resolved by SDS-PAGE and transferred to nitrocellulose, and subsequently probed with β -actin and PSD95 antibodies. The left panel shows representative western blots (position of molecular weight markers is shown on the left), whereas the right panel shows quantified data from 3 KO and 3 WT mouse whole brain homogenates. Statistical analysis using an unpaired t-test indicated that there was no significant difference in PSD95 expression between WT and KO samples ($p > 0.05$).

The targeting of PSD95 to the post-synaptic density is regulated by palmitoylation (El-Husseini et al., 2000). Therefore its palmitoylation level was examined by Acyl-RAC in whole brain and hippocampus of WT and KO animals without any significant finding (Figure 5.27).

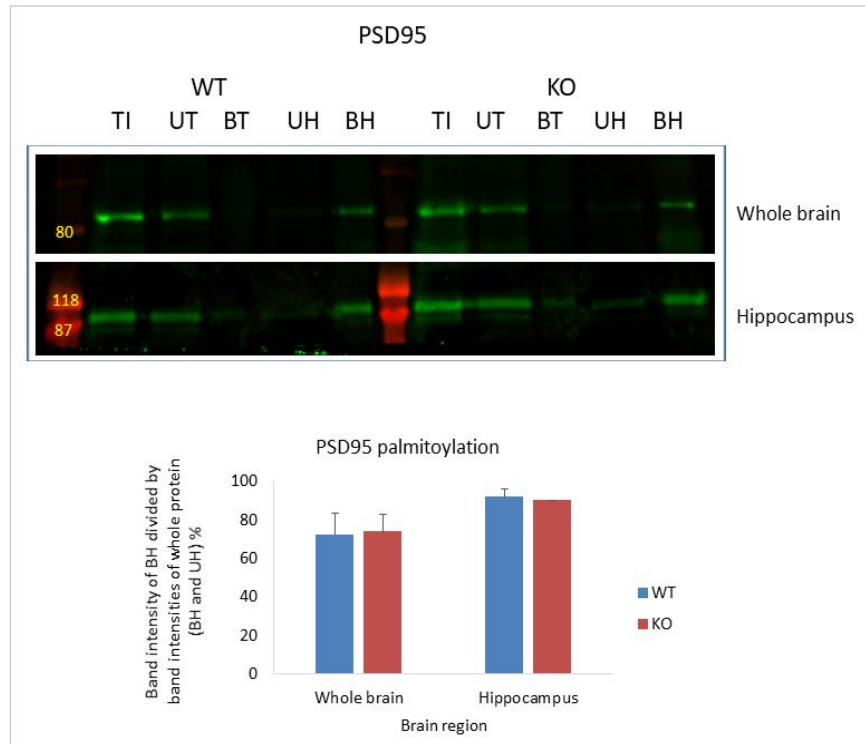


Figure 5.27 Quantification of PSD95 palmitoylation in whole brain and hippocampi of WT and Zdhhc9 KO mice. Acyl-RAC samples from whole brain or hippocampi were resolved by SDS-PAGE and transferred to nitrocellulose and subsequently probed with PSD95 antibody. The upper panel shows representative western blots (position of molecular weight markers is shown on the left), whereas the lower panel shows quantified data from whole brain or hippocampi of 3 KO and 3 WT mice. Statistical analysis using an unpaired t-test indicated that there was no significant difference in PSD95 palmitoylation between WT and KO samples ($p > 0.05$). TI: total input, UT: Unbound Tris treated fraction, BT: Bound Tris treated fraction, UH: Unbound HA treated fraction, BH: Bound HA treated fraction.

Finally, expression and palmitoylation of the NR2b subunit of NMDA receptors was investigated as this protein is also known to be regulated by palmitoylation (Hayashi et al., 2009). After studying its protein level in whole brain homogenates, no significant difference was revealed between WT and KO mouse brain (Figure 5.28).

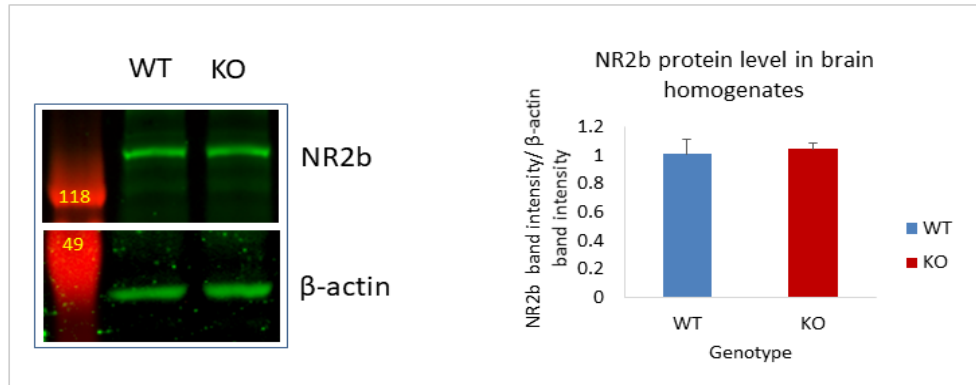


Figure 5.28 Quantification of NR2b protein level in brain homogenates. Whole brain homogenates (13 μ g) were resolved by SDS-PAGE and transferred to nitrocellulose, and subsequently probed with β -actin and NR2b antibodies. The left panel shows representative western blots (position of molecular weight markers is shown on the left), whereas the right panel shows quantified data from 3 KO and 3 WT mouse whole brain homogenates. Statistical analysis using an unpaired t-test indicated that there was no significant difference in NR2b expression between WT and KO samples ($p > 0.05$).

Similar results were obtained after studying its palmitoylation in whole brain from WT and KO animals, the palmitoylated protein had similar levels in both groups (Figure 5.29).

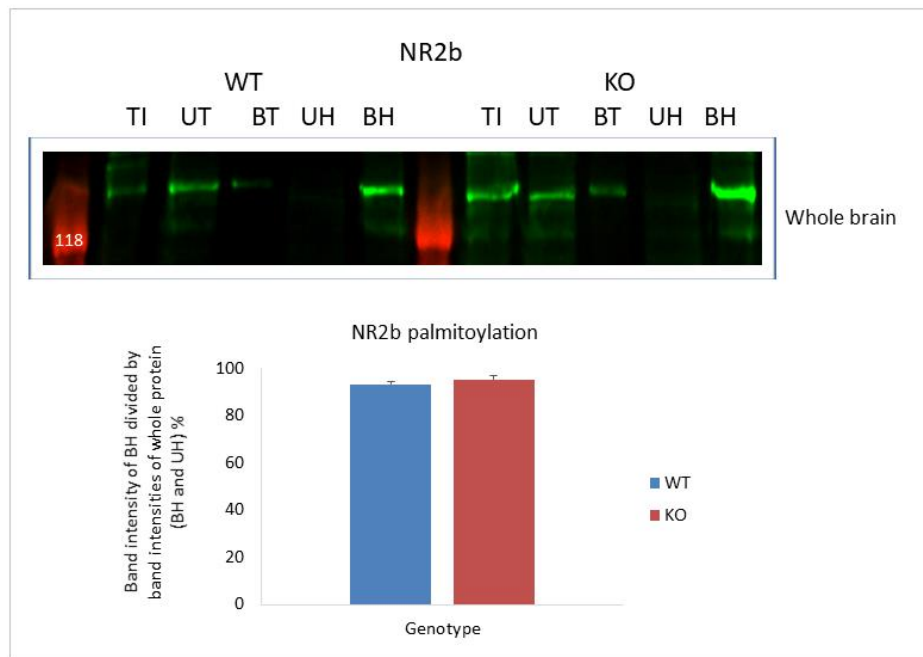


Figure 5.29 Quantification of NR2b palmitoylation in whole brain of WT and Zdhhc9 KO mice. Acyl-RAC samples from whole brain were resolved by SDS-PAGE and transferred to nitrocellulose, and subsequently probed with NR2b antibody. The upper panel shows representative western blot (position of molecular weight markers is shown on the left), whereas the lower panel shows quantified data from whole brain of 3 KO and 3 WT mice. Statistical analysis using an unpaired t-test indicated that there was no significant difference in NR2b palmitoylation between WT and KO samples ($p > 0.05$). TI: total input, UT: Unbound Tris treated fraction, BT: Bound Tris treated fraction, UH: Unbound HA treated fraction, BH: Bound HA treated fraction.

5.2.6 Proteomic analysis of changes in palmitoylated proteins in Zdhhc9 KO mouse brain

As no change in the expression or palmitoylation of a variety of pre- and post-synaptic proteins was identified by immunoblotting apart from a small decrease in VAMP2 protein level in brain homogenates of Zdhhc9 KO animals, an unbiased

proteomics strategy was adopted. Acyl-RAC fractions (BH and BT) were isolated from whole WT and KO mouse brain (n=2) and analysed by MS.

1179 proteins were identified as likely to be palmitoylated. After applying a filter for proteins with a fold change ≥ 2 (upregulated in KO) and ≤ 0.5 (downregulated in KO), 300 proteins appeared to meet those criteria. From them, 230 proteins had reduced palmitoylation and are presented in Table 5.1.

Table 5.1 Proteins with reduced palmitoylation in *Zdhhc9* KO mouse brain.

Gene name of protein	Average Ratio KO/WT
<i>Usp20</i>	WT specific
<i>Dhx15</i>	WT specific
<i>Ralgapb</i>	WT specific
<i>Tbck</i>	WT specific
<i>Eif3a</i>	WT specific
<i>Uhrf1bp1</i>	WT specific
<i>Mtmr3</i>	WT specific
<i>Ccr5</i>	WT specific
<i>Stxbp3</i>	WT specific
<i>Tmem57</i>	WT specific
<i>Rnpep</i>	WT specific
<i>Ikbkb</i>	WT specific
<i>Sae1</i>	WT specific
<i>Nell2</i>	0.004

<i>Gdap1</i>	0.012
<i>Ppm1a</i>	0.013
<i>Pip4k2a</i>	0.052
<i>Jam3</i>	0.053
<i>Tpi1</i>	0.058
<i>Tns1</i>	0.078
<i>Ndufb8</i>	0.082
<i>Map3k4</i>	0.084
<i>Dnajc6</i>	0.088
<i>Abcb8</i>	0.091
<i>Scn3a</i>	0.093
<i>Zc2hc1a</i>	0.106
<i>Uchl5</i>	0.109
<i>Atp6v1g1</i>	0.110
<i>Synrg</i>	0.111
<i>Sept3</i>	0.118
<i>Gpi</i>	0.125
<i>Apeh</i>	0.129
<i>Rab13</i>	0.137
<i>Ctsd</i>	0.137

<i>Necab2</i>	0.152
<i>Arhgap26</i>	0.152
<i>Lancl1</i>	0.153
<i>Lzts1</i>	0.153
<i>Hapln1</i>	0.155
<i>Luc7l</i>	0.157
<i>Psmc6</i>	0.158
<i>Map2k2</i>	0.160
<i>Sorbs1</i>	0.162
<i>Gad1</i>	0.166
<i>Mat2b</i>	0.167
<i>Scrn1</i>	0.174
<i>Asrgl1</i>	0.176
<i>Arfgap2</i>	0.177
<i>Bcat1</i>	0.184
<i>Unc13c</i>	0.184
<i>Sirt2</i>	0.184
<i>Mbnl1</i>	0.186
<i>Tnpo1</i>	0.188
<i>Kif3a</i>	0.200

<i>Impa1</i>	0.201
<i>Eif3i</i>	0.204
<i>Uchl1</i>	0.224
<i>Atp6v1g2</i>	0.231
<i>Arhgap5</i>	0.231
<i>Irs2</i>	0.233
<i>Ndrp4</i>	0.235
<i>Hnrnpa2b1</i>	0.239
<i>Cpe</i>	0.241
<i>Adrbk1</i>	0.244
<i>Cdc42ep4</i>	0.244
<i>Trappc8</i>	0.248
<i>Ddn</i>	0.249
<i>Pam</i>	0.251
<i>Wars</i>	0.253
<i>Vps51</i>	0.255
<i>Tjp1</i>	0.255
<i>Got1</i>	0.259
<i>Hba1</i>	0.260
<i>Sept7</i>	0.260

<i>Arsb</i>	0.260
<i>Vps4a</i>	0.260
<i>Nfs1</i>	0.267
<i>Sh2b1</i>	0.268
<i>Opa1</i>	0.271
<i>Gpsm1</i>	0.272
<i>Igfbp1</i>	0.274
<i>Apmap</i>	0.274
<i>Exoc8</i>	0.275
<i>Celf4</i>	0.275
<i>Abhd17a</i>	0.275
<i>Ctnn</i>	0.275
<i>Dpysl4</i>	0.278
<i>Coro1a</i>	0.278
<i>Hsp90ab1</i>	0.281
<i>Rpsa</i>	0.281
<i>Map2k4</i>	0.284
<i>Dnaja3</i>	0.286
<i>Txn1l1</i>	0.292
<i>Zyx</i>	0.299

<i>Npepps</i>	0.299
<i>Dgke</i>	0.300
<i>Kctd12</i>	0.302
<i>Acaa2</i>	0.303
<i>Rap1gap</i>	0.310
<i>Sf3b3</i>	0.312
<i>Bsg</i>	0.313
<i>Sars</i>	0.313
<i>Ocr1</i>	0.318
<i>Hsp90aa1</i>	0.320
<i>Appl2</i>	0.322
<i>Pgk1</i>	0.328
<i>Slc24a2</i>	0.331
<i>Prkar2a</i>	0.331
<i>ldh3a</i>	0.333
<i>Cpeb3</i>	0.339
<i>Stom</i>	0.341
<i>Slc29a1</i>	0.343
<i>Cat</i>	0.345
<i>Ddx1</i>	0.346

<i>Fam217b</i>	0.350
<i>Pdma5</i>	0.351
<i>Ankrd63</i>	0.352
<i>Tns2</i>	0.356
<i>Mblac2</i>	0.360
<i>Mtmr12</i>	0.361
<i>Pde2a</i>	0.362
<i>Fga</i>	0.362
<i>Tlhc1</i>	0.363
<i>Acs16</i>	0.363
<i>Usp4</i>	0.364
<i>Rnf214</i>	0.368
<i>Ube2v2</i>	0.370
<i>Hnrnp2</i>	0.371
<i>Lrrc16a</i>	0.371
<i>Ppia</i>	0.372
<i>Rps16</i>	0.373
<i>Vps37b</i>	0.373
<i>Vps35</i>	0.376
<i>Necap1</i>	0.376

<i>Stxbp5</i>	0.377
<i>Dpysl5</i>	0.377
<i>Cnn3</i>	0.379
<i>Cst3</i>	0.380
<i>Aldh5a1</i>	0.381
<i>Vps8</i>	0.382
<i>Syt4</i>	0.382
<i>Plcb1</i>	0.382
<i>C1qtnf4</i>	0.383
<i>Golga7b</i>	0.384
<i>Elavl2</i>	0.385
<i>Lamb2</i>	0.388
<i>Csnk1e</i>	0.389
<i>Plxna1</i>	0.395
<i>Qdpr</i>	0.397
<i>Dtna</i>	0.399
<i>Clcn6</i>	0.403
<i>Abce1</i>	0.405
<i>Synpo</i>	0.410
<i>Trim32</i>	0.412

<i>Fam21</i>	0.413
<i>Fech</i>	0.415
<i>Crmp1</i>	0.417
<i>Pde10a</i>	0.417
<i>Spred2</i>	0.419
<i>Atp6v1b2</i>	0.423
<i>Pura</i>	0.424
<i>Cadps</i>	0.427
<i>Gmppa</i>	0.428
<i>Pycrl</i>	0.428
<i>Inpp5j</i>	0.429
<i>Dlgap4</i>	0.430
<i>Fam63b</i>	0.432
<i>Thsd7a</i>	0.433
<i>Lasp1</i>	0.435
<i>Ago1</i>	0.438
<i>Blmh</i>	0.439
<i>Slc2a3</i>	0.448
<i>Gabra1</i>	0.451
<i>Hcn1</i>	0.451

<i>Tkt</i>	0.452
<i>Lars</i>	0.452
<i>Ncor2</i>	0.452
<i>Cops3</i>	0.452
<i>Asap2</i>	0.454
<i>Itsn1</i>	0.455
<i>Nckipsd</i>	0.456
<i>Camkv</i>	0.459
<i>Mprip</i>	0.459
<i>App1</i>	0.461
<i>Wasl</i>	0.461
<i>Mgea5</i>	0.462
<i>Wdfy3</i>	0.462
<i>Aip</i>	0.464
<i>Dgkb</i>	0.464
<i>Agap3</i>	0.466
<i>Apc</i>	0.466
<i>Coro1b</i>	0.466
<i>Eno1</i>	0.469
<i>Shc3</i>	0.469

<i>Rab6a</i>	0.469
<i>Wasf1</i>	0.469
<i>Map7d2</i>	0.470
<i>Gdi1</i>	0.473
<i>Add3</i>	0.474
<i>Zc3h4</i>	0.475
<i>Fn1</i>	0.476
<i>Usp15</i>	0.477
<i>Nipsnap1</i>	0.477
<i>Osbpl8</i>	0.477
<i>Macf1</i>	0.478
<i>Ehbp1</i>	0.480
<i>Ak5</i>	0.480
<i>Nsf</i>	0.481
<i>Ccdc88a</i>	0.483
<i>Slc30a3</i>	0.483
<i>Farp1</i>	0.485
<i>Asap1</i>	0.486
<i>Ulk1</i>	0.486
<i>Col4a2</i>	0.487

<i>Larp1</i>	0.488
<i>Pfas</i>	0.489
<i>Ubr5</i>	0.489
<i>Lrba</i>	0.489
<i>Kbtbd11</i>	0.490
<i>Usp7</i>	0.490
<i>Rnf11</i>	0.490
<i>Gnl1</i>	0.490
<i>Calcoco1</i>	0.495
<i>Nisch</i>	0.495
<i>Myo16</i>	0.496
<i>Pgbd5</i>	0.496
<i>Tpp2</i>	0.498
<i>Ewsr1</i>	0.498
<i>Tex264</i>	0.499
<i>Irgq</i>	0.500

5.2.7 Validation of proteomics with immunoblotting

Some of the proteomic hits were tested for validation using immunoblotting. CCR5 (C-C chemokine receptor type 5) was detected in only palmitoylated samples from WT mice and not KO mice. However immunoblotting analysis showed that no CCR5 could be detected in the palmitoylated fractions (BH) (n= 2 WT, 2 KO from

proteomics). In addition, no change in CCR5 expression was observed in brain homogenates from WT and KO mice (Figure 5.30).

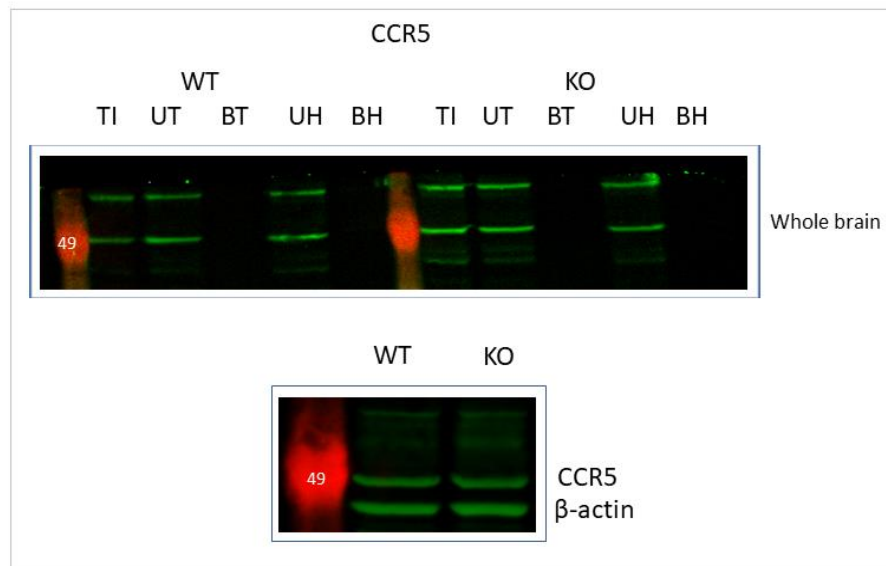


Figure 5.30 CCR5 expression in Acyl-RAC fractions and brain homogenates from WT and *Zdhhc9* KO mice. The upper panel shows representative western blot after Acyl-RAC from whole mouse brain. The samples were resolved by SDS-PAGE and transferred to nitrocellulose and subsequently probed with CCR5 antibody. The lower panel shows representative western blot of CCR5 protein levels in brain homogenates. Whole brain homogenates (13 μ g) were resolved by SDS-PAGE and transferred to nitrocellulose, and subsequently probed with β -actin and CCR5 antibodies. TI: total input, UT: Unbound Tris treated fraction, BT: Bound Tris treated fraction, UH: Unbound HA treated fraction, BH: Bound HA treated fraction. Position of molecular weight markers are shown on the left side of all immunoblots.

Pde10a (cAMP and cAMP-inhibited cGMP 3,5-cyclic phosphodiesterase 10A) was also downregulated in KO samples (0.42 KO vs WT) based on proteomics so its palmitoylation and expression was also studied by immunoblotting (Figure 5.31). No change in palmitoylation of Pde10a was identified by immunoblotting of the Acyl-

RAC samples (n= 2 WT, 2 KO from proteomics), and no change in Pde10a expression was observed by immunoblotting of brain homogenates (Figure 5.31).

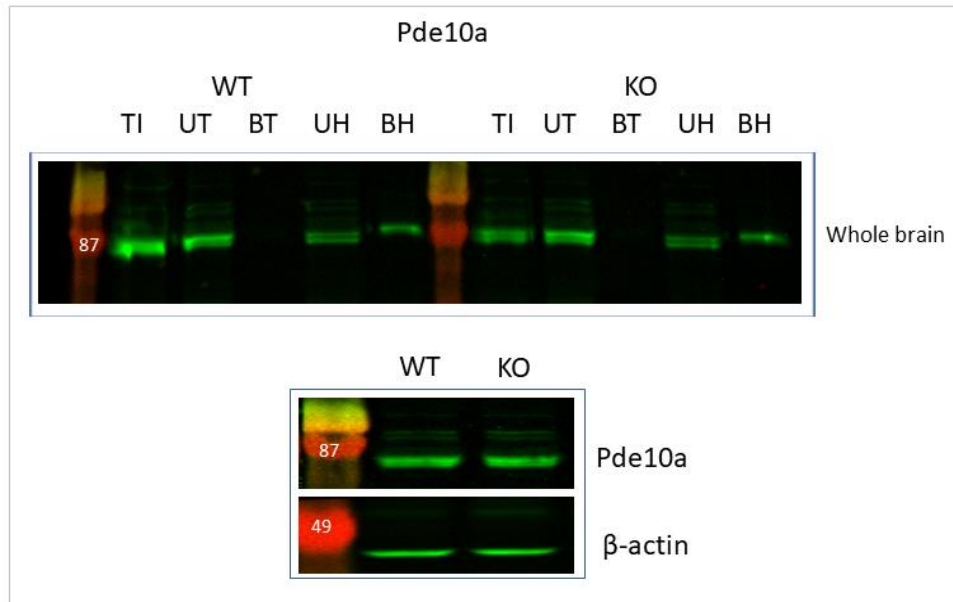


Figure 5.31 Pde10a expression in Acyl-RAC fractions and brain homogenates from WT and *Zdhhc9* KO mice. The upper panel shows representative western blot after Acyl-RAC from whole mouse brain. The samples were resolved by SDS-PAGE and transferred to nitrocellulose, and subsequently probed with Pde10a antibody. The lower panel shows representative western blot of Pde10a protein levels in brain homogenates. Whole brain homogenates (13 μ g) were resolved by SDS-PAGE and transferred to nitrocellulose, and subsequently probed with β -actin and Pde10a antibodies. TI: total input, UT: Unbound Tris treated fraction, BT: Bound Tris treated fraction, UH: Unbound HA treated fraction, BH: Bound HA treated fraction. Position of molecular weight markers are shown on the left side of all immunoblots.

Synaptophysin was also downregulated in KO samples (0.56 KO vs WT) based on proteomics so its palmitoylation was also studied by immunoblotting (Figure 5.32). No change in palmitoylation of Synaptophysin was identified by

immunoblotting of the Acyl-RAC samples (n= 2 WT, 2 KO from proteomics, Figure 5.32).

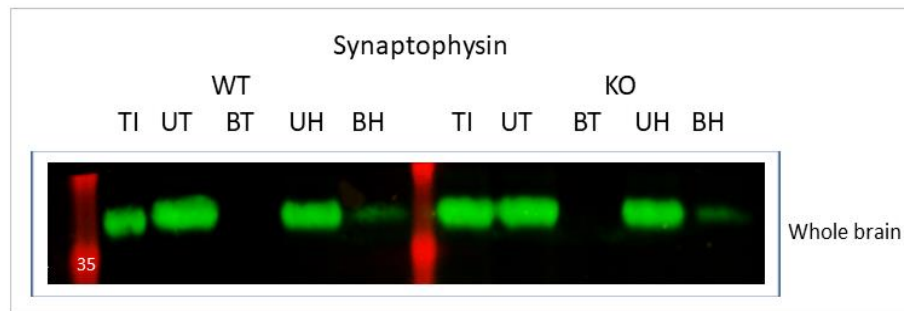


Figure 5.32 Synaptophysin expression in Acyl-RAC fractions from WT and Zdhhc9 KO mice. Representative western blot after Acyl-RAC from whole mouse brain. The samples were resolved by SDS-PAGE and transferred to nitrocellulose and subsequently probed with Synaptophysin antibody. TI: total input, UT: Unbound Tris treated fraction, BT: Bound Tris treated fraction, UH: Unbound HA treated fraction, BH: Bound HA treated fraction. Position of molecular weight markers is shown on the left side of the immunoblot.

Calnexin was also downregulated in KO samples (0.57 KO vs WT) based on proteomics therefore its palmitoylation and expression was also studied by immunoblotting (Figure 5.33). No change in palmitoylation of Calnexin was identified by immunoblotting of the Acyl-RAC samples (n= 2 WT, 2 KO from proteomics) and no change in Calnexin expression was observed by immunoblotting of brain homogenates (Figure 5.33).

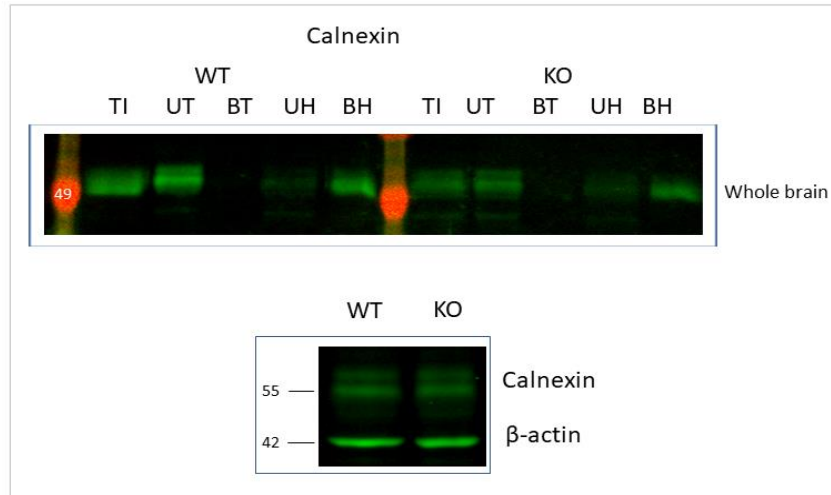


Figure 5.33 Calnexin expression in Acyl-RAC fractions and brain homogenates from WT and *Zdhhc9* KO mice. The upper panel shows representative western blot after Acyl-RAC from whole mouse brain. The samples were resolved by SDS-PAGE and transferred to nitrocellulose and subsequently probed with Calnexin antibody. The lower panel shows representative western blot of Calnexin protein levels in brain homogenates. Whole brain homogenates (13 μ g) were resolved by SDS-PAGE and transferred to nitrocellulose, and subsequently probed with β -actin and Calnexin antibodies. TI: total input, UT: Unbound Tris treated fraction, BT: Bound Tris treated fraction, UH: Unbound HA treated fraction, BH: Bound HA treated fraction. Position of molecular weight markers are shown on the left side of all immunoblots.

Flotillin 2 was also downregulated in KO samples (0.66 KO vs WT) based on proteomics therefore its palmitoylation and expression was also studied by immunoblotting (Figure 5.34). No change in palmitoylation of Flotillin 2 was identified by immunoblotting of the Acyl-RAC samples (n= 2 WT, 2 KO from proteomics), and no change in Flotillin 2 expression was observed by immunoblotting of brain homogenates (Figure 5.34).

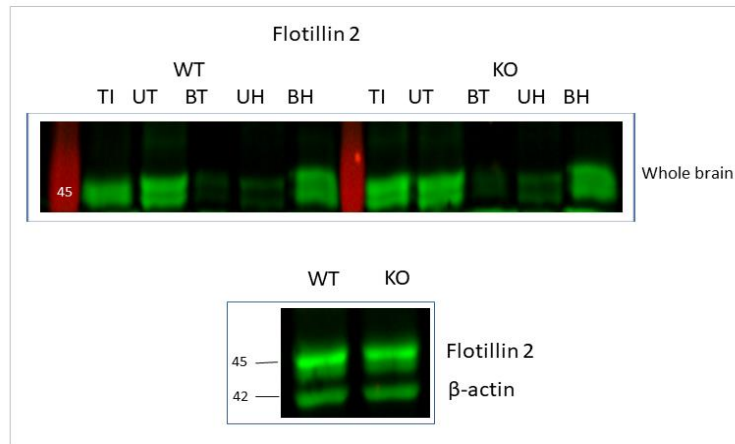


Figure 5.34 Flotillin 2 expression in Acyl-RAC fractions and brain homogenates from WT and *Zdhhc9* KO mice. The upper panel shows representative western blot after Acyl-RAC from whole mouse brain. The samples were resolved by SDS-PAGE and transferred to nitrocellulose and subsequently probed with Flotillin 2 antibody. The lower panel shows representative western blot of Flotillin 2 protein levels in brain homogenates. Whole brain homogenates (13 μ g) were resolved by SDS-PAGE and transferred to nitrocellulose and subsequently probed with β -actin and Flotillin 2 antibodies. TI: total input, UT: Unbound Tris treated fraction, BT: Bound Tris treated fraction, UH: Unbound HA treated fraction, BH: Bound HA treated fraction. Position of molecular weight markers are shown on the left side of all immunoblots.

Among the proteomic hits, some already studied proteins were found: VAMP1 (0.75 KO vs WT), VGLUT1 (0.85 KO vs WT), NR2b (0.86 KO vs WT), GluR1 (1.34 KO vs WT), H-Ras (1.98 KO vs WT), but there was no significant change in the palmitoylation or expression of those proteins as already demonstrated.

5.3 Discussion

In this chapter, a variety of presynaptic and postsynaptic proteins that are known to be palmitoylated were investigated. First, protein levels of each protein

were examined in brain homogenates and then palmitoylation of each protein was studied by Acyl-RAC. The results indicate that *Zdhhc9* KO mice do not show any significant changes in protein expression or palmitoylation of the synaptic proteins studied with the exception of VAMP2. Comparison of the isolated palmitoylomes from WT and *Zdhhc9* KO mice identified a number of marked changes; however immunoblotting of the same samples that were analysed by MS failed to validate any of these changes.

A decrease in protein expression of the presynaptic plasma membrane protein VAMP2 was identified, which was statistically significant based on quantification of band intensities in immunoblots. In neurons, vesicle-associated membrane protein (VAMP2 or Synaptobrevin-2) is an important v-SNARE protein (Elferink et al., 1989). SNARE (Soluble NSF Attachment Protein Receptor) proteins form a large protein family that mediate vesicle fusion. The v-SNARE VAMP2 interacts with the plasma membrane SNARE proteins Syntaxin 1 and Snap25 proteins (Söllner et al., 1993; Söllner et al., 1993). The formation of this ternary SNARE complex forms a link between the synaptic vesicle and plasma membrane that mediates exocytosis and neurotransmitter release (Weber et al., 1998). VAMP2 expression is essential for presynaptic neurotransmitter release (Schoch et al., 2001). Although VAMP2 expression was significantly reduced, it could be argued that the size of this change is not sufficient to cause a dysfunction. However, it is possible that small changes in protein expression can cause neurological disorders.

As it has been proved in animal models of VAMP2 dysfunction, VAMP2 is essential for fast neurotransmitter exocytosis and fast endocytosis which is important for synaptic vesicle recycling (Schoch et al., 2001; Deák et al., 2004). It is possible therefore that small changes in VAMP2 expression could cause a defect in neurotransmitter exocytosis and slower synaptic vesicle recycling, which could then cause behavioural deficits in *Zdhhc9* KO mice. It would be interesting to know if

heterozygous mice for Vamp2 show a deficit in synaptic vesicle recycling, as functional studies have only been conducted in Vamp2 KO neurons.

Some proteins whose palmitoylation was examined in this chapter, are known to be palmitoylated by other zDHHC enzymes. Csp can be palmitoylated by zDHHC3, -7, -15, and -17 (Greaves et al., 2008). Snap25 is palmitoylated by zDHHC-3, -7 and -17 (Lemonidis et al., 2014). Synaptotagmin 1 is palmitoylated by zDHHC17 (Huang et al., 2004). zDHHC-2, -3, -7 and -15 are PATs for PSD95 (Fukata et al., 2004). NR2b and GluR1/2 are palmitoylated by zDHHC3 (Hayashi et al., 2005, 2009). It is not yet known which specific enzymes palmitoylate VAMP1/2/3 and vGlut1/2.

After studying protein levels of H-Ras and N-Ras in membrane fractions from mouse brain homogenates, it was demonstrated that the association of those proteins with the membranes does not change in Zdhhc9 KO mice. This finding suggested that palmitoylation of H- and N-Ras is not disrupted in Zdhhc9 KO mice and this was confirmed by subsequent immunoblotting analysis of isolated Acyl-RAC fractions. This was a surprising observation as these proteins are thought to be major substrates of the zDHHC9 enzyme (Swarthout et al., 2005; Chai et al., 2013) and yet stable membrane association of these proteins is dependent on palmitoylation (Hancock et al., 1989).

Previous work has identified H-Ras and N-Ras as targets of zDHHC9 and this enzyme was shown to be a target of miR-134 in somatostatin interneurons (Chai et al., 2013). Interestingly, knockdown of zDHHC9 was shown to perturb membrane binding of H-Ras, implying zDHHC9-H-Ras is a functional enzyme-substrate pair. In contrast, other work has questioned the specific requirement of zDHHC9 for Ras palmitoylation (Rocks et al., 2010) suggesting that other enzymes can palmitoylate Ras and may compensate for the loss of zDHHC9.

However, it is possible that changes in palmitoylation of H- and N-Ras could be occurring in specific brain regions and that these effects were diluted out by the

analysis of whole brain samples. However as no change in palmitoylation was detected in the hippocampus, this suggests that the deficits observed in the hippocampal-dependent Morris water maze task are not linked to changes in Ras palmitoylation.

The hippocampus is an important brain region for spatial learning and memory, which is essential in order to perform the Morris water maze task (Logue et al., 1997). Palmitoylation of presynaptic and postsynaptic hippocampal proteins was specifically examined in this chapter but no changes were observed. It is likely that there are specific molecular changes occurring in the hippocampus of *Zdhhc9* KO mice and that additional work will be required to pinpoint the specific molecular deficits. Moreover, hippocampal volume was unaffected in KO mice suggesting that the behavioural deficits revealed in MWM are not caused by any gross anatomical changes in the hippocampus but instead they are likely to reflect molecular changes that affect its function. However, it is also possible that this brain region may not be responsible for the mild deficit in performance of *Zdhhc9* KO mice in this spatial learning and memory task. Although the hippocampus is central to performance in the Morris water maze, it is known that other brain regions contribute to successful completion of the task. Lesions in regions like striatum, basal forebrain, cerebellum and cerebral cortex have been shown to cause deficits in performance of Morris water maze (D'Hooge and De Deyn, 2001).

The corpus callosum could be an interesting brain region to study at the molecular level, given the fact that it has a reduced volume in *Zdhhc9* KO animals. The corpus callosum is the largest white matter tract in the mammalian brain (Luders et al., 2010), and is forming at E18.5 in mice. Thus, it will be interesting to determine when the defect in corpus callosum develops in *Zdhhc9* KO mice and what molecular changes might underlie its agenesis.

Proteomics is a useful approach in order to identify new substrates of enzymes or protein interactors as an unbiased strategy. After proteomic analysis of

palmitoylated proteins in WT and Zdhhc9 KO mouse brains, 300 proteins appeared as highly likely to be palmitoylated. 230 out of the 300 proteins had reduced palmitoylation such as VAMP1, VGLUT1, NR2b, GluR1, H-Ras, CCR5, Pde10a, Synaptophysin, Calnexin and Flottilin 2. Validation of proteomics is a step that not all studies include before publication of the results and was presented as a challenging step in this chapter. Among the 10 aforementioned proteins that were studied in order to be validated, significant changes in palmitoylation or protein expression were not confirmed by immunoblotting. It is interesting to note that validation was conducted on the same samples as proteomics was conducted, making it surprising to prove that the changes in palmitoylation detected by MS could not be detected by immunoblotting of the same samples.

MS is a sensitive technique that can probably detect small changes that cannot be detected by immunoblotting (Tuli & Ransom., 2009). However, immunoblotting is still a 'gold standard' technique for protein detection that cannot be omitted. A limitation of the current proteomic study is the small sample size (n=2KO, 2WT) that does not permit any statistical analysis in order to identify significant changes. Normally an n number of 3 is sufficient for analysis (Wan et al., 2013). Future work can include more samples. Moreover another possibility could be to perform different quantitative MS methods such as iTRAQ or spectral counting.

Palmitoyl-proteomics has also been conducted on zDHHc5 KO and zDHHc17 hypomorphic mice (Li et al., 2012; Wan et al., 2013). Using ABE/SILAM, a proteomic strategy that couples acyl-biotinyl exchange (ABE) purification of palmitoylated proteins to whole animal stable isotope labelling (SILAM) in zDHHc17 hypomorphic mice, biggest disease changes were noted for astrocytes and oligodendrocytes of mutant mice rather than for neuronal cells (Wan et al., 2013). The proteins that showed the largest reduction in palmitoylation were Flot1, Flot2 and Arhgap21 (36 % decrease for Flot1 and Flot2, 30 % decrease for Arhgap21) followed by Ank2, Add1 and Syn2 (22% , 19% and 18% decrease respectively). Moreover, a quantitative

proteomic analysis of stable isotope-labeled (SILAC) neuronal stem cell cultures from forebrains of DHHC5- gene-trapped mice using the palmitate analog 17-octadecynoic acid identified Flot2 as substrate of DHHC5 (Li et al., 2012). Although strong evidence for a steady-state pool of unacylated proteins in the DHHC5-GT cells was not found, the SILAC ratio (WT/GT) for Flot-2 was 3.06 making it a possible DHHC5 substrate. Validation experiments confirmed this possibility (Li et al., 2012). Palmitoylation and oligomerization of Flot2 was abolished in DHHC5-GT neuronal stem cells. The study also suggested that palmitoylation can be regulated through changes in palmitoyltransferase levels in response to differentiation signals.

Overall, our results indicate that a variety of important pre- and post-synaptic proteins including H- and N-Ras do not exhibit changes in expression or palmitoylation in *Zdhhc9* KO animals in either whole brain or hippocampus. Those results highlight the need to undertake further screening methods (e.g. MS approaches with improved quantification) to identify proteins with altered palmitoylation in *Zdhhc9* KO mice. The search for novel zDHHC9 substrates might also benefit from analysis of cell lines, for example, examining how knockdown or over-expression of zDHHC9 affects cellular palmitoylation profiles using approaches such as SILAC. These complementary approaches may circumvent issues such as secondary or compensatory changes that might occur in KO mice through development. Moreover, our results support the opinion for the effort of always validating omics approaches such as proteomics.

CHAPTER 6

6 Metabolomic investigation of the effect of *Zdhhc9* KO

6.1 Introduction

Generating a comprehensive characterisation of KO mice is challenging as it requires a broad array of different techniques and approaches. In this project, possible changes in *Zdhhc9* KO animals were investigated at the behavioural, neuroanatomical and molecular level. The results of previous chapters have shown that the *Zdhhc9* KO mice exhibit clear behavioural changes in tests of anxiety and also in the Morris Water Maze task. Furthermore, a significant change in corpus callosum volume was detected, consistent with that observed in patients with *ZDHHC9* mutations (Baker et al., 2015). However, the results of the previous chapter were not able to pinpoint important molecular changes that could account for the behavioural and anatomical changes present in the *Zdhhc9* KO mice.

Omics approaches such as transcriptomics and proteomics have gained the attention of researchers as untargeted methods during the past decades (Westerhoff and Palsson, 2004). These approaches are now widely used despite their challenges, which have been briefly discussed in the previous chapter regarding proteomics.

Metabolomics is a relatively newer omics approach (compared to proteomics and transcriptomics) and has been a valuable method in order to decipher metabolic pathways that are dysregulated in a variety of diseases such as cancer, cardiovascular disease and diabetes. Its clinical significance is being proved very important as it can give information about development of a complex disease, treatment and drug assessment (Dias and Koal, 2016).

In this chapter, a metabolomic approach was followed in order to identify metabolic pathways that might be dysregulated in *Zdhhc9* KO animals. In addition to identifying metabolic changes, this analysis has the potential to support the identification of protein-level changes by highlighting affected pathways and processes, which ultimately could explain the behavioural and neuroanatomical changes seen in the *Zdhhc9* KO mice. Moreover, integrated pathway analysis was used in order to combine results from metabolomics and transcriptomics.

6.2 Results

6.2.1 Metabolomics

Metabolomic analysis from urine of 3 KO and 3 WT adult male mice showed that 108 metabolites were elevated and 41 decreased in the KO animals compared to WT after applying the filter of $p < 0.05$. Pathway analysis was conducted for those molecules with the MetaboAnalyst. Two pathways had a $p < 0.05$, the pathways of tryptophan metabolism and of phenylalanine, tyrosine and tryptophan biosynthesis (Table 6.1). The pathways are based on KEGG database.

Table 6.1 Pathways that are potentially dysregulated in *Zdhhc9* KO mice based on metabolomic data analysis using MetaboAnalyst. Match status indicates the number of metabolites in our dataset that belong to this pathway divided by the number of total metabolites of the pathway. Pathways with a p value < 0.05 are highlighted by blue colour.

Pathway Name	Match Status	p value
Tryptophan metabolism	6/40	0.010
Phenylalanine, tyrosine and tryptophan biosynthesis	2/4	0.012

Glycerophospholipid metabolism	3/30	0.051
Vitamin B6 metabolism	2/9	0.065
Ubiquinone and other terpenoid-quinone biosynthesis	1/3	0.137
Arginine and proline metabolism	4/44	0.156
D-Glutamine and D-glutamate metabolism	1/5	0.218
Pentose phosphate pathway	2/19	0.230
Linoleic acid metabolism	1/6	0.255
Alanine, aspartate and glutamate metabolism	2/24	0.321
Taurine and hypotaurine metabolism	1/8	0.325
Ascorbate and aldarate metabolism	1/9	0.358
alpha-Linolenic acid metabolism	1/9	0.358
Nitrogen metabolism	1/9	0.358
Phenylalanine metabolism	1/11	0.418
Aminoacyl-tRNA biosynthesis	4/69	0.425
Glycine, serine and threonine metabolism	2/31	0.443
Caffeine metabolism	1/12	0.447
Glycosylphosphatidylinositol(GPI)-anchor biosynthesis	1/14	0.499
Arachidonic acid metabolism	2/36	0.523
Histidine metabolism	1/15	0.523
Pentose and glucuronate	1/16	0.546

interconversions		
Pyrimidine metabolism	2/41	0.595
Starch and sucrose metabolism	1/19	0.609
Tyrosine metabolism	2/44	0.634
Sphingolipid metabolism	1/21	0.646
Butanoate metabolism	1/22	0.663
Cysteine and methionine metabolism	1/27	0.738
Inositol phosphate metabolism	1/28	0.751
Purine metabolism	1/68	0.967

6.2.2 Integrated pathway analysis

Microarray data showed expression of 127 genes being downregulated and 239 upregulated in the KO mouse brain after filtering of p value <0.05 and fold change of >1.5 in upregulation/downregulation. Analysis of those data using g:Profiler did not show any pathways being significantly dysregulated in KO mouse brain in gene expression level.

After performing integrated pathway analysis including the metabolomic data, the top pathways that emerged are presented in Table 6.2 with ascending p value order for each MetaboAnalyst pathway.

Table 6.2 Pathways that are dysregulated in Zdhhc9 KO mice based on integrated metabolomic and transcriptomic data analysis using MetaboAnalyst. Pathways with a p value < 0.05 are highlighted by blue colour.

Pathway Name	Total molecules of the pathway	Hits in our dataset	p-value
Tryptophan metabolism	84	7	3.29E-04
Phenylalanine, tyrosine and tryptophan biosynthesis	12	2	0.015
Vitamin B6 metabolism	17	2	0.030
Taurine and hypotaurine metabolism	18	2	0.033
Aminoacyl-tRNA biosynthesis	91	4	0.058
Alanine, aspartate and glutamate metabolism	58	3	0.066
Ubiquinone and other terpenoid-quinone biosynthesis	5	1	0.078
Arginine and proline metabolism	102	4	0.082
Lysine biosynthesis	7	1	0.108
Ascorbate and aldarate metabolism	36	2	0.115
D-Glutamine and D-glutamate metabolism	8	1	0.123
Glycerophospholipid metabolism	119	4	0.125
Pentose phosphate pathway	49	2	0.189
Butanoate metabolism	50	2	0.195
Pentose and glucuronate interconversions	50	2	0.195
Linoleic acid metabolism	51	2	0.201

Glycosphingolipid biosynthesis - ganglio series	14	1	0.205
Glycosaminoglycan biosynthesis - chondroitin sulfate	14	1	0.205
Starch and sucrose metabolism	66	2	0.292

6.3 Discussion

From the metabolomics analysis, two main pathways emerged as significantly dysregulated in *Zdhhc9* KO mice: the pathways of tryptophan metabolism and of phenylalanine, tyrosine and tryptophan biosynthesis (Figure 6.1, Figure 6.2).

The pathway of tryptophan metabolism includes forty molecules and six of these were significantly changed in *Zdhhc9* KO urine samples compared with WT: L-Tryptophan, 5-Hydroxykynurenamine, L-Kynurenine, Formylanthranilic acid, Indoleacetic acid and 5-Hydroxyindoleacetic acid (Figure 6.1).

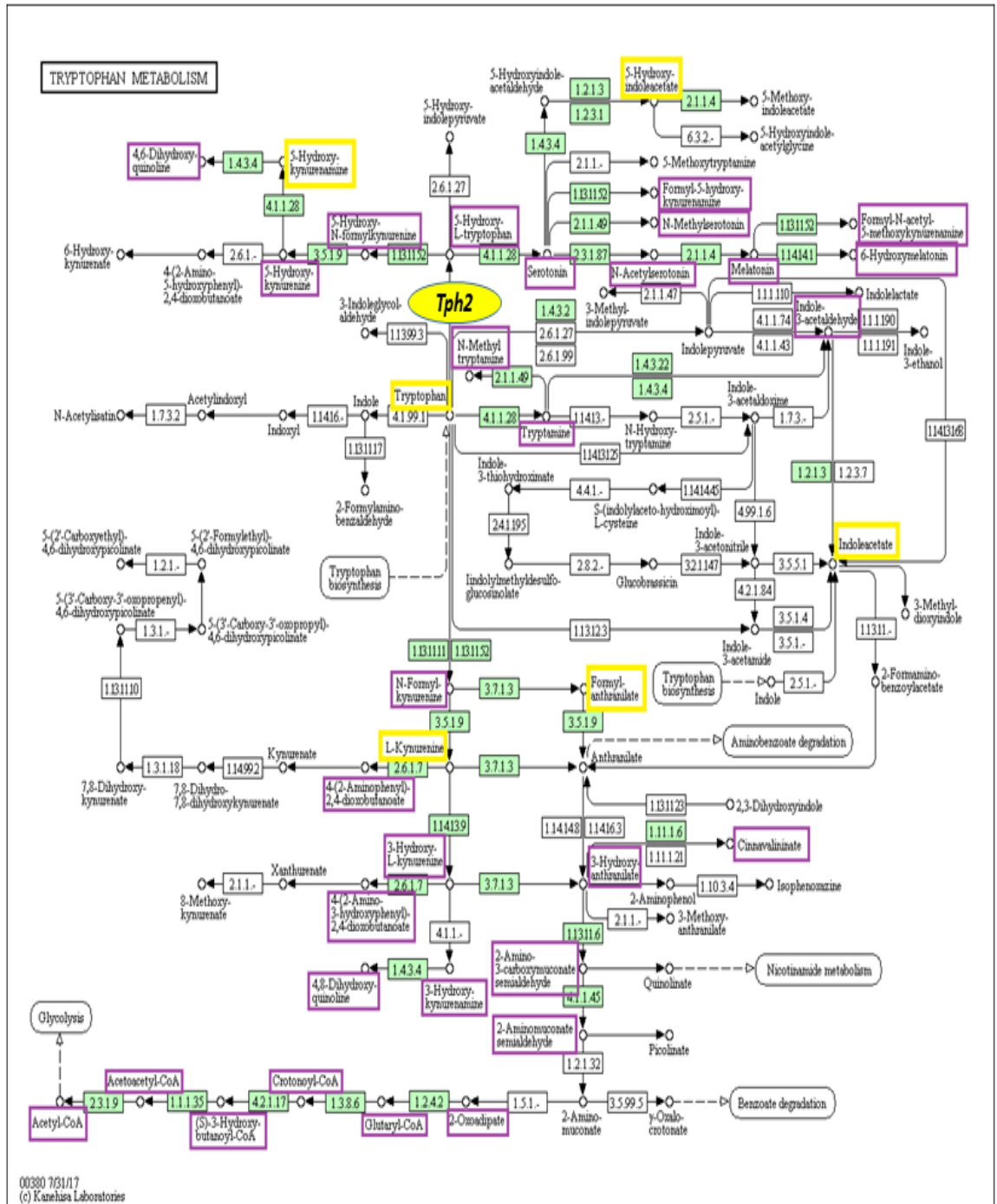


Figure 6.1 The pathway of tryptophan metabolism from KEGG pathway website. The diagram is modified in order to highlight metabolites contained in MetaboAnalyst database which are shown in purple rectangles. Metabolites included in MetaboAnalyst database and also detected as upregulated in urine of Zdhhc9 KO mice are shown in yellow rectangles.

Tph2 mRNA expression was upregulated in brain of Zdhhc9 KO mice and is shown in yellow circle.

L-tryptophan was elevated in urine of Zdhhc9 KO animals (3.68 KO vs WT). Tryptophan is an essential amino acid and precursor to the neurotransmitter serotonin and the hormone melatonin (Slominski et al., 2002). Tryptophanuria (elevated tryptophan in urine) is common in hypertryptophanemia, a metabolic disorder that results in an enormous increase of tryptophan in blood (Snedden et al., 1982). Moreover indoleacetic acid, which was also elevated in the Zdhhc9 KO mice has been reported to be increased in urine of patients with this disorder (Snedden et al., 1982). The patients also show speech abnormalities, perceptual hypersensitivity, mood swings, aggressive behaviour, optical strabismus and myopia (Snedden et al., 1982).

A study showed that urinary metabolites displaying the largest changes in young ASD (autism spectrum disorder) children compared to normal children belonged to the tryptophan and purine metabolic pathways (Gevi et al., 2016). Also, vitamin B6, phenylalanine-tyrosine-tryptophan biosynthesis and pyrimidine metabolism differed significantly in these children. Interestingly, these pathways show a trend for dysregulation in our dataset from Zdhhc9 KO mice, however their p value did not reach significance. In addition, the gut microbiome contributes to altered tryptophan metabolism, yielding increased levels of Indoleacetic acid in urine (Gevi et al., 2016). Interestingly, indoleacetic acid (Indole-3-acetate) was elevated in the Zdhhc9 KO animals (2.85 KO vs WT). Recently, changes in gut microbiome have been proved to alter brain development and neurological function, and they can even lead to mental illness (Rogers et al., 2016).

Another metabolite of the same pathway that was elevated in the Zdhhc9 KO dataset is 5-Hydroxyindoleacetic acid (5-HIAA) (3.65 KO vs WT). It has previously

been shown that urinary 5-HIAA was significantly greater in hyperserotonemic autistic subjects compared to normal controls, revealing a link between hyperserotonemia, autism and this metabolite (Minderaa et al, 1987).

In addition, L-Kynurenine (3.37 KO vs WT) is a central compound of the pathway of tryptophan metabolism as it can change to the neuroprotective agent kynurenic acid or to the neurotoxic agent quinolinic acid. Cognitive deficits in schizophrenia are associated with imbalances in the enzymes that break down kynurenine (Wonodi et al., 2011). The kynurenine pathway is also upregulated in Alzheimer's disease based on an immunohistochemical study (Guillemin et al., 2005).

The pathway of phenylalanine, tyrosine and tryptophan biosynthesis includes four molecules, two of which were highlighted in the *Zdhhc9* KO dataset: Phenylpyruvic acid and 4-Hydroxyphenylpyruvic acid (Figure 6.2).

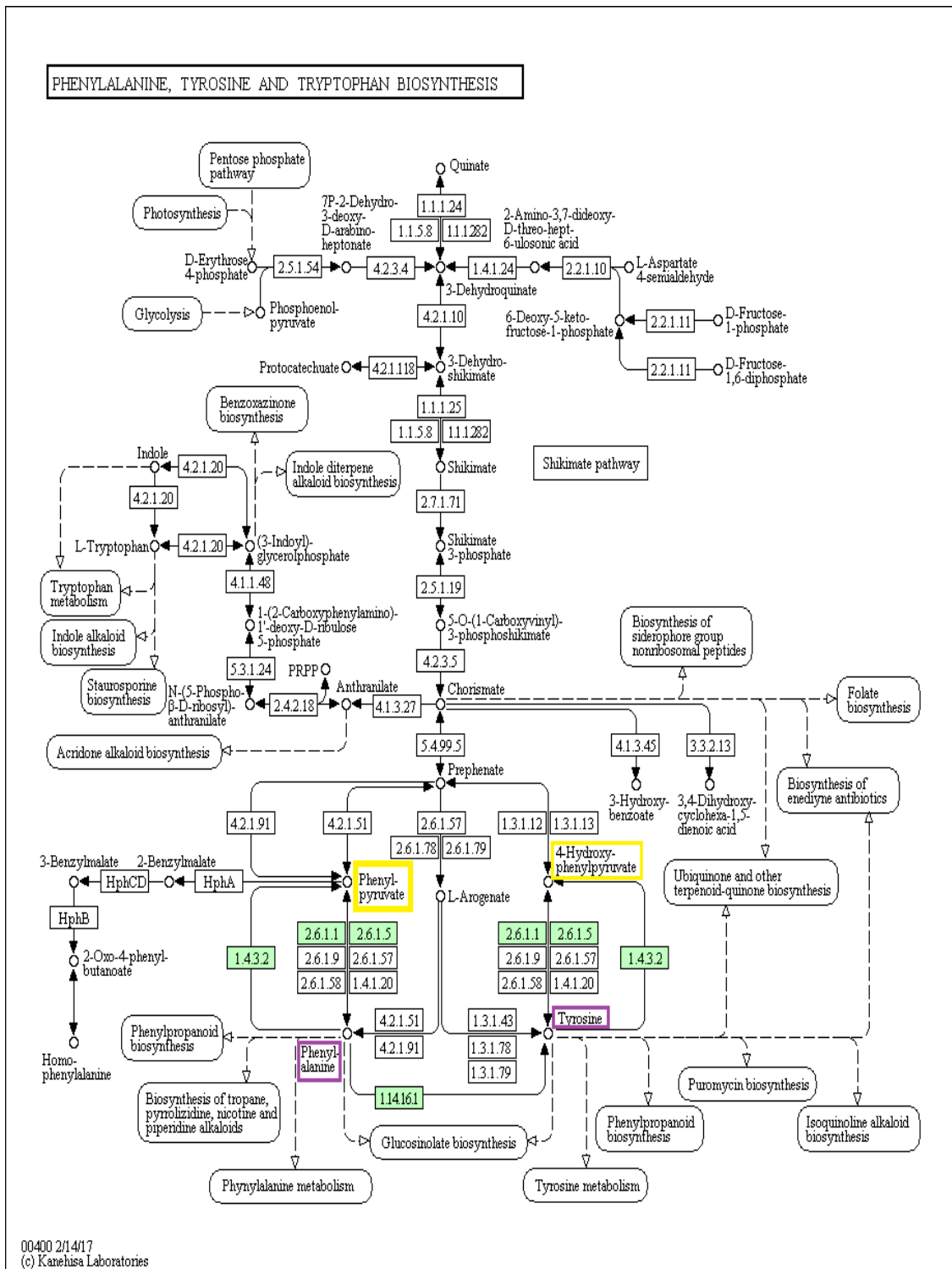


Figure 6.2 The pathway of phenylalanine, tyrosine and tryptophan biosynthesis from KEGG pathway website. The diagram is modified in order to highlight metabolites contained in MetaboAnalyst database which are shown in purple rectangles. Metabolites

included in MetaboAnalyst database and also detected as upregulated in urine of *Zdhhc9* KO mice are shown in yellow rectangles.

Phenylpyruvic acid (5.52 KO vs WT) was highly increased in *Zdhhc9* KO mice. Phenylketonuria (PKU) is a genetic disorder characterised by urinary excretion of phenylpyruvic acid (Meister, 1958) and is caused by decreased metabolism of the amino acid phenylalanine (Goldstein, 1961). Untreated PKU can lead to intellectual disability, seizures and behavioural problems (Yu, 1970).

4-Hydroxyphenylpyruvic acid (4-hydroxyphenylpyruvate) was also elevated in *Zdhhc9* KO mice (2.89 KO vs WT). Patients with PKU also show excretion of this acid in urine (Chalmers & Watts, 1974). In addition, Tyrosinemia Type 3 is a disorder caused by deficiency in the activity of 4-hydroxyphenylpyruvate dioxygenase (HPD) and is characterized by elevated blood tyrosine and urine excretion of its derivatives such as 4-hydroxyphenylpyruvate (Tomoeda et al., 2000). Patients with this disorder show mild ID and/or convulsions (Tomoeda et al., 2000).

The integrated pathway analysis showed that significantly dysregulated pathways were the pathways of tryptophan metabolism and of phenylalanine, tyrosine and tryptophan biosynthesis, which were also present in the non-integrated pathway analysis.

Apart from the six metabolites that were dysregulated in the tryptophan metabolism pathway, transcriptomic analysis showed that *Tph2* (tryptophan hydroxylase 2) gene expression was also upregulated 1.75 fold in the KO mouse brain and is involved in this pathway. The encoded protein catalyses the first and rate limiting step in the biosynthesis of serotonin (Richard et al., 2009). More specifically, brain tryptophan is converted to 5-hydroxytryptophan by tryptophan hydroxylase and then 5-hydroxytryptophan is converted to serotonin by tryptophan decarboxylase (Richard et al., 2009).

Mutations in *Tph2* that cause loss of function or reduced function of the enzyme, are associated with Attention Deficit Hyperactivity Disorder and major depression, while SNPs have been associated to bipolar disorder (Zhang et al., 2005; Cichon et al., 2008; McKinney et al., 2008). Mice with reduced function of *Tph2* show increased anxiety-like behaviour (Osipova et al., 2009), fact that could explain why the *Zdhhc9* KO mice have reduced anxiety; because of elevated *Tph2*.

On the other side, elevated levels of *Tph2* mRNA has been found in raphe nuclei of depressed suicides as a homeostatic mechanism to elevate abnormally low serotonin levels (Bach-Mizrachi et al., 2008).

The taurine and hypotaurine metabolism did not emerge as significantly dysregulated in the non-integrated pathway analysis ($p=0.326$). However, it emerged from the integrated pathway analysis (Figure 6.3). In this pathway, *Gad1* (Glutamate Decarboxylase 1) expression was 1.56 fold upregulated in *Zdhhc9* KO mouse brain. *Gad1* catalyses the conversion of glutamic acid to gamma-aminobutyric acid (GABA), the major inhibitory neurotransmitter in the vertebral central nervous system (Dirkx et al., 1995).

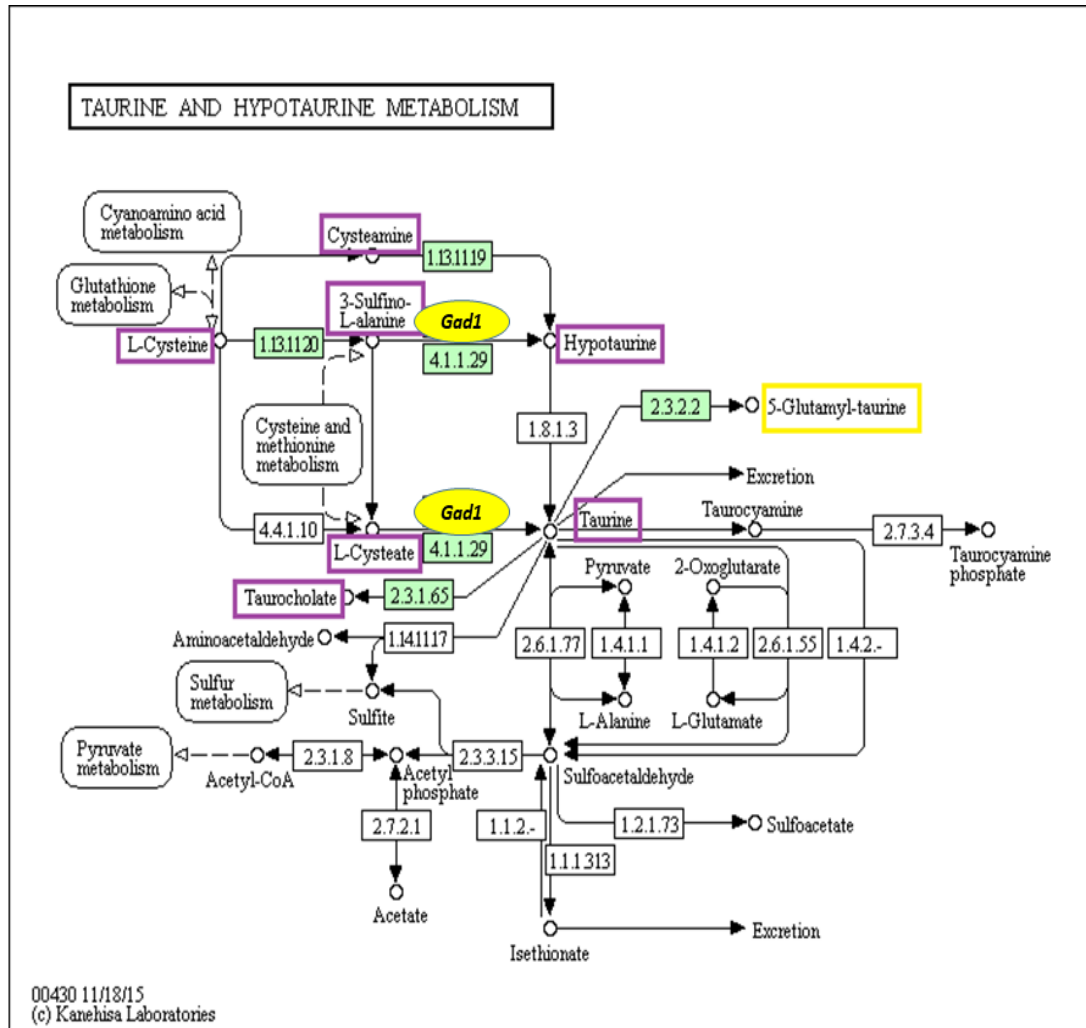


Figure 6.3 The pathway of taurine and hypotaaurine metabolism from KEGG pathway website. The diagram is modified in order to highlight metabolites contained in MetaboAnalyst database which are shown in purple rectangles. The metabolite 5-Glutamyl-taurine which is included in MetaboAnalyst database and also detected as upregulated in urine of *Zdhc9* KO mice is shown in yellow rectangle. *Gad1* mRNA expression was upregulated in brain of *Zdhc9* KO mice and is shown in yellow circle.

A mutation in *GAD1* causes Spastic Quadriplegic Cerebral Palsy 1 (Lynex et al., 2004). Patients show moderate to severe ID and spasticity including hypertonicity and hyperreflexia (Mitchell & Bunday, 1997; McHale et al., 1999). When *GAD1*

expression is upregulated, it facilitates metastasis outgrowth in brain cancer (Schnepp et al., 2017).

5-Glutamyl-aurine which is involved in the same pathway was upregulated in *Zdhhc9* KO mice (2.88 KO vs WT). This molecule was shown to reduce aversion or phobia and/or anxiety of rats and moreover it has anti-epileptic effect (Bittner et al., 2005).

Collectively, the results of the metabolomics and transcriptomics analyses reveal interesting changes that could be relevant to the neurological impairments in *Zdhhc9* KO mice and humans with *ZDHC9* mutations. It will be interesting to examine if similar changes are seen in *ZDHC9* patients. Future work should initially seek to examine changes in a larger cohort of WT and KO mice and examine urine from mice taken at different ages.

CHAPTER 7

7 General Discussion

Despite *ZDHHC9* mutations being associated with ID, epilepsy, and speech and attention deficits, to-date there has not been any detailed examination of the effects of *Zdhhc9* mutations in a genetic mouse model. In this study, we report the first behavioural characterization of a *Zdhhc9* mutant mouse line. Generation of appropriate mouse models is important to understand how neurological disorders develop and the associated underlying molecular and cellular deficits. Several deficits were uncovered in the *Zdhhc9* mutant line, which are broadly consistent with either phenotypes of humans with *ZDHHC9* mutations or phenotypes reported for other mouse models with mutations in ID genes. Collectively, these data suggest that this mutant mouse line may provide a good model system to dissect the underlying neurodevelopmental changes that lead to ID and other impairments in humans with disruptive *ZDHHC9* mutations. Although *ZDHHC9* mutations are rare, the consistent neurological impairments caused by these mutations may allow easier identification of causative molecular and cellular changes, in contrast to ID caused by more complex genetic processes.

The results of this thesis showed that *Zdhhc9* male KO mice are born at lower numbers than WT male littermates suggesting a semi-lethal phenotype is caused by disruption of *Zdhhc9*. This suggests that *Zdhhc9* may be important for embryonic development but not crucial, and implies that development of mutant embryos may be susceptible to failure. Nevertheless, the male KO mice that do survive are fertile and do not show any gross physical abnormalities.

End-point and quantitative PCR analysis confirmed that the first coding exon of *Zdhhc9* is deleted in the mutant mice. However, a shorter transcript was detected in KO mouse brain in statistically lower numbers to the WT transcript suggesting that a

shorter zDHHC9 protein construct could be produced. Analysis of an HA-tagged form of this shorter zDHHC9 protein showed that it was mis-localised at the subcellular level, mainly present on ER membranes rather than Golgi. This raises questions about whether this truncated protein could functionally replace WT zDHHC9 even if it was expressed. It will be useful to test whether this truncated protein is functional by studying palmitoylation of H-/N-Ras *in vitro* and if it still interacts with GPC16, an important co-factor of zDHHC9. Following completion of the work in this thesis, a zDHHC9 antibody was identified that successfully recognised the protein in cell lysates. Immunoblotting of brain samples from WT and KO mice demonstrated that the zDHHC9 protein was eliminated in KO brain and also showed that there was no noticeable expression of a truncated protein in KO mice.

This thesis also included the first thorough behavioural characterization of *Zdhhc9* KO mice covering important aspects such as motor coordination and balance, locomotor activity and anxiety, sensorimotor gating, anhedonia, sociability and social novelty, learning and memory and visuospatial attention. Some notable differences were identified between KO and WT mice. *Zdhhc9* KO mice show enhanced visual placing reflex but lower grip strength, reduced anxiety levels, impaired thigmotaxis and reduced startle reactivity. Moreover, they show impaired acquisition of spatial learning and spatial reversal learning. As regards visuospatial attention, they work harder completing more trials than the WT animals while achieving similar percentage of correct responses. They also have shorter correct reaction time and show hyperactivity in the final part of the visuospatial attention task. Many of the identified behavioural changes have also been reported in other well-characterised murine models of ID such as Down syndrome, Fragile X syndrome and Rett syndrome (Peier et al., 2000; Altafaj et al., 2001; Nielsen et al., 2002; Zang et al., 2009).

Zdhhc9 KO mice were also found to exhibit shrinkage of corpus callosum which is the largest white matter tract in the human brain and connects the two cerebral hemispheres (Luders et al. 2010). Volumetric reduction of this area could be explained by reduced white matter in the KO mouse brain. Diffusion tensor imaging would be interesting to further investigate this hypothesis. It would also be interesting to follow development of the corpus callosum in Zdhhc9 KO mice to determine the molecular/cellular basis of this defect. MRI volumetric analysis of the corpus callosum at a range of developmental ages starting from E18.5 (when the corpus callosum is forming) would allow the temporal nature of this defect to be studied. Further analysis could examine if there is a deficit in the growth of callosal neurons or if there is ongoing neuronal death/apoptosis in this area. Apart from that, it would be interesting to test if ZDHC9 expression is particularly important in other brain regions such as the hippocampus even though its volume was not affected in KO animals. Producing and testing conditional knock out animals specifically for hippocampus or other brain regions could prove if the expression of the gene is important for these specific brain regions.

Changes in dendritic spines can be a cause of ID as changes in spine number or morphology in the hippocampus has been reported in other ID mouse models (Kooy, 2003; Iwase et al., 2016). Therefore, it would be important to study the dendritic spine morphology in isolated neurons or brain slices from the Zdhhc9 KO mice. For example, *IL1RAPL1* (IL-1 receptor accessory protein-like 1) KO mice have impaired spatial reference and working memories and decreased spine density (Yasumura et al., 2014). Thus, changes in hippocampal-dependent function can be linked to changes in neuronal connectivity.

Overall, the KO mice recapitulate characteristics noted in humans with *ZDHC9* mutations such as hypotonia and shrinkage of corpus callosum. Another consistent finding in patients with *ZDHC9* mutations is focal seizures similar to Rolandic Epilepsy (Baker et al., 2015), and therefore it will be valuable to test by

electrophysiology if epileptic activity is present in KO mouse brain, for example by analysis of electroencephalogram (EEG) recordings. Apart from that, with electrophysiological approaches we could test LTP to identify post-synaptic dysfunctions or paired pulse facilitation (PPF) for pre-synaptic alterations. Furthermore, it will be interesting to examine further attention in *Zdhhc9* KO mice. Although KO mice were able to identify correct stimuli in the 5-choice serial reaction time trial, it will be interesting to examine further their inhibitory control. This could be examined by including specific “no-go” trials to which the mouse must inhibit a response as in the 5-choice continuous performance task (Young et al., 2009). Another aspect of the human phenotype that merits attention is the speech defect. As a starting point, tongue movements of the *Zdhhc9* KO mice could be examined using a lickometer to identify any deficits that might correlate with speech issues in humans. The *Zdhhc9* KO mouse model can serve as a valuable model of the human condition. Moreover, in order to eliminate the use of animals, a cellular model could be developed for the zDHHC9 dysfunction using either mouse embryonic fibroblasts (MEFs) of KO mice or induced pluripotent stem cells from patients with *ZDHC9* mutations.

Zdhhc9 KO mice do not show any significant changes in protein expression or palmitoylation of major pre- and postsynaptic proteins studied with the exception of VAMP2 whose expression was very modestly (but significantly) decreased in KO brain homogenates. Surprisingly, H- and N-Ras do not exhibit changes in expression or palmitoylation in either whole brain or hippocampus of KO animals, urging the need to identify novel zDHHC9 substrates and/or novel zDHHC9 functions. The observed behavioural and anatomical deficits in *Zdhhc9* KO mice are likely linked to palmitoylation dysfunction based on the fact that human mutations in this gene cause ID but we should always keep in mind the fact that this enzyme may also exert other functions. Knock-in technology in mice where the sequence encoding the DHHC motif is mutated to instead encode DHHA in the *Zdhhc9* gene could prove if the reported changes are due to dysfunction in palmitoylation. The knock-in mice

could be tested in similar tasks to the *Zdhhc9* KO mice and if the results are similar, we could conclude that disrupted palmitoylation is the cause of the behavioural deficits. Comparison of the isolated palmitoylomes from WT and *Zdhhc9* KO mice identified a number of marked changes; however immunoblotting of the same samples failed to validate any of these changes. In addition, my results show the importance of always validating proteomic approaches. It will be important to investigate the substrates of zDHHC9 in further detail using more quantitative methods and higher n numbers. For example, it might be beneficial to generate embryonic fibroblasts (MEFs) from the *Zdhhc9* KO mice and WT mice and apply techniques such as SILAC labelling to increase the quantitative power of the MS-based substrate identification.

In *Zdhhc9* KO neurons, it would be interesting to study proteins, dysfunction in which has been implicated in ID. Mutations in genes that encode for presynaptic proteins, cause ID by disrupting important presynaptic processes such as presynaptic vesicle recycling (Vaillend et al., 2008). Among them, mutations in *GD1* gene cause non-syndromic XLID. This gene encodes for $\text{GDI}\alpha$, a protein that regulates the sequestration of GDP-bound forms of Rab proteins after their exit from empty vesicles (Ishizaki et al., 2000). In mice, loss of $\text{GDI}\alpha$ disrupts the distribution of proteins Rab4-5 and causes enhanced short-term plasticity and impaired short-term memory (Ishizaki et al., 2000; D'Adamo et al., 2002). The IL1 receptor accessory protein like (IL1RAPL), which is also implicated in non-syndromic XLID, inhibits calcium-dependent exocytosis and neurotransmitter release, probably via its interaction with neuronal calcium sensor-1 (NCS-1), a protein associated to hippocampal LTP and associative learning in *C. elegans* (Genin et al., 2001; Gomez et al., 2001). Rab3 GAP, which is mutated in the Warburg Micro syndrome characterized by abnormal brain development and severe ID, limits the amount of GTP-bound Rab3A (Aligianis et al., 2005). Mutations in the gene that encodes the protein in mice cause inhibition of glutamate release and altered short-term plasticity (Sakane et al., 2006). Genetic loss of ID pre-synaptic proteins is associated

with changes in presynaptic function, such as enhanced paired-pulse facilitation (PPF) and short-term synaptic plasticity (STP), while LTP is unaltered. Disruption of ID genes, oligophrenin 1 (OPHN1) and LIM kinase 1 (LIMK1), which have established postsynaptic function but are also detected pre-synaptically, have also been associated with altered pre-synaptic mechanisms such as PPF or synaptic depression (Meng et al., 2002; Govak et al., 2004; Khelifaoui et al., 2007). However, we should note that we do not know if zDHHC9 is more important for palmitoylation of pre- or post- synaptic proteins therefore both protein groups should be examined. It would be interesting to study surface levels of GluR and NMDA receptors and their presences in dendritic spines versus shafts.

The search for novel zDHHC9 substrates might also benefit from analysis of cell lines, for example, examining how knockdown or over-expression of zDHHC9 affects cellular palmitoylation profiles. These complementary approaches may circumvent issues such as secondary or compensatory changes that might occur in KO mice through development. Studying WT neurons where *Zdhhc9* is knocked out by siRNA would be a valuable tool to delineate those issues. In addition to measuring palmitoylation as a way of identifying zDHHC9 substrates, it may also be useful to apply protein interaction studies, such as co-immunoprecipitation, pull-down experiments with recombinant proteins or more recent methodologies such as Bio-ID.

This study also included the first metabolomic analysis of *Zdhhc9* KO mice showing some common dysregulated metabolites between the KO mice and a well-known cause of ID, Phenylketonuria (PKU). PKU is a genetic disorder characterised by urinary excretion of phenylpyruvic acid (Meister, 1958) and 4-Hydroxyphenylpyruvic acid (Chalmers & Watts, 1974). Untreated PKU can lead to intellectual disability, seizures and behavioural problems (Yu, 1970). Two main pathways emerged as significantly dysregulated in KO mice: the pathway of tryptophan metabolism and of phenylalanine, tyrosine and tryptophan biosynthesis

with Phenylpyruvic and 4-Hydroxyphenylpyruvic acid being highly increased in *Zdhhc9* KO mice. It would be useful to test if humans with *ZDHHC9* mutations show excretion of those metabolites in urine. Metabolic profiling of this mouse model can add to our knowledge of studying biomarkers of ID, a field that not much research has been conducted on. Moreover, it would be important to follow-up the metabolomic work conducted in this thesis and as a first step by increasing the number of samples analysed. Apart from that, examining a range of developmental ages would be useful in order to test if metabolic changes correlate in time with corpus callosum changes.

Overall, this study provides useful information for the study of ID, highlights a key role for *ZDHHC9* in brain development and behaviour, and supports the utility of the *Zdhhc9* mutant mouse line to investigate molecular and cellular changes linked to ID and other deficits in the human population.

CHAPTER 8

8 References

Abdul Rahman, N. Z. et al. (2016) 'Mitogen-Activated Protein Kinase Phosphatase-2 Deletion Impairs Synaptic Plasticity and Hippocampal-Dependent Memory', *The Journal of Neuroscience*, 36(8), pp. 2348–54. doi: 10.1523/JNEUROSCI.3825-15.2016.

Abel, T. and Lattal, K. M. (2001) 'Molecular mechanisms of memory acquisition, consolidation and retrieval', *Current Opinion in Neurobiology*, 11(2), pp. 180–187. doi: 10.1016/S0959-4388(00)00194-X.

Adachi, N. et al. (2016) 'S-palmitoylation of a Novel Site in the β 2 -adrenergic Receptor Associated with a Novel Intracellular Itinerary', *Journal of Biological Chemistry*, 291(38), pp. 20232-46. doi: 10.1074/jbc.M116.725762.

Ahearn, I.M. et al. (2011) FKBP12 binds to acylated H-ras and promotes depalmitoylation, *Molecular Cell*, 41(2), pp. 173–185.

Alexander, A. L. et al. (2007) 'Diffusion Tensor Imaging of the Brain', *Neurotherapeutics*, 4(3), pp. 316–329. doi: 10.1016/j.nurt.2007.05.011.

Ali, A. M. et al. (2016) 'Metabolomic Profiling of Submaximal Exercise at a Standardised Relative Intensity in Healthy Adults', *Metabolites*, 6(1), pii: E9. doi: 10.3390/metabo6010009.

Aligianis, I. A., et al. (2005) Mutations of the catalytic subunit of RAB3GAP cause Warburg Micro syndrome, *Nature Genetics*, 37(3), pp. 221-223.

Altafaj, X. et al. (2001) 'Neurodevelopmental delay, motor abnormalities and cognitive deficits in transgenic mice overexpressing Dyrk1A (minibrain), a murine model of Down's

syndrome', *Human Molecular Genetics*, 10(18), pp. 1915–1923. doi: 10.1093/hmg/10.18.1915.

Anami, K, et al. (2010) Search for transmembrane protein in gastric cancer by the Escherichia coli ampicillin secretion trap: expression of DSC2 in gastric cancer with intestinal phenotype, *The Journal of Pathology*, 221(3), pp. 275–284.

Apolloni, A. et al. (2000) 'H-ras but not K-ras traffics to the plasma membrane through the exocytic pathway', *Molecular and cellular biology*, 20(7), pp. 2475–2487. doi: 10.1128/MCB.20.7.2475-2487.2000.

Bach-Mizrachi, H. et al. (2008) 'Elevated expression of tryptophan hydroxylase-2 mRNA at the neuronal level in the dorsal and median raphe nuclei of depressed suicides', *Molecular Psychiatry*, 13(5), pp. 507–513. doi: 10.1038/sj.mp.4002143.

Baker, K. et al. (2015) 'Epilepsy, cognitive deficits and neuroanatomy in males with ZDHHC9 mutations', *Annals of Clinical and Translational Neurology*, 2(5), pp. 559-69. doi: 10.1002/acn3.196.

Bakker, C. et al. (1994) 'Fmr1 Knockout Mice: A Model to Study Fragile X Mental Retardation', *Cell*, 78(1), pp. 23–33. doi: 10.1016/0092-8674(94)90569-X.

Bakker, C.E., et al. (1994) Fmr1 knockout mice: a model to study fragile X mental retardation. The Dutch-Belgian Fragile X Consortium, *Cell*; 78(1), pp. 23–33.

Bakker, C.E., Oostra BA. (2003) Understanding fragile X syndrome: insights from animal models, *Cytogenetics and Genome Research*, 100(1-4), pp. 111–23, doi: 10.1159/000072845.

Bakker, M. J. et al. (2009) 'Increased whole-body auditory startle reflex and autonomic reactivity in children with anxiety disorders', *Journal of Psychiatry and Neuroscience*, 34(4), pp. 314–322.

Banerjee, S., Neveu, P., Kosik, K.S. (2009) A coordinated local translational control point at the synapse involving relief from silencing and MOV10 degradation, *Neuron*, 64(6), pp. 871–884.

Barria, A., et al. (1997) Regulatory phosphorylation of AMPA-type glutamate receptors by CaM-KII during long-term potentiation, *Science*, 276(5321), pp. 2042–2045.

Bast, T., Zhang, W. N. and Feldon, J. (2001) ‘Hippocampus and classical fear conditioning’, *Hippocampus*, 11(6), pp. 828–831. doi: 10.1002/hipo.1098.

Baum, M. L. (2016) ‘The Neuroethics of Biomarkers: What the Development of Bioprediction Means for Moral Responsibility, Justice, and the Nature of Mental Disorder’, *Oxford Series in Neuroscience, Law, and Philosophy*, 6(38), pp. 45–66.

Bayés, À. et al. (2011) ‘Characterisation of the proteome, diseases and evolution of the human postsynaptic density’, *Nature Neuroscience*, 14(1), pp. 19–21. doi: 10.1038/nn.2719.Characterisation.

Belichenko, N.P., et al. (2009) The “Down Syndrome Critical Region” Is Sufficient in the Mouse Model to Confer Behavioural, Neurophysiological, and Synaptic Phenotypes Characteristic of Down Syndrome, *Journal of Neuroscience*, 29(18), pp. 5938–48, doi: 10.1523/JNEUROSCI.1547-09.2009.

Belichenko, P.V., et al. (2007) Synaptic and cognitive abnormalities in mouse models of Down syndrome: exploring genotype-phenotype relationships, *Journal of Comparative Neurology*, 504(4), pp. 329–45, doi: 10.1002/cne.21433.

Bennett, M. K. et al. (1993) ‘The syntaxin family of vesicular transport receptors’, *Cell*, 74(5), pp. 863–873. doi: 10.1016/0092-8674(93)90466-4.

Berger-Sweeney, J. (2003), Using mice to model cognitive deficits in neurologic disorders: narrowing in on Rett syndrome, *Current Neurology and Neuroscience Reports*, 3(3), pp. 185-7.

Bernardet, M. and Crusio, W. E. (2006) ‘Fmr1 KO Mice as a Possible Model of Autistic Features’, *The Scientific World Journal*, 6(1), pp. 1164–1176. doi: 10.1100/tsw.2006.220.

Bhattacharya, S. et al. (2002) ‘Members of the synaptobrevin/vesicle-associated membrane protein (VAMP) family in *Drosophila* are functionally interchangeable in vivo for neurotransmitter release and cell viability’, *Proceedings of the National Academy of*

Sciences of the United States of America, 99(21), pp. 13867–13872. doi: 10.1073/pnas.202335999.

Biennu, T, et al. (1998) Non-specific X-linked semidominant mental retardation by mutations in a Rab, GDP-dissociation inhibitor, *Human Molecular Genetics*, 7(8), pp. 1311–5.

Birkenkamp-Demtroder, K, et al. (2002) Gene expression in colorectal cancer, *Cancer Research* 62(15), pp. 4352–4363.

Bittner, S., Win, T. and Gupta, R. (2005) 'γ-L-glutamyltaurine', *Amino Acids*, 28(4), pp. 343–356. doi: 10.1007/s00726-005-0196-7.

Blanc, M, et al. (2015) SwissPalm: Protein Palmitoylation database, *F1000Res*, 4:261. doi: 10.12688/f1000research.6464.1. eCollection 2015.

Boone, P. M. et al. (2010) 'Detection of clinically relevant exonic copy-number changes by array CGH', *Human Mutation*, 31(12), pp. 1326–1342. doi: 10.1002/humu.21360.

Bosmans, F., Milescu, M. and Swartz, K. J. (2011) 'Palmitoylation influences the function and pharmacology of sodium channels', *Proceedings of the National Academy of Sciences*, 108(50), pp. 20213–20218. doi: 10.1073/pnas.1108497108.

Bula, C.M. et al. (2005) Presence of a truncated form of the vitamin D receptor (VDR) in a strain of VDR-knockout mice, *Endocrinology*, 146(12), pp. 5581-6.

Branchi, I. et al. (2003) 'Animal models of mental retardation: From gene to cognitive function', *Neuroscience and Biobehavioral Reviews*, 27(1–2), pp. 141–153. doi: 10.1016/S0149-7634(03)00016-2.

Brigidi, G. S et al. (2014) Palmitoylation of δ-catenin by DHHC5 Mediates Activity-Induced Synapse Plasticity, *Nature Neuroscience*, 17(4), pp. 522–532. doi: 10.1038/nn.3657.

Brown, T. C. et al. (2005) NMDA receptor-dependent activation of the small GTPase Rab5 drives the removal of synaptic AMPA receptors during hippocampal LTD, *Neuron*, 45(1), pp. 81–94.

Bussey, T. J. et al. (2008) 'The touchscreen cognitive testing method for rodents: how to get the best out of your rat', *Learning & memory* (Cold Spring Harbor, N.Y.), 15(7), pp. 516–523. doi: 10.1101/lm.987808.

Bustos, F. J. et al. (2014) 'PSD95 suppresses dendritic arbor development in mature hippocampal neurons by occluding the clustering of NR2B-NMDA receptors', *PLoS ONE*, 9(4), doi: 10.1371/journal.pone.0094037.

Camp, L.A. et al. (1994) Molecular cloning and expression of palmitoyl-protein thioesterase, *Journal of Biological Chemistry*, 269(37), pp. 23212-9.

Campbell, S.L. et al. (1998) 'Increasing complexity of the Ras signaling', *Oncogene*, 17(11 Reviews), pp. 1395-413. doi: 10.1074/jbc.273.32.19925.

Canfield, M.A. et al. (2006) National estimates and race/ethnic-specific variation of selected birth defects in the United States, *Birth Defects Research Part A: Clinical and Molecular Teratology*, 76(11), pp. 747-56.

Casey, P. J. et al. (1989) 'P21Ras Is Modified By a Farnesyl Isoprenoid.', *Proceedings of the National Academy of Sciences of the United States of America*, 86(21), pp. 8323–8327. doi: 10.1073/pnas.86.21.8323.

Centerwall, S.A., Centerwall, W.R. (2000) The discovery of phenylketonuria: the story of a young couple, two retarded children, and a scientist, *Paediatrics*, 105(1 Pt 1), pp. 89-103.

Chai, S. et al. (2013) 'MicroRNA-134 activity in somatostatin interneurons regulates H-Ras localization by repressing the palmitoylation enzyme, DHHC9', *Proceedings of the National Academy of Sciences of the United States of America*, 110(44), pp. 17898-903. doi: 10.1073/pnas.1317528110/-
/DCSupplemental.www.pnas.org/cgi/doi/10.1073/pnas.1317528110.

Chalmers, R.A., Watts, R.W. (1974) Quantitative studies on the urinary excretion of unconjugated aromatic acids in phenylketonuria, *Clinica Chimica Acta*, 55(3), pp. 281-94.

- Chamberlain, L. H. and Burgoyne, R. D. (1996) 'Identification of a novel cysteine string protein variant and expression of cysteine string proteins in non-neuronal cells', *Journal of Biological Chemistry*, 271(13), pp. 7320–7323. doi: 10.1074/jbc.271.13.7320.
- Chamberlain, L. H. and Shipston, M. J. (2015) 'The Physiology of Protein S-acylation', *Physiological Reviews*, 95(2), pp. 341–376. doi: 10.1152/physrev.00032.2014.
- Chan, A. W. et al. (2007) 'Resistance of presynaptic CaV2.2 channels to voltage-dependent inactivation: Dynamic palmitoylation and voltage sensitivity', *Cell Calcium*, 42(4–5), pp. 419–425. doi: 10.1016/j.ceca.2007.04.009.
- Chandran, J. S. et al. (2017) 'Site Specific Modification of Adeno-Associated Virus Enables Both Fluorescent Imaging of Viral Particles and Characterization of the Capsid Interactome', *Scientific Reports*, 7(1), pp. 1–17. doi: 10.1038/s41598-017-15255-2.
- Chapman, E. R. et al. (1996) 'Fatty Acylation of Synaptotagmin in PC12 Cells and Synaptosomes', *Biochemical and Biophysical Research Communications*, 225(1), pp. 326–32.
- Chaudhry, A. et al. (2015) 'Phenotypic spectrum associated with PTCHD1 deletions and truncating mutations includes intellectual disability and autism spectrum disorder', *Clinical Genetics*, 88(3), pp. 224–233. doi: 10.1111/cge.12482.
- Chelly, J. (1999) Breakthroughs in molecular and cellular mechanisms underlying X-linked mental retardation. *Human Molecular Genetics*, 8(10), pp. 1833–8.
- Chen, R.Z. et al. (2001) Deficiency of methyl-CpG binding protein-2 in CNS neurons results in a Rett-like phenotype in mice, *Nature Genetics*, 27(3), pp. 327–31.
- Chien, A. J. et al. (1996) 'Identification of palmitoylation sites within the L-type calcium channel beta2a subunit and effects on channel function', *The Journal of biological chemistry*, 271(43), pp. 26465–26468.
- Chung, H. J. et al. (2000) Phosphorylation of the AMPA receptor subunit GluR2 differentially regulates its interaction with PDZ domain-containing proteins. *Journal of Neuroscience*, 20(19), pp. 7258–67.

- Chung, H. J. et al. (2003) Requirement of AMPA receptor GluR2 phosphorylation for cerebellar long-term depression, *Science*, 300(5626), pp. 1751-5.
- Cichon, S. et al. (2008) 'Brain-specific tryptophan hydroxylase 2 (TPH2): A functional Pro206Ser substitution and variation in the 5'-region are associated with bipolar affective disorder', *Human Molecular Genetics*, 17(1), pp. 87–97. doi: 10.1093/hmg/ddm286.
- Comery, T.A. et al. (1997) Abnormal dendritic spines in fragile X knockout mice: maturation and pruning deficits. *Proceedings of the National Academy of Sciences of the United States of America*, 94(10), pp. 5401–4.
- Contopoulos-Ioannidis, D. G., Manoli, E. N., Ioannidis, J. P. A. (2005) Meta-analysis of the association of beta-2-adrenergic receptor polymorphisms with asthma phenotypes, *The Journal of Allergy and Clinical Immunology*, 115(5), pp. 963-72.
- Costa, A. C., Walsh, K. and Davisson, M. T. (1999) 'Motor dysfunction in a mouse model for Down syndrome', *Physiology & Behavior*, 68(1–2), pp. 211–220. doi: 10.1016/S0031-9384(99)00178-X.
- Coussons-Read, M.E., Crnic, L.S. (1996) Behavioral assessment of the Ts65Dn mouse, a model for Down syndrome: altered behavior in the elevated plus maze and open field, *Behavioural Genetics*, 26(1):7–13.
- Cox, J. et al. (2014) 'Accurate Proteome-wide Label-free Quantification by Delayed Normalization and Maximal Peptide Ratio Extraction, Termed MaxLFQ', *Molecular & Cellular Proteomics*, 13(9), pp. 2513–2526. doi: 10.1074/mcp.M113.031591.
- Crawley, J. N. (2000) *What's Wrong With My Mouse? Behavioral Phenotyping of Transgenic and Knockout Mice* (Wiley, New York).
- Curia, G. et al. (2009) Downregulation of tonic GABAergic inhibition in a mouse model of fragile X syndrome, *Cerebral Cortex*, 19(7), pp. 1515-20. doi: 10.1093/cercor/bhn159.
- D'Adamo, P. et al. (1998) Mutations in GDI1 are responsible for X-linked non-specific mental retardation. *Nature Genetics*, 19(2), pp. 134–9.

D'Adamo, P. et al. (2002) Deletion of the mental retardation gene *Gdi1* impairs associative memory and alters social behavior in mice, *Human Molecular Genetics*, 11(21), pp. 2567–80.

D'Hooge, R. et al. (1997) Mildly impaired water maze performance in male *Fmr1* knockout mice, *Neuroscience*, 76(2), pp. 367–76.

D'Hooge, R. and De Deyn, P. P. (2001) Applications of the Morris water maze in the study of learning and memory, *Brain Research Reviews*, 36(1), pp. 60-90. doi: 10.1016/S0165-0173(01)00067-4.

D'Hooge, R. et al. (1997) 'Mildly impaired water maze performance in male *Fmr1* knockout mice', *Neuroscience*, 76(2), pp. 367–376. doi: 10.1016/S0306-4522(96)00224-2.

Davare, M.A., et al. (2001) A beta2 adrenergic receptor signalling complex assembled with the Ca²⁺ channel Cav1.2, *Science*, 293(5527), pp. 98-101.

Davis, M. (2006) 'Neural systems involved in fear and anxiety measured with fear-potentiated startle', *The American Psychologist*, 61(8), pp. 741–756.

Davisson, M.T., et al. (1993) Segmental trisomy as a mouse model for Down syndrome, *Progress in clinical and biological research*, 384:117-33.

De Bin, R., Herold, T. and Boulesteix, A. L. (2014) 'Added predictive value of omics data: Specific issues related to validation illustrated by two case studies', *BMC Medical Research Methodology*, 14(1), pp. 1–23. doi: 10.1186/1471-2288-14-117.

Deák, F. et al. (2004) 'Synaptobrevin is essential for fast synaptic-vesicle endocytosis', *Nature Cell Biology*, 6(11), pp. 1102–1108. doi: 10.1038/ncb1185.

Del Beato T, A. A. (2014) 'Potential Biomarkers for Intellectual Disability: A Gipsy Family Study', *Hereditary Genetics*, 3(3). doi: 10.4172/2161-1041.1000138.

Denayer, E. et al. (2012) 'NRAS mutations in Noonan syndrome', *Molecular Syndromology*, 3(1), pp. 34–38. doi: 10.1159/000338467.

Derkach, V., Barria, A., and Soderling, T. R. (1999) Ca²⁺/calmodulin-kinase II enhances channel conductance of alpha-amino-3-hydroxy-5-methyl-4-isoxazolepropionate type

glutamate receptors. *Proceedings of the National Academy of Sciences of the United States of America*, 96(6), pp. 3269-74.

DiAntonio, A., et al. (2001) Ubiquitination-dependent mechanisms regulate synaptic growth and function, *Nature*, 412(6845), pp. 449-52.

Dias, D. A. and Koal, T. (2016) 'Progress in Metabolomics Standardisation and its Significance in Future Clinical Laboratory Medicine', *Ejifcc*, 27(4), pp. 331–343. Available at: <https://www.ncbi.nlm.nih.gov/pmc/articles/PMC5282916/pdf/ejifcc-27-331.pdf> <http://www.ncbi.nlm.nih.gov/pubmed/28149265> <http://www.pubmedcentral.nih.gov/articlerender.fcgi?artid=PMC5282916>.

Dierssen, M., et al. (1997) Alterations of central noradrenergic transmission in Ts65Dn mouse, a model for Down syndrome, *Brain Research*; 749(2), pp. 238–44.

Dirkx, R. et al. (1995) 'Targeting of the 67-kDa isoform of glutamic acid decarboxylase to intracellular organelles is mediated by its interaction with the NH₂- terminal region of the 65-kDa isoform of glutamic acid decarboxylase', *Journal of Biological Chemistry*, pp. 2241–2246. doi: 10.1074/jbc.270.5.2241.

Duncan, J.A., Gilman, A.G. (1998) A cytoplasmic acyl-protein thioesterase that removes palmitate from G protein alpha subunits and p21(RAS), *Journal of Biological Chemistry*, 273(25), pp. 15830-7.

Dunn, H.G., MacLeod, P.M. (2001) Rett syndrome: review of biological abnormalities, *The Canadian Journal of Neurological Sciences*, 28(1), pp. 16–29.

Ehlers, M. D. (2000) 'Reinsertion or degradation of AMPA receptors determined by activity-dependent endocytic sorting', *Neuron*, 28(2), pp. 511–525. doi: 10.1016/S0896-6273(00)00129-X.

Ehlers, M. D. (2003) Ubiquitin and synaptic dysfunction: ataxic mice highlight new common themes in neurological disease, *Trends in Neuroscience*, 26(1), pp. 4-7.

Eichenbaum, H., Clegg, R.A., Feeley, A. (1983) Reexamination of functional subdivisions of the rodent prefrontal cortex, *Experimental Neurology*, 79(2), pp. 434-51.

Elferink, L. A., Trimble, W. S. and Scheller, R. H. (1989) 'Two vesicle-associated membrane protein genes are differentially expressed in the rat central nervous system', *The Journal of biological chemistry*, 264(19), pp. 11061–4. Available at: <http://www.ncbi.nlm.nih.gov/pubmed/2472388>.

El-Husseini, A. E. D. and Brecht, D. S. (2002) 'Protein palmitoylation: A regulator of neuronal development and function', *Nature Reviews Neuroscience*, 3(10), pp. 791–802. doi: 10.1038/nrn940.

El-Husseini, A. E. D. et al. (2002) 'Synaptic strength regulated by palmitate cycling on PSD-95', *Cell*, 108(6), pp. 849–863. doi: 10.1016/S0092-8674(02)00683-9.

El-Husseini, A. E. et al. (2000) 'Dual palmitoylation of PSD-95 mediates its vesiculotubular sorting, postsynaptic targeting, and ion channel clustering', *Journal of Cell Biology*, 148(1), pp. 159–171. doi: 10.1083/jcb.148.1.159.

Epstein, C.J. (1995) Down syndrome (Trisomy 21). In: Scriver CR, et al. *The Metabolic and Molecular Basis of Inherited disease*, pp. 749–94.

Escorihuela, R. M. et al. (1998) 'Impaired short- and long-term memory in Ts65Dn mice, a model for Down syndrome.', *Neuroscience letters*, 247(2–3), pp. 171–174. doi: 10.1016/S0304-3940(98)00317-6.

Esposito, M.S. et al. (2005) Neuronal differentiation in the adult hippocampus recapitulates embryonic development, *Journal of Neuroscience*, 25(44), pp. 10074-86.

Fang, C. et al. (2006) 'GODZ-mediated palmitoylation of GABA(A) receptors is required for normal assembly and function of GABAergic inhibitory synapses.', *The Journal of neuroscience*, 26(49), pp. 12758–12768. doi: 10.1523/JNEUROSCI.4214-06.2006.

Fotaki, V., et al. (2002) Dyrk1A haploinsufficiency affects viability and causes developmental delay and abnormal brain morphology in mice, *Molecular Cell Biology*, 22(18), pp. 6636–47.

Friez, M. J. et al. (2006) Recurrent Infections, Hypotonia, and Mental Retardation Caused by Duplication of MECP2 and Adjacent Region in Xq28, *Paediatrics*, 118(6):e1687-95.

- Fu, A. K. et al. (2011) APCCdh1 mediates EphA4-dependent downregulation of AMPA receptors in homeostatic plasticity, *Nature Neuroscience*, 14(2), pp. 181–18.
- Fukata, M. et al. (2004) 'Identification of PSD-95 Palmitoylating Enzymes', *Neuron*, 44(6), pp. 987–996.
- Fukata, Y. and Fukata, M. (2010) 'Protein palmitoylation in neuronal development and synaptic plasticity', *Nature Reviews Neuroscience*, 11(3), pp. 161–175. doi: 10.1038/nrn2788.
- Gao, J. et al. (2010) 'A novel pathway regulates memory and plasticity via SIRT1 and miR-134', *Nature*, 466(7310), pp. 1105–1109.
- Gautam, V., et al. (2013) Nedd4 is a specific E3 ubiquitin ligase for the NMDA receptor subunit GluN2D, *Neuropharmacology*, 74, pp. 96–107.
- Genin, A., et al. (2001) Regulated expression of the neuronal calcium sensor-1 gene during long-term potentiation in the dentate gyrus in vivo, *Neuroscience*, 106(3), pp. 571-7.
- Gevi, F. et al. (2016) 'Urinary metabolomics of young Italian autistic children supports abnormal tryptophan and purine metabolism', *Molecular Autism*, 7(1), p. 47. doi: 10.1186/s13229-016-0109-5.
- Goldstein, F. B. (1961) 'Biochemical Studies on Phenylketonuria: I. Experimental Hyperphenylalanemia in the rat', *The Journal of biological chemistry*, 236(10), pp. 2656–2661.
- Gomez, M., et al. (2001) Ca²⁺ signaling via the neuronal calcium sensor-1 regulates associative learning and memory in *C. elegans*, *Neuron*, 30(1), pp. 241–8.
- Gonnord, P. et al. (2009) 'Palmitoylation of the P2X7 receptor, an ATP-gated channel, controls its expression and association with lipid rafts', *The FASEB journal*, 23(3), pp. 795–805. doi: 10.1096/fj.08-114637.
- Govek, E.E., et al. (2004) The X-linked mental retardation protein oligophrenin-1 is required for dendritic spine morphogenesis. *Nature Neuroscience*, 7(4), pp. 364-72.

Graybiel, A. M. (2000) 'The Basal Ganglia', *Current Biology*, 10(14), pp. 509–11. doi: 10.1007/978-3-319-42743-0.

Greaves, J. et al. (2008) Palmitoylation and membrane interactions of the neuroprotective chaperone cysteine-string protein, *Journal of Biological Chemistry*, 283(36), pp. 25014-26. doi: 10.1074/jbc.M802140200.

Greaves, J. et al. (2017) 'Molecular basis of fatty acid selectivity in the zDHHC family of S-acyltransferases revealed by click chemistry', *Proceedings of the National Academy of Sciences*, 114(8), pp. E1365–E1374. doi: 10.1073/pnas.1612254114.

Gubitosi-Klug, R. A., Mancuso, D. J. and Gross, R. W. (2005) 'The human Kv1.1 channel is palmitoylated, modulating voltage sensing: Identification of a palmitoylation consensus sequence', *Proceedings of the National Academy of Sciences of the United States of America*, 102(17), pp. 5964–5968. doi: 10.1073/pnas.0501999102.

Guillemin, G. J. et al. (2005) 'Indoleamine 2,3 dioxygenase and quinolinic acid Immunoreactivity in Alzheimer's disease hippocampus', *Neuropathology and Applied Neurobiology*, 31(4), pp. 395–404. doi: 10.1111/j.1365-2990.2005.00655.x.

Gunbey, H. P. et al. (2017) 'Structural brain alterations of Down's syndrome in early childhood evaluation by DTI and volumetric analyses', *European Radiology*, 27(7), pp. 3013–3021. doi: 10.1007/s00330-016-4626-6.

Gundersen, C. B. et al. (1994) 'Extensive lipidation of a Torpedo cysteine string protein', *Journal of Biological Chemistry*, 269(30), pp. 19197–19199.

Gutierrez, L. et al. (1989) 'Post-translational processing of p21ras is two-step and involves carboxyl-methylation and carboxy-terminal proteolysis', *The EMBO journal*, 8(4), pp. 1093–1098.

Guy, J., et al. (2001) A mouse Mecp2- null mutation causes neurological symptoms that mimic Rett syndrome. *Nature Genetics*; 27(3):322–6.

- Hagerman, R. J. and Hagerman, P. J. (2002) 'The fragile X premutation: Into the phenotypic fold', *Current Opinion in Genetics and Development*, 12(3), pp. 278–283. doi: 10.1016/S0959-437X(02)00299-X.
- Halgren, C. et al. (2012) 'Corpus callosum abnormalities, intellectual disability, speech impairment, and autism in patients with haploinsufficiency of ARID1B', *Clinical Genetics*, 82(3), pp. 248–255. doi: 10.1111/j.1399-0004.2011.01755.x.
- Hall, B., Limaye, A., Kulkarni, A. B. (2009) 'Overview: Generation of Gene Knockout Mice', *Current Protocols in Cell Biology*, Chapter 19:Unit 19.12, pp. 1–17. doi: 10.1002/0471143030.cb1912s44.
- Hamdan, F. F. et al. (2009) 'De novo STXBP1 mutations in mental retardation and nonsyndromic epilepsy', *Annals of Neurology*, 65(6), pp. 748–753. doi: 10.1002/ana.21625.
- Hammerle, B., et al. (2002) Mnb/Dyrk1A is transiently expressed and asymmetrically segregated in neural progenitor cells at the transition to neurogenic divisions, *Developmental Biology*, 246(2), pp. 259–73.
- Han, J. Y. et al. (2017) 'The first patient with sporadic X-linked intellectual disability with de novo ZDHHC9 mutation identified by targeted next-generation sequencing', *European Journal of Medical Genetics*, 60(10), pp. 499–503. doi: 10.1016/j.ejmg.2017.07.002.
- Hancock, J. F. et al. (1989) 'All ras proteins are polyisoprenylated but only some are palmitoylated', *Cell*, 57(7), pp. 1167–1177. doi: 10.1016/0092-8674(89)90054-8.
- Hawrylycz, M. J. et al. (2012) 'An anatomically comprehensive atlas of the adult human brain transcriptome', *Nature*, 489(7416), pp. 391–399. doi: 10.1038/nature11405.An.
- Hayashi, T., and Huganir, R. L. (2004) Tyrosine phosphorylation and regulation of the AMPA receptor by SRC family tyrosine kinases, *Journal of Neuroscience*, 24(27), pp. 6152–60.
- Hayashi, T., Rumbaugh, G. and Huganir, R. L. (2005) 'Differential regulation of AMPA receptor subunit trafficking by palmitoylation of two distinct sites', *Neuron*, 47(5), pp. 709–723. doi: 10.1016/j.neuron.2005.06.035.

Hayashi, T., Thomas, G. M. and Huganir, R. L. (2009) 'Dual Palmitoylation of NR2 Subunits Regulates NMDA Receptor Trafficking', *Neuron*, 64(2), pp. 213–226. doi: 10.1016/j.neuron.2009.08.017.

Heilstedt, H. A., Shahbazian, M. D. and Lee, B. (2002) 'Infantile hypotonia as a presentation of Rett syndrome', *American Journal of Medical Genetics*, 111(3), pp. 238–242. doi: 10.1002/ajmg.10633.

Herbst, DS, Miller, JR. (1980) Nonspecific X-linked mental retardation. II: the frequency in British Columbia, *American Journal of Medical Genetics*, 7(4): 461–9.

Hess, D. T. et al. (1992) 'The 25 kDa synaptosomal-associated protein SNAP-25 is the major methionine-rich polypeptide in rapid axonal transport and a major substrate for palmitoylation in adult CNS', *The Journal of Neuroscience*, 12(12), pp. 4634–4641.

Hevner, RF, et al. (2006) Transcription factors in glutamatergic neurogenesis: conserved programs in neocortex, cerebellum, and adult hippocampus, *Neuroscience Research*, 55(3), pp. 223-33.

Ho, G. P. et al. (2011) 'S-nitrosylation and S-palmitoylation reciprocally regulate synaptic targeting of PSD-95.', *Neuron*, 71(1), pp. 131–141. doi: 10.1016/j.neuron.2011.05.033.S-Nitrosylation.

Holtzman, DM, et al. (1996) Developmental abnormalities and age-related neurodegeneration in a mouse model of Down syndrome. *Proceedings of the National Academy of Science USA*, 93(23), pp. 13333–8.

Huang, K et al. (2004) Huntingtin-interacting protein HIP14 is a palmitoyl transferase involved in palmitoylation and trafficking of multiple neuronal proteins, *Neuron*, 44(6), pp. 977-86.

Huang, K, et al. (2011) Wild-type HTT modulates the enzymatic activity of the neuronal palmitoyl transferase HIP14, *Human Molecular Genetics*, 20(17), pp. 3356–3365.

Hurley, J. H. et al. (2000) 'The role of dynamic palmitoylation in Ca²⁺ channel inactivation', *Proceedings of the National Academy of Sciences of the United States of America*, 97(16), pp. 9293–9298. doi: 10.1073/pnas.160589697.

Insausti, AM, et al. (1998) Hippocampal volume and neuronal number in Ts65Dn mice: a murine model of Down syndrome, *Neuroscience Letters*, 253(3):175–8.

Ishizaki, H, et al. (2000) Role of rab GDP dissociation inhibitor alpha in regulating plasticity of hippocampal neurotransmission, *Proceedings of the National Academy of Science USA*, 97(21), pp. 11587-92.

Iwase, S. et al. (2016) 'A Mouse Model of X-linked Intellectual Disability Associated with Impaired Removal of Histone Methylation', *Cell Reports*, 14(5), pp. 1000–1009. doi: 10.1016/j.celrep.2015.12.091.

Jenkins, M. A., and Traynelis, S. F. (2012) PKC phosphorylates GluA1- Ser831 to enhance AMPA receptor conductance, *Channels (Austin)*, 6(1), pp. 60-4.

Jennings, B. C. and Linder, M. E. (2012) 'DHHC protein S-acyltransferases use similar ping-pong kinetic mechanisms but display different Acyl-CoA specificities', *Journal of Biological Chemistry*, 287(10), pp. 7236–7245. doi: 10.1074/jbc.M111.337246.

Jindal, H. K. et al. (2008) 'Posttranslational modification of voltage-dependent potassium channel Kv1.5: COOH-terminal palmitoylation modulates its biological properties', *American journal of physiology. Heart and circulatory physiology*, 294(5), pp. H2012–H2021. doi: 10.1152/ajpheart.01374.2007.

Johnston, M.V., et al. (2001) Neurobiology of Rett syndrome: a genetic disorder of synapse development, *Brain Development*, 23(1):S206–13.

Johnston, M.V., Hohmann, C., Blue, M.E. (1995) Neurobiology of Rett syndrome, *Neuropediatrics*, 26(2), pp. 119–22.

Joneson, T. and Bar-Sagi, D. (1997) 'Ras effectors and their role in mitogenesis and oncogenesis', *Journal of Molecular Medicine*, 75(8), pp. 587–593. doi: 10.1007/s001090050143.

- Jurd, R., et al. (2008) Mind bomb-2 is an E3 ligase that ubiquitinates the N-methyl-D-aspartate receptor NR2B subunit in a phosphorylation-dependent manner, *Journal of Biological Chemistry*, 283(1), pp. 301–310.
- Kang, J.U., et al. (2008) Gain at chromosomal region 5p15.33, containing TERT, is the most frequent genetic event in early stages of non-small cell lung cancer, *Cancer Genetics and Cytogenetics*, 182(1), pp. 1–11.
- Kang, R. et al. (2008) 'Neural palmitoyl-proteomics reveals dynamic synaptic palmitoylation', *Nature*, 456(7224), pp. 904–909. doi: 10.1038/nature07605.
- Kato, A. S., et al. (2010) TARPs differentially decorate AMPA receptors to specify neuropharmacology, *Trends in Neuroscience*, 33(5), 241–248.
- Keller, C. A et al. (2004) 'The gamma2 subunit of GABA(A) receptors is a substrate for palmitoylation by GODZ.', *The Journal of neuroscience*, 24(26), pp. 5881–5891. doi: 10.1523/JNEUROSCI.1037-04.2004.
- Khandjian, E.W. (1999) Biology of the fragile X mental retardation protein, an, RNA-binding protein, *Biochemistry and Cell Biology*, 77(4), pp. 331–42.
- Khelifaoui, M., et al. (2007) Loss of X-linked mental retardation gene oligophrenin1 in mice impairs spatial memory and leads to ventricular enlargement and dendritic spine immaturity, *Journal of Neuroscience*, 27(35), pp. 9439–50.
- Klug, A. and Rhodes, D. (1987) Zinc fingers: a novel protein fold for nucleic acid recognition, *Cold Spring Harbor Symposia on Quantitative Biology*, 52, pp. 473-82.
- Koch, M. (1999) 'The neurobiology of startle', *Progress in Neurobiology*, 59(2), pp. 107–128. doi: 10.1016/S0301-0082(98)00098-7.
- Kooy, R. F. (2003) 'Of mice and the fragile X syndrome', *Trends in Genetics*, 19(3), pp. 148–154. doi: 10.1016/S0168-9525(03)00017-9.
- Kristensen, A. S., et al. (2011) Mechanism of Ca²⁺/calmodulin-dependent kinase II regulation of AMPA receptor gating, *Nature Neuroscience*, 14(6), pp. 727–735.

Large, V., et al. (1997) Human beta-2 adrenoceptor gene polymorphisms are highly frequent in obesity and associate with altered adipocyte beta-2 adrenoceptor function, *Journal of Clinical Investigation*, 100(12): 3005-3013.

LaSalle, J.M., Yasui, D.H. (2009) Evolving role of MeCP2 in Rett syndrome and autism, *Epigenomics*, 1(1), pp. 119–30, doi: 10.2217/epi.09.13.

Lavezzari, G., et al. (2003) Differential binding of the AP-2 adaptor complex and PSD-95 to the C-terminus of the NMDA receptor subunit NR2B regulates surface expression, *Neuropharmacology*, 45(6), 729–737.

Lee, H. K. et al. (2003) 'Phosphorylation of the AMPA receptor GluR1 subunit is required for synaptic plasticity and retention of spatial memory', *Cell*, 112(5), pp. 631–643. doi: 10.1016/S0092-8674(03)00122-3.

Lejeune, J., Gautier, M., Turpin, R. (1959) Study of somatic chromosomes from 9 mongoloid children, *Comptes rendus de l'Académie des Sciences*, 248(11), pp. 1721-2.

Lemonidis, K. et al. (2014) 'The Golgi S-acylation machinery comprises zDHC enzymes with major differences in substrate affinity and S-acylation activity', *Molecular Biology of the Cell*, 25(24), pp. 3870–3883. doi: 10.1091/mbc.E14-06-1169.

Levy, A. D. et al. (2011) 'Subcellular Golgi localization of stathmin family proteins is promoted by a specific set of DHC palmitoyl transferases', *Molecular Biology of the Cell*, 22(11), pp. 1930–1942. doi: 10.1091/mbc.E10-10-0824.

Li, Y. et al. (2010) 'DHC5 interacts with PDZ domain 3 of post-synaptic density-95 (PSD-95) protein and plays a role in learning and memory', *Journal of Biological Chemistry*, 285(17), pp. 13022–13031. doi: 10.1074/jbc.M109.079426.

Li, Y. et al. (2012) 'DHC5 protein palmitoylates flotillin-2 and is rapidly degraded on induction of neuronal differentiation in cultured cells', *Journal of Biological Chemistry*, 287(1), pp. 523–530. doi: 10.1074/jbc.M111.306183.

Lin, A., et al. (2011) Nedd4-mediated AMPA receptor ubiquitination regulates receptor turnover and trafficking, *Journal of Neurochemistry*, 119(1), 27–39.

- Liu, P. et al. (2016) 'Palmitoyltransferase Zdhhc9 inactivation mitigates leukemogenic potential of oncogenic Nras', *Leukemia*, 30(5), pp. 1225–1228. doi: 10.1038/leu.2015.293.
- Lobo, S. et al. (2002) 'Identification of a Ras palmitoyltransferase in *Saccharomyces cerevisiae*', *Journal of Biological Chemistry*, 277(43), pp. 41268–41273. doi: 10.1074/jbc.M206573200.
- Logue, S. F., Paylor, R. and Wehner, J. M. (1997) 'Hippocampal lesions cause learning deficits in inbred mice in the Morris water maze and conditioned-fear task', *Behavioral Neuroscience*, 111(1), pp. 104–113. doi: 10.1037/0735-7044.111.1.104.
- Lu, W., and Roche, K. W. (2012) Posttranslational regulation of AMPA receptor trafficking and function, *Current Opinion in Neurology*, 22(3), pp. 470–479.
- Luders, E., Thompson, P. M. and Toga, A. W. (2010) 'The Development of the Corpus Callosum in the Healthy Human Brain', *Journal of Neuroscience*, 30(33), pp. 10985–10990. doi: 10.1523/JNEUROSCI.5122-09.2010.
- Lumbreras, M.A. et al. (1995) A behavioral assessment of Ts65Dn mice: a putative Down syndrome model, *Neuroscience Letters*, 199(2), pp. 143–6, doi: 10.1016/0304-3940(95)12052-6.
- Lundberg, S., Frylmark, A., Eeg-Olofsson, O. (2005) Children with rolandic epilepsy have abnormalities of oromotor and dichotic listening performance, *Developmental Medicine & Child Neurology*, 47(9), pp. 603–608.
- Lussier, M. P., et al. (2012) Ubiquitin ligase RNF167 regulates AMPA receptor-mediated synaptic transmission, *Proceedings of the National Academy of Sciences of the United States of America*, 109(47), pp. 19426–19431.
- Lussier, M. P., Nasu-Nishimura, Y., and Roche, K.W. (2011) Activity-dependent ubiquitination of the AMPA receptor subunit GluA2, *The Journal of Neuroscience*, 31(8), pp. 3077-81.
- Lynex, C. N. et al. (2004) 'Homozygosity for a missense mutation in the 67 kDa isoform of glutamate decarboxylase in a family with autosomal recessive spastic cerebral palsy:

parallels with Stiff-Person Syndrome and other movement disorders', *BMC Neurology*, 4(1), p. 20. doi: 10.1186/1471-2377-4-20.

Mabb, A. M., and Ehlers, M. D. (2010) Ubiquitination in postsynaptic function and plasticity. *Annual Review of Cell and Developmental Biology*, 26, pp. 179–210.

Magee, A. I. et al. (1987) 'Dynamic fatty acylation of p21N-ras.', *The EMBO journal*, 6(11), pp. 3353–7.

Mammen, A. L., et al. (1997) Phosphorylation of the α -Amino-3-hydroxy-5-methylisoxazole4-propionic Acid Receptor GluR1 Subunit by Calcium/ Calmodulin-dependent Kinase II, *Journal of Biological Chemistry*, 272(51), pp. 32528-33.

Mansilla, F. et al. (2007) 'Differential expression of DHH9 in microsatellite stable and instable human colorectal cancer subgroups', *British journal of cancer*, 96(12), pp. 1896–1903. doi: 10.1038/sj.bjc.6603818.

Mansour, S.L., Thomas, K.R., Capecchi, M.R. (1988) 'Disruption of the proto-oncogene int-2 in mouse embryo-derived stem cells: a general strategy for targeting mutations to non-selectable genes', *Nature*, 336(6197), pp. 348–352. doi: 10.1038/332141a0.

Mansouri, M. R. et al. (2005) 'Loss of ZDHH15 expression in a woman with a balanced translocation t(X;15)(q13.3;cen) and severe mental retardation', *European journal of human genetics*, 13(8), pp. 970–977. doi: 10.1038/sj.ejhg.5201445.

Manti, S. et al. (2018) 'Inflammatory biomarkers and intellectual disability in patients with Down syndrome', *Journal of Intellectual Disability Research*, 62(5), pp. 382-390, doi: 10.1111/jir.12470.

Masurel-Paulet, A. et al. (2014) 'Expanding the clinical phenotype of patients with a ZDHH9 mutation', *American Journal of Medical Genetics*, 164(3), pp. 789–795. doi: 10.1002/ajmg.a.36348.

Masuya, H. et al. (2005) 'Implementation of the modified-SHIRPA protocol for screening of dominant phenotypes in a large-scale ENU mutagenesis program', *Mammalian Genome*, 16(11), pp. 829–837. doi: 10.1007/s00335-005-2430-8.

- Matsuda, S., Mikawa, S., and Hirai, H. (1999) Phosphorylation of serine-880 in GluR2 by protein kinase C prevents its C terminus from binding with glutamate receptor-interacting protein, *Journal of Neurochemistry*, 73(4), pp. 1765–1768.
- Maulik, P. K. et al. (2011) 'Prevalence of intellectual disability: A meta-analysis of population-based studies', *Research in Developmental Disabilities*, 32(2), pp. 419–436. doi: 10.1016/j.ridd.2010.12.018.
- McHale, D. P. et al. (1999) 'A gene for autosomal recessive symmetrical spastic cerebral palsy maps to chromosome 2q24-25.', *American journal of human genetics*, 64(2), pp. 526–32. doi: 10.1086/302237.
- McKinney, J. et al. (2008) 'A loss-of-function mutation in tryptophan hydroxylase 2 segregating with attention-deficit/hyperactivity disorder', *Molecular Psychiatry*, 13(4), pp. 365–367. doi: 10.1038/sj.mp.4002152.
- Meister, A. (1958) 'Phenylpyruvic Oligophrenia', *Pediatrics*, 21(1), pp. 1021–1031.
- Meng, Y, et al. (2002) Abnormal spine morphology and enhanced LTP in LIMK-1 knockout mice, *Neuron*, 35(1), pp. 121–33.
- Milligan, G., Parenti, M., Magee, A.I. (1995) The dynamic role of palmitoylation in signal transduction, *Trends in Biochemical Sciences*, 20(5), pp. 181-7.
- Milnerwood, A. J. et al. (2013) 'Memory and synaptic deficits in Hip14/DHHC17 knockout mice.', *Proceedings of the National Academy of Sciences of the United States of America*, 110(50), pp. 20296–20301. doi: 10.1073/pnas.1222384110.
- Minderaa, R. B. et al. (1987) 'Urinary 5-hydroxyindoleacetic acid and whole blood serotonin and tryptophan in autistic and normal subjects', *Biological Psychiatry*, 22(8), pp. 933–940. doi: 10.1016/0006-3223(87)90002-3.
- Mineur, Y. S. et al. (2002) 'Behavioral and neuroanatomical characterization of the Fmr1 knockout mouse', *Hippocampus*, 12(1), pp. 39–46. doi: 10.1002/hipo.10005.

- Mitchell, D. A. et al. (2006) 'Protein palmitoylation by a family of DHHC protein S-acyltransferases', *Journal of lipid research*, 47(7), pp. 1107–1118. doi: 10.1194/jlr.R600007-JLR200.
- Mitchell, D. A. et al. (2010) 'Mutational analysis of *Saccharomyces cerevisiae* Erf2 reveals a two-step reaction mechanism for protein palmitoylation by DHHC enzymes', *Journal of Biological Chemistry*, 285(49), pp. 38104–38114. doi: 10.1074/jbc.M110.169102.
- Mitchell, D. A. et al. (2014) 'Mutations in the X-linked intellectual disability gene, *zDHHC9*, alter autopalmitoylation activity by distinct mechanisms', *Journal of Biological Chemistry*, 289(26), pp. 18582–18592. doi: 10.1074/jbc.M114.567420.
- Mitchell, S. and Bunday, S. (1997) 'Symmetry of neurological signs in Pakistani patients with probable inherited spastic cerebral palsy', *Clinical Genetics*, 51(1), pp. 7–14.
- Moeschler, J. B. and Shevell, M. (2014) 'Comprehensive Evaluation of the Child With Intellectual Disability or Global Developmental Delays', *Pediatrics*, 134(3), pp. e903–e918. doi: 10.1542/peds.2014-1839.
- Morris, R. G. (1989) 'Synaptic plasticity and learning: selective impairment of learning rats and blockade of long-term potentiation in vivo by the N-methyl-D-aspartate receptor antagonist AP5', *The Journal of Neuroscience*, 9(9), pp. 3040–3057.
- Mukai, J., et al. (2004) Evidence that the gene encoding *ZDHHC8* contributes to the risk of schizophrenia, *Nature Genetics*, 36(7), pp. 725–31.
- Murphy, J. A., et al. (2014) Phosphorylation of Ser1166 on *GluN2B* by PKA is critical to synaptic NMDA receptor function and Ca²⁺ signalling in spines, *Journal of Neuroscience*, 34(3), pp. 869–879.
- Murray, A. J. et al. (2015) 'Parvalbumin-positive interneurons of the prefrontal cortex support working memory and cognitive flexibility', *Scientific Reports*, 5(16778), pp. 1–14. doi: 10.1038/srep16778.
- Na, C. H., et al. (2012) Synaptic protein ubiquitination in rat brain revealed by antibody-based ubiquitome analysis, *Journal of Proteome Research*, 11(9), pp. 4722–32.

Nadolski, M. J. and Linder, M. E. (2007) 'Protein lipidation', *FEBS Journal*, 274(20), pp. 5202–5210. doi: 10.1111/j.1742-4658.2007.06056.x.

Naidu, S. (1997) Rett syndrome: a disorder affecting early brain growth, *Annals of Neurology*, 42(1), pp. 3–10.

Nakajima, J. et al. (2015) 'De novo EEF1A2 mutations in patients with characteristic facial features, intellectual disability, autistic behaviors and epilepsy', *Clinical Genetics*, 87(4), pp. 356–361. doi: 10.1111/cge.12394.

Nelson, L. et al. (2005) 'Learning and memory as a function of age in Down syndrome: A study using animal-based tasks', *Progress in Neuro-Psychopharmacology and Biological Psychiatry*, 29(3), pp. 443–453. doi: 10.1016/j.pnpbp.2004.12.009.

Nielsen, D. M. et al. (2002) 'Alterations in the auditory startle response in Fmr1 targeted mutant mouse models of fragile X syndrome', *Brain Research*, 927(1), pp. 8–17. doi: 10.1016/S0006-8993(01)03309-1.

Noritake, J. et al. (2009) 'Mobile DHHC palmitoylating enzyme mediates activity-sensitive synaptic targeting of PSD-95', *Journal of Cell Biology*, 186(1), pp. 147–160. doi: 10.1083/jcb.200903101.

Northam, G. B. et al. (2012) 'Interhemispheric temporal lobe connectivity predicts language impairment in adolescents born preterm', *Brain*, 135(12), pp. 3781–3798. doi: 10.1093/brain/aws276.

O'Dowd, B. F., et al. (1989) Palmitoylation of the human β 2-adrenergic receptor: mutation of Cys-341 in the carboxyl tail leads to an uncoupled nonpalmitoylated form of the receptor, *Journal of Biological Chemistry*, 264(13), pp. 7564–7569.

Ohno, Y. et al. (2006) Intracellular localization and tissue-specific distribution of human and yeast DHHC cysteine-rich domain-containing proteins, *Biochimica et Biophysica Acta*, 1761(4), pp. 474-83.

Ohta, E. et al. (2003) 'Identification and Characterization of GCP16, A Novel Acylated Golgi Protein That Interacts with GCP170', *Journal of Biological Chemistry*, 278(51), pp. 51957–51967. doi: 10.1074/jbc.M310014200.

Ohyama, T. et al. (2007) 'Huntingtin-interacting protein 14, a palmitoyl transferase required for exocytosis and targeting of CSP to synaptic vesicles', *Journal of Cell Biology*, 179(7), pp. 1481–1496. doi: 10.1083/jcb.200710061.

Okui, M., et al. (1999) High-level expression of the Mnb/Dyrk1A gene in brain and heart during rat early development, *Genomics*, 62(2), pp. 165–71.

Okun, E. et al. (2010) 'Toll-like receptor 3 inhibits memory retention and constrains adult hippocampal neurogenesis', *Proceedings of the National Academy of Sciences of the United States of America*, 107(35), pp. 15625–15630. doi: 10.1073/pnas.1005807107.

Oostra, B.A., Chiurazzi P. (2001) The fragile X gene and its function, *Clinical Genetics*, 60(6), pp. 399–408, doi: 10.1034/j.1399-0004.2001.600601.x

Osipova, D. V., Kulikov, A. V. and Popova, N. K. (2009) 'C1473G polymorphism in mouse tph2 gene is linked to tryptophan hydroxylase-2 activity in the brain, intermale aggression, and depressive-like behavior in the forced swim test', *Journal of Neuroscience Research*, 87(5), pp. 1168–1174. doi: 10.1002/jnr.21928.

Oyama, T., et al. (2000) Isolation of a novel gene on 8p21.3–22 whose expression is reduced significantly in human colorectal cancers with liver metastasis, *Genes Chromosomes Cancer*, 29(1), pp. 9–15.

Panayiotopoulos, C. P. et al. (2008) 'Benign childhood focal epilepsies: Assessment of established and newly recognized syndromes', *Brain*, 131(9), pp. 2264–2286. doi: 10.1093/brain/awn162.

Pasinelli, P. et al. (1995) Long-term potentiation and synaptic protein phosphorylation, *Behavioural Brain Research*, 66(1-2), pp. 53–59.

- Paul, L. K. (2011) 'Developmental malformation of the corpus callosum: A review of typical callosal development and examples of developmental disorders with callosal involvement', *Journal of Neurodevelopmental Disorders*, 3(1), pp. 3–27, doi: 10.1007/s11689-010-9059-y.
- Peier, A. M. et al. (2000) '(Over)correction of FMR1 deficiency with YAC transgenics: behavioral and physical features', *Human molecular genetics*, 9(8), pp. 1145–1159. doi: 10.1093/hmg/9.8.1145.
- Pernot, F. et al. (2010) 'Selection of reference genes for real-time quantitative reverse transcription-polymerase chain reaction in hippocampal structure in a murine model of temporal lobe epilepsy with focal seizures', *Journal of Neuroscience Research*, 88(5), pp. 1000–1008. doi: 10.1002/jnr.22282.
- Pevsner, J., Hsu, S. C. and Scheller, R. H. (1994) 'n-Sec1: a neural-specific syntaxin-binding protein.', *Proceedings of the National Academy of Sciences of the United States of America*, 91(4), pp. 1445–9. doi: 10.1073/pnas.91.4.1445.
- Pickering, D. S. et al. (1995) 'Palmitoylation of the GluR6 kainate receptor', *Proceedings of the National Academy of Sciences of the United States of America*, 92(26), pp. 12090–12094. doi: 10.1073/pnas.92.26.12090.
- Pieretti, M. et al. (1991) Absence of expression of the FMR-1 gene in fragile X syndrome, *Cell*, 66(4):817–22.
- Poirier, K. et al. (2010) 'Mutations in the neuronal β -tubulin subunit TUBB3 result in malformation of cortical development and neuronal migration defects', *Human Molecular Genetics*, 19(22), pp. 4462–4473. doi: 10.1093/hmg/ddq377.
- Powell, S. B., Zhou, X. and Geyer, M. A. (2009) 'Prepulse inhibition and genetic mouse models of schizophrenia', *Behavioural Brain Research*, 204(2), pp. 282–294. doi: 10.1016/j.bbr.2009.04.021.Prepulse.
- Prybylowski, K., et al. (2005) The synaptic localization of NR2B-containing NMDA receptors is controlled by interactions with PDZ proteins and AP-2, *Neuron* 47(6), 845–857.

- Rana, M.S., et al. (2018) Fatty acyl recognition and transfer by an integral membrane S-acyltransferase, *Science*, 359(6372), pii: eaa06326, doi: 10.1126/science.aao6326.
- Rathenberg, J., Kittler, J. T. and Moss, S. J. (2004) 'Palmitoylation regulates the clustering and cell surface stability of GABAA receptors', *Molecular and Cellular Neuroscience*, 26(2), pp. 251–257. doi: 10.1016/j.mcn.2004.01.012.
- Raymond, F. L. et al. (2007) 'Mutations in ZDHHC9, which encodes a palmitoyltransferase of NRAS and HRAS, cause X-linked mental retardation associated with a Marfanoid habitus.', *American journal of human genetics*, 80(5), pp. 982–987. doi: 10.1086/513609.
- Raymond, K. N. and Pierre, V. C. (2005) 'Next generation, high relaxivity gadolinium MRI agents', *Bioconjugate Chemistry*, 16(1), pp. 3–8. doi: 10.1021/bc049817y.
- Reeves, R.H., et al. (1995) A mouse model for Down syndrome exhibits learning and behaviour deficits, *Nature Genetics*, 11(2), pp. 177–84.
- Resh, M. D. (2012) 'Targeting protein lipidation in disease', *Trends in Molecular Medicine*, 18(4), pp. 206–214. doi: 10.1016/j.molmed.2012.01.007.
- Resh, M. D. (2016) 'Fatty acylation of proteins : The long and the short of it', *Progress in Lipid Research*, 63, pp. 120–131. doi: 10.1016/j.plipres.2016.05.002.
- Resh, MD. (2006) Trafficking and signalling by fatty-acylated and prenylated proteins, *Nature Chemical Biology*, 2(11), pp. 584-90.
- Richard, D. M. et al. (2009) 'L -Tryptophan : basic metabolic functions, behavioral research and therapeutic indications', *International Journal of Tryptophan Research*, 2, pp. 45–60. doi: 10.2964/jsik.kuni0223.
- Roche, K. W., et al. (1996) Characterization of multiple phosphorylation sites on the AMPA receptor GluR1 subunit, *Neuron*, 16(6), pp. 1179–1188.
- Rocks, O., et al. (2005) An acylation cycle regulates localization and activity of palmitoylated Ras isoforms, *Science*, 307(5716), pp. 1746-52.

- Rocks, O. et al. (2010) 'The palmitoylation machinery is a spatially organizing system for peripheral membrane proteins', *Cell*, 141(3), pp. 458–471. doi: 10.1016/j.cell.2010.04.007.
- Rodenburg, R.N.P. et al. (2017) Stochastic palmitoylation of accessible cysteines in membrane proteins revealed by native mass spectrometry, *Nature Communications*, 8(1):1280. doi: 10.1038/s41467-017-01461-z.
- Rogers, D.C., et al. (1999) Use of SHIRPA and discriminant analysis to characterise marked differences in the behavioural phenotype of six inbred mouse strains, *Behavioural Brain Research*, 105(2), pp. 207-17.
- Rogers, G. B. et al. (2016) 'From gut dysbiosis to altered brain function and mental illness: Mechanisms and pathways', *Molecular Psychiatry*, 21(6), pp. 738–748. doi: 10.1038/mp.2016.50.
- Roizen, N. J. (2001) 'Down Syndrome: Progress in research', *Mental retardation and developmental disabilities research reviews*, 7(1), pp. 38–44.
- Rose, S.P. (1995) Glycoproteins and memory formation, *Behavioural Brain Research*, 66(1-2), pp. 73–78.
- Roth, A.F. et al. (2002) The yeast DHHC cysteine-rich domain protein Akr1p is a palmitoyl transferase, *Journal of Cell Biology*, 159(1), pp. 23-8.
- Sago, H., et al. (1998) Ts1Cje, a partial trisomy 16 mouse model for Down syndrome, exhibits learning and behavioral abnormalities, *Proceedings of the National Academy of Sciences of the United States of America.*, 95(11), pp. 6256–61, doi: 10.1073/pnas.95.11.6256.
- Sago, H., et al. (2000) Genetic dissection of region associated with behavioral abnormalities in mouse models for down syndrome, *Pediatric Research*, 48(5), pp. 606–13.
- Saitoh, F. et al. (2004) 'NIDD, a novel DHHC-containing protein, targets neuronal nitric-oxide synthase (nNOS) to the synaptic membrane through a PDZ-dependent interaction and regulates nNOS activity', *Journal of Biological Chemistry*, 279(28), pp. 29461–29468. doi: 10.1074/jbc.M401471200.

- Sakane, A., et al. (2006) Rab3 GTPase-activating protein regulates synaptic transmission and plasticity through the inactivation of Rab3, *Proceedings of the National Academy of Sciences of the United States of America*, 103(26), pp. 10029-34.
- Salaün, C., James, D.J., Chamberlain, L.H. (2004) Lipid rafts and the regulation of exocytosis, *Traffic*, 5(4), pp. 255-64.
- Samaco, R. C. et al. (2008) 'A partial loss of function allele of Methyl-CpG-binding protein 2 predicts a human neurodevelopmental syndrome', *Human Molecular Genetics*, 17(12), pp. 1718–1727. doi: 10.1093/hmg/ddn062.
- San Martín, A., Pagani, M.R. (2014) Understanding intellectual disability through RASopathies, *Journal of Physiology Paris*, 108(4-6), pp. 232-9, doi: 10.1016/j.jphysparis.2014.05.003.
- Sanders, S.S., Hayden, M.R. (2015) Aberrant palmitoylation in Huntington disease, *Biochemical Society Transactions*, 43(2), pp. 205-10, doi: 10.1042/BST20140242.
- Sanz-Clemente, A., et al. (2010) Casein kinase 2 regulates the NR2 subunit composition of synaptic NMDA receptors, *Neuron*, 67(6), pp. 984-96.
- Schlesinger, M.J., Magee, A.I., Schmidt, M.F. (1980) Fatty acid acylation of proteins in cultured cells, *Journal of Biological Chemistry*, 255(21), pp. 10021-4.
- Schmidt, J. W. and Catterall, W. A. (1987) 'Palmitoylation, sulfation, and glycosylation of the alpha subunit of the sodium channel. Role of post-translational modifications in channel assembly', *Journal of Biological Chemistry*, 262(28), pp. 13713–13723.
- Schmidt, M.F., Schlesinger, M.J. (1979) Fatty acid binding to vesicular stomatitis virus glycoprotein: a new type of post-translational modification of the viral glycoprotein, *Cell*, 17(4), pp. 813-9.
- Schnepp, P. M. et al. (2017) 'GAD1 upregulation programs aggressive features of cancer cell metabolism in the brain metastatic microenvironment', *Cancer Research*, 77(11), pp. 2844–2856. doi: 10.1158/0008-5472.CAN-16-2289.

Schoch, S. et al. (2001) 'SNARE Function Analyzed in Synaptobrevin / VAMP Knockout Mice', *Science*, 294 (5544), pp. 1117–1123, doi: 10.1126/science.1064335.

Schratt, G. M. et al. (2006) 'A brain-specific microRNA regulates dendritic spine development', *Nature*, 439(7074), pp. 283–289, doi: 10.1038/nature04367.

Schwartz, C. E. et al. (2007) 'The original Lujan syndrome family has a novel missense mutation (p.N1007S) in the MED12 gene', *Journal of Medical Genetics*, 44(7), pp. 472–477. doi: 10.1136/jmg.2006.048637.

Schwarz, L. A., Hall, B. J., and Patrick, G. N. (2010) Activity-dependent ubiquitination of GluA1 mediates a distinct AMPA receptor endocytosis and sorting pathway, *Journal of Neuroscience*, 30(49), 16718–16729.

Scorza, C. A. and Cavalheiro, E. A. (2011) 'Animal models of intellectual disability: towards a translational approach', *Clinics (Sao Paulo)*, 66 Suppl 1, pp. 55–63, doi: 10.1590/S1807-59322011001300007.

Scott, B.S., Becker, L.E., Petit, T.L. (1983) Neurobiology of Down's syndrome, *Progress in Neurobiology*, 21(3), pp. 199–237.

Scudder, S. L., et al. (2014) Synaptic strength is bidirectionally controlled by opposing activity-dependent regulation of Nedd4–1 and USP8, *Journal of Neuroscience*, 34(50), pp. 16637–49.

Seidl, R., Cairns, N., Lubec, G. (2001) The brain in Down syndrome, *Journal of Neural Transmission. Supplementum*, (61), pp. 247–61.

Shahbazian, M., et al. (2002) Mice with truncated MeCP2 recapitulate many Rett syndrome features and display hyperacetylation of histone H3, *Neuron*, 35(2), pp. 243–54.

Shepherd, J. D., and Huganir, R. L. (2007) The cell biology of synaptic plasticity: AMPA receptor trafficking, *Annual Review of Cell and Developmental Biology*, 23, pp. 613–643.

- Shigeri, Y., Seal, R. P. and Shimamoto, K. (2004) 'Molecular pharmacology of glutamate transporters, EAATs and VGLUTs', *Brain Research Reviews*, 45(3), pp. 250–265. doi: 10.1016/j.brainresrev.2004.04.004.
- Siarey, R.J., et al. (2005) Abnormal synaptic plasticity in the Ts1Cje segmental trisomy 16 mouse model of Down syndrome, *Neuropharmacology*, 49(1), pp. 122–8, doi: 10.1016/j.neuropharm.2005.02.012.
- Siegel, G., et al. (2009) A functional screen implicates microRNA-138-dependent regulation of the depalmitoylation enzyme APT1 in dendritic spine morphogenesis, *Nature Cell Biology*, 11(6), pp. 705–716.
- Singaraja, R. R. et al. (2002) 'HIP14, a novel ankyrin domain-containing protein, links huntingtin to intracellular trafficking and endocytosis', *Human molecular genetics*, 11(23), pp. 2815–2828. doi: 10.1093/hmg/11.23.2815.
- Singaraja, R. R. et al. (2011) 'Altered palmitoylation and neuropathological deficits in mice lacking HIP14', *Human Molecular Genetics*, 20(20), pp. 3899–3909. doi: 10.1093/hmg/ddr308.
- Slominski, A. et al. (2002) 'Conversion of L -tryptophan to serotonin and melatonin in human melanoma cells', *FEBS Letters*, 511(1–3), pp. 102–106. doi: 10.1016/S0014-5793(01)03319-1.
- Smith, D.J., et al. (1997) Functional screening of 2 Mb of human chromosome 21q22.2 in transgenic mice implicates minibrain in learning defects associated with Down syndrome, *Nature Genetics*, 16(1), pp. 28–36.
- Snedden, W., Mellor, C. S., Martin, J. R. (1982) 'Hypertryptophanemia and Indoleketonuria in Two Mentally Subnormal Siblings', *The New England Journal of Medicine*, 307(22), pp. 1405–1405.
- Söllner, T., Bennett, M. K., et al. (1993) 'A protein assembly-disassembly pathway in vitro that may correspond to sequential steps of synaptic vesicle docking, activation, and fusion', *Cell*, 75(3), pp. 409–418. doi: 10.1016/0092-8674(93)90376-2.

- Söllner, T., Whiteheart, S. W., et al. (1993) 'SNAP receptors implicated in vesicle targeting and fusion', *Nature*, 362(6418), pp. 318–324. doi: 10.1038/362318a0.
- Spencer, C. M. et al. (2005) 'Altered anxiety-related and social behaviors in the Fmr1 knockout mouse model of fragile X syndrome', *Genes, Brain and Behavior*, 4(7), pp. 420–430. doi: 10.1111/j.1601-183X.2005.00123.x.
- Spencer, M. D. et al. (2005) 'Qualitative assessment of brain anomalies in adolescents with mental retardation', *American Journal of Neuroradiology*, 26(10), pp. 2691–2697.
- Stearns, N.A. et al. (2007) Behavioral and anatomical abnormalities in Mecp2 mutant mice: a model for Rett syndrome, *Neuroscience*, 146(3), pp. 907-21.
- Swank, M.W. and Sweatt, J.D. (2001) Increased histone acetyltransferase and lysine acetyltransferase activity and biphasic activation of the ERK/RSK cascade in insular cortex during novel taste learning, *Journal of Neuroscience*, 21(10), pp. 3383–3391.
- Swarthout, J. T. et al. (2005) 'DHHC9 and GCP16 constitute a human protein fatty acyltransferase with specificity for H- and N-Ras', *Journal of Biological Chemistry*, 280(35), pp. 31141–31148. doi: 10.1074/jbc.M504113200.
- Swerdlow, N. R. et al. (1995) 'Impaired prepulse inhibition of acoustic and tactile startle response in patients with Huntington's disease', *Journal of Neurology, Neurosurgery, and Psychiatry*, 58(2), pp. 192–200. doi: 10.1136/jnnp.58.2.192.
- Takashima, S., et al. (1981) Abnormal neuronal development in the visual cortex of the human fetus and infant with down's syndrome. A quantitative and qualitative Golgi study, *Brain Research*, 225(1), pp. 1–21.
- Tang, T. et al. (2010) A mouse knockout library for secreted and transmembrane proteins, *Nature Biotechnology*, 28(7), pp. 749-55. doi: 10.1038/nbt.1644.
- Tarpey, P. S. et al. (2010) 'A systematic, large-scale resequencing screen of X-chromosome coding exons in mental retardation', *Nature Genetics*, 41(5), pp. 535–543. doi: 10.1038/ng.367.A.

Tezuka, T. et al. (1999) PSD-95 promotes Fyn-mediated tyrosine phosphorylation of the N-methyl-D-aspartate receptor subunit NR2A, *Proceedings of the National Academy of Sciences U S A*, 96(2), pp. 435-40.

Thomas, G. M. et al (2012) 'Palmitoylation by DHHC5/8 targets GRIP1 to dendritic endosomes to regulate AMPA-R trafficking', *Neuron*, 29(6), pp. 997–1003. doi: 10.1016/j.biotechadv.2011.08.021.Secreted.

Tian, L. et al. (2008) 'Palmitoylation gates phosphorylation-dependent regulation of BK potassium channels.', *Proceedings of the National Academy of Sciences of the United States of America*, 105(52), pp. 21006–21011. doi: 10.1073/pnas.0806700106.

Tian, L. et al. (2010) 'Multiple palmitoyltransferases are required for palmitoylation-dependent regulation of large conductance calcium- and voltage-activated potassium channels', *Journal of Biological Chemistry*, 285(31), pp. 23954–23962. doi: 10.1074/jbc.M110.137802.

Tomoeda, K. et al. (2000) 'Mutations in the 4-Hydroxyphenylpyruvic Acid Dioxygenase Gene Are Responsible for Tyrosinemia Type III and Hawkinsinuria', *Molecular Genetics and Metabolism*, 71(3), pp. 506–510. doi: 10.1006/mgme.2000.3085.

Toniolo, D., D'Adamo, P. (2000) X-linked non-specific mental retardation, *Current Opinion in Genetics & Development*, 10(3), pp. 280–5.

Toniolo, D. (2000) In search of the MRX genes, *American Journal of Medical Genetics*, 97(3), pp. 221–7.

Tönissoo, T. et al. (2006) 'Heterozygous mice with Ric-8 mutation exhibit impaired spatial memory and decreased anxiety', *Behavioural Brain Research*, 167(1), pp. 42–48. doi: 10.1016/j.bbr.2005.08.025.

Tristan, C. et al. (2011) 'The diverse functions of GAPDH: Views from different subcellular compartments', *Cellular Signalling*, 23(2), pp. 317–323. doi: 10.1016/j.cellsig.2010.08.003.

- Tsien, J. Z., Huerta, P. T. and Tonegawa, S. (1996) 'The essential role of hippocampal CA1 NMDA receptor-dependent synaptic plasticity in spatial memory', *Cell*, 87(7), pp. 1327–1338. doi: 10.1016/S0092-8674(00)81827-9.
- Tuli, L., Resson, H. W. (2009) 'LC-MS Based Detection of Differential Protein Expression', *Journal of Proteomics and Bioinformatics*, 1(2), pp. 416–438. doi: 10.4172/jpb.1000102.LC.
- Turner, G., et al. (1996) Prevalence of fragile X syndrome, *American Journal of Medical Genetics*, 64(1), pp. 196–7.
- Tzschach, A. et al. (2015) 'Next-generation sequencing in X-linked intellectual disability', *European Journal of Human Genetics*, 23(11), pp. 1513–1518. doi: 10.1038/ejhg.2015.5.
- Vaillend, C., Poirier, R. and Laroche, S. (2008) 'Genes, plasticity and mental retardation', *Behavioural Brain Research*, 192(1), pp. 88–105. doi: 10.1016/j.bbr.2008.01.009.
- Valdez- Taubas, J., Pelham, H. (2005) Swf1-dependent palmitoylation of the SNARE Tlg1 prevents its ubiquitination and degradation, *The EMBO Journal*, 24(14), pp. 2524-32.
- Van Buggenhout, G. and Fryns, J. P. (2006) 'Lujan-Fryns syndrome (mental retardation, X-linked, marfanoid habitus)', *Orphanet journal of rare diseases*, 1, p. 26. doi: 10.1186/1750-1172-1-26.
- Veit, M., Becher, A. and Ahnert-Hilger, G. (2000) 'Synaptobrevin 2 is palmitoylated in synaptic vesicles prepared from adult, but not from embryonic brain', *Molecular and Cellular Neurosciences*, 15(4), pp. 408–416. doi: 10.1006/mcne.1999.0830.
- Verheij, C., et al. (1993) Characterization and localization of the FMR-1 gene product associated with fragile X syndrome. *Nature*, 363(6431), pp. 722–4.
- Vesa, J., et al. (1995) Mutations in the palmitoyl protein thioesterase gene causing infantile neuronal ceroid lipofuscinosis, *Nature*, 376(6541), pp. 584-7.
- Viergge, P., and Froster-Iskenius, U. (1989) Clinico-neurological investigations in the fra(X) form of mental retardation, *Journal of Neurology*, 236(2), pp. 85-92.

- Wagner, S. A., et al. (2012) Proteomic analyses reveal divergent ubiquitylation site patterns in murine tissues, *Molecular & Cellular Proteomics*, 11(12), pp. 1578–1585.
- Walker, D. L. and Davis, M. (1997) 'Anxiogenic effects of high illumination levels assessed with the acoustic startle response in rats', *Biological Psychiatry*, 42(6), pp. 461–471. doi: 10.1016/S0006-3223(96)00441-6.
- Wan, J. et al. (2013) 'Tracking brain palmitoylation change: Predominance of glial change in a mouse model of Huntington's disease', *Chemistry and Biology*, 20(11), pp. 1421–1434. doi: 10.1016/j.chembiol.2013.09.018.
- Webb, T., Latif, F. (2001) Rett syndrome and the MECP2 gene, *Journal of Medical Genetics*, 38(4), pp. 217–23.
- Weber, T. et al. (1998) 'SNAREpins: Minimal machinery for membrane fusion', *Cell*, 92(6), pp. 759–772. doi: 10.1016/S0092-8674(00)81404-X.
- Wells, M. F. et al. (2016) 'Thalamic reticular impairment underlies attention deficit in Ptchd1(Y/-) mice', *Nature*, 532(7597), pp. 58–63. doi: 10.1038/nature17427.
- Wentholt, R. J., et al. (1996) Evidence for multiple AMPA receptor complexes in hippocampal CA1/ CA2 neurons, *Journal of Neuroscience*, 16(6), pp. 1982–1989.
- Westerhoff, H. V. and Palsson, B. O. (2004) 'The evolution of molecular biology into systems biology', *Nature Biotechnology*, 22(10), pp. 1249–1252. doi: 10.1038/nbt1020.
- Widagdo, J., et al. (2015) Activity-dependent ubiquitination of GluA1 and GluA2 regulates AMPA receptor intracellular sorting and degradation, *Cell Reports*, pii: S2211-1247(15)00028-5. doi: 10.1016/j.celrep.2015.01.015.
- Wonodi, I., et al. (2011) 'Downregulated Kynurenine 3-Monooxygenase Gene Expression and Enzyme Activity in Schizophrenia and Genetic Association With Schizophrenia Endophenotypes', *Archives of General Psychiatry*, 68(7), pp. 665-74. doi: 10.1001/archgenpsychiatry.2011.71.Downregulated.

Woods, Y.L. et al. (2001) The kinase DYRK phosphorylates protein-synthesis initiation factor eIF2Bepsilon at Ser539 and the microtubule-associated protein tau at Thr212: potential role for, DYRK as a glycogen synthase kinase 3-priming kinase, *Biochemical Journal*, 355(Pt 3), pp. 609–15.

Yamamoto, Y., et al. (2007) Gain of 5p15.33 is associated with progression of bladder cancer, *Oncology*, 72(1-2), pp. 132–138.

Yan, S.M., et al. (2013) Reduced expression of ZDHHC2 is associated with lymph node metastasis and poor prognosis in gastric adenocarcinoma, *PLoS One*, 8(2):e56366. doi: 10.1371/journal.pone.0056366.

Yanai, A., et al. (2006) Palmitoylation of huntingtin by HIP14 is essential for its trafficking and function, *Nature Neuroscience*, 9(6), pp. 824–831.

Yang, E.J., Ahn, Y.S., Chung, K.C. (2001) Protein kinase Dyrk1 activates cAMP response element-binding protein during neuronal differentiation in hippocampal progenitor cells, *Journal of Biological Chemistry*, 276(43), pp. 39819–24.

Yang, G. et al. (2009) 'Subunit-selective palmitoylation regulates the intracellular trafficking of AMPA receptor', *European Journal of Neuroscience*, 30(1), pp. 35–46. doi: 10.1111/j.1460-9568.2009.06788.x.

Yasumura, M. et al. (2014) 'IL1RAPL1 knockout mice show spine density decrease, learning deficiency, hyperactivity and reduced anxiety-like behaviours', *Scientific reports*, 4, p. 6613. doi: 10.1038/srep06613.

Yeste-Velasco, M., et al. (2014) Identification of ZDHHC14 as a novel human tumour suppressor gene, *Journal of Pathology*, 232(5), pp. 566–577.

Young, J.W. et al. (2009) The 5-choice continuous performance test: evidence for a translational test of vigilance for mice, *PLoS One*, 4(1), pp. e4227. doi: 10.1371/journal.pone.0004227.

Yu, C. et al. (2008) 'White matter tract integrity and intelligence in patients with mental retardation and healthy adults', *NeuroImage*, 40(4), pp. 1533–1541. doi: 10.1016/j.neuroimage.2008.01.063.

Yu, J. S. (1970) 'Phenylketonuria : a review', *Postgraduate Medical Journal*, 46(1), pp. 430–446.

Yu, L., et al. (2011) Activation of a novel palmitoyltransferase ZDHHC14 in acute biphenotypic leukemia and subsets of acute myeloid leukemia, *Leukemia*, 25(2), pp. 367–371.

Yudowski, G. A. et al. (2013) 'Acute Inactivation of PSD-95 Destabilizes AMPA Receptors at Hippocampal Synapses', *PLoS ONE*, 8(1), pp. 1–9. doi: 10.1371/journal.pone.0053965.

Yuen, E. Y., et al. (2012) Repeated stress causes cognitive impairment by suppressing glutamate receptor expression and function in prefrontal cortex, *Neuron*, 73(5), pp. 962–977.

Zang, J. B. et al. (2009) 'A mouse model of the human fragile X syndrome I304N mutation', *PLoS Genetics*, 5(12), pp. 1–16. doi: 10.1371/journal.pgen.1000758.

Zhang, X. et al. (2005) 'Loss-of-function mutation in tryptophan hydroxylase-2 identified in unipolar major depression', *Neuron*, 45(1), pp. 11–16. doi: 10.1016/j.neuron.2004.12.014.

Online links

<http://biit.cs.ut.ee/gprofiler/index.cgi>

<http://brainspan.org/>

<http://mmrrc.mousebiology.org/phenotype/Genentech/MEM695N1-treeFrame.html>


<http://mouse.brain-map.org/>

<http://www.metaboanalyst.ca/faces/ModuleView.xhtml>

https://www.ebi.ac.uk/Tools/psa/emboss_water/


https://www.ensembl.org/Mus_musculus/Transcript/ProteinSummary?db=core;g=ENSMUSG00000036985;r=X:48171969-48208878;t=ENSMUST00000037960

Appendix I




University of Strathclyde
Sciences

Knockout of *ZDHHC9*, a gene associated with X-linked intellectual disability, causes reduced anxiety and a spatial learning deficit in adult male mice




Chamberlain
LAB
UNIVERSITY OF STRATHCLYDE



BIOCHEMICAL SOCIETY

Marianna Kouskou¹, David M. Thomson¹, Lee Wheeler¹, Mark O. Collins², Ros R. Brett¹, Judith A. Pratt¹, and Luke H. Chamberlain¹

¹Strathclyde Institute of Pharmacy and Biomedical Sciences, University of Strathclyde, Glasgow, UK. ²Department of Biomedical Science, The University of Sheffield, Sheffield, UK.



INTRODUCTION

Mutations in Zinc finger DHHC domain- containing protein 9 (*ZDHHC9*) gene located in the Xq26 chromosomal region cause mild to moderate intellectual disability (ID) along with oromotor impairment and hypoplasia of corpus callosum (Baker et al. 2015). *ZDHHC9* (Fig.1) encodes the main part of a heterodimer palmitoyltransferase for H- and N- Ras (Swarthout et al. 2005) highly expressed in human and mouse brain.

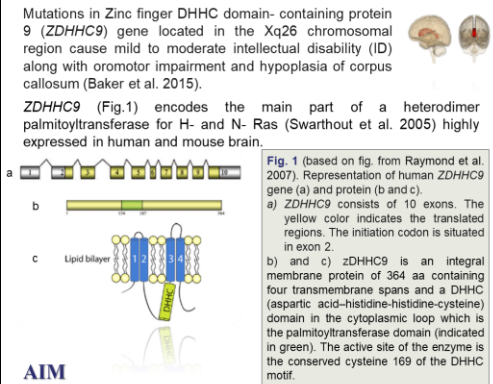



Fig. 1 (based on fig. from Raymond et al. 2007). Representation of human *ZDHHC9* gene (a) and protein (b and c). a) *ZDHHC9* consists of 10 exons. The yellow color indicates the translated regions. The initiation codon is situated in exon 2. b) and c) *ZDHHC9* is an integral membrane protein of 364 aa containing four transmembrane spans and a DHHC (aspartic acid-histidine-histidine-cysteine) domain in the cytoplasmic loop which is the palmitoyltransferase domain (indicated in green). The active site of the enzyme is the conserved cysteine 169 of the DHHC motif.

AIM

To examine how knockout (KO) of *Zdhhc9* in mice affects cognitive processing and cell pathways.

METHODS

Zdhhc9 KO mice were purchased from Mutant Mouse Regional Resource Centers. A genomic region of 207 bp including most of exon 2 (coding exon 1) of *Zdhhc9* was deleted in the KO mice. In order to achieve KO mice with the mutation in a C57BL/6 genetic background, backcrossing was performed for at least 6 generations. Then, behavioural tasks were conducted in adult (8-10 weeks) male KO and WT mice to study motor coordination and sensorimotor gating, locomotor activity and anxiety, learning and memory.



Moreover, ex-vivo MRI (9.4 Tesla) of KO brain was conducted to assess the volume of corpus callosum and hippocampus. In addition, Western blot on brain homogenates, cell fractions and isolated palmitoylated proteins of KO and WT mouse brain was conducted to assess levels of H/N-Ras.

RESULTS

All error bars represent standard error of the mean. Statistical analysis was conducted using SPSS version 22 and applying either general linear model repeated measures or unpaired t-test.

• *Zdhhc9* KO mice exhibit hypotonia on the hanging wire but normal motor coordination on the rotarod.




Fig. 2. KO mice spend significantly less time on the hanging wire (a) but they exhibit no difference in the time spent on the rotarod (b) compared to the WT mice (n=14 KO, 20 WT).

• *Zdhhc9* KO mice exhibit reduced startle reactivity but normal pre-pulse inhibition.

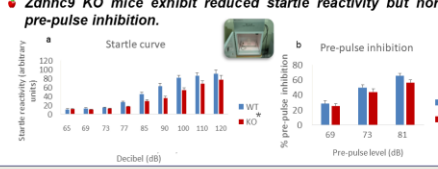


Fig. 3. KO mice start startling at higher decibels than WT (a) but they exhibit normal pre-pulse inhibition (b) indicating normal sensorimotor gating (n=22 KO, 24 WT).

• *Zdhhc9* KO mice exhibit normal general locomotor activity in the Open Field Test but behavior in the Elevated Plus Maze suggests they have reduced anxiety levels.

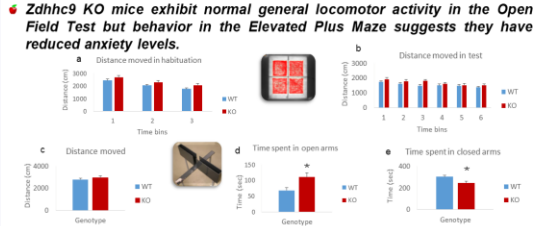


Fig. 4. KO mice exhibit normal locomotor activity in the habituation and test period of the Open Field Test (a, b) as well as in the Elevated Plus Maze (c). However they spent significantly more time in the open arms (d) of the Elevated Plus Maze (n=14 KO, 20 WT) and less time in closed arms (e). A time bin represents a period of 5 min.

• *Zdhhc9* KO mice exhibit no change in learning and cognitive flexibility in the pairwise visual discrimination task but show a different pattern of spatial learning in the Morris Water Maze.

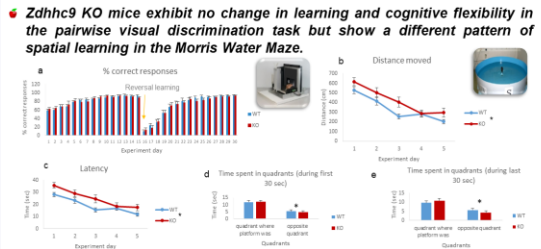


Fig. 5. KO mice perform normally in the pairwise discrimination (a), (n= 12KO, 12WT). However in the Morris water maze they show a different pattern of spatial learning based on distance moved (b) and latency (c). In the probe trial where platform was removed both groups spend significantly more time in the quadrant where platform was (d,e), (n= 20KO, 26WT).

• *Zdhhc9* KO mice show reduced corpus callosum but not hippocampal volume (preliminary results, n=2KO, 2WT).

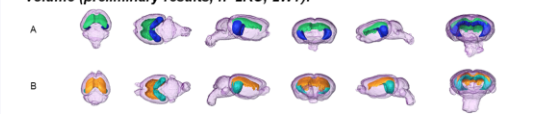


Fig. 6. Reconstruction of WT (A) and KO (B) mouse brain using Amira 6.01 software after MRI scan. Volumetric analysis showed 34% reduction in the total volume of corpus callosum (orange in panel B) in KO brain but not in hippocampus (light blue in panel B).

• H- and N-Ras are detected in normal levels in brain homogenates and membrane fractions of KO brain. Moreover, palmitoylation of H-Ras is not affected in whole brain and hippocampal KO samples suggesting that other unknown substrates may be affected.

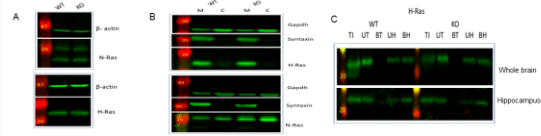


Fig. 7. Western blots of WT and KO brain homogenates (A), cell fractions (B) and Acyl-Resin Assisted Capture (Acyl-RAC, panel C) of WT and KO brain samples (n=3KO, 3WT). Panel A: β -actin was used as loading control. Panel B: M is membrane fraction, C is cytoplasmic fraction. Gapdh was used as a cytoplasmic control while Syntaxin as membrane control. Panel C: During Acyl-RAC, Hydroxylamine (HA) treatment cleaves thioester bonds of palmitoylated proteins. Tris was used as negative control treatment. TI: total input, UT: Unbound Tris fraction, BT: Bound Tris, UH: Unbound HA, BH: Bound HA.


DISCUSSION

Zdhhc9 KO mice exhibit hypotonia, reduced anxiety levels and a deficit in spatial learning. Moreover their reduced startle reactivity can be explained by reduced anxiety levels. Hypotonia is also found in some patients with *ZDHHC9* mutations. Overall, this phenotype is common in other models of ID. Future work will be focused on finding new substrates of *ZDHHC9* enzyme in order to explain the phenotype. Moreover, mouse embryonic fibroblasts from KO mice will help us develop a cellular model of *ZDHHC9* dysfunction.

ACKNOWLEDGMENTS


This work is funded by the University of Strathclyde.

Appendix II



University of Strathclyde
Glasgow


Exploring the links between the *ZDHHC9* gene and intellectual disability



Chamberlain
UNIVERSITY OF STRATHCLYDE

Marianna Kouskou¹, David M. Thomson¹, Lee Wheeler¹, Mark O. Collins², Ros R. Brett¹, Judith A. Pratt¹, and Luke H. Chamberlain¹

¹Strathclyde Institute of Pharmacy and Biomedical Sciences, University of Strathclyde, Glasgow, UK. ²Department of Biomedical Science, The University of Sheffield, Sheffield, UK.



INTRODUCTION

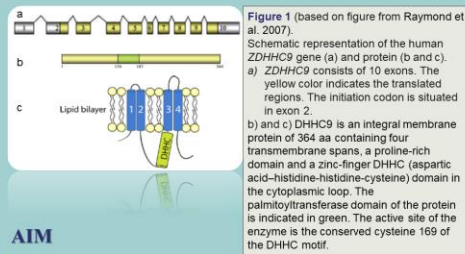
Mutations in Zinc finger DHH domain-containing protein 9 (*ZDHHC9*) gene located in the Xq26 chromosomal region cause X-linked intellectual disability (ID) with Marfanoid habitus (MH) (Raymond et al. 2007) or epilepsy and hypoplasia of corpus callosum (Baker et al. 2015).



MH is a constellation of symptoms resembling those of Marfan syndrome including tall stature, arm span greater than the height of the individual, long hyperlax fingers and toes and long limbs.



ZDHHC9 (Fig.1) encodes the main part of a heterodimer that acts as a palmitoyltransferase highly expressed in brain (Swarthout et al. 2005).




AIM


To examine how the knockout (KO) of *Zdhhc9* in mice affects cognitive processing.

METHODS


The *Zdhhc9* KO mice were purchased from Mutant Mouse Regional Resource Centers (MMRRC). A genomic region of 207 bp including most of exon 2 (coding exon 1) of *Zdhhc9* was deleted in the KO mice. In order to achieve KO mice with the mutation in a C57BL/6 genetic background, backcrossing was performed for 6 generations. Then behavioural tasks were conducted in adult (8-10 weeks) male KO and WT mice to study:



Motor coordination and sensorimotor gating



Locomotor activity and anxiety



Learning and memory

RESULTS

***Zdhhc9* KO mice exhibit hypotonia in the hanging wire but normal motor coordination on the rotarod.**

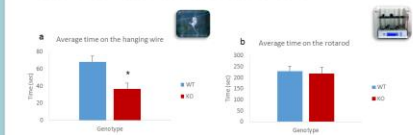


Figure 2. The KO mice spent statistically significantly less time on the hanging wire (a) but they exhibit no difference in the time spent on the rotarod (b) compared to the WT mice (n=14 KO, 20 WT). Statistical analysis was conducted using an unpaired t-test with SPSS version 22. Error bars represent standard error of the mean (SEM).

***Zdhhc9* KO mice exhibit reduced startle reactivity but normal pre-pulse inhibition.**

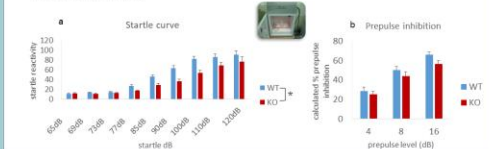


Figure 3. The KO mice start starting at higher decibels than the WT (a) but they exhibit a normal pre-pulse inhibition (b) indicating normal sensorimotor gating (n=22 KO, 24 WT). Statistical analysis was conducted using a general linear model, repeated measures with SPSS version 22. Error bars represent SEM.

***Zdhhc9* KO mice exhibit normal general locomotor activity in the Open Field Test but behavior in the Elevated Plus Maze suggests they have reduced anxiety levels.**

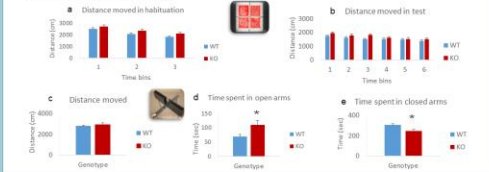


Figure 4. The KO mice exhibit normal locomotor activity in the habituation and test period of the Open Field Test (a, b) as well as in the Elevated Plus Maze (c). However they spent statistically significantly more time in the open arms (d) of the Elevated Plus Maze (n=14 KO, 20 WT). Statistical analysis was conducted using either general linear model, repeated measures or unpaired t-test with SPSS version 22. A time bin represents a period of 5 min. Error bars represent SEM.

***Zdhhc9* KO mice exhibit no change in learning and cognitive flexibility in the pairwise visual discrimination task but show a different pattern of spatial learning in the Morris Water Maze.**

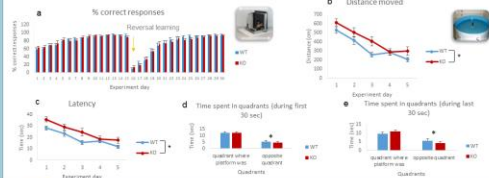


Figure 5. The KO mice perform normally in the pairwise discrimination (a), (n=12KO, 12WT). However in the Morris water maze they show a different pattern of spatial learning based on distance moved (b) and latency (c). In the probe trial where platform was removed both groups spent statistically significantly more time in the quadrant where platform was ((d, e), n=20KO, 26WT). Statistical analysis was conducted using either general linear model, repeated measures or paired t-test with SPSS version 22. Error bars represent SEM.

CONCLUSION AND FUTURE WORK

Our results indicate that the *Zdhhc9* KO mice exhibit hypotonia, reduced anxiety levels and a deficit in spatial learning. Moreover their reduced startle reactivity can be explained by reduced anxiety levels. This phenotype is common in other models of ID. Future work will be focused on explaining the phenotype studying the KO brain architecture using immunohistochemistry and cell pathways using proteomics in order to identify other substrates of DHH9C enzyme.

REFERENCES

- Baker K et al. Epilepsy, cognitive deficits and neuroanatomy in males with *ZDHHC9* mutations. *Ann Clin Transl Neurol.* 2015 May;2(5):559-69.
- Raymond FL et al. Mutations in *ZDHHC9*, which encodes a palmitoyltransferase of NRAS and HRAS, cause X-linked mental retardation associated with a Marfanoid habitus. *Am J Hum Genet.* 2007 May;80(5):982-7.
- Swarthout JT et al. DHH9C and GCP16 constitute a human protein fatty acyltransferase with specificity for H- and N-Ras. *J Biol Chem.* 2005 Sep 2;280(35):31141-8.

ACKNOWLEDGMENTS

This work is funded by the University of Strathclyde.

Appendix III



Exploring the links between the *ZDHHC9* gene and intellectual disability



Marianna Kouskou¹, David M. Thomson¹, Mark O. Collins² and Luke H. Chamberlain¹

¹Strathclyde Institute of Pharmacy and Biomedical Sciences, University of Strathclyde, Glasgow, UK.
²Department of Biomedical Science, The University of Sheffield, Sheffield, UK.



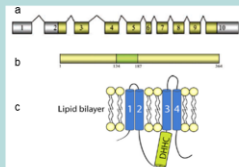
INTRODUCTION

Mutations in Zinc finger DHC domain-containing protein 9 (*ZDHHC9*) gene located in the Xq26 chromosomal region cause X-linked intellectual disability with Marfanoid habitus (MH) (Raymond et al. 2007) or Rolandic epilepsy (RE) (Baker et al. 2015).



MH is a constellation of symptoms resembling those of Marfan syndrome including tall stature, arm span greater than the height of the individual, long hyperlax fingers and toes (arachnodactyly and hypermobility of joints) and long limbs (dolichostenomelia).

RE also known as Benign Childhood Epilepsy with Centro-Temporal Spikes, (BECTS) is the most frequently diagnosed epilepsy syndrome of childhood (Panayiotopoulos et al. 2008). *ZDHHC9* (Fig.1) encodes the main part of a heterodimer that acts as a palmitoyltransferase (PAT) (Swarthout et al. 2005).



AIM

To examine how the knockout (KO) of *Zdhhc9* in mice affects cognitive processing, neuronal function and cell pathways.

METHODS

✓The *ZDHHC9* KO mice were purchased from Mutant Mouse Regional Resource Centers (MMRRC). A genomic region of 207 bp including most of exon 2 (coding exon 1) of *Zdhhc9* was deleted in the KO mice. The selection cassette contained both Neomycin (Neo) and LacZ. In order to achieve KO mice with the mutation in a C57BL/6 genetic background, backcrossing was performed for 6 generations. During the backcrosses, behavioural tests were conducted in adult (8-10 weeks) male mice.



✓Moreover proteomic profiling of the KO brain was conducted after enriching for palmitoylated proteins with Resin-Assisted Capture of S-acylated proteins (Acy-RAC).

RESULTS

BEHAVIOURAL TESTS

We identified statistically significant behavioral differences between KO and WT mice in locomotor activity (distance travelled) and anxiety in the open field test and the elevated plus maze as well as in reversal learning using the pairwise discrimination task.

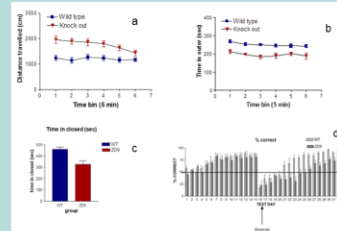


Figure 2. Statistically significant behavioral differences between WT and KO mice in the a) open field test, c) elevated plus maze and d) reversal learning using the pairwise discrimination task.

PROTEOMICS

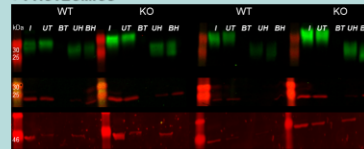


Figure 3. Western blotting from 2 KO and 2 WT adult mouse brains after Acyl-RAC using antibodies against a) CSPα and b) Snap25 as positive controls and c) β-actin as negative control. I: total input, UT: unbound Tris treated fraction, BT: bound Tris treated fraction, UH: unbound HA treated fraction, BH: bound HA treated fraction.

Protein names	Gene names	Average KOWT
Elongation factor 1-alpha 2	Erf1a2	0.147
Potassium voltage-gated channel subfamily D member 3	Kcnd3	0.148
Alpha-intensin	Itia	0.059
Tubulin beta-3 chain	Tubb3	0.079
Tubulin alpha-4A chain	Tuba4a	0.081
Myelin basic protein	Mbp	0.082
Brain-enriched guanylate kinase-associated protein	Began	0.104
Voltage-dependent L-type calcium channel subunit beta4	Cacnb4	0.127
Tubulin alpha-1B chain	Tuba1b	0.142
Astractin-1	Astr1	0.155
Protein-rich transmembrane protein 3	Prtc3	0.157
Myelin proteolipid protein	Plp1	0.168
Ankyrin repeat and sterile alpha motif domain-containing protein 18	Ank18	0.169
Rho guanine nucleotide exchange factor 33	Arhgef33	0.170
Protein kinase C, protein kinase C alpha type	Pkca	0.181
Tubulin beta-4A chain	Tuba4a	0.182
Rho-related GTP-binding protein RhoB	RhoB	0.186
Plasminogen	Plg	0.189
Synaptic vesicle 2-related protein	Svpp	0.194
Kinesin light chain 2	Klc2	0.211
Protein myo-inositol cotransporter	Slc3a13	0.213
FXYD domain-containing ion transport regulator 6	Fxyd6	0.219
Kelch repeat and BTB domain-containing protein 11	Klrbt11	0.233
Claudin-12	Cldn12	0.235
Cysteine and glycine rich protein 1	Cgrp1	0.238
Rho guanine nucleotide exchange factor 9	Arhgef9	0.243
GTPase HRas, GTPase HRas, N-terminally processed	Hras	0.245

Table 1. List of the 25 proteins being mostly downregulated in KO mouse brain. Results were obtained with LC-MS/MS on an orbitrap (on trap mass analyzer). The relative levels of proteins in each purification were quantified by label-free quantification. Data were processed with MaxQuant.

CONCLUSION AND FUTURE WORK

Preliminary behavioural results indicate that the *ZDHHC9* KO mice exhibit increased locomotor activity and reduced anxiety as well as deficit in reversal learning. This phenotype is common in models of ID. Moreover, proteomic analysis of the palmitoylated proteomes of KO and WT mice with proteins important for neuronal function being significantly down-regulated (up to 21 times) in the KO brain, Hras which is one of the substrates of *ZDHHC9* enzyme was among those proteins, showing a down-regulation of palmitoylation of 75% in the KO brain. Future work will be focused on confirming the preliminary behavioral results after the final backcrossing and explaining the phenotype based on deficits in neuronal function using neuronal cultures.

REFERENCES

- Baker K et al. Epilepsy, cognitive deficits and neuroanatomy in males with *ZDHHC9* mutations. *Ann Clin Transl Neurol.* 2015 May;2(5):559-69.
- Panayiotopoulos CP et al. Benign childhood focal epilepsies: assessment of established and newly recognized syndromes. *Brain* 2008 Sep;131(Pt 9):2264-86.
- Raymond FL et al. Mutations in *ZDHHC9*, which encodes a palmitoyltransferase of NRAS and HRAS, cause X-linked mental retardation associated with a Marfanoid habitus. *Am J Hum Genet.* 2007 May;80(5):982-7.
- Swarthout JT et al. *ZDHHC9* and *GCP16* constitute a human protein fatty acyltransferase with specificity for H- and N-Ras. *J Biol Chem.* 2005 Sep 2;280(35):31141-8.

ACKNOWLEDGMENTS

This work is funded by the University of Strathclyde.